
Taming the Zoo of Tetraquarks and Pentaquarks using the HISH Model

Michal Michael Green
mickeygreen@mail.tau.ac.il

Jacob Sonnenschein
cobi@tauex.tau.ac.il

School of Physics and Astronomy,
The Raymond and Beverly Sackler Faculty of Exact Sciences,
Tel Aviv University, Ramat Aviv 69978, Israel
February 14, 2024

Abstract

In this paper we scan over all possible charmed tetraquarks and pentaquarks. Using the holography inspired stringy hadron (HISH) model we determine the trajectories associated with each of the exotic hadron candidates. The trajectories include further exotic states with higher angular momentum or higher stringy excited states. A trajectory is a property of a genuine exotic hadron and can be used to distinguish between the latter and a molecule. We examine 71 tetraquarks and 210 pentaquarks. Few of these states have already been found but most of the predicted zoo have yet not been discovered. We analyze the strong decay processes of these exotic hadrons and compute the corresponding decay widths of part of them. The predictions are summarized in tables 107 and 223. The results for each of the exotic candidates are at sections 7.2 and 7.5.

Contents

1	Introduction	4
2	Brief review of HISH (holography inspired string hadron) model	7
2.1	The HISH mapping	8
2.2	Massive Strings in Flat Spacetime	8
2.3	Hadron Constructions	9
2.4	Action and equations of motion	10
2.5	Classical Regge trajectories	12
2.6	The quantum static string	12
2.7	Quantum Regge trajectories	13
2.7.1	Repulsive Casimir force	14
2.8	Baryonic structures	15
2.9	The decay width of stringy hadrons	15
2.9.1	Hadronic decay through string breaking	16
2.9.2	Hadronic decay via annihilation	18
3	Exotic hadrons	18
4	Tetraquarks	20
4.1	The spin structure of tetraquarks	22
4.2	Tetraquark Creation	23
4.2.1	Excited Meson Decay	23
4.2.2	Mesons Decay Through Scattering	24
4.3	Decay mechanisms of tetraquarks	24
5	Pentaquarks	26
5.1	Pentaquark configurations	26
5.1.1	A single BV	27
5.1.2	Configuration with BV anti-BV and a BV	28
5.2	Decays of the pentaquarks	29
5.2.1	Decay of a configuration with a single BV	29
5.2.2	Decay of a configuration with BV anti-BV and a BV	30
6	Confronting Experimental Data	31
6.1	Fitting Procedure	31
6.2	Width estimation	32
6.3	Fitting Models	33
6.4	Predictions of J and n	34
6.5	Mesons	34
6.6	Baryons	34
6.7	Tetraquarks	35
6.8	Pentaquarks	35
7	Exotic Hadron Candidates	36
7.1	HISH Exotic Candidates selection Criteria	36
7.2	Tetraquarks Candidates	37
7.2.1	Minimal content $T_{u\bar{u}d\bar{d}}$ or $T_{\bar{u}d\bar{d}\bar{d}}$	40
7.2.2	$T_{u\bar{d}\bar{u}\bar{d}}$ or $T_{d\bar{d}\bar{d}\bar{d}}$	41

7.2.3	$T_{u\bar{s}\bar{u}s}$ or $T_{d\bar{s}\bar{d}s}$	43
7.2.4	$K(3100)$ ($T_{s\bar{u}u\bar{d}}$)	48
7.2.5	$T_{c\bar{u}u\bar{s}}$ or $T_{c\bar{d}u\bar{s}}$	50
7.2.6	T_{cs} (with quark content $c\bar{d}s\bar{u}$)	52
7.2.7	$T_{c\bar{s}}^a$ (with quark content $c\bar{s}d\bar{u}$ or $c\bar{s}u\bar{d}$)	53
7.2.8	$X(3350)$ ($T_{c\bar{d}d\bar{u}}$ or $T_{c\bar{u}u\bar{u}}$)	55
7.2.9	$T_{c\bar{d}c\bar{u}}$	59
7.2.10	$T_{c\bar{c}u\bar{d}}$ or $T_{c\bar{c}d\bar{u}}$	61
7.2.11	$T_{c\bar{c}u\bar{s}}$ or $T_{c\bar{c}d\bar{s}}$	70
7.2.12	$T_{\psi\phi}$ (quark content $c\bar{c}s\bar{s}$)	72
7.2.13	$T_{\psi\psi}$ (quark content $c\bar{c}c\bar{c}$)	77
7.3	Tetraquarks and Mesons Global Fit	80
7.4	Tetraquarks HMRTs predictions	87
7.4.1	Detailed Predictions for Genuine and Semi-Genuine Tetraquarks	96
7.4.2	$T_{c\bar{u}d\bar{u}}$	96
7.4.3	$T_{c\bar{d}u\bar{d}}$	97
7.4.4	$T_{c\bar{d}u\bar{s}}$	98
7.4.5	$T_{c\bar{s}d\bar{u}}$	99
7.4.6	$T_{c\bar{u}s\bar{u}}$	100
7.4.7	$T_{c\bar{d}s\bar{u}}$	101
7.4.8	$T_{c\bar{d}s\bar{d}}$	102
7.4.9	$T_{c\bar{s}u\bar{s}}$	103
7.4.10	$T_{c\bar{s}d\bar{s}}$	104
7.4.11	$T_{c\bar{c}d\bar{u}}$	105
7.4.12	$T_{c\bar{c}s\bar{u}}$	106
7.4.13	$T_{c\bar{c}s\bar{d}}$	107
7.4.14	$T_{c\bar{c}d\bar{s}}$	108
7.4.15	$T_{c\bar{u}c\bar{u}}$	109
7.4.16	$T_{c\bar{d}c\bar{d}}$	110
7.4.17	$T_{c\bar{s}c\bar{u}}$	111
7.4.18	$T_{c\bar{d}c\bar{s}}$	112
7.4.19	$T_{c\bar{s}c\bar{s}}$	113
7.4.20	$T_{c\bar{c}c\bar{u}}$	114
7.4.21	$T_{c\bar{c}c\bar{d}}$	115
7.4.22	$T_{c\bar{c}c\bar{s}}$	116
7.4.23	$T_{c\bar{b}d\bar{u}}$	117
7.4.24	$T_{c\bar{b}u\bar{d}}$	118
7.4.25	$T_{c\bar{b}s\bar{u}}$	119
7.4.26	$T_{c\bar{b}u\bar{s}}$	120
7.4.27	$T_{c\bar{b}d\bar{s}}$	121
7.4.28	$T_{c\bar{b}s\bar{d}}$	122
7.4.29	$T_{b\bar{u}c\bar{u}}$	123
7.4.30	$T_{b\bar{d}c\bar{u}}$	124
7.4.31	$T_{b\bar{d}c\bar{d}}$	125
7.4.32	$T_{b\bar{s}c\bar{u}}$	126
7.4.33	$T_{b\bar{d}c\bar{s}}$	127
7.4.34	$T_{b\bar{s}c\bar{s}}$	128
7.4.35	$T_{b\bar{c}c\bar{u}}$	129
7.4.36	$T_{c\bar{b}u\bar{c}}$	130
7.4.37	$T_{c\bar{b}c\bar{u}}$	131

7.4.38	$T_{c\bar{b}c\bar{d}}$	132
7.4.39	$T_{c\bar{b}d\bar{c}}$	133
7.4.40	$T_{b\bar{c}c\bar{d}}$	134
7.4.41	$T_{b\bar{c}c\bar{s}}$	135
7.4.42	$T_{c\bar{b}c\bar{s}}$	136
7.4.43	$T_{c\bar{b}s\bar{c}}$	137
7.4.44	$T_{c\bar{b}c\bar{c}}$	138
7.4.45	$T_{b\bar{b}c\bar{u}}$	139
7.4.46	$T_{b\bar{b}c\bar{d}}$	140
7.4.47	$T_{b\bar{b}c\bar{s}}$	141
7.4.48	$T_{c\bar{b}u\bar{b}}$	142
7.4.49	$T_{c\bar{b}d\bar{b}}$	143
7.4.50	$T_{c\bar{b}s\bar{b}}$	144
7.4.51	$T_{b\bar{b}c\bar{c}}$	145
7.4.52	$T_{c\bar{b}c\bar{b}}$	146
7.4.53	$T_{b\bar{b}c\bar{b}}$	147
7.5	Pentaquarks Candidates	147
7.6	$P_\psi^{N^+}$ (quark content $c\bar{c}uud$)	148
7.6.1	$P_\psi^{N^+}$ baryonic configuration fit	148
7.6.2	$P_\psi^{N^+}$ tetraquark-like configuration fit	149
7.7	$P_{c\bar{c}sud}$	149
7.7.1	$P_{c\bar{c}sud}$ baryon configuration HMRTs	150
7.7.2	$P_{c\bar{c}sud}$ tetra configuration fit	150
7.8	Pentaquarks HMRTs Predictions	151
8	Summary and Conclusions	166
9	Open Questions	168
10	Acknowledgment	169
A	Mesons Fits	176
B	Baryons Fits	190
B.1	Baryons (n, M^2) Global Fit.	192

1 Introduction

THE Question of whether nature exhibits compact multiquark hadron states aside from mesons, baryons, and glueballs is still not fully resolved. Observations in recent years provide direct and indirect evidence for the existence of such exotic hadrons, yet there is no consensual picture about exotic hadron states in the hadronic spectrum. For reviews of the experimental and theoretical status see [1], [2], [3], [4],[5] and [6].

The main challenges of any theoretical description of exotic hadrons is the determinations of their spectra and decay widths. In previous works, the spectra of mesons [7], baryons [8], glueballs [9] and tetraquarks [10] were analysed in the context of the HISH (holography inspired stringy hadron) model [11] [12]. It was found that most of the known hadron resonances match nicely the HISH modified Regge trajectories (HMRT) generated by the model. The model also provides mechanisms for strong hadronic decays [13] from which one can predict not only the masses of the resonances, but also their corresponding decay width and branching ratios.

The description of hadrons in terms of strings was one of the origins of string theory. In the “old days” various aspects of hadron physics have been analyzed in terms of a stringy behavior. For a review and references therein see [14]. The “modern” arena of stringy hadron physics has been sourced by the holographic string/gauge duality. In particular the HISH framework[11] provides a phenomenological stringy description of hadrons based on a map between string configurations that reside in holographic confining backgrounds and strings in four dimensional flat space-time. One should notice the difference between the holographic stringy picture of hadrons and the field theory gravity/gauge duality approach where hadrons associate with fluctuations of the bulk fields and flavor D branes. For a review and references about this approach see[15]. Several other descriptions of hadrons, and in particular exotic ones, in terms of strings have been proposed in the past, in fact from the early days of strings and up to recent years. Such models can be found for instance in [16], [17], [18],[19] , [20], and and [21].

In the HISH model mesons are described as open strings with massive particles (“quarks”) that carry electric charge and spin on their endpoints, baryons as strings stretched between a quark and a baryonic vertex (BV) to which a di-quark is attached and glueballs as closed strings. The stringy hadron can rotate thus generating an orbital angular momentum to a meson, baryon and glueball respectively. The stringy hadrons furnish the HMRT. These trajectories, described in the plane of M^2 and J the total angular momentum which is sum of the orbital angular momentum of the string and the spin of the endpoint particles. Another class of trajectories is in the plane of M^2 and n the string excitation number. In both cases the trajectories which are not linear are characterized by the masses of the endpoint particles, by the slope which relates to the string tension and by the intercept that relates to the quantum Casimir energy of the string. The latter depends on the properties of the endpoint particles, the masses [12], the electric charges [22] and the spins.

Naturally the string description of hadrons can accommodate on top of mesons, baryons and glueballs, also “exotic hadrons”. These include states without quarks, namely, exotic glueballs and with quarks but with vanishing baryon number: tetraquarks, hexaquarks and hybrids of glueballs and mesons. States with unit baryon number: pentaquarks, septaquarks etc. including hybrids with glueballs. One can also easily construct configurations with baryon number equal to two or higher like sexaquarks[23] etc. In fact, trajectories of tetraquarks candidates where analysed in the past in [10] and [24]. In the former exotic states associated with Y(4630) and in the latter with X(6900).

Tetraquarks and pentaquarks have been thoroughly investigated from both the experimental and theoretical points of view. For reviews and references therein see for the the former [2], [25]and [26]. Reviews and references about pentaquark can be found in[27] and [5]

Exotic resonances can have light or heavy string endpoint quarks. In recent years the focus of the study of exotic hadrons has been on states that include a heavy quark. For that reason, in the present work we systematically analyze all the stringy tetraquarks and pentaquarks states that include at least one charmed quark. As a warm up we also describe several candidates of exotic hadrons that do not include a charm quark. We analyse the exotic hadron candidates in the context of the HISH model. We sketch the possible arrangements constructed from the basic building blocks - open strings, massive endpoints (“quarks” or “di-quarks”), and baryonic vertices. Using data extracted from the HMRT of relevant mesons and baryons we determine the trajectories of the tetraquarks and pentaquark. This includes predicting the mass, angular momentum J and string excitation number n of the states that reside on the trajectories.

In this paper we study “genuine” exotic hadrons. We do not study molecules of hadrons. The latter can be described as disconnected string configurations. The stringy description of molecules and mixtures of them and genuine connected exotic hadrons was analyzed in several papers. See for instance [28] and [29].

Associated with each tetraquark state there are two thresholds: (i) The sum of the masses

of the two stringy mesons that have the quark content of the original tetraquark (ii) The sum of the masses of the baryon and anti-baryon that can result from the breaking of the string of the tetraquark. In fact the most natural decay mode of any stringy hadron, if permitted by energy considerations, is through breaking apart. In the case of the tetraquark simplest configuration (Fig-11) it is the decay to a baryon-antibaryon pair (see Fig-18). Obviously, this decay can occur only provided the mass of the tetraquark is higher than the sum of the masses of the daughter baryon and anti-baryon. Due to the structure of the tetraquark, the computation of the decay width of such a process is similar to that of a meson decaying into two mesons [30]. When the mass is below the threshold for decay through tearing, a tetraquark decay can take place through BV-anti-BV annihilation, which results in two mesons (see Fig-17 and 4.3). Most of the recently observed exotics were below the baryonia threshold, and instead reconstructed through a mesons pair channel.

For pentaquarks, the possible configurations are more complex. There are two possible structures, the first (see Fig-21) is baryon-like, with the addition of a quark anti-quark pair attached to a BV. The second is constructed similarly to a tetraquark (see Fig-23), where there are two BVs with diquarks and an additional anti-BV attached to an antiquark between them. Both structures will be discussed in this paper along with the criteria with which one determines the structure that takes place.

An important question regarding exotic candidates observations is whether they are genuine multiquarks or bound states of mesons and baryons. The HISH model, where the stringy exotic hadrons are genuine, provides two ways to distinguish between the genuine exotic hadrons and the molecules:(i) If the exotic states furnish a HMRT it means that they all are string configuration and are genuine. (ii) If a state decays into a baryon anti-baryon it is probably a genuine tetraquark which decays via a breaking of its string. Similarly, an outcome of two baryon and anti- baryon and in fact also of a baryon and two mesons are smoking guns of pentaquarks.

In this paper We analyze 71 candidates of charmed tetraquarks. For each of them we determine the thresholds to decay into two mesons and into a baryon and anti-baryon. The masses of the excited states are determined. We group all the states into 31 separate cases for which we write down the HMRT, the and widths associated with breaking of the string and with an annihilation process. 210 different candidates of Pentaquarks are analyzed. Again we write down the threshold for decay, this time to a baryon and a meson, draw the HMRTs and compute the two different decay widths.

Our procedure of determining the HMRTs of all the tetraquark candidates was based relating the spectra and the various decay channels. One assumption that we made was that the first tetraquark state that can decay into a baryon and an anti-baryon is of a mass which is 40-125 MEV higher than the baryonic threshold . This is based on the few cases with such a decay that have been already discovered[10] and [24]. Using this assumption we determined the approximated value of the intercept. We also assumed that in between the threshold of decaying into two mesons and that of a baryon anti-baryon decay two low lying states reside on the trajectory, so that the first state with the later decay is characterized by $J + n = 3$. We determined the full HMRT. For that we used the endpoint masses, the intercept and the slope determined from meson and baryon trajectories with similar endpoint particles. Altogether we determined on each HMRT 5 states. Out of them can decay only into two mesons and in the other three a decay to a baryon and anti-baryon is also possible.

The paper is organized as follows. In section 2 we briefly review the HISH model and the important results that will aid confronting the data. It includes the basic ingredients, the simplest configurations of the different multiquarks, the classical and quantum HISH modified Regge trajectories and decay channels and widths. The following section 3 is dedicated to the general structure of stringy exotics hadrons, In section 4 we discuss the tetraquark structure and

decay mechanisms, as well as the mechanisms through which tetraquarks are created. In section 5 we analyse the pentaquark structure and decays. At last, in section 7 we confront experimental data. We will first present the fitting procedures and phenomenological methodology to be used to analyse the observations and predict further states on the HMRTs. Then we will discuss all possible charm tetraquarks configurations, we will examine the data for those with an observed candidates, and provide predictions for those that do not. We will also confront, for the first time, pentaquark candidates for the few that were observed. We end up with a summary section, a section of open questions and an appendix that includes fitting of the HISH to the meson spectra.

2 Brief review of HISH (holography inspired string hadron) model

The AdS/CFT duality conjecture is an equivalence between bulk string theories and field theories that live on the boundary. Realistic field theories should be non-supersymmetric, non-conformal and confining. The dual string background on the other hand, should admit confining Wilson lines, dual to a boundary with a matter sector that is invariant under a chiral flavor symmetry that is spontaneously broken (an example review paper on how to achieve these requirements [31]).

Unlike most of the applications of the holographic duality, in which hadrons loose their stringy properties due to taking the $\alpha' \rightarrow 0$ limit, the HISH framework preserves these characteristics. In particular, it admits the semi-linear Regge behavior that arise naturally for strings. Moreover, the model is mostly consistent with the data for mesons [7] and baryons [32].

The idea behind the HISH model is to construct a phenomenological unitary string model that is in accordance with as much as possible experimental data of hadron physics and then use it to predict properties and phenomena that have not been measured so far. The model is in flat four dimensions but is based on mapping hadronic string configurations of holographic backgrounds.

The prescription for building and using the model includes the following steps:

- Determining a prototype confining holographic background with flavor branes. A confining holographic background means a background for which the Maldacena-Wilson line admits an area law behavior[33].
- Analyzing in the holographic confining background classical strings, in particular rotating ones, that correspond to hadrons: (i) Mesons- open strings between flavor D branes, (ii) Glueballs- closed strings, (iii) Baryons- systems that include a baryonic vertex (B.V) with two short strings (di-quark) connected to flavor branes attached to it that is connected with a long string to a flavor D brane and (iv) Exotic hadrons- strings between a B.V and an anti- B.V to which a di-quark and an anti-diquark are attached respectively.
- “Mapping” the classical holographic strings, in particular the rotating ones, to strings with massive particles on their ends in four flat dimensions. The endpoint particles “quarks” carry electric and flavor charges but not a color charge and a spin. The B.V is mapped into a string junction that carries a unit baryon number with , a net number $N_c = 3$ of three strings coming out of it and a net number of three strings coming into an anti-string junction of baryon number -1.
- Examining for the stringy baryons the classical stability against classical fluctuations of the Y shape versus the single string configuration between a quark and a B.V with attached diquark.

- Solving the classical equations of motion for rotating string and computing the classical energy and angular momentum of the strings with massive particles on their ends. This constitutes the classical HMRT (HISH modified Regge trajectory)
- Quantizing the fluctuations around the classical stringy hadrons subjected to the boundary conditions associated with the endpoint particles with masses, electric charges, and spins. and to the baryonic vertices. Determining the eigenfrequencies of the fluctuations, namely, the spectrum.
- Renormalizing the world sheet Hamiltonian using a “Cauchy Casimir-like method”. Determining the intercept and the quantum HMRT. This includes the contribution of the Liouville mode associated the fact taht the string resides in d=4 non-critical dimension.
- Confronting the outcome of the model, in particular the HMRTs with experimental spectra examining the fitness of the theoretical model and extracting the best fit values for the string tension(slope), endpoint masses and intercepts from all the hadron (meson and baryon) trajectories. Predicting the masses and quantum numbers of resonances that have yet not been detected.
- Determining the strong decay width of hadrons including (i) Computing the total decay width associated with possible breaking of the parent string into two daughter strings. (ii) Evaluating the probability of a particular pair creation at the breaking point and hence the branching ratios, (iii) Approximating the width associated with annihilation of a b.v and an anti-b.v. Comparing the measured decay width to the corresponding results of the HISH and predicting yet unknown decay widths.

2.1 The HISH mapping

Confining holographic backgrounds are characterized by a “wall” that truncates in one way or another the range of the holographic radial direction. A common feature to all the holographic stringy hadrons is that there is a segment of the string that stretches along a constant radial coordinate in the vicinity of the “wall”, as in figure 1 [11, 34]. For a stringy glueball it is the whole folded closed string that rotates there. For an open string it is part of the string, the horizontal segment, that connects with vertical segments either to the boundary for a Wilson line or to flavor branes for a meson or baryon. This fact that the classical solutions of the flatly rotating strings reside at fixed radial direction is a main rationale behind the map between rotating strings in curved spacetime and rotating strings in flat spacetime described in figure 1. In the HISH picture, the vertical segments are represented as m_{sep} - the endpoint masses of the string in flat spacetime. As mentioned, the HISH approximation improves as the horizontal string becomes longer with respect to its endpoint masses - hence, the higher the excitation, the better the HISH model describes the state.

A key player of the map is the “string endpoint mass”, m_{sep} [34], that provides in the flat space-time description the dual of the string action associated with the vertical string segments. It is important to note that upon extracting this mass from the fits to experimental data, it turns out that this mass is neither the QCD mass parameter (the current quark mass) nor the constituent quark mass. Notice also that the massive endpoint as a map of an exactly vertical segment is an approximation that is more accurate the longer the horizontal string is.

2.2 Massive Strings in Flat Spacetime

The HISH model basic building blocks are:

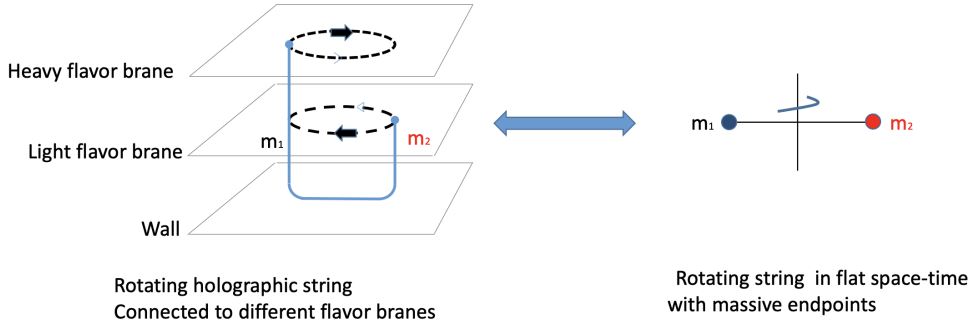


Figure 1: **Left:** Rotating holographic open string. **Right:** The corresponding open string with massive endpoints in flat spacetime. In this case we show a heavy-light meson.

- Open strings, characterized by a slope $\alpha' = \frac{1}{2\pi T}$ (T is the string tension). The string, which rotates in general, possesses mass and angular momentum. In the quantum level, the angular momentum has a contribution from an intercept a , that can be interpreted as a "Casimir force" that prevents the string ground state from collapsing into itself.
- Quarks - massive particles ($m_{u/d}$, m_s , m_c , m_b) that are attached to the ends of open strings. These masses are the parameters of the HISH model from a pure flat spacetime picture. They have been determined in previous works ([7], [11]) by fitting.
- "Baryonic vertex" (BV) - a massive vertex that is connected to an N_c number of strings. Hadronic structures that include BVs connected to one long string and two short strings attached to quarks are called "diquarks". Unlike other models, these are not part of the basic building block of the theory, rather a configuration that is always attached to a BV.
- Closed strings - the closed strings slope is half that of the open string ($\alpha'_{closed} = \frac{1}{2}\alpha'_{open}$). Their angular momentum (hence, the excitation number) of the closed string is always even. Their intercept is also expected to be twice that of an open string.

The total mass of the hadron is determined by its presenting configuration of all of these building blocks.

2.3 Hadron Constructions

Each of the hadron types can be constructed from the above ingredients. There are multiple possible configurations for each type. The simplest constructions of the basic multiquark structures are as follows:

- Meson - a single open string attached to a quark on one end and an antiquark on the other end.



Figure 2: Meson - (a) is a meson with content $u/d\bar{s}$ in the stringy picture. (b) is the mapping of the meson to the HISH picture

- Baryon - Apriori there are several possible configurations for the HISH baryon. However, as will be discussed in subsection (2.8), in nature it takes the form of a single open string attached to a quark on one endpoint and a diquark on the other as depicted in figure (3).

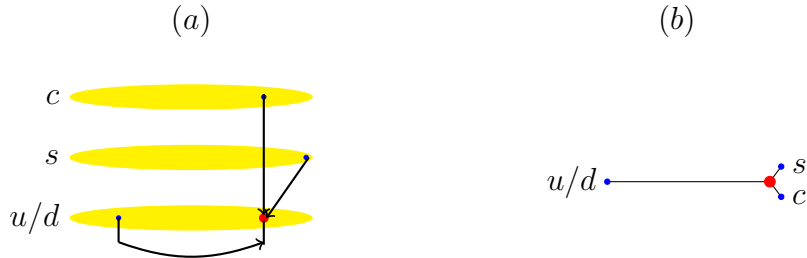


Figure 3: Baryon - (a) is a baryon with content u/dsc in the stringy picture. (b) is the mapping of the baryon to the HISH picture

- Glueball - a single closed string is the simplest configuration for glueballs. A more complex configuration can be achieved using BVs and anti-BVs configurations that creates closed structures (see Fig-8).

Since in this paper we concentrate on exotic hadrons, the configurations for tetraquarks and pentaquarks are analysed in dedicated sections 4, 5.

2.4 Action and equations of motion

The action of the HISH model includes the worldsheet action of an open bosonic string and the action of the endpoint particles. For closed strings obviously the latter is not included. The action reads

$$S = S_{st} + (S_{pm} + S_{pq} + S_{ps})|_{\sigma=0} + (S_{pm} + S_{pq} + S_{ps})|_{\sigma=\ell}. \quad (1)$$

where S_{st} is the string worldsheet action. and $S_{pm} + S_{pq} + S_{ps}$ are the particle action terms associated with the mass, electric charge and spin of the particle¹.

For the action of the string we take the Nambu-Goto action. Viewing the action as an effective action of a long string one can add additional higher order terms[35] and in particular an extrinsic curvature term [36]² However here we use only the Nambu-Goto action given by

$$S_{st} = -T \int d\tau d\sigma \sqrt{-h} = -T \int d\tau d\sigma \sqrt{\dot{X}^2 X'^2 - (\dot{X} \cdot X')^2}. \quad (2)$$

¹In fact the charge generalized to the electroweak one. It is important to note that the endpoint charges do not carry QCD color charges

²This is probably relevant for folded string solutions.

where $h_{\alpha\beta} = \eta_{\mu\nu}\partial_\alpha X^\mu\partial_\beta X^\nu$ is the induced metric on the worldsheet and h is its determinant, the indices α, β being either τ or σ . The target space is d dimensional $\mu, \nu = 0, \dots, d-1$. In this paper we take $d = 4$. The action is defined on the strip: $-\infty < \tau < \infty$ and $-l \leq \sigma \leq \ell$.

The particles located at both endpoints of the string $\sigma = -l$ and $\sigma = \ell$ have an action that is built from three parts. First is a mass term S_{pm} given by

$$S_{pm} = m_i \int d\tau \sqrt{-\dot{X}^2} \quad (3)$$

The second term on the boundary action S_{pq} respectively

$$S_{pq} = T q_i \int d\tau A_\mu(X) \dot{X}^\mu \quad (4)$$

The parameters m_i and q_i are the mass and charge of the endpoint particles. The electromagnetic interaction of the charges follows the usual Maxwell action that has to be added:

$$S \rightarrow S - \frac{1}{4g^2} \int d^4x F_{\mu\nu} F^{\mu\nu} \quad (5)$$

The third term on the boundary, the spin term can be written in a form which is analogous to the string Green Schwarz term as follows

$$S_{ps} = \int d\tau \left[\frac{-i\dot{X}^\mu(\bar{\psi}\gamma_\mu\partial_\tau\psi)}{2\sqrt{-\dot{X}^2}} - m_i \sqrt{-\dot{X}^2}\bar{\psi}\psi \right] \quad (6)$$

The system of an open bosonic string with massive endpoints was considered first in [37] and was addressed afterwards by many authors.

Next come the equations of motion. Since the charges and spins will not play a major role in the analysis of this paper we set them to zero from here on.

Using the two dimensional reparameterization symmetry we fix the orthogonal gauge

$$\dot{X}^2 + X'^2 = \dot{X} \cdot X' = 0. \quad (7)$$

In this gauge the bulk equations of motion read

$$\partial_\sigma^2 X^\mu - \ddot{X}^\mu = 0 \quad (8)$$

and the boundary conditions

$$T X'^\mu + m_1 \partial_\tau \frac{\dot{X}^\mu}{\sqrt{-\dot{X}^2}} = 0 \quad \sigma = -\ell \quad (9)$$

$$T X'^\mu - m_2 \partial_\tau \frac{\dot{X}^\mu}{\sqrt{-\dot{X}^2}} = 0 \quad \sigma = \ell \quad (10)$$

$$\quad . \quad (11)$$

The equations of motion admit several types of solutions: (i) static solutions, (ii) Yo-Yo vibrating solutions and (iii) rotating solutions. Classically, in the static case the string collapses to zero size. This will not be the case in the full quantum picture. The vibrating solution was studied in [38]. Since it does not play an important role for the spectra, we will not consider it here.

2.5 Classical Regge trajectories

The rotating solution takes the following form configuration

$$X^0 = \tau, X^1 = R(\sigma) \cos(\omega\tau), X^2 = R(\sigma) \sin(\omega\tau) \quad (12)$$

for any choice of $R(\sigma)$.

The energy and angular momentum associated with this solution for an open string with masses m_1 and m_2 on its endpoints constitute the classical trajectories referred to as HMRT (his modified Regge trajectory).

$$E = \sum_{i=1,2} m_i \left(\frac{\beta_i \arcsin \beta_i + \sqrt{1 - \beta_i}}{1 - \beta_i^2} \right) \quad (13)$$

$$J = \sum_{i=1,2} \pi \alpha' m_i^2 \frac{\beta_i^2}{(1 - \beta_i^2)^2} \left(\arcsin \beta_i + \beta_i \sqrt{1 - \beta_i} \right) \quad (14)$$

where $\beta_i = \omega l_i$ is the velocity of the i -th endpoint and l_i is the length of the i -th string segment from the center of mass.

The velocities are related by the boundary condition:

$$\frac{T}{\omega} = m_1 \frac{\beta_1}{1 - \beta_1^2} = m_2 \frac{\beta_2}{1 - \beta_2^2} \quad (15)$$

By taking the relativistic limit ($\beta_i \rightarrow 1$) where $m \ll E$:

$$J = \alpha' E^2 \times \left(1 - \sum_{i=1}^2 \left(\frac{4\sqrt{\pi}}{3} \left(\frac{m_i}{E} \right)^{3/2} + \frac{2\sqrt{\pi^3}}{10\sqrt{2}} \left(\frac{m_i}{E} \right)^{5/2} + \dots \right) \right) \quad (16)$$

where in the limit $m_i \rightarrow 0$ the linear Regge trajectory is recovered:

$$J = \alpha' E^2 \quad (17)$$

The high mass limit ($\beta_i \rightarrow 0$) where
 $\Delta E \equiv E - m_1 - m_2 / (m_1 + m_2) \ll 1$:

$$J = \frac{4\pi}{3\sqrt{3}} \alpha' \sqrt{\frac{m_1 m_2}{m_1 + m_2}} (\Delta E)^{3/2} + \frac{7\sqrt{2}\pi}{27\sqrt{3}} \alpha' \frac{m_1^2 - m_1 m_2 + m_2^2}{m_1 m_2 \sqrt{(m_1 + m_2)^3}} (\Delta E)^{5/2} + \dots \quad (18)$$

2.6 The quantum static string

The mass of a static string with massive endpoints is the sum of the masses of the endpoints and the energy of the string, namely

$$M = m_1 + m_2 + TL \quad (19)$$

Classically, unless the endpoints are nailed, the static string collapses to zero length since the force on the massive endpoints due to the tension is not balanced. In classical rotating strings the as was discussed above the centrifugal force is balancing the tension. Quantum mechanically a static string may have a non-vanishing length if the Casimir force acting on the endpoint particles is repulsive opposing the tension. The Casimir force is related to the intercept in the following form

$$F_C = -2\pi \frac{a}{L^2} \quad (20)$$

If $a > 0$, as it is in the ordinary bosonic string, the force is attractive and it will add up to the tension and would not balance it. However, if $a < 0$ we have a repulsive force. The equilibrium length of the string in that case is

$$L = \sqrt{\frac{2\pi|a|}{T}}, \quad (21)$$

and hence the total mass associated with the ground state of the static string is given by

$$M = m_1 + m_2 + \sqrt{\frac{|a|}{\alpha'}} \quad (22)$$

For the n excited state the relation between the mass and n is given by

$$n = \alpha'(M - (m_1 + m_2))^2 + a \quad (23)$$

2.7 Quantum Regge trajectories

In the quantum string the classical rotating configuration is dressed by quantum fluctuations. In $d=4$ there are fluctuations along one transverse and one planar directions. The eigenfrequencies w_n of fluctuations when the endpoints carry the same mass m are solutions of the transcendental equation

$$\tan(w_n L) = \frac{2mTw_n}{m^2w_n^2 - T^2} \quad (24)$$

The worldsheet hamiltonian associated with these fluctuations is characterized by the intercept.

$$a = -\frac{1}{w} \langle H_{ws} \rangle \quad (25)$$

The computation of the $\langle H_{ws} \rangle$ requires a renormalization which we perform using a “Cauchy-Casimir like” procedure[12] The intercept gets a contribution also from the Polchinski-Strominger term [39]. For the simplified case of two identical masses m the intercept, which are small, namely, $\frac{2m}{TL} \ll 1$ the intercept can be expanded in the form

$$a = a_t + a_p + a_{PS} \sim 1 - \frac{11}{6\pi} \left[\frac{2m}{TL} \right]^{1/2} + \frac{143}{240\pi} + \left[\frac{2m}{TL} \right]^{3/2} \quad (26)$$

The classical HMRT trajectory turns into a quantum one by

$$J_{cl} = \alpha'E_{cl}^2 \rightarrow J + w_n = \alpha'E^2 + a \sim J + n = \alpha'E^2 + a \quad (27)$$

Since the eigenfrequencies w_n are close in value to n we will use in what follows the latter expression.

As was discussed above for the static string, the existence of the intercept implies a non-vanishing Casimir force, repulsive for $a < 0$ and attractive for $a > 0$. The Casimir force modified the classical balancing between the tension and the centrifugal force. Quantum mechanically it reads

$$\frac{T}{\gamma_i} = \frac{\gamma_i m_i \beta_i^2}{l_i} - \frac{2\pi a}{L^2} \quad (28)$$

From relating the angular velocities:

$$\frac{\beta_1}{l_1} = \frac{\beta_2}{l_2} \rightarrow l_2 = \frac{\beta_2}{\beta_1} l_1 \quad (29)$$

The solution for l_1

$$l_1 = \frac{\gamma_1}{2T} \left(\gamma_1 m_1 \beta_1^2 + \sqrt{(\gamma_1 m_1 \beta_1^2)^2 - \frac{8\pi a T}{\gamma_1 (1 + \beta_2/\beta_1)}} \right) \quad (30)$$

To obtain β_2 numerically:

$$\frac{T}{\gamma_2} = \frac{\gamma_2 m_2 \beta_1 \beta_2}{l_1} - \frac{2a}{l_1^2 (1 + \beta_2/\beta_1)^2} \quad (31)$$

From here we can estimate L using the expression for l_1 and (29).

2.7.1 Repulsive Casimir force

Ground state hadrons, mesons and baryons have zero orbital angular momentum. As was mentioned in (2.6) these states do not collapse and have non-vanishing length only provided that there is a repulsive Casimir force that balances the string tension. A repulsive Casimir force means a negative intercept. Two questions immediately raise: (i) Is indeed the observed experimental intercept always negative? (ii) Can we write down a theoretical string theory that admits a negative intercept. As for the experimental picture, the Casimir force is in fact not related to the intercept a but rather to the following modified intercept

$$\tilde{a} = a - S \quad (32)$$

where S is the spin (not the total angular momentum J) of the hadron. This follows from the fact that a is extracted from the relation between the hadron mass M and J , but what is relevant for the Casimir force is the relation between M and L_{oam} the orbital angular momentum. For a string with no massive endpoints

$$J = L_{oam} + S = \alpha' M^2 + a \rightarrow \quad L_{oam} = \alpha' M^2 + a - S = \alpha' M^2 + \tilde{a} \quad (33)$$

A similar situation occurs for a string with massive endpoints. In [40] the values of \tilde{a} were extracted for all the hadronic trajectories and indeed it was found that

$$\tilde{a}_{obs} < 0 \quad (34)$$

As for the theoretical picture, the situation has not yet been fully clarified. It is well known that for the ordinary critical open bosonic string $\tilde{a} = 1$. In fact, as was firstly derived in [41], and proved in a different way in [12], $\tilde{a} = 1$ also for any non-critical string at $d \neq 26$ dimensions upon incorporating the Liouville mode. For strings with massive endpoints the intercept \tilde{a} depends on the endpoints masses. When the latter are equal it is always positive but in an asymmetric setup, in particular when one side is massive and the other is massless, \tilde{a} can be negative [12]. However, this of course cannot explain the situation for strings with the same endpoints as is the case for flavorless hadrons. Adding electric charges to the endpoints also modifies the value of the intercept \tilde{a} but cannot make it negative [22]. Spins at the endpoints probably affect the intercept but that has not yet been determined. An option to get negative intercepts is to involve also fermionic strings. It is well known that for a Ramond boundary condition a transverse mode contributes $-1/24$ to the intercept. The problem with this possibility is that it affects the statistics of the hadron and so it can be relevant only for baryonic hadronic strings.

2.8 Baryonic structures

What is a baryon in holography? Since an end of a string connected to a flavor brane is a ‘‘quark’’, a baryon has to be built from N_c strings. It turns out [42] that to a D_p brane that wraps a non-trivial p cycle with a flux of an RR field of value N_c , there must be N_c strings attached to it. Thus, such a structure in holography provides the baryonic vertex (BV). Correspondingly a baryon in a confining holographic background is a system that includes a BV and N_c strings connecting it to various flavor branes. This idea was first implemented in a confining background in [43]. A priori there could be different metastable configurations of the BV and the N_c strings. The location of the BV in the holographic direction, and whole structure is determined minimizing the energy of the system [44].

In HISH map described in figure (3), for $N_c = 3$ in four flat space-time the baryon can have Y shape structure or it can be a single string connected on one end to a quark and on the other end to a BV and a diquark. These configurations are two out of the four possible ones that connect three quarks. They are depicted in figure (4).

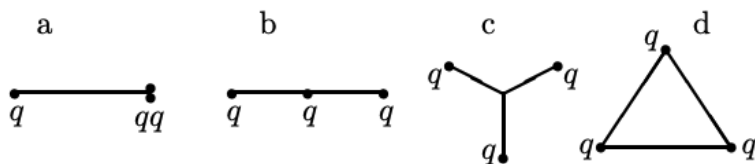


Figure 4: Baryonic configurations - (a) the quark-diquark model, (b) the linear structure, (c) the Y configuration and (d) the triangle.

The different possible structures have been analysed in [45], [46], [47] and [48]. The conclusions were that the quark-diquark and delta structure are stable, whereas the Y model is unstable and with a small perturbation would collapse to the linear configuration ($q-q-q$) [45]. The linear configuration was analysed in [49] and was found to be unstable as well, but its periodic behavior prevent it from collapsing to the quark-diaquark structure as was initially expected.

In the HISH picture, the delta and linear structure is not possible for baryons, since the model restricts BVs and anti-BVs connections to N_c , whereas quarks are not connected with more than one string.

The Y structure instability was deduced by assuming that all the quarks are identical. For baryons with quarks of different masses the analysis has to be repeated and a priori it is not obvious they are also unstable. However, there is another argument in favor of the single string configuration. Had a symmetric Y-shape string been stable, the baryon trajectory slope α_B should have been $\alpha_B = (2/3)\alpha_m$, where α_m is that of a meson. However, as was shown in [32], the slope of the baryonic trajectory is within 5% the same as that of a meson trajectory. This fact, that the slopes of baryons and mesons with similar endpoint masses, exclude the non-single string configurations also for non-symmetric baryons, namely with different quark masses.

2.9 The decay width of stringy hadrons

The decays of stringy hadrons can involve (i) breaking up of a string, (ii) annihilation of endpoint particles, (iii) annihilation of a BV and an anti-BV and (iv) electroweak decay of endpoint particles. For this paper only the first and third mechanisms will be relevant. We briefly summarize in this section both mechanisms according to the analysis done in [13] and [30].

2.9.1 Hadronic decay through string breaking

An open string of Type I string theory can break apart at any point along the string. However, in holographic backgrounds which are based on Type II string theory strings cannot break in thin air, namely, where the created endpoints are in the bulk but rather only when the later are on flavor branes. This can occur due to quantum fluctuations. This process is demonstrated in figure (5), where fluctuations of a meson built from one heavy and one light endpoints reach a medium flavor brane.

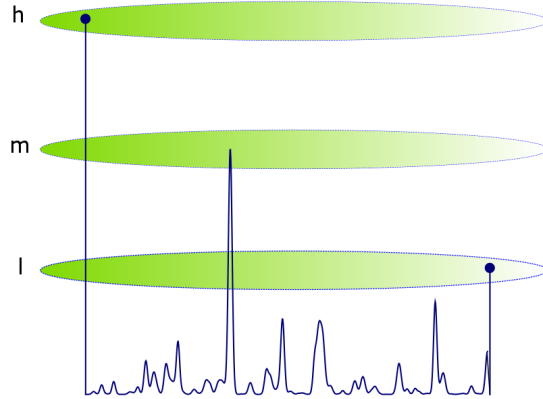


Figure 5: Quantum fluctuations of the horizontal segment of a heavy-light meson reach the medium flavor brane.

In fact as shown in figure (6) there are more than one possibility for the decay of such a holographic meson.

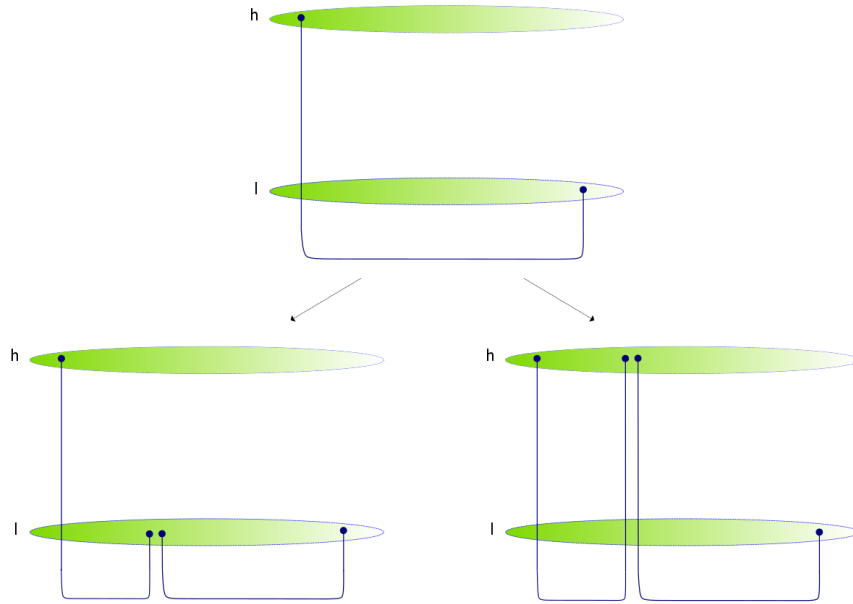


Figure 6: Possible decays of a heavy-light meson via light or heavy quark pair creation. The ratio between the two channels will include an exponential suppression term of the form $e^{-C(m_h^2 - m_l^2)/T}$.

Quantum fluctuations can reach the light or heavier flavor branes. Of course, there are also kinematical constraints on whether or not a hadron can decay in a channel where heavier

quarks are created. A calculation of the probability of the fluctuations of the horizontal segment of a hadronic string to reach a flavor brane was first performed in [14]. The result was found to be

$$\mathcal{P} = \text{Exp}\left[-2\pi C \frac{m_q^2}{T}\right] \quad (35)$$

where m_q is the mass of the quark created at the breaking point and C is a dimensionless coefficient of order 1 discussed in [13].

Once this probability is taken into account, one can compute the width of the breaking mechanism as if it is an Type I open string. Moreover, since the profile of the holographic string is of a flat horizontal string that stretches along a "wall" with additional vertical segments we can consider it as a breaking of a string with massive endpoints in flat space-time. The decay width of a Type I open string in flat space-time with no massive endpoints, described in figure (7), was computed in [50]and[51]. This is done using the optical theorem by computing the

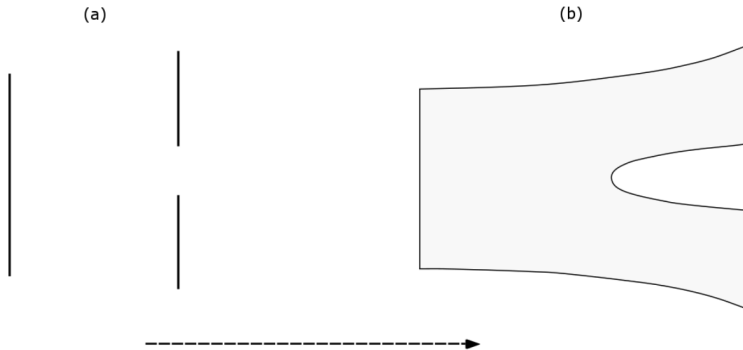


Figure 7: An open string breaks into two open strings. (a) Snapshots of before and after the split. (b) The worldsheet diagram of the split. The arrow represents the time direction.

imaginary part of the string self energy diagram. In [50] the corresponding loop diagram was mapped into a disk tree level diagram. The final result for the total decay width for long strings takes the form

$$\Gamma = \frac{\pi}{2} ATL(M, m_1, m_2, T) \quad (36)$$

namely, it admits a linear dependence on the string length L , as expected since the string can break at any point. The constant A is dimensionless, and proportional to the square of the string coupling .It is equal to the asymptotic ratio of $\frac{\Gamma}{L}$ for large L . It supposed to be universal for the decay of all stringy hadrons.

The partial width to decay via a particular breaking channel i with a pair with a mass m_{sep} and with the probability given in (35) takes the form

$$\frac{\Gamma_i}{\Gamma} = \Phi_i \text{Exp}\left[-2\pi C \frac{m_q^2}{T}\right] \quad (37)$$

where Φ_i is the phase space

$$\Phi(M, M_1, M_2) \equiv 2 \frac{|p_f|}{M} = \sqrt{\left(1 - \left(\frac{M_1 + M_2}{M}\right)^2\right) \left(1 - \left(\frac{M_1 - M_2}{M}\right)^2\right)}. \quad (38)$$

and where M is the mass of the parent hadron and M_1 and M_2 are the masses of the two daughter hadrons. The branching ratio formula is the HISH analog of the CNN formula of breaking of QCD flux tube [52].

2.9.2 Hadronic decay via annihilation

As was mentioned above, in addition to decaying by string break up, a stringy hadron can decay also by annihilation either of the string endpoints or of a BV and an anti-BV. The former is relevant for flavorless mesons like quarkonia, which in the holographic picture means that the two endpoints are on the same flavor brane. The latter is relevant, as will be discussed in section (4.3), for the decay of tetraquarks when breaking is energetically not allowed.

In [13] the probability of the annihilation process was estimated to be

$$\mathcal{P}_{anh} \sim \sqrt{\frac{\pi}{2T_{av}}} e^{-T_{av}L^2/2} = \sqrt{\frac{\pi}{2T_{av}}} e^{\frac{-4(M-(m_1+m_2))^2}{9T_{av}}} \quad (39)$$

In the last expression we assumed that the string is not rotating. For the decay of quarkonia T_{av} is the tension averaged over the holographic direction from the wall to the location of the flavor brane. For the annihilation of a BV anti-BV pair it is the ordinary tension, namely that at the vicinity of the wall. As discussed in [13] the result of the annihilation of the endpoint quarks in the quarkonia case is a glueball that decay via breaking into two mesons.

3 Exotic hadrons

The toolkit for constructing exotic stringy hadronic configurations includes the following building blocks: (i) Strings which can be closed or open. In this note we discuss only the latter ones. (ii) “Quarks”, which are massive particles carrying electric and flavor charges (but not color ones) and spins, located at the endpoints of open strings. (iii) BV’s and anti-BV’s. These string junctions can in general be connected to three strings in a Y shape form, or to a diquark, namely two short strings with a quark on their ends, and a regular string with a quark on its end or a tri-quark. Based on the baryonic configurations found in nature, one may anticipate that also for exotic hadrons only the second option exists. Never the less we check the two options for each exotic hadron separately.

With these building blocks a variety of configurations can be constructed.

- In general if the number of BV’s is the same as the number of anti-BV’s namely, $n_{BV} = n_{\bar{BV}}$ the configuration has the same number of external quarks and anti-quarks and hence it is non-baryonic. There are two types of such configurations:
- Configurations with no quarks involved, namely generalizations of glueballs. Note that the basic glue ball is a simple closed string but, as is described in figure (8), there are also “glueballs” built from open strings. It is interesting to note that whereas the ordinary glueball that corresponds to a closed string has a tension that is twice the meson tension since for rotating strings it is a folded string [9], the glue ball depicted in (a) has a tension, that is three times, and in general N_c times that of an ordinary meson tension. Thus, the mass of these objects will be linear in N_c and hence claims of a similarity between $N_c = 3$ and large N_c are wrong for these states.
- Configurations that do include quarks at the ends of strings and hence are generalizations of mesons. Examples for such exotic hadrons are *tetraquarks* and *hexaquarks* etc.
- If on one the other hand $n_{BV} = n_{\bar{BV}} + 1$ then $n_q - n_{\bar{q}} = 3$ and the configuration carries baryon number $B = 1$. The simplest objects in this class are of course the baryons which have more complicated cousins in the form of *pentaquarks* and *septaquarks* etc.

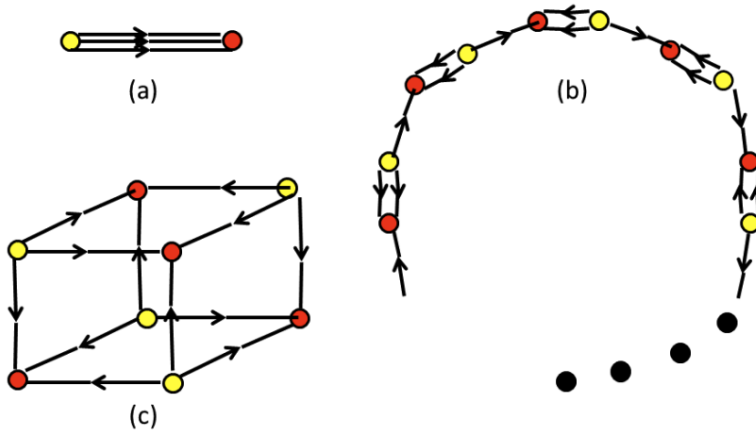


Figure 8: Gluballs - different configurations of BVs and anti-BVs. (a) Three strings connecting one BV and one anti-BV. (b) A planar polygon. (c) A cube.

- In a similar manner one can also construct objects with $n_{BV} > n_{\bar{BV}} + 1$ which are multi-baryon states. There is a whole zoo of stringy multibaryons. It is easy to draw the corresponding figures. For example, figure(9) describes a di-baryon build from 3 BV's and one anti-BV. When the endpoint di-quarks contain two u, d and s the stringy configuration corresponds to the sexaquark[23]. In analogy to the collapse of the Y shape in the case of a baryon, one may expect also here a configuration with parallel double strings with 3 quarks on their ends. In this note we will not discuss these multi-baryon states.
- In the introduction we made a distinction between genuine exotic hadrons that can be described by a connected string diagram and molecules that take the form of disconnected diagram. One can further classify the genuine exotic hadrons into two classes. The first will be referred as *not obviously genuine exotic hadrons*. In this case their decay products can also be the products of the decays of mesons and baryons. More specifically, two daughter mesons from a parent tetraquark that can be produced also by a decay of a meson, and a baryon and a meson that can be the result of a decay of a baryon. When the decay products cannot be a result of a decay of a meson, for tetraquarks, and a decay of a baryon for pentaquarks, these will be referred as *obvious genuine exotic hadrons* or for short *genuine exotic hadrons*. Genuine tetraquarks can carry electric charges of +2 or -2 which clearly cannot be carried by a meson. Similarly genuine pentaquarks can carry charge of +3. This will be further elaborated in section (7.4). In the following sections will discuss both types of tetraquarks and pentaquarks.
- Another type of configurations to consider are exotic hadrons that decay through channels containing mesons that are a superposition of quark-antiquark compositions. These "mixed" products should be translated to mixed exotic hadrons that are also a superposition of a few configurations, such as $u\bar{u}d\bar{d}$ and $u\bar{d}d\bar{d}$, which is expected to decay to a product that includes for example π^0 . The HISH picture does not deal directly with these mixture, but when confronting experimental data, we expect the only affect of it to be on the value of the endpoint masses for light quarks (u, d and s). This means the results are not affected significantly when only u and d are involved, since u and d are not separated when we fit $m_{u/d}$. We will elaborate more on how we treated these cases in the results section.

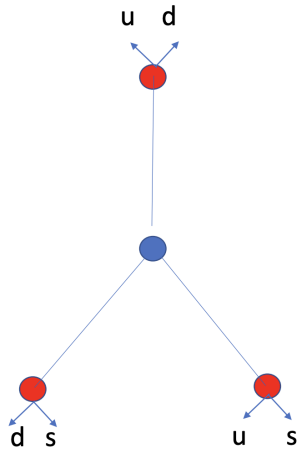


Figure 9: Sexaquark configuraiton. BV is denoted by red blobb and anti-BV by a blue one.

4 Tetraquarks

The simplest construction of a tetraquark is a single open string attached to a BV connected to a diquark on one endpoint and an anti BV connected to an antidiquark at the other (10) . As discussed above in (2.8) the stringy baryon can be in principle in a Y shape or in a shape of a single string with a di-quark and a quark on both ends. . In a similar manner the stringy tetraquark can be a single string or in the shape built from 5 strings as described in figure (10).

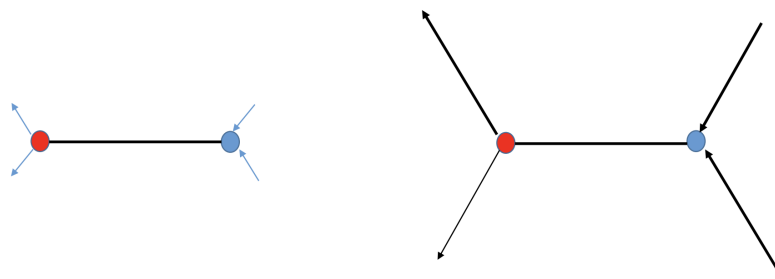


Figure 10: On the left a tetraquark built from a single string connecting a BV and an anti-BV. Adi-quark is attached to the BV and an anti-diquark to the anti-BV. On the right a 5 strings configuration with one string connecting the BV and the anti-BV

For the baryon the main reasons to adopt the single string picture were the theoretical stability of the configuration} and [47] and [46] and more importantly the fact that the slope of the baryonic trajectories is very close to that of mesons with similar endpoints. We will adopt the same criterion also for the tetraquarks for determining the preferred structure. It should be emphasized though that unlike for the baryons, for the tetraquarks there have not been yet determined trajectories from which we would be able to examine the relations between their corresponding α' and that of the mesons.

In fig-11 an example of a $c\bar{c}c\bar{s}$ is depicted both in the holographic setup (a) and in the HISH one (b). In fact the tetraquark may have an even more complex configuration as the one in Fig-12. We will assume here that it does not correspond to the low lying tetraquarks.

Following [10] we refer to this configuration as the *V-baryonium*. We consider here mainly charmed tetraquarks which include at least one charmed (or anti-charmed) quark and all the way to a $c\bar{c}c\bar{c}$ states. All together there are 125 different charmed tetraquarks including 40 with a single charmed quark and 40 with one anti-charmed quark, 10 with two charmed quarks and 10 with two anti-charmed quarks, 16 with $c\bar{c}$, 4 with $cc\bar{c}$, 4 with $\bar{c}\bar{c}c$ and one $cc\bar{c}\bar{c}$ state. The list of charmed tetraquarks includes 5 symmetric states which have the form $q_1\bar{q}_1q_2,\bar{q}_2$. These state are obviously charge-less and with no flavor charge. There are 44 semi-symmetric states of the form $q_1\bar{q}_1q_2\bar{q}_3$ which are *not obviously genuine tetraquarks* and 60 asymmetric states of the form $q_1\bar{q}_2q_3\bar{q}_4$ which are *genuine tetraquarks* carrying flavor charges that cannot be carried by mesons and have electric charge $-2, -1, 0, 1, 2$.

The *V-baryonium* tetraquarks are characterized by the following properties:

- Since the *V-baryonium* is basically a string, then like all other stringy hadrons it must have trajectories of higher excited states, one trajectory of states with higher angular momentum, and one of higher radial excitation number. Here again we refer to such a trajectory as a HISH modified Regge trajectory (HMRT) [53]. Since the mesons, baryons, and *V-baryonium* tetraquarks can all be seen as a single string with massive particles on its end, the function describing the trajectories is the same for the different types of hadrons. The differences between all of them are the masses on the endpoints, the intercepts and whether there is a BV or a pair of BV and anti-BV at the endpoints.
- The ground state which has vanishing angular momentum has a mass given by

$$M_T = M_{diquark_L} + M_{BV_L} + M_{diquark_R} + M_{BV_R} + \sqrt{\frac{|a_T|}{\alpha'}} \quad (40)$$

where $M_{diquark_L}$, $M_{diquark_R}$, M_{BV_L} and M_{BV_R} are the masses of the left and right di-quarks and BVs respectively.

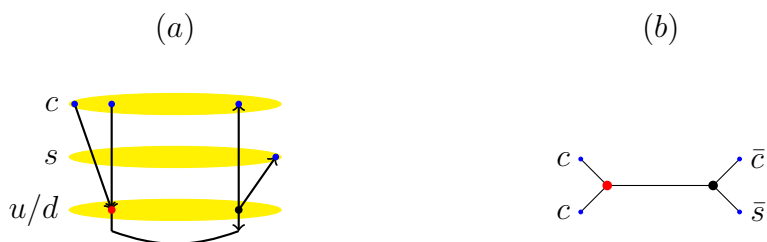


Figure 11: Tetraquark - (a) is a tetraquark with content $c\bar{c}c\bar{s}$ in the stringy picture. (b) is the mapping of the tetraquark to the HISH picture. The red and black vertices represents BV and anti-BV respectively.



Figure 12: (a) is an example of a holographic tetraquark built with two baryonic and two anti-baryonic vertices. (b) is the HISH mapping of this tetraquark structure.

In holography for the case that the single string is preferred over the Y shapes, two out of the three strings that connect to a BV are spanned only along the holographic direction and not along the ordinary space direction. To be more precise their span along the latter direction is much shorter than the string that connects the BV and anti-BV. Thus the endpoints in this picture are now composed from the BV (or anti-BV) contribution with the addition of the diquark contribution neglecting the contribution of the short strings. Since the structure of the tetraquarks resembles that of the mesons, we expect the tetraquark α' to resemble that of mesons with similar quark content (e.g $T_{c\bar{c}u\bar{u}}$ should have similar α' to ψ).

The location of the BV along the holographic direction is determined by the requirement of minimal energy. In figure (11) it is placed on the light-quark flavor brane but it could also reside on the “wall” or on the other flavor branes and in fact even between them. The location of the BV was discussed in details in [44]. Here we briefly summarize the issue. The total energy of the system is the sum of the energy of the baryonic vertex, which is a function of its location, and the energy associated with the strings that connect it to the flavor branes.

$$E_{sys} = E_{BV}(u_{BV}) + \sum_{i=1}^2 \int_{u_{BV}}^{u_{f_i}} T(u) du \quad (41)$$

where u_{BV} and u_{f_i} are the locations of the BV and the i^{th} flavor brane respectively. $E_{BV}(u)$ is the energy of the BV wrapped brane. It is a function of the location u but this dependence is not universal and varies in the different holographic models. $T(u)$ is the tension. Its dependence on u is also model dependent. From previous fits to mesons and baryons[53] we will assume in this paper that the BV is located on the wall so that

$$E_{sys} = M_{BV} + M_{diquark} = M_{BV} + \sum_{i=1}^2 m_{q_i} \quad (42)$$

where m_{q_i} are the holographic masses of the two quarks that built the di-quark. This means that we simply assume that the mass of the di-quark is the sum of the masses of its two quarks.

4.1 The spin structure of tetraquarks

It is well known that mesons with a give quark anti-quark content appear with two possible spins. There are (pseudo) scalar mesons of spin $s = 0$ and vector mesons of spin $s = 1$. Correspondingly there are separate HMRT associated with the former and later spins. For instance there are different trajectories for K and K^* of strange mesons with spin zero and one respectively, for D and D^* , B and B^* and so on. It was found out in [53] that the trajectories associated with the pseudo scalar and vector trajectories are different.

In a similar manner baryons can have for their ground states (with zero orbital angular momentum) spin 1/2 and spin 3/2 for instance the nucleons and the deltas. Again here as well, there are different trajectories associated with the different spins with different intercepts.

The HISH tetraquarks are described by a string that has a di-quark and an anti di-quark on its ends. Thus, the spin of each end can be either 0 or 1 and the total spin of the system can take the values of 0, 1 and 2. Given a tetraquark T of spin zero there are also a spin one tetraquark that we denote by T^* and a tetraquark of spin 2 T^{**} . We want to emphasize that we discuss here the spin and not the total angular momentum. Naturally, we anticipate that there are separate HMRTs for the three different spins with different corresponding intercepts. It is obvious from (40) that the mass difference between M_{T^*} and M_T and similarly with $M_{T^{**}}$

$$M_{T^*} - M_T = \sqrt{\frac{|a_{T^*}|}{\alpha'}} - \sqrt{\frac{|a_T|}{\alpha'}} \quad (43)$$

4.2 Tetraquark Creation

In this section we will heuristically describe the mechanism through which mesons may decay into tetraquarks in the HISH picture. In particular we will state the process for the formation of the X(3350) through B meson decay (in which this state was discovered), as well as the possible mechanisms in which baryon-antibaryon pairs are created from a meson. However, quantifying the decay width in these types of processes will require further research.

As mentioned above, the search for tetraquarks that would comply with the HISH model mainly includes searches for resonances that decay predominantly to baryon-antibaryon pairs and are above the mass threshold for this type of decay. This is since in the HISH model the string breaking is the main mechanism through which excited hadrons can decay, assuming they are above the mass threshold. While these are rare to find in the PDG data, there are quite a few baryonic decays that might be explained by an intermediate tetraquark state.

4.2.1 Excited Meson Decay

Since a tetraquark contains a BV and an anti-BV, in the simplest decay, the meson has to go through a 1 loop BV-anti-BV diagram where one of the strings connecting the loop would break (13).

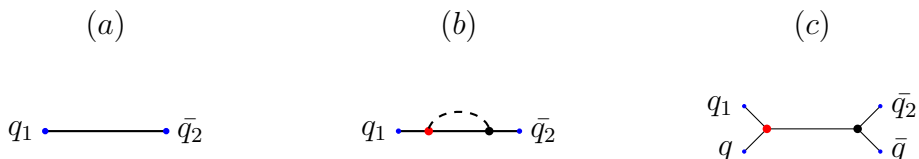


Figure 13: the decay process of an excited meson to a tetraquark in the HISH picture (from (a) to (c)). A BV-anti BV pair loop is created, and one of the strings breaks with a pair of light quark-antiquark (u, d and s with lower probability).

Since the meson transformation to tetraquark includes energy conversion to the tetraquark mass, the meson has to be excited. For the specific decay $B \rightarrow (\Lambda_c^+ \bar{p})_s \pi$ we expect the B meson to first go through a weak decay where two mesons would form, then one of the remaining mesons (the excited one) would go through a decay to a tetraquark, see fig-(13).

The total probability to that type of decay is expected to be:

$$P_{tetra} = V_{bc} * V_{ud}^* * P_{BV-anti-BV} * P_{tear} \quad (44)$$

Where V_{bc} and V_{ud}^* are the CKM matrix elements and P_{tear} is described at 2.9.1. In future work, we will try to estimate $P_{BV-anti-BV}$ (the probability for the creation of a BV-antiBV vertices) by analysing the baryonic decays of the B mesons.

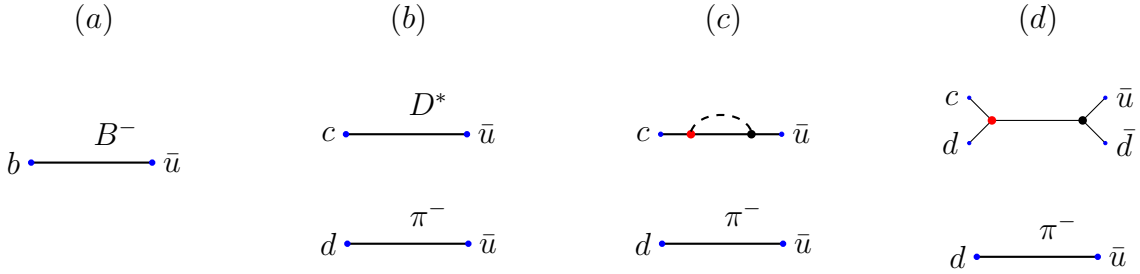


Figure 14: The decay process of a B meson to a tetraquark in the HISH picture. First a D^* meson is created and π^- through a weak decay of the b quark to $c\bar{u}d$. Then the D^* decays to a tetraquark through the process described in 13.

4.2.2 Mesons Decay Through Scattering

Another option for the formation of a BV-anti-BN vertex is through meson-meson scattering. In this process we need to calculate the S-Matrix element of a two mesons as the $|in>$ state, and a tetraquark as the $<out|$ state. The diagrams of the process are in Fig-(15). The details of this process were worked out in [54].

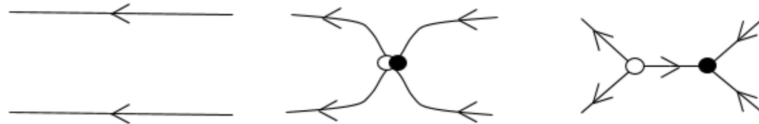


Figure 15: A scattering of two mesons to a tetraquark.

For the specific case that we are reviewing, the process diagrams would look as in (16).

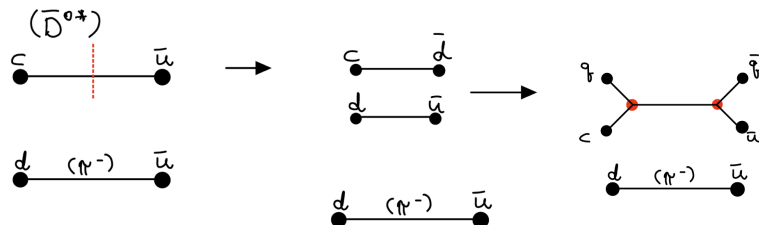


Figure 16: The decay of a B meson to a meson and a tetraquark through meson pair scattering (left to right). The B meson first decays to D^{*0} and $-$ through weak decay of the b quark. Then the excited D^{*0} decay again to π^- and D^+ . The latter then scatter to a tetraquark.

4.3 Decay mechanisms of tetraquarks

Is it possible that a tetraquark state is stable against strong decays? For a tetraquark to be stable all its possible channels of decay should be forbidden. Above in sections 2.9.1 and 2.9.2 the mechanisms of string breaking and annihilation of a BV and an anti-BV were analyzed. Assuming that these are the only possible decays, stability of a tetraquark can occur only provided that its mass is smaller than the masses of the decay products. For the annihilation process the condition of stability takes the form

$$M_T - (M_{m_a} + M_{m_b}) < 0 \quad (45)$$

where the two mesons m_a and m_b are the mesons strings that result from the annihilation which can be either with endpoints $(q_L^1 \bar{q}_R^1)$ and $((q_L^2 \bar{q}_R^2)$ or $(q_L^1 \bar{q}_R^2)$ and $((q_L^2 \bar{q}_R^1)$. Using (40) for the mass

of the tetraquark and (2.6) for the mass of a meson we get

$$M_T - (M_{m_a} + M_{m_b}) = M_{BV_L} + M_{BV_R} \sqrt{\frac{|a_T|}{\alpha'_T}} - \sqrt{\frac{|a_{m_a}|}{\alpha'_{m_a}}} - \sqrt{\frac{|a_{m_b}|}{\alpha'_{m_b}}} \quad (46)$$

where M_{BV_L} and M_{BV_R} are the masses of the BV and anti-BV respectively and (a_T, a_{m_a}, a_{m_b}) and $(\alpha'_T, \alpha'_{m_a}, \alpha'_{m_b})$ are the intercepts and slopes associated with a tetraquark, and the two mesons respectively. Note that the masses of the quarks cancel out in this expression. In fact, we can partially relate this difference to measured quantities. Using a baryon that includes a di-quark identical to the one in the tetraquark and a third quark denoted by \tilde{q}_L and similarly for an anti-baryon on the right we find

$$M_T - (M_{m_a} + M_{m_b}) = +\sqrt{\frac{|a_T|}{\alpha'_T}} - (\sqrt{\frac{|a_{B_L}|}{\alpha'_{B_L}}} + \sqrt{\frac{|a_{B_R}|}{\alpha'_{B_R}}}) + (M_{B_L} + M_{B_R}) - (m_{\tilde{q}_L} + m_{\tilde{q}_R}) - (M_{m_a} + M_{m_b}) \quad (47)$$

We can use in principle this relation to check the stability and also in case that the tetraquark is unstable to strong disintegration and to predict its ground state mass. However, for that we will need reliable information about the various intercepts that will be acquired when more tetraquarks are identified. We demonstrate the decay via annihilation for the case of a tetraquark candidate with content of $(cc\bar{c}\bar{s})$ in figure (17). On the left is the holographic outcome and on the right the outcome in the HISH model.

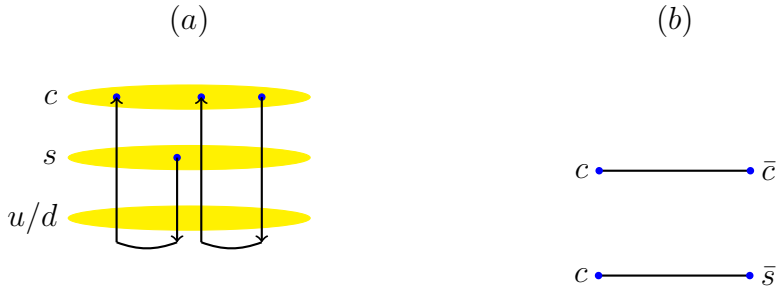


Figure 17: Tetraquark annihilation - (a) is a demonstration of the outcome of a tetraquark BV-antiBV annihilation with content $c\bar{c}c\bar{s}$ in the stringy picture, which results in two mesons. (b) is the mapping of the mesons to the HISH picture.

As was explained in (2.9.1) the most natural decay of a stringy hadron is a breakup of the string. This applies also to the string of the *V-baryonium* tetraquark. However, often the mass of the parent tetraquark is below the threshold for a string breakup. Obviously the condition for a breakup is

$$M_T > M_{B_L} + M_{B_R} \quad (48)$$

where M_{B_L} is the mass of the baryon produced at the left of the string and M_{B_R} is the mass of the anti-baryon at the right of the string. The total decay width of a tetra quark to any possible pair of a baryon and an anti-baryon is given in (36) and the partial decay width into a particular channel is given by (37). The process of a decay via a breakup is drawn in figure (18) for the case of a tetraquark candidate (s, s, \bar{s}, \bar{s}) decaying into Ξ^0 and $\bar{\Xi}^0$

In the breaking mechanism, the content of the di-quark and anti-di-quark of the original tetraquark is the same as the that of the outcome baryon and anti-baryon. There are however, decays of tetraquarks to a baryon anti-baryon pair with quarks which are lighter than the ones of the exotic hadron. There are several decay processes that can yield such a situation:

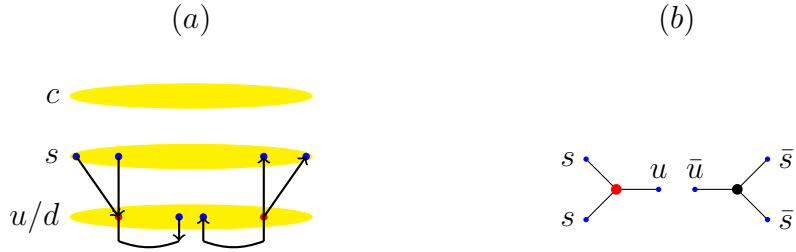


Figure 18: Tetraquark tear decay - (a) is a demonstration of the tetraquark decay through string tear to two baryons with content $s\bar{s}s\bar{s}$ in the stringy picture. (b) is the demonstration of the decay in the HISQ picture.

(i) A decay mechanism through an annihilation of a quark which is part of the di-quark and an anti-quark which is part of the anti-di-quark. This will yield an exotic meson which includes a BV and and anti-BV connected with two strings. This state may further decay into a tetraquark with content which is different than the original one, and then depending on its mass decaying either via a breaking or via an annihilation of the BV and anti-BV. This mechanism is relevant only for not obviously genuine states, which includes a pair of quark anti-quark of the same flavor.

(ii) One or more weak decays of a quark of heavy flavor (like c or b) to a lighter quark (like s or u/d), or similarly for an anti-quark. After the weak decay the tetraquark will include a di-quark (or an anti- diquark) with flavor lighter than the original one that can afterwards decay via breaking or annihilation.

5 Pentaquarks

Tetraquarks are the simplest exotic hadrons that relate to mesons since they are of vanishing baryon number. In a similar manner there are also exotic hadrons related to baryons which carry baryon number $B = 1$. These are referred to as pentaquarks since they involve four quarks and one anti-quark.

The total number of possible configurations of pentaquarks (excluding the top quark) is 350 in total - there are five possibilities for the antiquark. Then for four different quarks there are 5 possible configurations to a total of 25. For $\bar{q}_1 q_2 q_3 q_4$ there are 150 configurations. For $\bar{q}_1 q_2 q_2 q_3 q_3$ we get 50 configurations, for $\bar{q}_1 q_2 q_2 q_2 q_3$ there are 100 configurations and there are another 25 configurations for $\bar{q}_1 q_2 q_2 q_2 q_2$.

In this paper we put emphasis on charmed configurations. There are 210 possible pentaquarks with c/\bar{c} - 70 with \bar{c} , 80, 40, 16 and 4 with one c , two, three and four respectively. Out of 210 possible charm configurations, there are 115 that are genuine (don't contain a quark and an antiquark with the same flavor) and another 50 that are semi-genuine (contain a heavy pair of quark and antiquark).

5.1 Pentaquark configurations

A tetraquark is built from a mesonic string by adding a BV and anti-BV at its two endpoints. One can similarly construct a pentaquark by adding such a pair to the baryonic string. However, it turns out that for pentaquarks there is another possibility which does not include the adding of such a pair. A BV by construction must have a net number of $N_c = 3$ strings coming out of it. This does not imply that there are only 3 strings attached to it since the total number can be preserved also if there are additional pairs of string anti-string (opposite orientation)

connected to it. The requirement is that $N_{out} - N_{in} = N_c$ where N_{out} and N_{in} are the outcome and incoming strings respectively.

Thus, the two simplest possible structures of a pentaquark are the following:

5.1.1 A single BV

A pentaquark structure based on a single baryonic vertex. One adds to the BV an incoming and an outgoing strings with an antiquark and a quark attached to their endpoints respectively. A priori, there are several possible structures depicted in figure (19): .

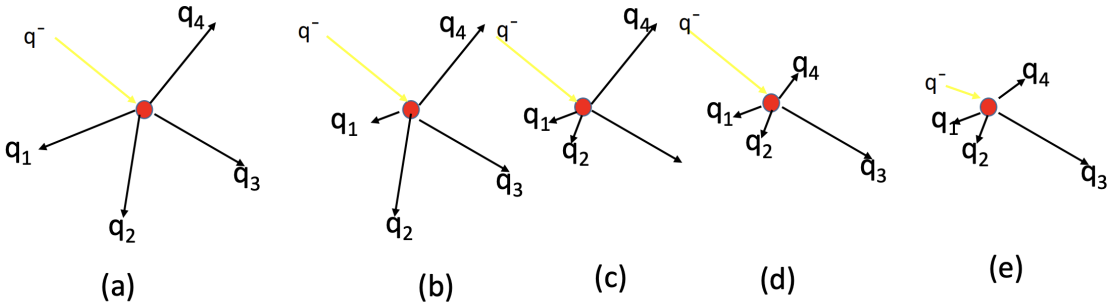


Figure 19: Possible setups of pentaquarks: (a) 5 strings attached to the BV, 4 with outward orientation (quark) and one inward (anti-quark) (b) After shrinking of one string, the quark q_1 is attached to the BV. (c) After two shrinkings a diquark is attached to the BV. (d) a triquark attached to the BV. (e) A diaquark and an pair of a quark antiquark. The BV, a string attached to a quark and a string attached to an anti-quark are drawn in red, black and yellow respectively.

(a) The analog of the Y shape of a baryon, a configuration with a BV with 4 outgoing strings attached to a quark and one inward string attached to an anti-quark. All the strings are of non-trivial lengths (b) A structure with one string shrank to zero size so the quark q_1 is attached to the BV. (c) A diquark (q_1, q_2) is attached to the BV in addition to an outgoing and incoming strings. (d) The BV is attached to a triquark and an incoming string (e) In the last option after a shrinkage of the incoming string associated with the anti-quark there is only one string q_3 that stretches in ordinary space and a diquark and a pair of quark anti-quark are attached to the BV. In the holographic picture The quarks q_1, q_2, q_4 and antiquark \bar{q} are connected with strings that stretch only along the holographic direction.

Even though we have not performed a stability analysis of these configurations, we assume following [45], [49] and [46] that the configuration (e) with only one string along a space direction will remain with finite length. On one end of this string there is an ordinary quark and on the other end a BV and a composite object that can be viewed as a diquark plus a quark anti-quark pair or a triquark plus an antiquark. From the point of view of the HISH the composite object

is relevant in determining the total mass, electric charge, flavor charges and spin of this end of the string.

Another issue relevant to this construction is whether the anti-quark \bar{q} carries the same flavor as one of the quarks q_1, q_2, q_4 . From the condition on the number of strings that connect to a given BV this we cannot determine the answer to this question. This issue is important for the possible decay channels of the pentaquark as will be discussed in (5.2).

In a similar manner to the fact that for a baryon there are several possibilities of what is the single quark and what quarks form the di-quark, also for a pentaquark of a general quark content of $(q_1, q_2, q_3, q_4, \bar{q})$, there are four possibilities for the single quark which is on the other side of the string. Currently we do not have a way to determine which option out of these four is preferable and we will assume that all of them are possible.

In (20) the holographic structure of a pentaquark of option (e) with a content of $(c, c, \bar{s}u/d, u/d)$ is drawn. In this example the single quark is a c quark and the diquark and pair of quark anti-quark are either $(c, u/d), (\bar{s}u/d)$ or $(u/d, u/d), (\bar{s}c)$.

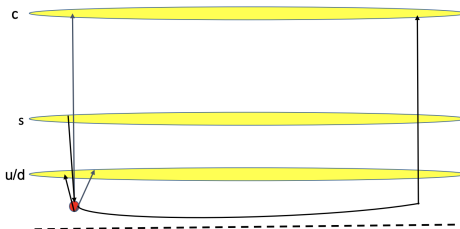


Figure 20: Pentaquark with the structure of one string and one BV. This an example of a content of $(c, c, \bar{s}u/d, u/d)$ and with c the quark at the end of the string that does not attach directly to the BV.

In (21) the HISH structure of the same pentaquark composed of $(c, c, \bar{s}u/d, u/d)$ is drawn. The diquark is taken to be of $(u/d, u/d)$ and the additional pair connected to the BV is that of (c, \bar{c}) .

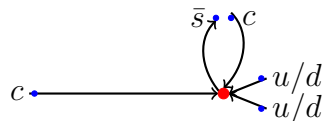


Figure 21: Pentaquark construction with one BV where an additional quark-antiquark pair is attached to it via two strings.

5.1.2 Configuration with BV anti-BV and a BV

- The other option includes an addition of a BV and anti-BV to a baryonic configuration. In this case the pentaquark is build from two finite size strings with diquarks on one of their endpoints and an anti-BV on the other end which is also attached to an antiquark through a string. For a content of $(q_1, q_2, q_3, q_4, \bar{q})$ there are 6 possibilities of forming the two diquarks.

In (Fig-22) and in (Fig-23) we show the holographic and HISH structures of the same content of quarks as the one above. .

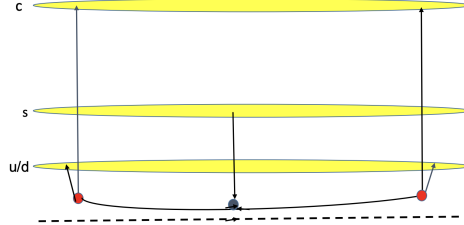


Figure 22: Pentaquark with a structure based on two strings stretch between a BV and an anti-BV and between the latter and another BV. This an example of a content of $(c, c, \bar{s}u/d, u/d)$ there are diquarks of $(u/d, c)$ attached to the two BVs.

Three comments are in order:(i) It is not necessary that the two strings that connect a BV and anti-BV are on a line. More generally they can be non-collinear. Minimizing the total action of system will determine the particular structure. (ii) In this setup since the anti-quark is separated in space from any of the quarks, one can have a pentaquark even when there is a quark and anti-quark of the same flavor, unlike in option (c) of the first type of structure. (iii) From fits to data of ordinary baryons, the contribution to the mass of the hadron a BV was found out to be small. Thus the second type of pentaquarks is not necessarily heavier than the first one. A detailed calculation of the mass is needed in each case.

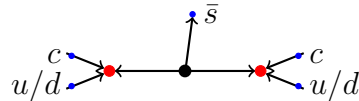


Figure 23: The HISH pentaquark construction with two BVs and one anti-BV.

5.2 Decays of the pentaquarks

Tetraquarks as we have seen in the previous section can decay either via an annihilation of a BV and an anti-BV or via a breakup of the string. For the pentaquarks these mechanism take place and there is another one, the detachment of a quark anti-quark from a BV. We discuss separately the decay of a structure based on a single BV and the a one with a BV anti-BV and a BV.

5.2.1 Decay of a configuration with a single BV

The petaquark that include a single BV can decay via two mechanisms: (i) A decay via breaking of the single long string producing a lower excited pentaquark and a meson. (ii) A decay via a detachment of the endpoints of an outgoing and incoming string on the BV. In holography as was described in (2.8), the BV is a wrapped D brane. On this D brane the endpoint of an attached string is a point particle with a “baryon number” charge, and that of a string

with opposite orientation is a point particle with the opposite “baryon number charge”. Due to fluctuations the two endpoints can get to the same point on the D brane and then annihilate. It is plausible that an annihilation of such a pair can take place if the other side of the strings are connected to the same flavor brane. Once the pair is detached from the BV one gets a mesonic string. If the annihilation, or detachment, is of a pair of the same flavor, the outcome meson will be flavorless like $\pi^0, \phi, J/\psi, botonium$.

If indeed the pair is of the same flavor, there is also a probability of the annihilation and detachment from the flavor brane. If the pentaquark configuration is of the setup (e) described in figure (19), then the process should be immediate. This implies that this configuration is not of a pentaquark but of a single baryon with a closed string attached to it. To have a pentaquark the two endpoints on the flavor brane should not be at the same points, namely, the corresponding strings have some non-vanishing length along space coordinates which occurs in configuration (d) for instance. An example of such a case is depicted in figure (Fig. 21). The latter emerge from the detachment of the quark anti-quark pair from the BV. This process for a pentaquark with the content given in (Fig. 21) is drawn in figure (24).

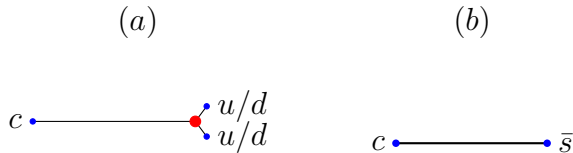


Figure 24: Pentaquark decay through the detachment of a quark-antiquark pair.

5.2.2 Decay of a configuration with BV anti-BV and a BV

The second type of pentaquark that is built on two BV and an anti-BV can decay via the following mechanisms:

(1) Decays via the annihilation of one of the two BVs with the anti-BV leaving over a baryon and a meson. Notice that in this case the annihilation does not yield two mesons but only one and the other quark of the annihilated BV connects to the other BV. This process is depicted in A of fig (25). We denote the left diquark by the quarks (q_L^1, q_L^2) and similarly for the right one by (q_R^1, q_R^2) and the quark attached to the anti-BV by \bar{q} . In figure A the string with its ends q_{L1} and \bar{q} forms a meson whereas the baryon is composed from q_L^2, q_R^1, q_R^2 . Obviously there are 4 possibilities of decay via such a process

$$(q_L^1, \bar{q}), (q_L^2, q_R^1, q_R^2) \quad (q_L^2, \bar{q}), (q_L^1, q_R^1, q_R^2) \quad (q_R^1, \bar{q}), (q_L^1, q_L^2, q_R^2) \quad (q_R^2, \bar{q}), (q_L^1, q_L^2, q_R^1) \quad (49)$$

(2) The other option is a decay via a breaking of a string yielding a tetraquark and a baryon. In figure (25) the baryon associates with $(q_{L1}, q_{L2}, \tilde{q})$ and the tetra quark with $((\bar{q}, \tilde{\bar{q}}, q_{R1}, q_{R2}))$. After this step there are two options denoted by B and C. In option B the tetraquark breaks apart into a baryon $(q_{L1}, q_{L2}, \tilde{q})$, anti baryon $(\bar{q}, \tilde{\bar{q}}, \tilde{\bar{q}})$ and a baryon $(q_{R1}, q_{R2}, \hat{q})$. It should be emphasized that whereas the products of the decay A can occur also in the decay of a molecule, the decays drawn in B and C can be an outcome only of a genuine pentaquark. The third option depicted in C of (25) is a process where the tetraquark decays into two mesons. In the figure $(q_{R1}\bar{q})$ and $(q_{R2}\tilde{\bar{q}})$. Clearly there is also the option of $(q_{R2}\bar{q})$ and $(q_{R1}\tilde{\bar{q}})$ and also there is the possibility that the annihilation will be between the anti-BV and the left BV. A sign on this channel is the fact that one of the anti-quarks of two mesons must have the same flavor as one of the quarks of the baryon since in the process they emerge from a breakup of a string. Note that this decay mechanism is also different from the one associated with the pentaquark built of a single BV.

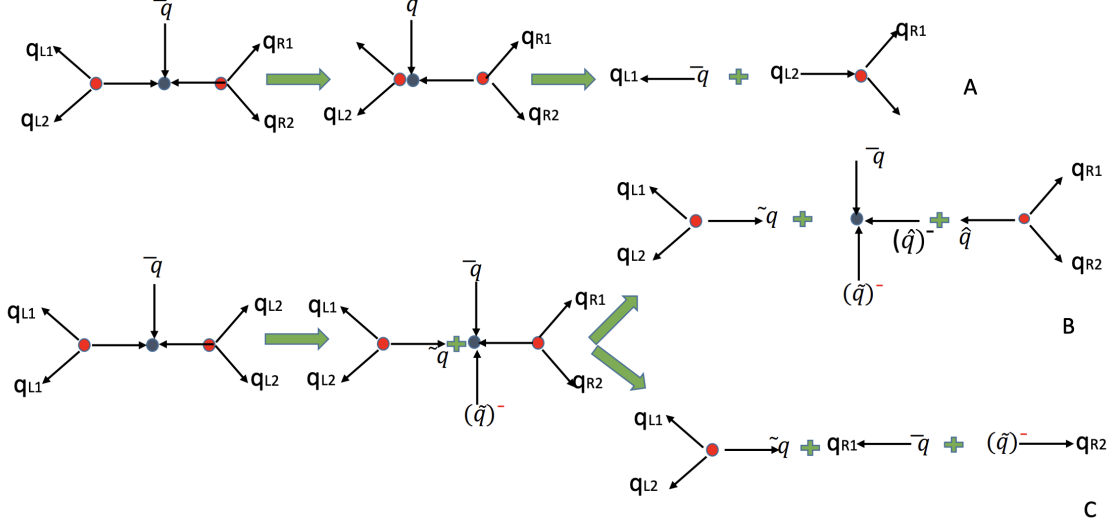


Figure 25: The decay mechanisms of a pentaquark constructed from a BV anti-BV and another BV. Option A follows from an annihilation of a BV and anti-BV. Option B and C follow from a breaking into a baryon and a tetraquark that can yield two baryons, and an anti-baryon B and two mesons and a baryon C

6 Confronting Experimental Data

In all our fits we assume the validity of (13) and (27), where there is a long horizontal string, attached to massive endpoints. These massive endpoints may be diquarks (or antidiquarks) with very short strings that connect to the quarks (antiquarks).

From this assumption we derive that the slope α' for a tetraquark should be similar to that of a meson but with the mass of an endpoint being that of a di-quark (anti-di-quark) plus the mass of a BV (anti-BV). As for pentaquarks, if the structure is as described in figure (21), we expect the slope to be similar to that of baryons with similar quark content. If the structure is as described in (23), we expect it to be similar to that of two strings attached at the anti-BV or maybe even an asymmetric Y shape where on one end there is a quark and on the other two there are BVs plus di-quarks.

Should the results admit an unexpected α' value, it is an indication that this postulation is not correct for certain exotic hadrons. Moreover, as discussed in subsections (5) and (2.8), hadrons may have more complex structures and while some are proven to be unstable, it is not obvious that this instability arguments can be applied to the exotic counterparts of these constructions.

6.1 Fitting Procedure

The fitting procedure will be done similarly to what was done in the previous works ([7], [32]) and was called "the massive fit". We will treat $M^2 = E^2(J + n)$ as the depended variable, where E relates to $J + n$ through the velocities β_1 and β_2 - according to (13):

$$E = E(m_1, m_2, \beta_1, \beta_2(m_1, m_2, \beta_1), \alpha', a) \quad (50)$$

Where the velocities are related through (15). The angular momentum according to (27):

$$J + n = (J + n)(\alpha', \beta_1, \beta_2(m_1, m_2, \beta_1), m_1, m_2, a) \quad (51)$$

Since $J + n$ is strictly monotonous in the domain we are interested in, assuming m_1, m_2, α' and a are known, we can calculate its inverse in terms of β_1 :

$$\beta_1 = \beta_1(J + n, \alpha', a, m_1, m_2,) \quad (52)$$

Then we can rewrite (50) as a direct dependency of the energy in the excitation level:

$$E = E(J + n, m_1, m_2, \alpha', a) \rightarrow M^2 = E^2(J + n, m_1, m_2, \alpha', a) \quad (53)$$

The fit degree-of-conformity will be measured according to the regular χ_r^2 :

$$\chi_r^2 = \frac{1}{\nu} \sum_{i=1}^n \frac{(M_{i,exp}^2 - M_{i,thry}^2)^2}{\sigma_i^2} \quad (54)$$

Where $M_{i,exp}$ is the estimated measured mass of each state, $M_{i,thry}$ is the predicted mass of the fit, σ is the total error of M_{exp}^2 and ν is the total number of DOFs which is the total number of measurements vs the number of fitting parameters that are not fixed. As usual, χ_r^2 is expected to be as close to 1 as possible to reflect a good fit. Since we don't seek a high level of precision, we have taken the masses error to be the max between 60 MeV and the total experimental error.

6.2 Width estimation

The hadrons width is composed at least of the width of each of the decay mechanisms - annihilation and string tear. According to (39), the annihilation decay width reduces exponentially with L^2 . To estimate the annihilation width of resonances that can break to baryon anti baryon pair, we assume that we need to know the full width of one of the states that decays predominantly through the annihilation mechanism:

$$\Gamma_{ann} = \Gamma_2 \frac{\exp\{-T_1 L^2|_{tear}\}}{\exp\{-T_2 L^2|_{ann}\}} \quad (55)$$

where Γ_2 is the width of one of the tetraquarks candidates.

The second mechanism is the tear of the string, which is calculated according to (36) and (37), resulting in:

$$\Gamma_{tear} = \frac{\pi}{2} ATL(M, m_1, m_2, T) \Phi(M, M_1, M_2) \quad (56)$$

Where M is the mass of the source hadron and M_1, M_2 are the masses of the two products - for tetraquarks it will be the masses of the baryon and antibaryon respectively.

The length of the string of each of these states can be estimated through:

$$L = l_1(E(\beta_1, m_1, \alpha', a)) + l_2(E(\beta_2(\beta_1, m_2, \alpha', a))) \quad (57)$$

where the expression for l_i is in accordance with (28) and (29).

6.3 Fitting Models

Tetraquarks and pentaquarks contain diquarks and anti-diquarks. These are connected to BVs and anti-BVs, and have a certain mass that is model dependant, as was shown in [55]. From [32] the results showed that the diquarks had mass that is usually the sum of the two quarks that are connected to the BV, implying that in the real world the BV is close to the wall where it's contribution to the endpoint mass is negligible with respect to the vertical strings that connect to the flavour branes and are mapped to the quarks masses at the flat-spacetime picture.

We will assume this conclusion also holds for the exotic hadrons, and expect the endpoint masses to be similar to the sum of the quarks (antiquarks) that compose the diquarks (anti-diquarks). The other assumption, as mentioned above (6) is that the slopes should be similar to that of mesons/baryons with accordance to the compact-multi-quarks structure and content.

In order to examine these assumptions, the fit of the exotic hadrons will be done according to (53) in four ways:

- Free fit - all parameters (α' , a , m_1 and m_2) will be free to vary. In this fit we expect to get values that are similar to these of our assumptions.
- Fixed masses - m_1 and m_2 will be fixed, each according to the sum of the quarks/antiquarks from which they are composed. α' and a on the other hand will be free to vary. The expectation is that the resulting α' will be similar to that of the mesons for tetraquarks.

For pentaquarks, we will fix the masses in two separate fits:

- o With fixed masses assuming the structure is similar to 21.
- o With fixed masses assuming the structure is similar to 23. In this case we will ignore the contribution of the middle anti-quark, assuming its velocity is close to zero (located close to the CM of the pentaquark).
- Fixed slope - α' will be fixed while the masses m_1 and m_2 will be free to vary. Here we expect again that the endpoint-masses will reflect our assumptions. Similarly to the fixed-masses fit, for pentaquarks, we will fix the slope once for each possible configuration (21, 23).
- Previous fit - α' , m_1 and m_2 will be fixed, while only the intercept a is free to vary. Similarly to the fixed-masses fit, for pentaquarks, we will fix all the parameters once for each possible configuration (21, 23).

If our assumptions are correct, we expect to see no significant variations between the different fits in terms of χ^2 and the predicted spectrum. We also expect the tetraquarks HMRTs slopes to be similar to these of the mesons.

Since there are two basic possible configurations - one that is similar to the tetraquarks structure, and another one that is similar to the baryonic configuration - the results for the pentaquarks may imply which configuration is a better description of these exotic hadrons.

The fit parameters will be bounded according to physical considerations - the endpoint masses will be bounded from below to zero and from above according to the mass of the lowest resonance in the trajectory.

From the fits we will calculate further resonances on the trajectory using (53) and the decays widths as described in 6.2.

6.4 Predictions of J and n

Not all the observed states have J known. In addition, the data measured is not guaranteed to have a full trajectory with no gaps - there can be states in between that weren't observed. Therefore, predictions of the full MRT will be done in the following steps:

- We will predict the trajectory for each quark content according to mesons/baryons thresholds - we will count the number of states that could rely on the same HMRT when building the trajectory around the thresholds.
- According to the fit, we will predict the value of $J + n$ for the candidates that fit the trajectories and the decay channels.

Since some states were added to the data collected since the last works [7], [32], we are repeating the fits to verify the validity of the previous results, and also to align with the new fitting procedure.

6.5 Mesons

In the previous HISH works [7] and [40], the mesons data was fit in both (J, M^2) and (n, M^2) planes. Our assumption is that the tetraquarks structure is similar to that of mesons, where there is a long string with massive endpoints. In the case of the tetraquarks these massive endpoints are diquark (or anti diquark), connected to quarks (anti quarks) with very short strings. If this assumption is correct, we expect the slope of tetraquarks with similar quark content to resemble that of mesons.

This assumption is based on the results of [32], where the baryons slopes were found to be similar to that of mesons. This observation reduces the chances of having a Y possible structure as detailed at 2.8, in which we expect the slope to be around 2/3 of mesons slope with similar quark content. Hence, tetraquarks with slope similar to 2/3 of their meson α' counterparts may be explained by having such a structure.

In this paper, we systematically predict the tetraquarks trajectories for all possible charm configurations. One of the conclusions from [7] was that for heavy quarks the slopes of the J and n trajectories differ significantly. For the (J, M^2) , a global fit was done for most of the mesons together, where the quarks masses are assumed to be global fit parameters of the model, that is common to all hadron configurations.

In order to provide trajectory predictions for tetraquarks in both planes - J and n excitations, we repeated the fit using the regular χ^2_r with global fit for each plane separately. At last we did a global fit for both planes together, assuming that the quark masses are constraint to be the same in both, where α' wasn't constrained. The idea behind a separate global fit for each plane was to estimate the degree-of-conformity of the quark-masses-constraint assumption vs that of separate parameters of each plane. The results of the last global fit will be used for both planes tetraquarks spectrum predictions.

The full results of the global fits done for the mesons and the states used are in the appendix A. This includes the states used for the fits in tables 229 and 232, as well as the graphs in 226-228 and fit values in table 224.

In this section at table 1 we summarize the global fits results which were used to predict the spectrum of all tetraquarks.

6.6 Baryons

The baryons fits were important for calculating the pentaquarks HMRTs, under the assumption of a baryonic structure (4). For the (J, M^2) trajectories, we used the results from [32] and [40]

$\alpha'_{n,light}$ [GeV $^{-2}$]	$\alpha'_{n,heavy}$ [GeV $^{-2}$]	$\alpha'_{j,light}$ [GeV $^{-2}$]	$\alpha'_{j,heavy}$ [GeV $^{-2}$]	$m_{u/d}$ [GeV]	m_s [GeV]	m_c [GeV]	m_b [GeV]
0.83	0.45	0.86	0.65	0.013	0.36	1.11	4.71

Table 1: Mesons universal fit parameters. These will be used for calculating tetraquarks and tetraquarks-like configurations trajectories.

as summarized in B. For the (n, M^2) trajectories, we did a universal fit (see B.1), similarly to the mesons fit. From this fit we extracted the light and heavy slopes of the baryons 235. The procedure was done in the following way:

- We assumed the universal values of the endpoint masses from the mesons fit holds for all configurations with quarks as endpoints.
- We went through all possible configurations for the baryons³, defining separately the diquarks masses.
- We fixed the quarks masses with the output of the masses obtained from the mesons global fit. But we let the diquarks masses vary with the restriction that their masses will be at least its heavy quark mass.
- The set of diquarks configurations that had the best universal fit was selected.

6.7 Tetraquarks

In the HISH framework, the natural decay of tetraquarks is to baryon-antibaryon due to the string breaking mechanism, given that they are above threshold. We searched for baryonia decays to find such candidates. In 2 we enlist all possible candidates of charmed tetraquarks. We enlist the state, quark content (assumed), mass, width, J^{PC} and the selected decay channels that match the HISH decay mechanisms (annihilation or string tear).

In table 107, we enlist all the possible tetraquark charm configurations, and for each we detail the possible decays into two mesons, the meson-meson threshold, decay into a baryon and anti-baryon and the corresponding threshold. In fact, as discussed above in (4.3) the latter decay can, if energy permits, follow several channels. For instance the first item (c, \bar{u}, u, \bar{u}) can in principle decay via a u, \bar{u} pair into $\Sigma_c^{++}, \bar{\Delta}^{--}$, a pair of d, \bar{d} into $\Lambda_c^+ p^-$, a pair of s, \bar{s} into $\Xi_c^+, \bar{\Sigma}^-$, and via c, \bar{c} and b, \bar{b} but of course the latter two are very improbable. The type of multiplicities may occur for all the states. In the table we write down only the most probable option when the string breaks by creating a light quark pair . The decay via annihilation of a given state is also not unique since there are two options of the quark anti-quark pairing. For instance the state (c, d, \bar{u}, \bar{d}) can decay into two mesons either via $(c, \bar{u}), (d\bar{d})$ or $(c, \bar{d}), (d\bar{u})$. Several of the candidates may have already been detected and they are mentioned in the prediction table of tetraquarks 107.

6.8 Pentaquarks

The natural decay of an excited pentaquark with baryonic configuration is through string tear mechanism, into another pentaquark and a meson. If it isn't excited, we expect it to decay

³By 'possible configurations' we mean that the baryons quark-diquark configuration is not always unambiguously established. For example Λ_c which consists of udc can either have endpoint masses $m_{BV_{u/d,u/d}}$ and m_c or $m_{BV_{c,u/d}}$ and $m_{u/d}$. We fitted all the possible sets of configurations for the global (n, M^2) fit and selected the set that provides the best χ^2_r .

through the detachment mechanism to a meson and a baryon. In the available data no pentaquark candidates 212 decayed to a pentaquark and meson. The tetraquark-like configuration is expected to decay through string break into a tetraquark and a baryon. If below threshold it is expected to decay through annihilation into a baryon-meson pair.

While the detachment vs annihilation mechanism may not tell us which configuration is more likely according to the products (in both cases we expect baryon-meson decay), we can still separate the two configurations. In both cases, the lowest (in energy) final product may be of two mesons and a baryon, if the pentaquark is above the string tear configuration. The first configuration will be consistent with the results if the baryon and meson are of the same mother particle, while the second is expected if the mesons are of the same origin - created through annihilation of the tetraquark.

Another possible product of the second configuration is of two baryons and an antibaryon. This will also be a clear evidence that the latter configuration is more likely.

In table 212 we enlist all the possible candidates, and in table 223 we calculate all possible predictions for pentaquarks based on both configurations and on the detachment/annihilation mechanism.

7 Exotic Hadron Candidates

In this section we will analyse in detail specific resonances that are suspected as tetraquarks or pentaquarks according to the HISH model. In order to identify candidates, we scanned all PDG data, searching for states that correspond to the HISH criteria for exotic hadrons. Each of these are presented here.

The search for the data was done in two phases. At first we searched for states that fit our criteria. Then we built each trajectories and finally, searched the PDG again for states that may fit the same trajectory.

At last, we built all possible charmed configurations in tables [107], than we went through the PDG data and searched for possible candidates with corresponding masses and decays that require more research.

This section is built as follows - I) we first describe the candidates selection criteria. II) Than we list all the exotic candidates, and elaborate on each of the candidates that have been observed. Each is confronted with the predictions and model assumptions. III) At last we list a table with the trajectories predictions for all the possible tetrauquarks configurations. We also elaborate on some of the pure tetraquarks predictions. IV) At last, we do the same for the pentaquarks.

7.1 HISH Exotic Candidates selection Criteria

In the HISH model, the natural decay of hadrons is through string tear. Hence, the best criteria for identifying tetraquarks was through scanning the PDG data for states that decay to baryon-antibaryon pairs. In addition, the candidate must admit the Modified Regge Trajectory behavior⁴.

Another criteria are decays through annihilation, especially for states that are below the baryon-antibaryon threshold. These criteria can be divided to three types. The first is for candidates that are composed solely from heavy content. Since string-tear decay probability exponentially decreases by the mass of the created $q\bar{q}$ pair ((37)), annihilation for a only heavy mesons is a strong indication that the mother particle is a tetraquark. The second is for states

⁴The HMRT criteria can only be confirmed when there are at lease three states. If there are two, we require that the slope and masses will be similar to the mesonic case (see 6.3).

that do not contain $q\bar{q}$ pair in their mesonic products, which implies that the products cannot come from a decay via breaking of a meson, hence these state are genuine tetraquark. The third are those states that do not belong to each of the previous ones, but do not belong to any of the mesonic trajectories.

For pentaquarks, we relied on candidates that were identified as pentaquarks (or molecules) by the experiments that found them. The candidates that were observed so far are charmed and contain $c\bar{c}$ pair. It is believed that these states are molecules and not genuine pentaquarks⁵. If on the other hand, it will be found in the future that there are excited states of them that furnish HMRT trajectories, then it will be a strong indication that they are genuine petaquarks.

7.2 Tetraquarks Candidates

In this paper, we focused on states with charm flavor. But, there are a few non-charm candidates that decay to baryon-antibaryon pairs that we analysed. We begin from these light candidates, and proceed to our main goal, which are the charmed ones. Table 2 summarizes the candidates and the measurements that were considered and used, followed by the detailed analysis of each state or trajectory.

The 'Selected Decay Channels' column includes the decay channels that matches the HISH decay possible mechanisms and imply the quark content of the states. As explained in section 7.1, the decay channel is used as part of the selection criteria for the states that should be considered, and this was our main consideration for selecting certain channels over others, rather than the width value of the channels.

The 'Quark Content' column is the assumed quark content according to the products. When there are more than one suggested compositions, it is either due to the products being a mixed ("superposition") configuration as explained in 3, or that the products minimal content is ambiguously established. When 'Molecule' is indicated, it means the state does not meet the HISH criteria for genuine compact-quark structure.

Candidate	Quarks Content	Selected Decay Channels	J^{PC}	Mass [MeV]	Width [MeV]	Ref.
$X(1855)$	Molecule	$\bar{p}n$? ^{??}	1856.6 ± 5	20 ± 5	[56]
$X(1835)$	Molecule	$p\bar{p}$	0^{-+}	$1826.5^{+13.0}_{-3.4}$	242^{+14}_{-15}	[57], [58], [59]
$f_4(2300)$	$ud\bar{u}d$ or $dd\bar{d}\bar{d}$	$N\bar{N}$	4^{++}	2320 ± 60	250 ± 80	[60], [61], [62], [63]
$f_2(1640)$	$u\bar{s}\bar{u}s$ or $d\bar{s}\bar{d}s$	$K\bar{K}$	2^{++}	1639 ± 6	99^{+60}_{-40}	[64], [65], [66]
$f_2(1750)$	$u\bar{s}\bar{u}s$ or $d\bar{s}\bar{d}s$	$K\bar{K}$	2^{++}	1755 ± 10	67 ± 12	[67]
$f_2(2300)$	$u\bar{s}\bar{u}s$ or $d\bar{s}\bar{d}s$	$\Lambda\bar{\Lambda}$	2^{++}	2297 ± 28	149 ± 40	[68]

⁵We thank M. Karliner for pointing this to us.

$\omega(2290)$	$u\bar{s}u\bar{s}$ or $d\bar{s}d\bar{s}$	$\Lambda\bar{\Lambda}$	1 ⁻⁻	2290 ± 20	275 ± 35	[69], [70], [71]
$f_3(2300)$	$u\bar{s}u\bar{s}$ or $d\bar{s}d\bar{s}$	$\Lambda\bar{\Lambda}$	3 ⁺⁺	2334 ± 25	200 ± 20	[69], [70]
$X(3250)$	$\bar{u}s u\bar{s}$ or $\bar{d}s d\bar{s}$	$\Lambda\bar{p}K^+$? ^{??}	$3250 \pm 8 \pm 20$	45 ± 18	[72]
$X(3250)$	$\bar{u}s u\bar{s}$ or $\bar{d}s d\bar{s}$	$\Lambda\bar{p}K^+\pi^\pm$ $K_S^0 p\bar{p}K^\pm$? ^{??}	$3245 \pm 8 \pm 20$	25 ± 11	[72]
$K(3100)^0$	$u\bar{s}u\bar{d}$	$\Sigma(1385)^+\bar{p}$? ^{??}	~ 3100	$\sim 10 - 70$	[72]
$X(2632)$	$c\bar{u}u\bar{s}$	D^0K^+ $D_s^+\eta$? ^{??}	2635.2 ± 3.3	< 17	[73]
$T_{cs0}(2900)^0$	$\bar{c}du\bar{s}$	D^-K^+	0 ⁺	2866 ± 7	57 ± 13	[74]
$T_{cs1}(2900)^0$	$\bar{c}d\bar{u}s$	D^-K^+	1 ⁻	2904 ± 5	110 ± 12	[74]
$T_{cs0}^a(2900)^0$	$\bar{c}s\bar{u}d$	$D_s^+\pi^-$	0 [?]	$2892 \pm 14 \pm 15$	$119 \pm 26 \pm 13$	[75]
$T_{cs0}^a(2900)^{++}$	$\bar{c}sud$	$D_s^+\pi^+$	0 [?]	$2921 \pm 17 \pm 20$	$137 \pm 32 \pm 17$	[75]
$X(3350)$	$cdd\bar{u}$	$\Lambda_c^+\bar{p}$	0 or 1 ^{??}	$3350^{+10}_{-20} \pm 20$	$70^{+40}_{-30} \pm 40$	[76], [77]
$X(3800)^6$	$cdd\bar{u}$	$\Lambda_c^+\bar{p}$? ^{??}	3840 ± 10	30 ± 30	[76]
$T_{cc}(3875)$	$c\bar{c}u\bar{d}$	$D^{*+}D^0$ $D^{*0}D^+$? [?]	3874 ± 0.11	0.41 ± 0.17	[78]
$Z_c(3900)$	$c\bar{c}u\bar{d}$ $c\bar{c}d\bar{u}$	$J/\psi\pi^\pm$ $DD^{*\pm}$	1 ⁺⁻	3887.1 ± 2.6	28.4 ± 2.6	Many, including [79]
$Z_c(4200)^\pm$	$c\bar{c}u\bar{d}$ or $c\bar{c}d\bar{u}$	$J/\psi\pi^+$	1 ⁺⁻⁷	4196^{+35}_{-32}	370^{+100}_{-150}	[80]
$Z_c(4430)^\pm$	$c\bar{c}u\bar{d}$ or $c\bar{c}d\bar{u}$	$\pi^+\psi(2S)$ π^+J/ψ	1 ⁺⁻⁷	4478^{+15}_{-18}	181 ± 31	[81], [82], [83], [84]
$X(4020)^\pm$	$c\bar{c}u\bar{d}$ or $c\bar{c}d\bar{u}$	$D^*\bar{D}^*$ $h_c(1P)\pi^\pm$? ^{?-}	4024.1 ± 1.9	13 ± 5	[85], [86] [87], [87]
$X(4051)^\pm$	$c\bar{c}u\bar{d}$ or $c\bar{c}d\bar{u}$	$\pi^+\chi_{c1}(1P)$? ^{?+}	4051^{+24}_{-40}	82^{+50}_{-28}	[88]
$X(4055)^\pm$	$c\bar{c}u\bar{d}$ or $c\bar{c}d\bar{u}$	$\pi^+\psi(2S)$? ^{?-}	4054 ± 3.2	45 ± 13	[89], [90] [91]
$X(4100)^\pm$	$c\bar{c}u\bar{d}$ or $c\bar{c}d\bar{u}$	$\pi^-\eta(1S)$? ^{??}	4096 ± 28	152^{+80}_{-70}	[92]

⁶Needs confirmation, seen at [76] but not at [77].

⁷C needs confirmation.

$R_{c0}(4240)^{\pm}$	$c\bar{c}ud$ or $c\bar{c}d\bar{u}$	$\pi^-\psi(2S)$	0^{--}	4239^{+50}_{-21}	220^{+120}_{-90}	[93]
$X(4250)^{\pm}$	$c\bar{c}ud$ or $c\bar{c}d\bar{u}$	$\pi^+\chi(1P)$	$?^{? -7}$	4248^{+190}_{-50}	177^{+320}_{-70}	[88]
$T_{\psi s1}^{\theta}(4000)^+$ also $Z_{cs}(4000)^+$	$c\bar{c}u\bar{s}$	$J/\psi K^+$ $D_s^+ \bar{D}^{*0}$ $D_s^{*+} \bar{D}^0$	1^+	$3980 - 4010$	$5 - 150$	[93]
$T_{\psi s1}(4220)^+$ also $Z_{cs}(4220)^+$	$c\bar{c}u\bar{s}$	$J/\psi K^+$	1^+	4216^{+50}_{-40}	233^{+110}_{-90}	[93]
$T_{\psi s1}^{\theta}(4000)^0$	$c\bar{c}d\bar{s}$	$J/\psi K_S^0$	1^+	3991^{+14}_{-20}	105^{+12+9}_{-10-17}	[94]
$X(3960)$	$c\bar{c}s\bar{s}$	$D_s^+ D_s^-$	0^{++}	$3956 \pm 5 \pm 10$	$43 \pm 13 \pm 8$	[95]
$X(4140)$	$c\bar{c}s\bar{s}$	$J/\psi\phi$	1^{++}	4146.5 ± 3.0	19^{+7}_{-5}	[96]
$X(4274)$	$c\bar{c}s\bar{s}$	$J/\psi\phi$	1^{++}	4286^{+8}_{-9}	51 ± 7	[97]
$\chi_{c0}(4500)$	$c\bar{c}s\bar{s}$	$J/\psi\phi$	0^{++}	4474 ± 4	77^{+12}_{-10}	[97]
$\chi_{c1}(4685)$	$c\bar{c}s\bar{s}$	$J/\psi\phi$	1^{++}	4684^{+15}_{-17}	126 ± 40	[93]
$\chi_{c0}(4700)$	$c\bar{c}s\bar{s}$	$J/\psi\phi$	0^{++}	4694^{+16}_{-5}	87^{+18}_{-10}	[97]
$X(4350)^8$	$c\bar{c}s\bar{s}$	$J/\psi\phi$	$?^{?+}$	4351 ± 5	13^{+18}_{-10}	[98]
$X(4630)$	$c\bar{c}s\bar{s}$	$J/\psi\phi$	1^{-+9}	4626^{+24}_{-110}	174^{+140}_{-80}	[93]
$\psi(4360)$	$c\bar{c}s\bar{s}$	$J/\psi\eta$	1^{--}	4374 ± 7	118 ± 12	[99], [100]
$\psi(4660)$	$c\bar{s}\bar{c}s$	$\Lambda_c^+ \bar{\Lambda}_c^-$ $D_s^+ D_{s1}^-(2536)$ $D_s^+ D_{s2}^{*-}(2573)$	1^{--}	4630 ± 6	72^{+14}_{-12}	[101]
$T_{\psi\psi}(6600)$	$c\bar{c}c\bar{c}$	$J/\psi J/\psi$	$?^{??}$	6630 ± 90	$350 \pm 11^{+110}_{-40}$	[102]
$T_{\psi\psi}(6600)$	$c\bar{c}c\bar{c}$	$J/\psi J/\psi$	$?^{??}$	$6552 \pm 10 \pm 12$	$124^{+32}_{-26} \pm 33$	[103]
$T_{\psi\psi}(6900)$	$c\bar{c}c\bar{c}$	$J/\psi J/\psi$	$?^{??}$	6886 ± 16	168 ± 80	[104]
$T_{\psi\psi}(6900)$	$c\bar{c}c\bar{c}$	$J/\psi J/\psi$	$?^{??}$	$6927 \pm 9 \pm 4$	$122^{+24}_{-21} \pm 18$	[103]
$T_{\psi\psi}(7300)$	$c\bar{c}c\bar{c}$	$J/\psi J/\psi$	$?^{??}$	$7287^{+20}_{-18} \pm 5$	$95^{+59}_{-40} \pm 19$	[103]

Table 2: Tetraquarks candidates summary. These states were analysed in detail in this paper and compared with the tetraquarks predicted HMRTs described at 107. The 'Selected Decay Channels' column includes the decay channels that matches the HISH decay mechanisms and imply the quark content. The 'Quark Content' column is the assumed quark composition, where 'Molecule' means it does not meet the HISH criteria for compact-quark structure.

For light tetraquarks candidates, we used the universal light slopes for (J, M^2) and (n, M^2) to calculate the spectrum for each HMRT. We set the sum of the diquark (antidiquark) masses as was outputed by the mesons fits to be the mass of each endpoint. We then extracted the intercepts a_J and a_n using all the other parameters along with the provided mass of one of the states on the trajectories.

Since we do not differentiate between u and d masses/D-brane, we treat contents containing them together. For example $T_{c\bar{d}d\bar{u}}$ is treated with $T_{c\bar{u}u\bar{u}}$ as the HISH model does not distinguish between them in terms of mass or preferable decay channel.

⁸Needs confirmation.

⁹ J^P needs confirmation.

For heavy candidates, we did the same, but used the mesons heavy slopes for both planes.

7.2.1 Minimal content $T_{u\bar{u}u\bar{d}}$ or $T_{\bar{u}d\bar{d}\bar{d}}$

In the available data there is the state $X(1855)$ (table 3) which corresponds to minimal quark content of either $u\bar{u}u\bar{d}$ or $\bar{u}d\bar{d}\bar{d}$. This resonance was observed only in the baryonic channel $\bar{p}n$. In the HISH framework, the criteria for identifying a molecule is that it shouldn't fit an HMRT. Another condition for a tetraquark decay through string tear is that its energy is above the baryon-antibaryon pair threshold, which is ~ 1877 in this case. Therefore, the state $X(1855)$ which has a mass of $\sim 1857 \pm 5$ is expected to be a molecule and not a genuine compact-multiparticle structure. Aside from these requirements, the description of molecules in the HISH framework requires more research as explained in the open-questions section.

Candidate	Quarks Content	Selected Decay Channels	J^{PC}	Mass [MeV]	Width [MeV]	Ref.
$X(1855)$	Molecule	$\bar{p}n$? ^{??}	1856.6 ± 5	20 ± 5	[56]

Table 3: $T_{u\bar{u}u\bar{d}}$ or $T_{\bar{u}d\bar{d}\bar{d}}$ exotic candidate.

Table 4 summarizes the thresholds for $T_{\bar{u}d\bar{d}\bar{d}}$ and the predicted annihilation and tear widths (in the 'Width' column the first value is the annihilation width, the second one is the tear width). Tables (5 and 6) provide the model HMRTs in planes (J, M^2) and (n, M^2) respectively. Indeed $X(1855)$ does not fit any of the trajectories. The predicted widths are also above the experimental value. Figure 26 contains the graphs of the predicted trajectories for $T_{\bar{u}d\bar{d}\bar{d}}$.

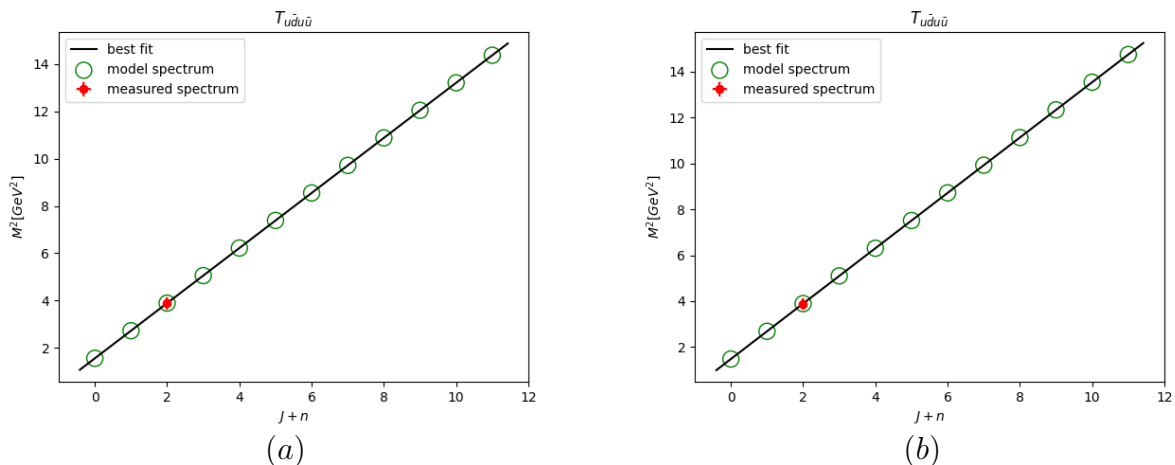


Figure 26: (a) is (J, M^2) $T_{\bar{u}d\bar{d}\bar{d}}$ predicted HMRT, (b) (n, M^2) $T_{\bar{u}d\bar{d}\bar{d}}$ HMRT. In both cases it is assumed to be a tetraquark due to its decay channel.

Thry Width [MeV]	Mesons Pair	Meson Threshold [MeV]	Baryon Anti-baryon	Baryonic Threshold [MeV]	Genuine
24 – 115	$\pi^+ \pi_u^0$	275	$p\bar{n}$	1878	
38 – 75	$\pi_u^0 \pi^+$	275	$\Delta^{++} \bar{p}$ $\Sigma^+ \bar{\Lambda}^0$	2170 2305	

Table 4: $T_{u\bar{d}u\bar{d}}$ thresholds.

J Spec	a_{T_J}
1161 – 1335	
1585 – 1717	
1918 – 2028	
2201 – 2297	
2451 – 2538	
2678 – 2758	
2887 – 2961	
3082 – 3152	
3266 – 3331	
3439 – 3502	
3604 – 3664	
3762 – 3819	-1.5–1.1

Table 5: $T_{u\bar{d}u\bar{u}}$ (J, M^2) predictions.

n Spec	a_{T_n}
1124 – 1303	
1572 – 1705	
1918 – 2028	
2210 – 2306	
2468 – 2555	
2702 – 2781	
2916 – 2990	
3116 – 3185	
3304 – 3369	
3482 – 3543	
3651 – 3710	
3812 – 3869	-1.4–1.0

Table 6: $T_{u\bar{d}u\bar{u}}$ (n, M^2) predictions.

7.2.2 $T_{u\bar{d}\bar{u}d}$ or $T_{d\bar{d}d\bar{d}}$

The $T_{u\bar{d}\bar{u}d}$ or $T_{d\bar{d}d\bar{d}}$ tetraquarks candidates that are considered are in the following table 7:

Candidate	Quarks Content	Selected Decay Channels	J^{PC}	Mass [MeV]	Width [MeV]	Ref.
$X(1835)$	Molecule	$p\bar{p}$ $\eta' \pi^+ \pi^-$ $\gamma\gamma$	0^{-+}	$1826.5^{+13.0}_{-3.4}$	242^{+14}_{-15}	[57], [58], [59]
$f_4(2300)$	$u\bar{d}\bar{u}d$ or $d\bar{d}d\bar{d}$	$N\bar{N}$ $\eta\eta$ $\omega\omega$ $\pi\pi$ $K\bar{K}$ $\rho\rho$ $\eta\pi\pi$	4^{++}	2320 ± 60	250 ± 80	[60], [61], [62], [63]

Table 7: $T_{u\bar{d}\bar{u}d}$ or $T_{d\bar{d}d\bar{d}}$ tetraquark candidates.

Similar to $X(1855)$ from previous section 7.2.1, the first state $X(1835)$ mass (~ 1826) is below the threshold for $p\bar{p}$ decay (~ 1877) by about 50 MeV. Therefore, we expect it to not be on the predicted HMRT for $T_{u\bar{d}\bar{u}d}$ or $T_{d\bar{d}d\bar{d}}$.

The other state in this category, $f_4(2300)$ have been observed in $N\bar{N}$ decay channel, as well as in meson-meson pair channels and one 3-body meson channel as can be seen from the table 7. Since the strongest indication of a tetraquark candidate according to this model is a decay to baryon-antibaryon pair, we consider $f_4(2300)$ to be a candidate. Another indication is that we couldn't fit this state into a meson trajectory, implying it does not belong to this regime. However, the determination of the exact quark content is ambiguous since the products are mixes of all light quarks - in general the model allows annihilation of a quark-antiquark of the same flavour brane followed by the creation of a different pair on another flavor-brane. This could be interpreted either by implying that there are multiple decay channels, or by the suggestion that the model always offers a mix of states when this annihilation is possible. This is another open question of the model.

The $f_4(2300)$ mass is roughly 440 MeV above the baryonic threshold (table 8). Other tetraquarks candidates that are above the baryon-antibaryon threshold are closer to it with only about 20 – 130 MeV above the threshold. Therefore, we assume it is not the first state on the trajectory that decay through $N\bar{N}$. In order to test it, we built the trajectories for $f_4(2300)$ in both (J, M^2) and (n, M^2) (tables 9 and 10, figure 27) to see if the $X(1835)$ state fits on any of the trajectories. We can see from table 9 that the state fits on the J trajectory, and from 8 that the predicted width also fits the measured value. Moreover, the second row in table 9 is the mass range of $J + n = 3$, and row three is the mass range of $J + n = 4$, which is consistent with the J value of $f_4(2300)$ with $n = 0$.

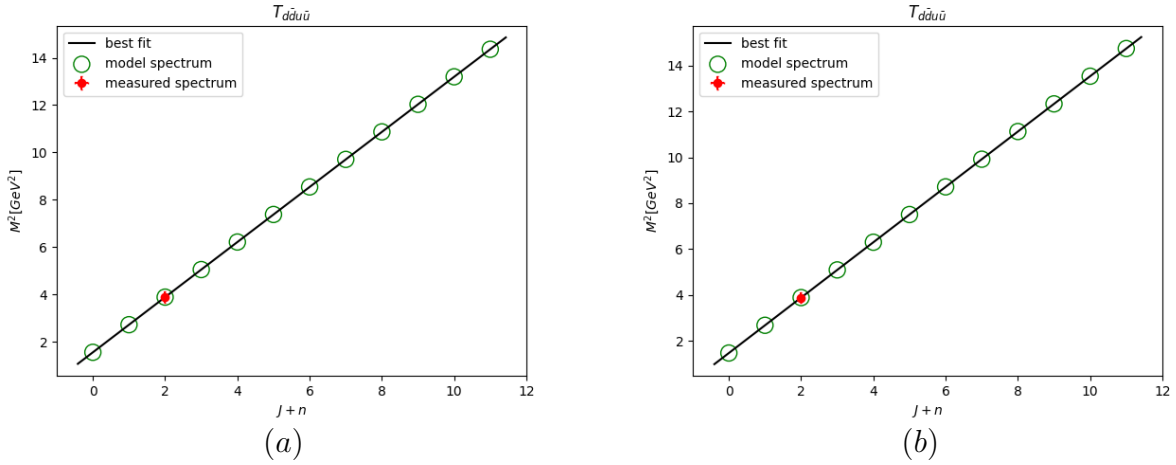


Figure 27: (a) is (J, M^2) $T_{u\bar{d}\bar{u}d}$ or $T_{d\bar{d}d\bar{d}}$ predicted HMRT, (b) (n, M^2) $T_{u\bar{d}\bar{u}d}$ or $T_{d\bar{d}d\bar{d}}$ predicted HMRT. In both cases it is assumed to be a tetraquark due to its decay channel.

Thry Width [MeV]	Mesons Pair	Meson Threshold [MeV]	Baryon Anti-baryon	Baryonic Threshold [MeV]	Genuine
25 – 115	$\pi_d^0 \pi_u^0$	270	$p\bar{p}$	1876	
38 – 75	$\pi^- \pi^+$	280	$n\bar{n}$ $\Lambda^0 \bar{\Lambda}^0$	1880 2232	

Table 8: $T_{d\bar{d}u\bar{u}}$ thresholds.

J Spec	a_{T_J}
1157 – 1332	
1583 – 1715	
1916 – 2026	
2199 – 2295	
2450 – 2536	
2677 – 2756	-1.5 – -1.1
2886 – 2960	
3081 – 3150	
3264 – 3330	
3438 – 3500	
3603 – 3663	
3761 – 3818	

Table 9: $T_{d\bar{d}u\bar{u}}(J, M^2)$ predictions.

n Spec	a_{T_n}
1120 – 1300	
1570 – 1702	
1916 – 2026	
2209 – 2305	
2467 – 2553	
2700 – 2779	-1.4 – -1.0
2915 – 2988	
3115 – 3184	
3303 – 3368	
3481 – 3542	
3650 – 3709	
3811 – 3868	

Table 10: $T_{d\bar{d}u\bar{u}}(n, M^2)$ predictions.

7.2.2.1 $f_4(2300)$

This state was observed in $f_4(2300) \rightarrow N\bar{N}$. Tables 11 and 12 are the built HMRT that includes the measured $f_4(2300)$ and 28 are the plot of these trajectories. These are consistent with table 9. The intercept values are $a_J = -0.52$ and $a_n = -0.37$.

State	M [MeV]	Thry M [MeV]	J	Thry n	Thry $J+n$
		1721			2
		2031			3
$f(2300)$	2300	2300	4	0	4
		2541			5
		2760			6

Table 11: $f_4(2300)(J, M^2)$ HMRT.

State	M [MeV]	Thry M [MeV]	J	Thry n	Thry $J+n$
		1696			2
		2021			3
$f(2300)$	2300	2300	4	0	4
		2549			5
		2775			6

Table 12: $f_4(2300)(n, M^2)$ HMRT.

7.2.3 $T_{u\bar{s}\bar{u}s}$ or $T_{d\bar{s}\bar{d}s}$

For a tetraquark with the quark content $u\bar{s}\bar{u}s$ or $d\bar{s}\bar{d}s$ the mesonic and baryonic thresholds are ~ 990 and ~ 2230 respectively. The candidate resonances are presented in table 13. Both states $X(3250)$ will be discussed separately, since they are special cases of 3-body and 4-body decays. We generated the predicted HMRTs for this quark content in tables 15 and 16, and the thresholds table 14 includes the predicted width. The HMRTs are also plotted in 27.

Candidate	Quarks Content	Selected Decay Channels	J^{PC}	Mass [MeV]	Width [MeV]	Ref.
$f_2(1640)$	$u\bar{s}\bar{u}s$ or $d\bar{s}\bar{d}s$	$K\bar{K}$	2^{++}	1639 ± 6	99_{-40}^{+60}	[64], [65], [66]

$f_2(1750)$	$u\bar{s}u\bar{s}$ or $d\bar{s}\bar{d}s$	$K\bar{K}$	2^{++}	1755 ± 10	67 ± 12	[67]
$f_2(2300)$	$u\bar{s}u\bar{s}$ or $d\bar{s}\bar{d}s$	$\Lambda\bar{\Lambda}$	2^{++}	2297 ± 28	149 ± 40	[68]
$\omega(2290)$	$u\bar{s}u\bar{s}$ or $d\bar{s}\bar{d}s$	$\Lambda\bar{\Lambda}$	1^{--}	2290 ± 20	275 ± 35	[69], [70], [71]
$f_3(2300)$	$u\bar{s}u\bar{s}$ or $d\bar{s}\bar{d}s$	$\Lambda\bar{\Lambda}$	3^{++}	2334 ± 25	200 ± 20	[69], [70]
$X(3250)$	$\bar{u}s u\bar{s}$ or $\bar{d}s d\bar{s}$	$\Lambda\bar{p}K^+$???	$3250 \pm 8 \pm 20$	45 ± 18	[72]
$X(3250)$	$\bar{u}s u\bar{s}$ or $\bar{d}s d\bar{s}$	$\Lambda\bar{p}K^+\pi^\pm$ $K_S^0 p\bar{p}K^\pm$???	$3245 \pm 8 \pm 20$	25 ± 11	[72]

Table 13: $T_{u\bar{d}u\bar{d}}$ or $T_{d\bar{d}d\bar{d}}$ tetraquark candidates.

Thry Width [MeV]	Mesons Pair	Meson Threshold [MeV]	Baryon Anti- baryon	Baryonic Threshold [MeV]	Genuine
79 – 364	K^-K^+	988	$\Lambda^0\bar{\Lambda}^0$	2232	
30 – 59	$\phi(1020)\pi_u^0$	1154	$\Sigma^+\bar{\Sigma}^-$ $\Xi^0\bar{\Xi}^0$	2378 2630	

Table 14: $T_{s\bar{s}u\bar{u}}$ thresholds.

J Spec	a_{T_j}	n Spec	a_{T_n}
1591 – 1755		1559 – 1727	
1968 – 2097		1956 – 2085	
2272 – 2382		2272 – 2382	
2535 – 2633		2544 – 2641	
2770 – 2859		2786 – 2875	
2985 – 3067		3008 – 3089	
3184 – 3261	-1.6--1.2	3212 – 3288	-1.5--1.1
3371 – 3443		3403 – 3475	
3547 – 3615		3584 – 3651	
3714 – 3779		3755 – 3819	
3873 – 3936		3918 – 3980	
4026 – 4086		4075 – 4134	

Table 15: $T_{s\bar{s}u\bar{u}}$ (J, M^2) predictions.

Table 16: $T_{s\bar{s}u\bar{u}}$ (n, M^2) predictions.

From table 16 we can see that indeed states $f_2(2300)$ and $f_2(1750)$ belong to the same predicted n trajectory. The second row is the first state above the baryon-antibaryon threshold.

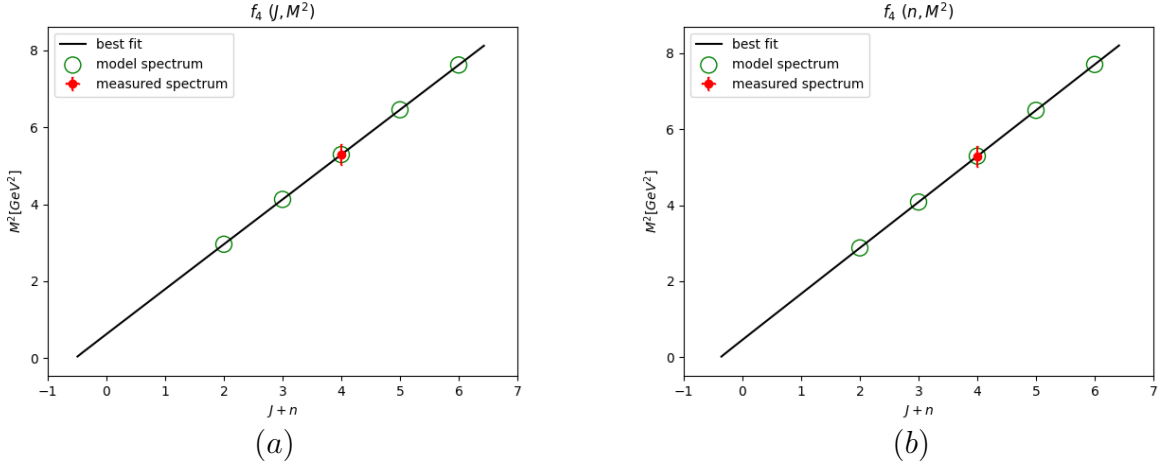


Figure 28: (a) is (J, M^2) $f_4(2300)$ MHRT, (b) (n, M^2) $f_4(2300)$ MHRT. In both cases it is assumed to be a tetraquark due to its decay channel.

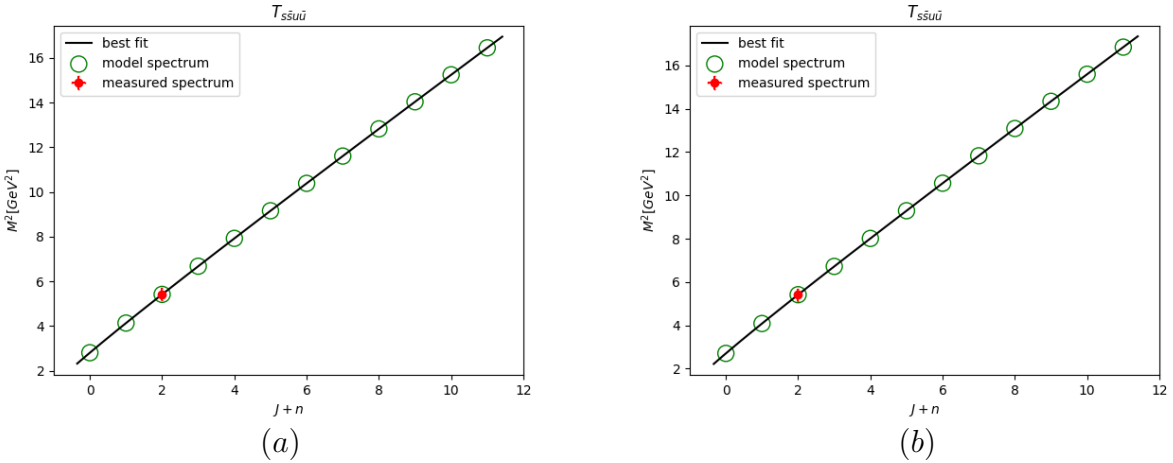


Figure 29: (a) is (J, M^2) $T_{u\bar{s}\bar{u}s}$ or $T_{d\bar{s}\bar{d}s}$ predicted HMRT, (b) (n, M^2) $T_{u\bar{s}\bar{u}s}$ or $T_{d\bar{s}\bar{d}s}$ predicted HMRT.

All states ($f_2(2300)$, $\omega(2290)$ and $f_3(2300)$) are on the predicted trajectories, differ only by the composition of $J + n$. The predicted width is a bit above the measured one for $f_2(2300)$ and $f_3(2300)$, but it provides a good estimation.

We first create a trajectory in the (n, M^2) plane for $f_2(1750)$ and $f_2(2300)$. The first state didn't match any f or ω/f trajectory so far, and it was selected since its meson-pair minimal quark content matches the $f_2(2300)$. We expect the fit to match the mesons slope and the endpoint masses to be similar to the sum of the m_s and $m_{u/d}$.

7.2.3.1 $\omega(2290)$

This state was observed in $\omega(2290) \rightarrow \Lambda\bar{\Lambda}$. This state was predicted to exist in [10] as the analog of the decay of $\psi(4660)$ into a pair of $\Lambda_c\bar{\Lambda}_c$.

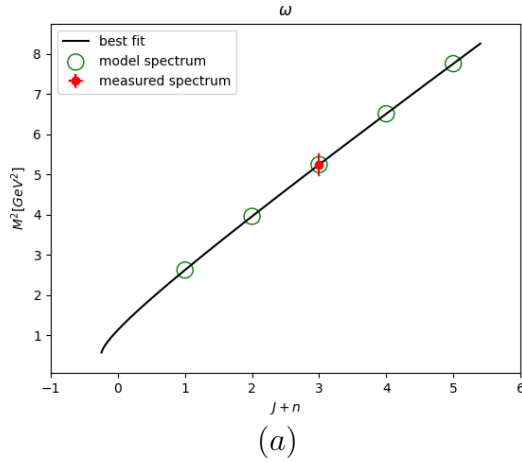
Tables 17 and 18 are the built HMRT that includes the measured $\omega(2290)$ and 30 are the plot of these trajectories. These are consistent with tables 15 and 16. The intercept values are $a_J = -0.24$ and $a_n = -1.13$.

<i>State</i>	M [MeV]	Thry M [MeV]	J	Thry n	Thry $J+n$
		1619			1
		1989			2
$\omega(2290)$	2290	2290	1	2	3
		2551			4
		2785			5

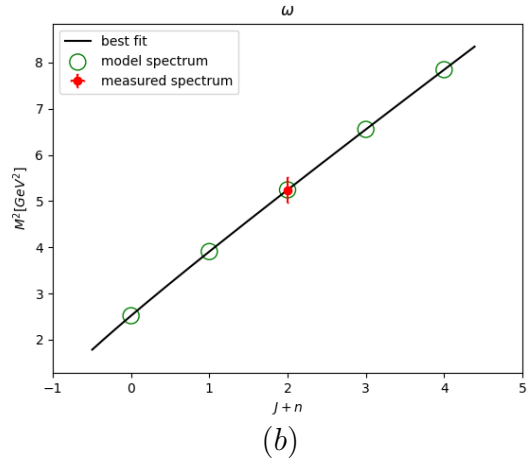
Table 17: $\omega(2290)(J, M^2)$ HMRT.

<i>State</i>	M [MeV]	Thry M [MeV]	J	Thry n	Thry $J+n$
		1587			0
		1977			1
$\omega(2290)$	2290	2290	1	1	2
		2560			3
		2801			4

Table 18: $\omega(2290)(n, M^2)$ HMRT.



(a)



(b)

Figure 30: (a) is (J, M^2) $\omega(2290)$ MHRT, (b) (n, M^2) $\omega(2290)$ MHRT. In both cases it is assumed to be a tetraquark due to its decay channel.

7.2.3.2 $f_2(2300)$

This state was observed in $f_2(2300) \rightarrow \Lambda\bar{\Lambda}$. Most of the states of f_2 do not match any meson trajectory that we built so far. The predicted (n, M^2) HMRT provides indication for the states that may be considered as tetraquarks, assuming $f_2(2300)$, which decays to $\Lambda\bar{\Lambda}$ just above threshold, is on the trajectory. We searched the f_2 known states for other states on the HMRT and found also $f_2(1640)$ that decays to $K\bar{K}$. Both $f_2(1750)$ and $f_2(1640)$ fit the (n, M^2) predicted tetraquark trajectory.

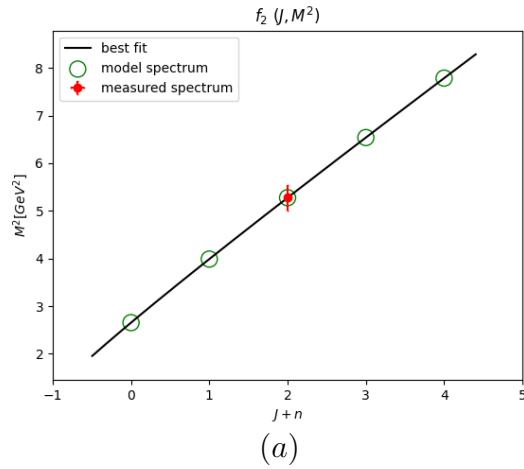
Tables 19 and 20 are the built HMRT that includes the measured $f_2(2300)$ and 31 are the plot of these trajectories. These are consistent with tables 15 and 16. The intercept values are $a_J = -1.27$ and $a_n = -1.15$.

<i>State</i>	M [MeV]	Thry M [MeV]	J	Thry n	Thry $J+n$
		1629			0
		1997			1
$f(2300)$	2297	2297	2	0	2
		2557			3
		2790			4

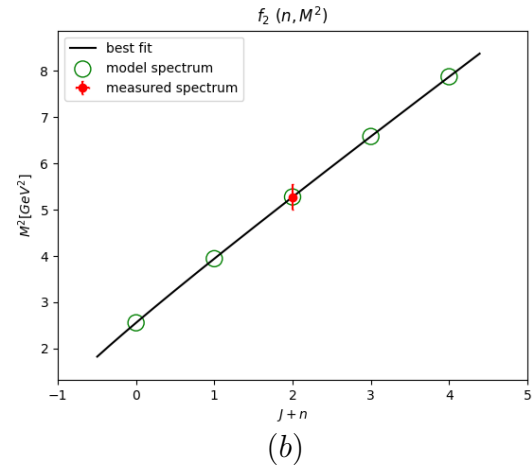
Table 19: $f_2(2300)(J, M^2)$ HMRT.

<i>State</i>	M [MeV]	Thry M [MeV]	J	Thry n	Thry $J+n$
		1598			0
		1985			1
$f(2300)$	2297	2297	2	0	2
		2566			3
		2806			4

Table 20: $f_2(2300)(n, M^2)$ HMRT.



(a)



(b)

Figure 31: (a) is (J, M^2) $f_2(2300)$ MHRT, (b) (n, M^2) $f_2(2300)$ MHRT. In both cases it is assumed to be a tetraquark due to its decay channel.

7.2.3.3 $f_3(2300)$

This state was observed in $f_3(2300) \rightarrow \Lambda\bar{\Lambda}$. Tables 21 and 22 are the built HMRT that includes the measured $f_3(2300)$ and 32 are the plot of these trajectories. These are consistent with tables 15 and 16. The intercept values are $a_J = -0.40$ and $a_n = -0.28$.

<i>State</i>	M [MeV]	Thry M [MeV]	J	Thry n	Thry $J+n$
		1685			1
		2041			2
$f(2300)$	2334	2334	3	0	3
		2590			4
		2820			5

Table 21: $f_3(2300)(J, M^2)$ HMRT.

<i>State</i>	M [MeV]	Thry M [MeV]	J	Thry n	Thry $J+n$
		1655			1
		2029			2
$f(2300)$	2334	2334	3	0	3
		2599			4
		2836			5

Table 22: $f_3(2300)(n, M^2)$ HMRT.

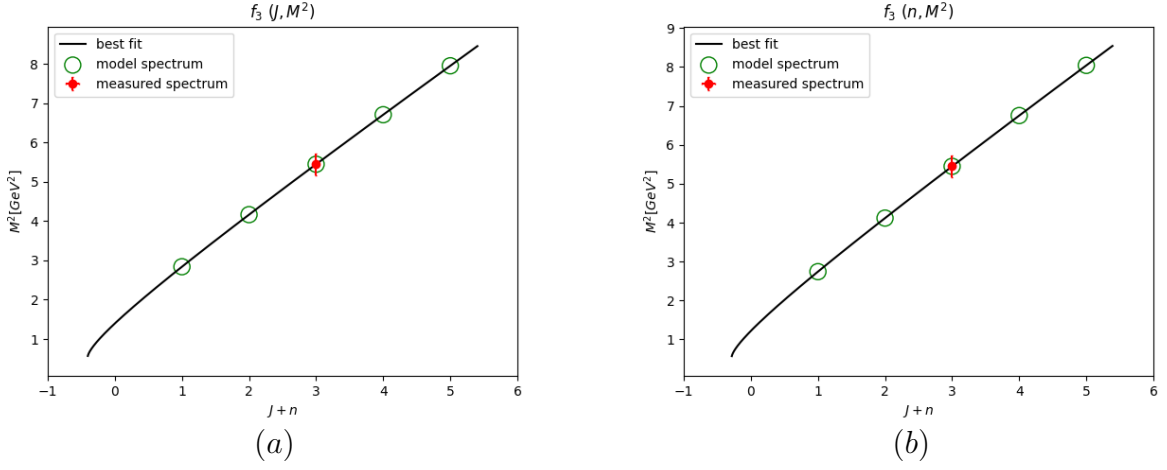


Figure 32: (a) is (J, M^2) $f_3(2300)$ MHRT, (b) (n, M^2) $f_3(2300)$ MHRT. In both cases it is assumed to be a tetraquark due to its decay channel.

7.2.3.4 $X(3250)$

This state is categorized as a meson in PDG database. Table 15 indeed predicts the mass of both $X(3250)$ states, implying they may be on the J trajectory of $T_{u\bar{s}\bar{u}\bar{s}}$.

However, the decay product combination $\Lambda\bar{p}K^+$ could originate from a tetraquark with a configuration as in 12, that decay through string tear to a tetra-like pentaquark and a baryon. In this paper we focused on the simple tetraquark configuration, therefore we leave the categorization of this state as an open question.

7.2.4 $K(3100)$ ($T_{s\bar{u}u\bar{d}}$)

This state (table 23) was observed only in baryonic decays, and decays also to $K(3100)^0 \rightarrow \Sigma^+\bar{p}$ [72]. Tables 25 and 26 are the predicted HMRTs in both planes. The thresholds and predicted width are at table 24.

Candidate	Quarks Content	Selected Decay Channels	J^{PC}	Mass [MeV]	Width [MeV]	Ref.
$K(3100)^0$	$u\bar{s}\bar{u}\bar{d}$	$\Sigma(1385)^+\bar{p}$???	~ 3100	$\sim 10 - 70$	[72]

Table 23: $T_{u\bar{u}\bar{u}\bar{d}}$ or $T_{\bar{u}d\bar{d}\bar{d}}$ exotic candidate.

Thry Width [MeV]	Mesons Pair	Meson Threshold [MeV]	Baryon Anti-baryon	Baryonic Threshold [MeV]	Genuine
45 – 209	$K^0\pi_u^0$	633	$n\bar{\Lambda}^0$	2056	
34 – 66	$\pi^-\bar{K}^+$	634	$p\bar{\Sigma}^-$ $\Lambda^0\bar{\Xi}^0$	2127 2431	

Table 24: $T_{d\bar{s}u\bar{u}}$ thresholds.

J Spec	a_{T_J}
1378 – 1547	
1778 – 1908	
2096 – 2206	
2369 – 2466	
2611 – 2699	
2832 – 2913	-1.5--1.2
3036 – 3112	
3227 – 3298	
3407 – 3474	
3577 – 3641	
3739 – 3800	
3894 – 3953	

Table 25: $T_{d\bar{s}u\bar{u}} (J, M^2)$ predictions.

n Spec	a_{T_n}
1344 – 1517	
1765 – 1896	
2096 – 2206	
2378 – 2475	
2628 – 2715	
2855 – 2935	
3065 – 3139	-1.4--1.0
3260 – 3330	
3444 – 3511	
3619 – 3682	
3785 – 3845	
3944 – 4001	

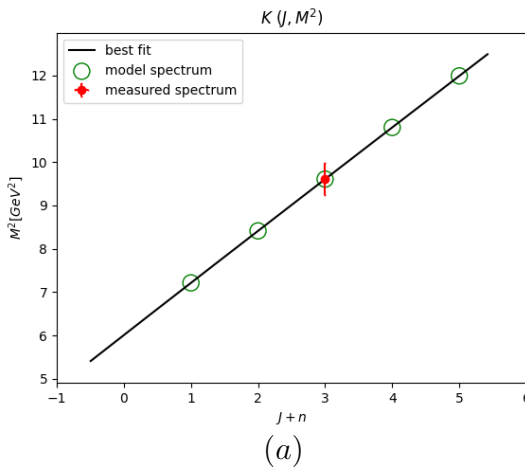
Table 26: $T_{d\bar{s}u\bar{u}} (n, M^2)$ predictions.

We built its HMRTs in (n, M^2) and (J, M^2) (tables 27 and 28) according to the mesonic case slopes, which are consistent with 27 and 28. The intercepts are $a_J = -4.22$ and $a_n = -3.81$.

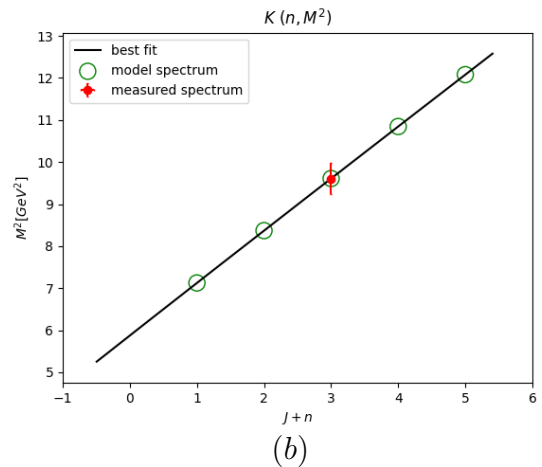
State	M [MeV]	Thry M [MeV]	J	Thry n	Thry $J + n$
		2686			1
		2901			2
$K(3100)^+$	3100	3100			3
		3287			4
		3463			5

Table 27: $K(3100)$ (J, M^2) HMRT.

State	M [MeV]	Thry M [MeV]	J	Thry n	Thry $J + n$
		2669			1
		2893			2
$K(3100)^+$	3100	3100			3
		3293			4
		3476			5

Table 28: $K(3100)$ (n, M^2) HMRT.

(a)



(b)

Figure 33: (a) is (J, M^2) $K(3100)$ MHRT, (b) (n, M^2) $K(3100)$ MHRT. In both cases it is assumed to be a tetraquark due to its decay channel.

7.2.5 $T_{c\bar{u}u\bar{s}}$ or $T_{\bar{c}d\bar{u}s}$

For a tetraquarks with the quark content $u\bar{u}s\bar{s}$ or $d\bar{d}s\bar{s}$ (table 29). The candidate resonances are presented in table. We generated the predicted HMRTs for this quark content in tables 31 and 32, and the thresholds table 30 includes the predicted width. The HMRTs are also plotted in 34.

Candidate	Quarks Content	Selected Decay Channels	J^{PC}	Mass [MeV]	Width [MeV]	Ref.
$X(2632)$	$c\bar{u}u\bar{s}$	D^0K^+ $D_s^+\eta$??	2635.2 ± 3.3	< 17	[73]
$T_{cs0}(2900)^0$	$\bar{c}du\bar{s}$	D^-K^+	0^+	2866 ± 7	57 ± 13	[74]
$T_{cs1}(2900)^0$	$\bar{c}d\bar{u}s$	D^-K^+	1^-	2904 ± 5	110 ± 12	[74]
$T_{c\bar{s}0}^a(2900)^0$	$c\bar{s}\bar{u}d$	$D_s^+\pi^-$	$0^?$	$2892 \pm 14 \pm 15$	$119 \pm 26 \pm 13$	[75]
$T_{c\bar{s}0}^a(2900)^{++}$	$c\bar{s}ud$	$D_s^+\pi^+$	$0^?$	$2921 \pm 17 \pm 20$	$137 \pm 32 \pm 17$	[75]

Table 29: $T_{c\bar{u}u\bar{s}}$ or $T_{\bar{c}d\bar{u}s}$ tetraquark candidates.

Thry Width [MeV]	Mesons Pair	Meson Threshold [MeV]	Baryon Anti-baryon	Baryonic Threshold [MeV]	Genuine
$98 - 147$	$\pi^- D_s^-$	2108	$\Sigma^-\Lambda_c^-$	3483	
$29 - 59$	D^-K^-	2364	$\Lambda^0\bar{\Sigma}_c^{--}$ $\Xi^-\bar{\Xi}_c^-$	3570 3790	**

Table 30: $T_{d\bar{c}s\bar{u}}$ thresholds.

J Spec	a_{T_J}	n Spec	a_{T_n}
2946 – 3085		2628 – 2791	
3252 – 3374		3121 – 3250	
3523 – 3633		3523 – 3633	
3769 – 3870		3872 – 3970	
3996 – 4091		4186 – 4275	
4209 – 4298		4473 – 4556	
4409 – 4493	-2.1--1.6	4740 – 4818	-1.5--1.2
4599 – 4679		4991 – 5064	
4780 – 4856		5228 – 5297	
4953 – 5027		5453 – 5519	
5120 – 5191		5668 – 5731	
5281 – 5349		5874 – 5935	

Table 31: $T_{d\bar{c}s\bar{u}}$ (J, M^2) predictions.

Table 32: $T_{d\bar{c}s\bar{u}}$ (n, M^2) predictions.

We can see from tables 31, 32 that $X(2632)$ fit the n HMRT, while the other states are within error range to the J trajectory. The difference between the actual mass of the states and the predicted one is related to the difference in quantum numbers and the actual quark content. The HISH model does not differentiate between u/d in terms of m .

In the next section, we analysed and fitted the T_{cs} measured states.

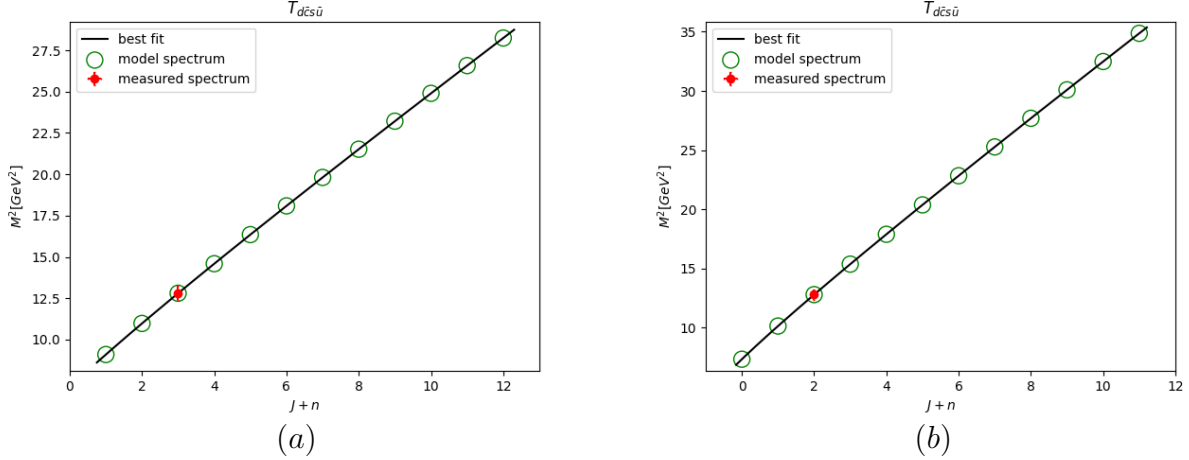


Figure 34: (a) is (J, M^2) $T_{c\bar{u}u\bar{s}}$ or $T_{cd\bar{u}\bar{s}}$ predicted HMRT, (b) (n, M^2) $T_{c\bar{u}u\bar{s}}$ or $T_{cd\bar{u}\bar{s}}$ predicted HMRT.

7.2.5.1 $X(2632)$

This state was observed in $X(2632) \rightarrow D^0 K^+$ and $X(2632) \rightarrow D_s^+ \eta$.

Tables 33 and 34 are the built HMRT that includes the measured $X(2632)$ and 35 are the plot of these trajectories. These are consistent with tables 31 and 32. The intercept values are $a_J = -0.77$ and $a_n = -1.23$.

State	M [MeV]	Thry M [MeV]	J	Thry n	Thry $J + n$
$X(2632)$	2635	2635			1
		2988			2
		3289			3
		3556			4
		3799			5

Table 33: $X(2632)$ (J, M^2) HMRT.

State	M [MeV]	Thry M [MeV]	J	Thry n	Thry $J + n$
$X(2632)$	2635	2635			0
		3127			1
		3528			2
		3876			3
		4190			4

Table 34: $X(2632)$ (n, M^2) HMRT.

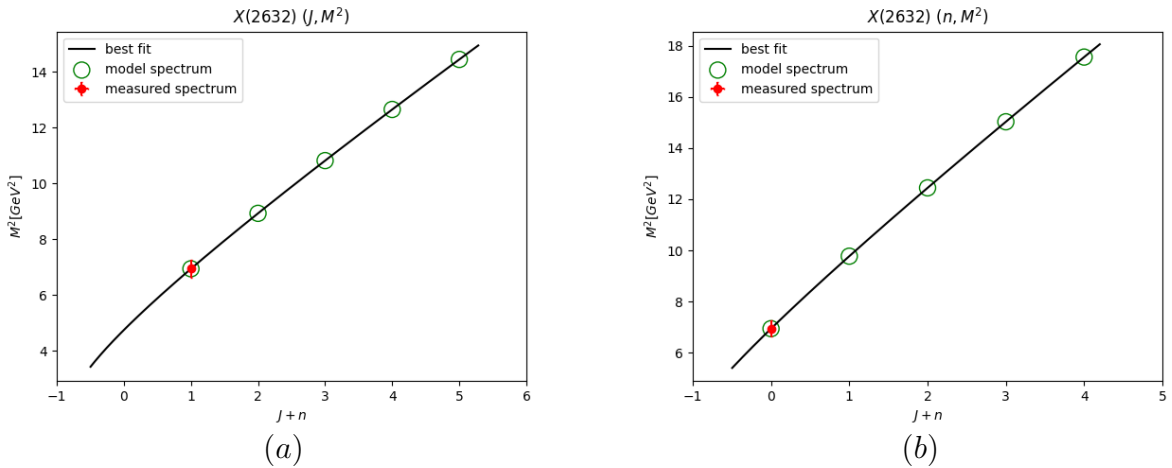


Figure 35: (a) is (J, M^2) $X(2632)$ MHRT, (b) (n, M^2) $X(2632)$ MHRT. In both cases it is assumed to be a tetraquark due to its decay channel.

7.2.6 T_{cs} (with quark content $c\bar{d}s\bar{u}$)

In [105] the states T_{cs0} and T_{cs1} were observed. Both tetraquarks candidates have roughly the same mass. This implies that the total quantity $J + n$ is the same. The decay channel in which these states were observed is D^-K^+ , which is according to the annihilation mechanism. This is expected, since the string tear threshold for baryonia ($\Xi_c p$ pair) creation is higher at around $3.4 GeV$. Both trajectories are built using the D_s slopes as calculated in [7].

7.2.6.1 T_{cs0}^0 HMRTs

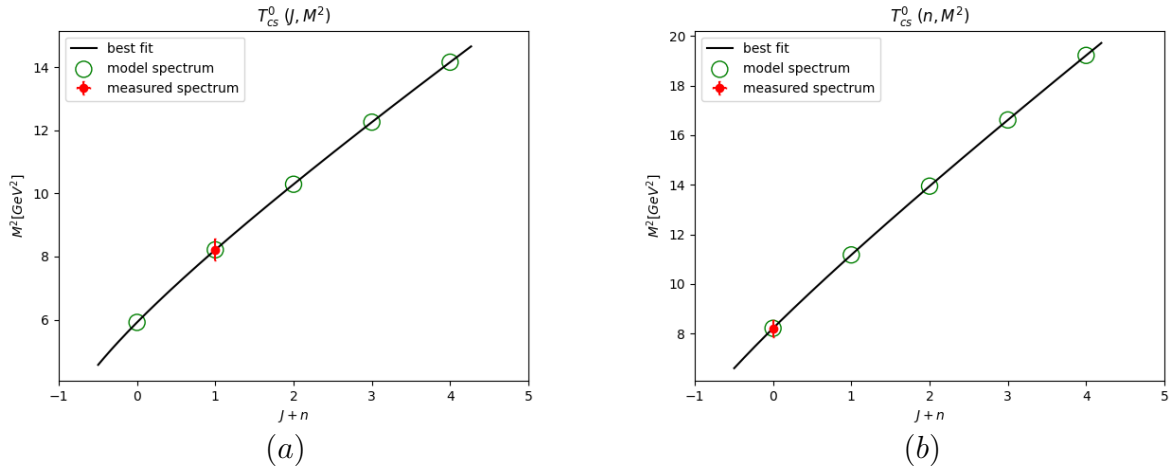


Figure 36: (a) is (J, M^2) T_{cs0}^0 MHRT, (b) (n, M^2) T_{cs0}^0 MHRT by a single point. The trajectory was built with fixed massive endpoints according to the universal fit done for mesons.

State	M [MeV]	Thry M [MeV]	J	Thry n	Thry $J + n$	State	M [MeV]	Thry M [MeV]	J	Thry n	Thry $J + n$
$T(2900)_0^{cs0}$	2866	2866	0	1	1	$T(2900)_0^{cs0}$	2866	2866	0	0	0
		3208			2			3343			1
		3501			3			3734			2
		3762			4			4076			3
		4001			5			4384			4

Table 35: $T_{cs}^0 (J, M^2)$ HMRT.

Table 36: $T_{cs}^0 (n, M^2)$ HMRT.

The intercept values are $a_j = -0.99$ and $a_n = -1.38$. The decays widths are $\Gamma_{tear} \lesssim 127 MeV$ and $\Gamma_{annihilation} \approx 5 MeV$. The sum of them is a good approximation for all the states widths except T_{cs0}

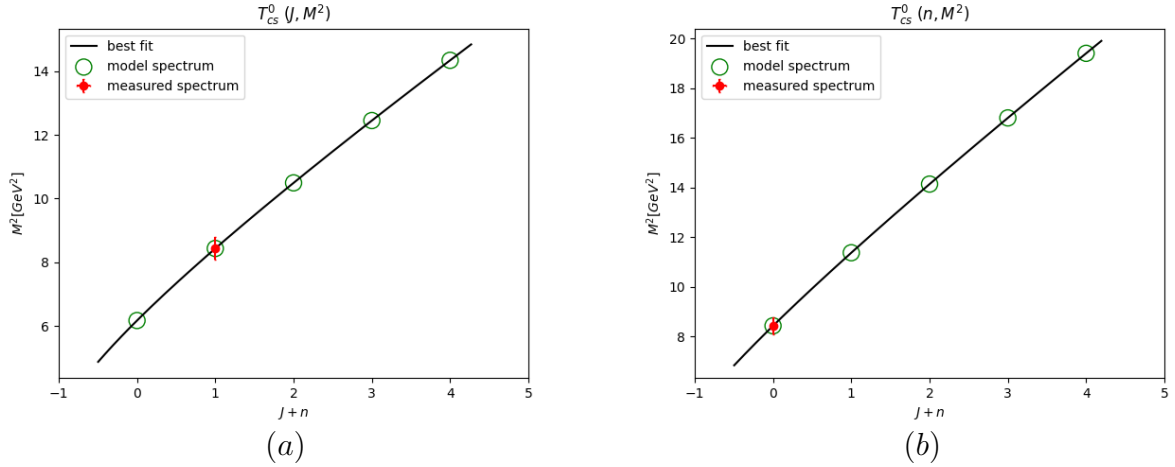


Figure 37: (a) is (J, M^2) T_{cs1}^0 MHRT, (b) (n, M^2) T_{cs1}^0 MHRT by a single point. The trajectory was built with fixed massive endpoints according to the universal fit done for mesons.

7.2.6.2 T_{cs1}^0 HMRTs

State	M [MeV]	Thry M [MeV]	J	Thry n	Thry $J + n$	State	M [MeV]	Thry M [MeV]	J	Thry n	Thry $J + n$
$T(2900)_{cs1}^0$	2904	2904	1	0	1	$T(2900)_{cs1}^0$	2904	2904	1	-1	0
		3240			2			3373			1
		3529			3			3760			2
		3788			4			4099			3
		4024			5			4405			4

Table 37: $T_{cs}^0(J, M^2)$ HMRT.

Table 38: $T_{cs}^0(n, M^2)$ HMRT.

The intercept values are $a_j = -1.10$ and $a_n = -1.45$. The decays widths are $\Gamma_{tear} \lesssim 107\text{MeV}$ and $\Gamma_{annihilation} \approx 22\text{MeV}$.

7.2.7 T_{cs}^a (with quark content $c\bar{s}d\bar{u}$ or $c\bar{s}u\bar{d}$)

In [106] the states $T_{c\bar{s}0}^{a0}$ and $T_{c\bar{s}0}^{a++}$ were observed. Both tetraquarks candidates have roughly the same mass. This implies that the total quantity $J + n$ is the same. All four trajectories in this section are built using the mesonic universal heavy n or J slopes as calculated in the appendix 6.5.

7.2.7.1 $T_{c\bar{s}0}^{a0}$

The neutral state was reconstructed in the decay channel $D_s^+\pi^-$. This is in accordance with the annihilation mechanism, which is expected, due to the string tear threshold for baryonia ($\Lambda\Lambda_c$ pair) creation which is around 3.4GeV . The intercept values are $a_j = -1.48$ and $a_n = -0.72$.

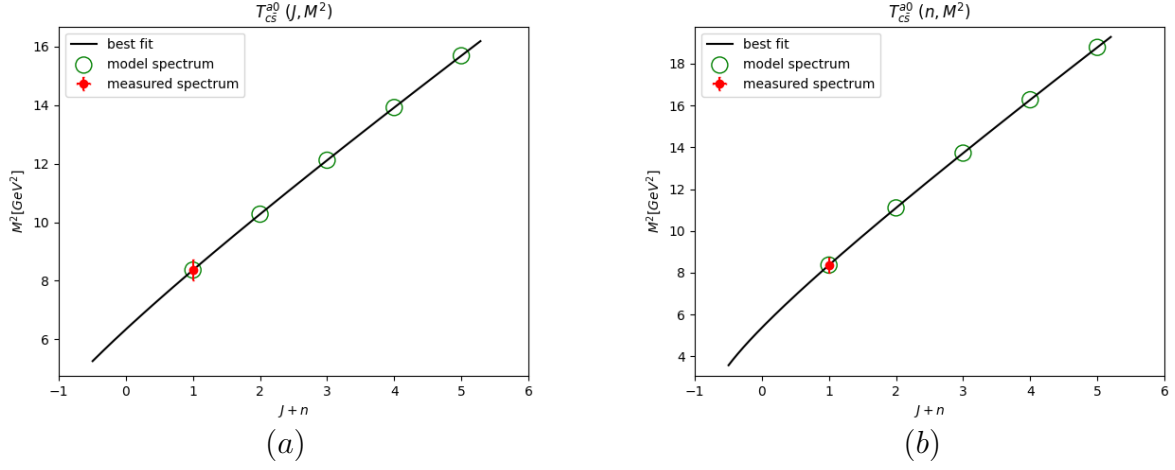


Figure 38: (a) is (J, M^2) $T_{c\bar{s}0}^{a0}$ MHRT, (b) (n, M^2) $T_{c\bar{s}0}^{a0}$ MHRT by a single point. The trajectory was built with fixed massive endpoints according to the universal fit done for mesons.

State	M [MeV]	Thry M [MeV]	J	Thry n	Thry $J + n$	State	M [MeV]	Thry M [MeV]	J	Thry n	Thry $J + n$
$T(2900)_{c\bar{s}0}^{a0}$	2892	2892	0	1	1	$T(2900)_{c\bar{s}0}^{a0}$	2892	2892	0	1	1
		3205			2			3332			2
		3481			3			3704			3
		3731			4			4034			4
		3961			5			4333			5

Table 39: $T_{c\bar{s}}^{a0}$ (J, M^2) HMRT.

Table 40: $T_{c\bar{s}}^{a0}$ (n, M^2) HMRT.

7.2.7.2 $T_{c\bar{s}0}^{a++}$

The positive state was reconstructed in the decay channel $D_s^+ \pi^+$. This is in accordance with the annihilation mechanism, which is expected, due to the string tear threshold for baryonia ($\Lambda\Lambda_c$ pair) creation which is around 3.4GeV . The intercept values are $a_j = -1.57$ and $a_n = -0.78$.

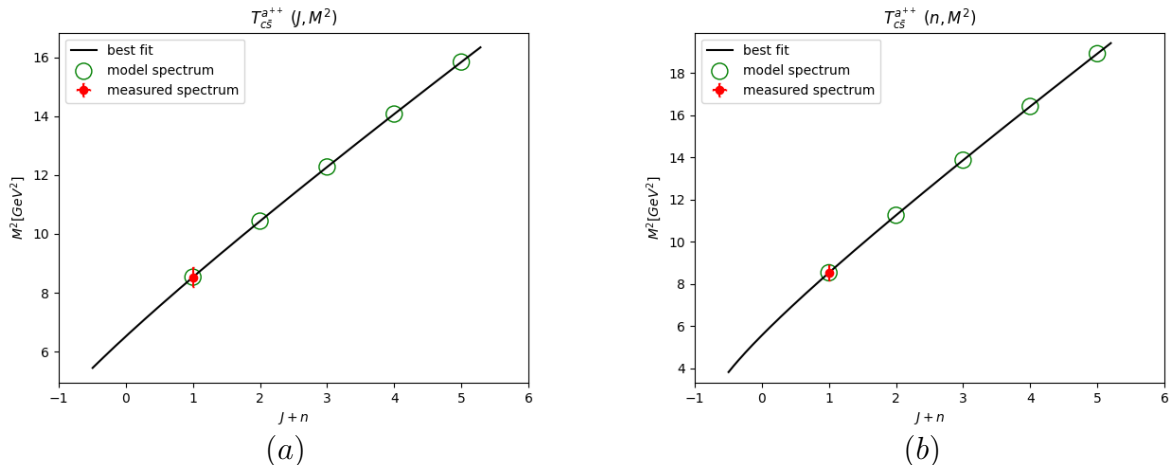


Figure 39: (a) is (J, M^2) $T_{c\bar{s}0}^{a++}$ MHRT, (b) (n, M^2) $T_{c\bar{s}0}^{a++}$ MHRT by a single point. The trajectory was built with fixed massive endpoints according to the universal fit done for mesons.

<i>State</i>	M [MeV]	Thry M [MeV]	J	Thry n	Thry $J + n$	<i>State</i>	M [MeV]	Thry M [MeV]	J	Thry n	Thry $J + n$
$T(2900)_{c\bar{s}0}^{a++}$	2921	2921	0	1	1	$T(2900)_{c\bar{s}0}^{a++}$	2921	2921	0	1	1
		3230			2			3355			2
		3504			3			3725			3
		3751			4			4053			4
		3980			5			4351			5

Table 41: $T_{c\bar{s}}^{a++}$ (J, M^2) HMRT.Table 42: $T_{c\bar{s}}^{a++}$ (n, M^2) HMRT.

7.2.8 $X(3350)$ ($T_{c\bar{d}d\bar{u}}$ or $T_{c\bar{u}u\bar{u}}$)

In [76] and [77] the $X(3350)$ have been observed, both in the decay channel of $\Lambda_c^+ \bar{p}$. There was another pick observed in the same channel in [76] at 3.8GeV², but wasn't observed in [77]. The states analysed in this section are summarized in table 43.

Tables 45 and 46 are the predicted HMRTs in both planes. The thresholds and predicted width are at table 44.

Candidate	Quarks Content	Selected Decay Channels	J^{PC}	Mass [MeV]	Width [MeV]	Ref.
$X(3350)$	$cdd\bar{u}$	$\Lambda_c^+ \bar{p}$	0 or 1??	$3350_{-20}^{+10} \pm 20$	$70_{-30}^{+40} \pm 40$	[76], [77]
$X(3800)^8$	$cdd\bar{u}$	$\Lambda_c^+ \bar{p}$???	3840 ± 10	30 ± 30	[76]

Table 43: $T_{u\bar{u}u\bar{u}}$ or $T_{\bar{u}d\bar{d}\bar{d}}$ exotic candidate.

Thry Width [MeV]	Mesons Pair	Meson Threshold [MeV]	Baryon Anti-baryon	Baryonic Threshold [MeV]	Genuine
79 – 118	$D^0 \pi_d^0$	2000	$\Lambda_c^+ \bar{p}$	3224	
30 – 61	$D^+ \pi^-$	2010	$\Sigma_c^0 \bar{n}$ $\Xi_c^0 \bar{\Lambda}^0$	3394 3586	

Table 44: $T_{c\bar{d}d\bar{u}}$ thresholds.

²This possible resonance was found in [76] with statistical significance of 2.8σ , and wasn't analysed further. We assumed it exists in order to build the HMRT.

J Spec	a_{T_J}
2634 – 2779	
2972 – 3095	
3264 – 3374	
3526 – 3626	
3766 – 3858	
3988 – 4075	-1.6 – -1.2
4197 – 4278	
4394 – 4471	
4581 – 4655	
4760 – 4831	
4931 – 5000	
5097 – 5162	

Table 45: $T_{c\bar{d}d\bar{u}}(J, M^2)$ predictions.

n Spec	a_{T_n}
2270 – 2448	
2829 – 2961	
3264 – 3374	
3635 – 3731	
3964 – 4051	
4263 – 4344	-1.2 – -0.92
4540 – 4615	
4799 – 4869	
5042 – 5109	
5273 – 5337	
5494 – 5554	
5705 – 5763	

Table 46: $T_{c\bar{d}d\bar{u}}(n, M^2)$ predictions.

Since $X(3800)$ needs confirmation, we built the HMRTs for the case in which it exists, and for the case in which we have only one point on the trajectory ($X(3350)$). We calculated both (n, M^2) and (J, M^2) HMRT. According to the predicted spectrum (45 and 46), we do expect a state to exist around $3.8 GeV$ on the (J, M^2) trajectory. Hence, it should have the same momentum value of $X(3350)$ plus 2.

7.2.8.1 $X(3350)(J, M^2)$ fit

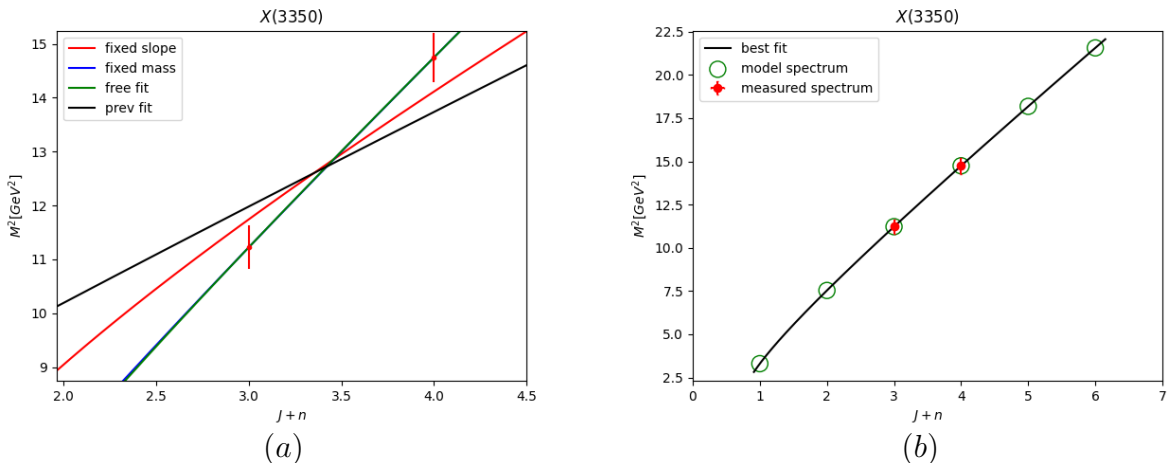


Figure 40: (a) $X(3350)(J, M^2)$ HMRT. The fit was done with fixed massive endpoints according to the universal fit for mesons 1. (b) (J, M^2) $X(3350)$ HMRT best fit is with the fixed masses.

The masses were taken to be $1.33 GeV$ and $0.03 GeV$ in accordance with the mesons universal fit, assuming the diquarks/antidiquarks weighing as the sum of the two quarks in each end. The results of all the fits are summarized at table 47. The spectrum of this trajectory can be found in table [107] including lower and higher states.

Since there are only two points on the trajectories, the best "fit" is the one that produced the lowest value of χ^2_r (where the points are on the trajectory).

χ^2_r	χ^2_{hish}	α'	a	m_1	m_2	Fit Type
0.00	0.00	0.34	0.98	1.34	0.04	free fit
8.37	0.06	0.65	-1.96	1.12	0.03	fixed m_1, m_2 and α'
3.56	0.03	0.65	1.00	2.07	0.01	fixed α'
0.00	0.00	0.32	0.74	1.12	0.03	fixed m_1 and m_2

Table 47: $X(3350)(J, M^2)$ output for each fit.

7.2.8.2 $X(3350)(n, M^2)$ fit

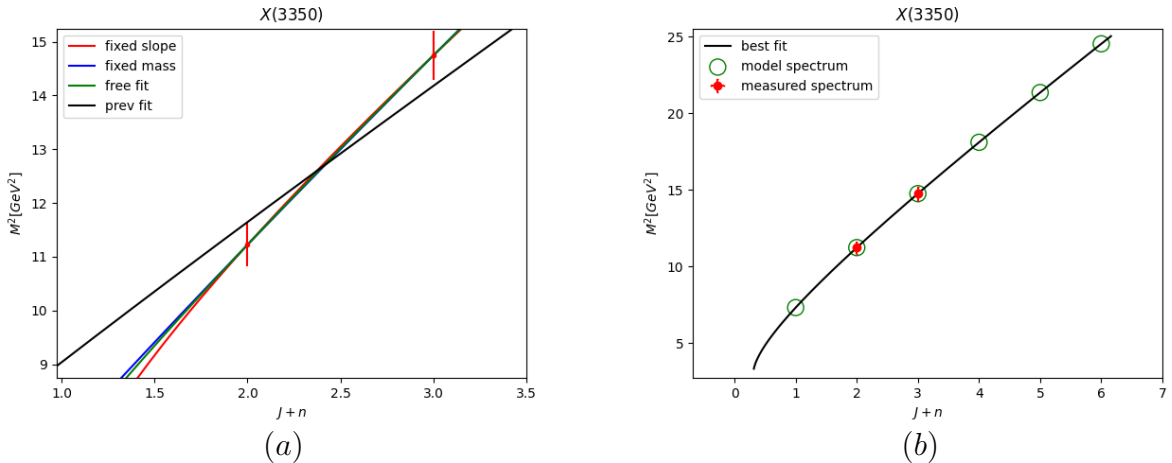


Figure 41: (a) $X(3350)(n, M^2)$ MHRT. The fit was done with fixed massive endpoints according to the universal fit done for mesons. (b) (n, M^2) $X(3350)$ MHRT best fit which was the free fit.

The masses were taken to be 1.33GeV and 0.03GeV with accordance to the universal fit, assuming the diquarks/antidiquarks weighing the same as the heavy quark. The spectrum of this trajectory can be found in table [50] including lower and higher states.

χ^2_r	χ^2_{hish}	α'	a	m_1	m_2	Fit Type
0.00	0.00	0.36	0.31	1.49	0.30	free fit
2.62	0.02	0.45	-1.30	1.12	0.03	fixed m_1, m_2 and α'
0.00	0.00	0.45	0.88	2.11	0.09	fixed α'
0.00	0.00	0.32	-0.26	1.12	0.03	fixed m_1 and m_2

Table 48: $X(3350)(n, M^2)$ output for each fit.

State	M [MeV]	Thry M [MeV]	J	Thry n	Thry $J + n$
		2076			1
		3008			2
$X(3350)$	3350	3427	0	3	3
$X(3800)$	3840	3757	1	3	4
		4040			5
		4292			6

Table 49: $X(3350)(J, M^2)$ HMRT.

State	M [MeV]	Thry M [MeV]	J	Thry n	Thry $J + n$
		2200			0
		2531			1
$X(3350)$	3350	3350	0	2	2
$X(3800)$	3840	3840	0	3	3
		4233			4
		4573			5

Table 50: $X(3350)(n, M^2)$ HMRT.

7.2.8.3 $X(3350)$ spectrum by one point

Since the second state ($X(3800)$) wasn't observed in another experiment, we also calculated the trajectories with a single point shown in the next figure. The intercept values are $a_j = -1.54$ and $a_n = -1.14$.

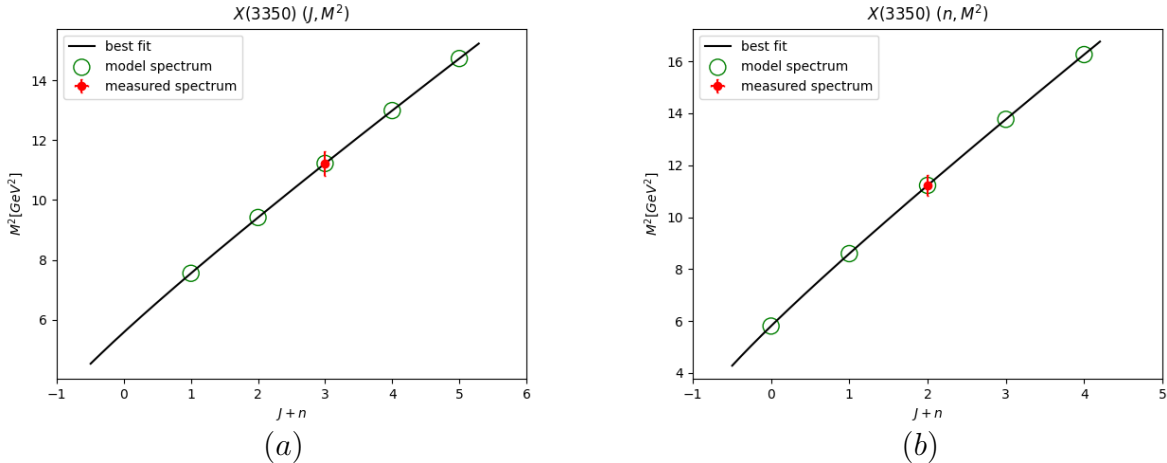


Figure 42: (a) is (J, M^2) $X(3350)$ MHRT, (b) (n, M^2) $X(3350)$ MHRT by a single point. In both cases it is assumed to be a tetraquark due to its decay channel.

State	M [MeV]	Thry M [MeV]	J	Thry n	Thry $J + n$
		2748			1
		3069			2
$X(3350)$	3350	3350			3
		3604			4
		3838			5

Table 51: $X(3350)(J, M^2)$ HMRT by ignoring the $X(3800)$ state. The slope used is the α' value for heavy mesons for J excitation trajectory.

State	M [MeV]	Thry M [MeV]	J	Thry n	Thry $J + n$
		2410			0
		2932			1
$X(3350)$	3350	3350			2
		3710			3
		4032			4

The decay width is estimated to be $\Gamma_{tear} \lesssim 45 MeV$. The ratio is:

$$\frac{\Gamma_{annihilation}}{\Gamma[\Psi(2710)]} = \frac{\exp(-\frac{TL^2}{2}|_{X(3350)})}{\exp(-\frac{TL^2}{2}|_{X(2710)})} \approx 0.41 \quad (58)$$

Based on the predicted state which is lower than the string-tear threshold, this might be the higher state of $D^*(2760)$, also according to its decay channel ($D^+\pi^-$). By taking the width of this state, we can estimate the width of the X(3350):

$$\Gamma_{annihilation} \lesssim 73 MeV \quad (59)$$

7.2.9 $T_{c\bar{d}c\bar{u}}$

For a tetraquarks with the quark content $T_{c\bar{d}c\bar{u}}$ (table 53). The candidate resonance are presented in table 53. We generated the predicted HMRTs for this quark content in tables 55 and 56, and the thresholds table 54 includes the predicted width. The HMRTs are also plotted in 43.

Candidate	Quarks Content	Selected Decay Channels	J^{PC}	Mass [MeV]	Width [MeV]	Ref.
$T_{cc}(3875)$	$cc\bar{u}\bar{d}$	$D^{*+}D^0$ $D^{*0}D^+$??	3874 ± 0.11	0.41 ± 0.17	[78]

Table 53: $T_{c\bar{d}c\bar{u}}$ tetraquark candidates.

Thry Width [MeV]	Mesons Pair	Meson Threshold [MeV]	Baryon Anti-baryon	Baryonic Threshold [MeV]	Genuine
	D^+D^0 D^0D^+	3735 3735	$\Xi_{cc}^+\bar{n}$ $\Xi_{cc}^{++}\bar{p}$ $\Omega_{cc}^+\bar{\Lambda}^0$	4459 4560	**

Table 54: $T_{c\bar{d}c\bar{u}}$ thresholds.

J Spec	a_{T_j}
3983 – 4118	
4255 – 4375	
4499 – 4609	
4723 – 4825	
4932 – 5027	
5128 – 5218	-3.7--3.3
5313 – 5399	
5490 – 5572	
5659 – 5738	
5822 – 5898	
5978 – 6052	
6130 – 6201	

Table 55: $T_{c\bar{d}c\bar{u}} (J, M^2)$ predictions.

n Spec	a_{T_n}
4499 – 4609	
4818 – 4917	
5107 – 5198	
5373 – 5458	
5622 – 5702	
5857 – 5932	
6080 – 6151	-3.0--2.6
6292 – 6361	
6496 – 6561	
6691 – 6755	
6880 – 6941	
7062 – 7122	

Table 56: $T_{c\bar{d}c\bar{u}} (n, M^2)$ predictions.

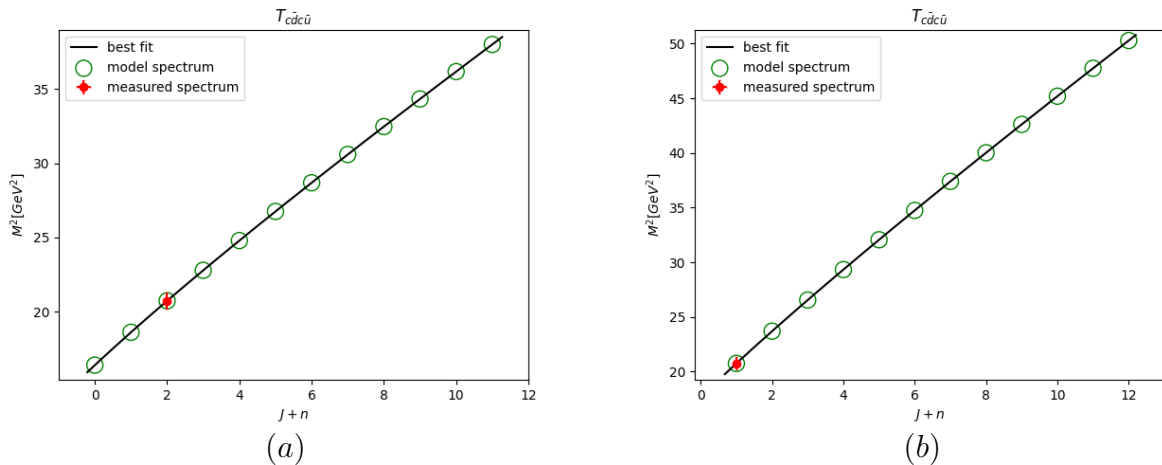


Figure 43: (a) is (J, M^2) $T_{c\bar{d}c\bar{u}}$ predicted HMRT, (b) (n, M^2) $T_{c\bar{d}c\bar{u}}$ predicted HMRT.

In [107] the state T_{cc}^+ was observed. It was also analysed in [108]. It was reconstructed in the decay channel $D^0 D^0 \pi^+$ in accordance with the annihilation mechanism. This is expected since the string tear threshold for baryonia ($\Xi_{cc}^+ p$ pair) creation is around $4.56 GeV$. The trajectories are built using the mesons heavy slopes as calculated at 6.5. The intercepts values are $a_J = -2.89$ and $a_n = -2.00$

State	M [MeV]	Thry M [MeV]	J	Thry n	Thry $J + n$	State	M [MeV]	Thry M [MeV]	J	Thry n	Thry $J + n$
$T(3875)_{cc0}^+$	3870	3870	0	0	0	$T(3875)_{cc0}^+$	3870	3870	0	0	0
		4155			1			4271			1
		4409			2			4615			2
		4640			3			4922			3
		4854			4			5203			4

Table 57: $T_{cc}^+ (J, M^2)$ HMRT.

Table 58: $T_{cc}^+ (n, M^2)$ HMRT.

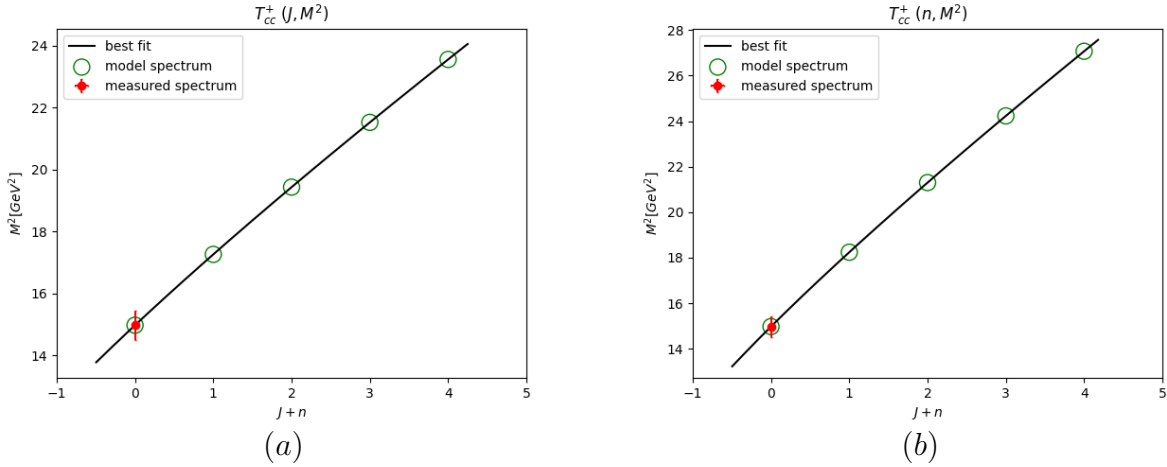


Figure 44: (a) is (J, M^2) T_{cc}^+ MHRT, (b) (n, M^2) T_{cc}^+ MHRT by a single point. The trajectory was built with fixed massive endpoints according to the universal fit done for mesons.

The interesting thing about this state is its width, which is very narrow (54), meaning it is stable. The HISH annihilation decay mechanism suggests that the BV and anti-BV will annihilate in a certain probability, that is dependant on the length of the horizontal string ([13]). In the case of $X(4630)/\psi(4660)$ and $X(6900)$ ([10] and [24]) it proved to be a good approximation to rely on the same $P_{\text{annihilation}}$ value for both states. In the case of T_{cc} , it seems the probability is much lower, despite the length of the string being similar. The conditions in which the annihilation can occur is still an open question. One possible explanation is that the asymmetry between the diquark and antidiquark affects the location of the vertices on the holographic space on the u direction, which reduces the annihilation probability. Anyhow, this requires more research.

7.2.10 $T_{c\bar{c}u\bar{d}}$ or $T_{c\bar{c}d\bar{u}}$

For a tetraquark with the quark content $T_{c\bar{c}u\bar{d}}$ or $T_{c\bar{c}d\bar{u}}$ (table 59). The candidate resonances are presented in table 59. We generated the predicted HMRTs for this quark content in tables 61 and 62, and the thresholds table 60 includes the predicted width. The HMRTs are also plotted in 45.

Candidate	Quarks Content	Selected Decay Channels	J^{PC}	Mass [MeV]	Width [MeV]	Ref.
$Z_c(3900)$	$c\bar{c}u\bar{d}$ $c\bar{c}d\bar{u}$	$J/\psi\pi^\pm$ $D\bar{D}^*\pm$	1^{+-}	3887.1 ± 2.6	28.4 ± 2.6	Many, including [79]
$Z_c(4200)^\pm$	$c\bar{c}u\bar{d}$ or $c\bar{c}d\bar{u}$	$J/\psi\pi^+$	1^{+-7}	4196^{+35}_{-32}	370^{+100}_{-150}	[80]
$Z_c(4430)^\pm$	$c\bar{c}u\bar{d}$ or $c\bar{c}d\bar{u}$	$\pi^+\psi(2S)$ π^+J/ψ	1^{+-7}	4478^{+15}_{-18}	181 ± 31	[81], [82], [83], [84]
$X(4020)^\pm$	$c\bar{c}u\bar{d}$ or $c\bar{c}d\bar{u}$	$D^*\bar{D}^*$ $h_c(1P)\pi^\pm$	$?^{?-}$	4024.1 ± 1.9	13 ± 5	[85], [86] [87], [87]

$X(4051)^\pm$	$c\bar{c}u\bar{d}$ or $c\bar{c}d\bar{u}$	$\pi^+\chi_{c1}(1P)$? [?] + ?	4051^{+24}_{-40}	82^{+50}_{-28}	[88]
$X(4055)^\pm$	$c\bar{c}u\bar{d}$ or $c\bar{c}d\bar{u}$	$\pi^+\psi(2S)$? [?] - ??	4054 ± 3.2	45 ± 13	[89], [90] [91]
$X(4100)^\pm$	$c\bar{c}u\bar{d}$ or $c\bar{c}d\bar{u}$	$\pi^-\eta(1S)$???	4096 ± 28	152^{+80}_{-70}	[92]
$R_{c0}(4240)^\pm$	$c\bar{c}u\bar{d}$ or $c\bar{c}d\bar{u}$	$\pi^-\psi(2S)$	0-- ?	4239^{+50}_{-21}	220^{+120}_{-90}	[93]
$X(4250)^\pm$	$c\bar{c}u\bar{d}$ or $c\bar{c}d\bar{u}$	$\pi^+\chi(1P)$? [?] -7 ?	4248^{+190}_{-50}	177^{+320}_{-70}	[88]

Table 59: $T_{c\bar{c}u\bar{d}}$ or $T_{c\bar{c}d\bar{u}}$ tetraquark candidates.

Thry Width [MeV]	Mesons Pair	Meson Threshold [MeV]	Baryon Anti- baryon	Baryonic Threshold [MeV]	Genuine
11 – 31 34 – 67	$\eta_c(1S)\pi^+$ $D^+\bar{D}^0$	3124 3735	$\Sigma_c^{++}\Lambda_c^-$ $\Lambda_c^+\bar{\Sigma}_c^0$ $\Xi_c^+\bar{\Xi}_c^0$	4740 4740 4938	*

Table 60: $T_{c\bar{c}u\bar{d}}$ thresholds.

J Spec	a_{T_J}	n Spec	a_{T_n}
4373 – 4497		4174 – 4306	
4583 – 4699		4491 – 4611	
4780 – 4890		4780 – 4890	
4967 – 5072		5047 – 5150	
5145 – 5245		5297 – 5394	
5316 – 5412		5533 – 5625	
5480 – 5572	-2.6--2.0	5757 – 5844	-2.0--1.6
5638 – 5727		5971 – 6054	
5790 – 5877		6176 – 6256	
5938 – 6023		6373 – 6450	
6082 – 6164		6563 – 6638	
6222 – 6301		6747 – 6819	

Table 61: $T_{c\bar{c}u\bar{d}} (J, M^2)$ predictions.

Table 62: $T_{c\bar{c}u\bar{d}} (n, M^2)$ predictions.

7.2.10.1 $Z_c (n, M^2)$

All Z_c states were observed in $Z_c \rightarrow J/\psi\pi$ decay channels, but more channels are detailed in table 59. Table 63 is the built HMRTs output that includes all three states $Z_c(3900)$, $Z_c(4200)$

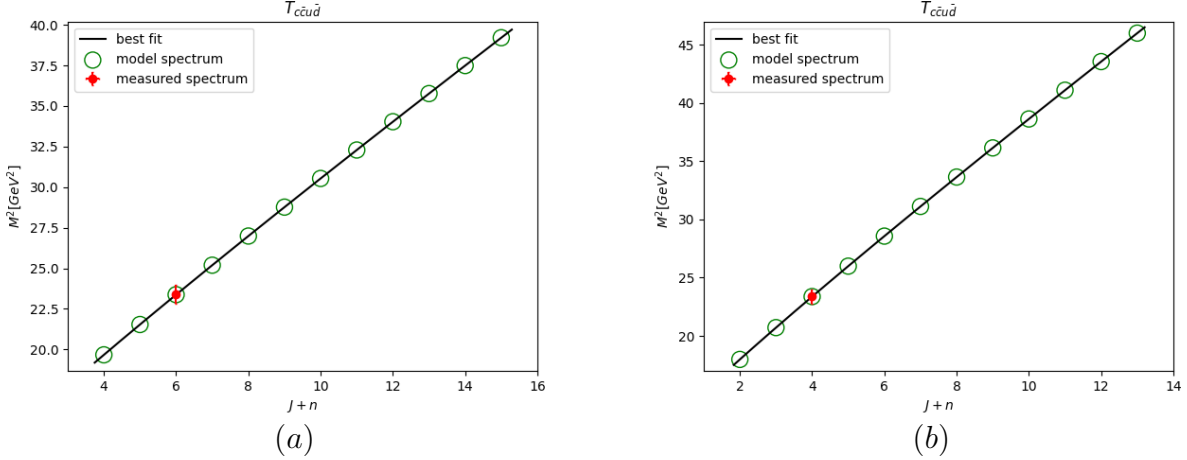


Figure 45: (a) is (J, M^2) $T_{c\bar{c}u\bar{d}}$ or $T_{c\bar{c}d\bar{u}}$ predicted HMRT, (b) (n, M^2) $T_{c\bar{c}u\bar{d}}$ or $T_{c\bar{c}d\bar{u}}$ predicted HMRT.

and $Z_c(4430)$. 46 are the plot of these trajectories. These are consistent with tables 15 and 16. Moreover, the predictions of the states in table 62 is close to the Z_c sample. The intercept value of the best fit is $a_n = -2.10$.

χ_r^2	χ_{hish}^2	α'	a	m_1	m_2	Fit Type
0.00	0.00	0.51	-2.14	1.11	1.11	free fit
0.41	0.00	0.45	-1.64	1.12	1.12	fixed m_1, m_2 and α'
0.75	0.00	0.45	-1.70	1.11	1.11	fixed α'
0.00	0.00	0.51	-2.10	1.12	1.12	fixed m_1 and m_2

Table 63: The fit for Z_c states (59) in the (n, M^2) plane. The best fit is with fixed α' , but all the fits provide similar results and are consistent with the assumption that tetraquarks should admit near slope as the mesons with similar flavour content.

State	M [MeV]	Thry M [MeV]	J	Thry n	Thry $J + n$
$Z(3900)_{c1}$	3887	3851	1	0	1
$Z(4200)_{c1}$	4196	4202	1	1	2
$Z(4430)_{c1}$	4478	4515	1	2	3
		4801			4
		5066			5
		5314			6
		5548			7

Table 64: $Z_c(n, M^2)$ HMRT.

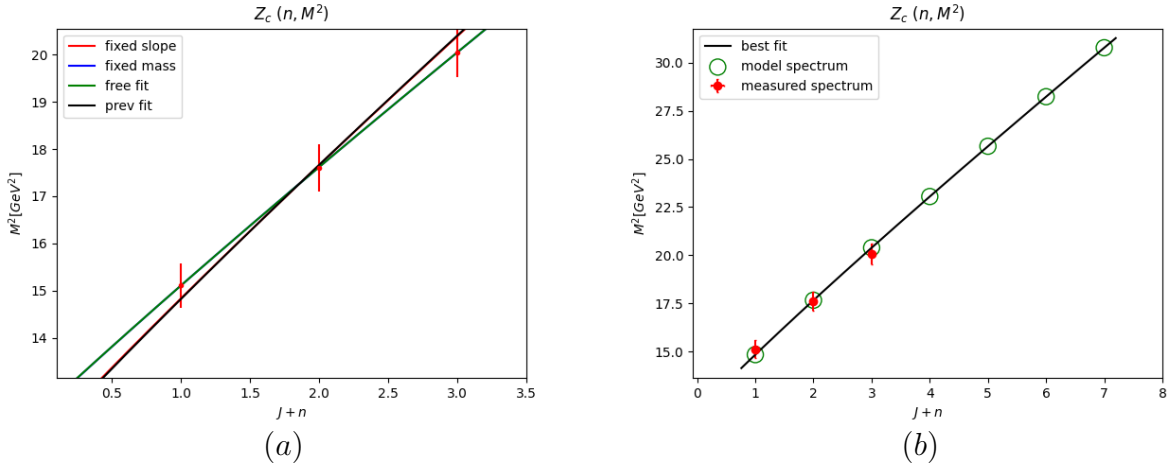


Figure 46: (a) $Z_c(n, M^2)$ HMRTs output, (b) $Z_c(n, M^2)$ best fit (fixed $\alpha' = 0.46$).

7.2.10.2 $Z_c(3900) (J, M^2)$

This state was observed in $Z_c(3900) \rightarrow J/\psi\pi$ and $Z_c(3900) \rightarrow D\bar{D}^*$. Table 65 includes the measured $Z_c(3900)$ and 47 is the plot of the HMRT. It is consistent with table 61. The intercept value is $a_J = -1.96$.

<i>State</i>	M [MeV]	Thry M [MeV]	J	Thry n	Thry $J + n$
		3301			0
		3614			1
$Z(3900)_{c1}$	3887	3887	1	1	2
		4133			3
		4359			4

Table 65: $Z_c(3900) (J, M^2)$ HMRT.

The preferred decay channel of this state is to $D\bar{D}^*$ as opposed to $J/\psi\pi$. One explanation is that it is a molecule and not a compact-multiquark structure. We leave it as an open question for future work.

7.2.10.3 $Z_c(4200) (J, M^2)$

This state was observed in $Z_c(4200) \rightarrow J/\psi\pi$. Table 66 includes the measured $Z_c(4200)$ and 48 is the plot of the HMRT. It is consistent with table 61. The intercept value is $a_J = -2.23$.

<i>State</i>	M [MeV]	Thry M [MeV]	J	Thry n	Thry $J + n$
		3691			1
		3956			2
$Z(4200)_{c1}$	4196	4196	1	2	3
		4417			4
		4624			5

Table 66: $Z_c(4200)$ (J, M^2) HMRT.

7.2.10.4 $Z_c(4430)$ (J, M^2)

This state was observed in $Z_c(4430) \rightarrow J/\psi\pi$ and $Z_c(4430) \rightarrow \psi(2S)\pi$. Table 67 includes the measured $Z_c(4430)$ and 49 is the plot of the HMRT. It is consistent with table 61. The intercept value is $a_J = -1.52$.

<i>State</i>	M [MeV]	Thry M [MeV]	J	Thry n	Thry $J + n$
		4027			3
		4261			4
$Z(4430)_{c1}$	4478	4478	1	4	5
		4681			6
		4873			7

Table 67: $Z_c(4430)$ (J, M^2) HMRT.

7.2.10.5 $X(4020)^{\pm}$

$X(4020)$ was observed in $X(4020) \rightarrow D^*\bar{D}^*$ and $X(4020) \rightarrow h_c(1P)\pi^{\pm}$. Tables 68 and 69 are the built HMRT that includes the measured $X(4020)^{\pm}$ and 50 are the plot of these trajectories. These are consistent with tables 61 and 62. The intercept values are $a_J = -1.51$ and $a_n = -1.12$.

<i>State</i>	M [MeV]	Thry M [MeV]	J	Thry n	Thry $J + n$
		3478			1
		3767			2
$X(4020)^+$	4024	4024			3
		4258			4
		4476			5

Table 68: $X(4020)$ (J, M^2) HMRT.

<i>State</i>	M [MeV]	Thry M [MeV]	J	Thry n	Thry $J + n$
		3179			0
		3643			1
$X(4020)^+$	4024	4024			2
		4357			3
		4657			4

Table 69: $X(4020)$ (n, M^2) HMRT.

7.2.10.6 $X(4051)^{\pm}$

$X(4051)$ was observed in $X(4051) \rightarrow \pi^+\chi_{c1}(1P)$. Tables 70 and 71 are the built HMRT that includes the measured $X(4051)^{\pm}$ and 51 are the plot of these trajectories. These are consistent with tables 61 and 62. The intercept values are $a_J = -1.62$ and $a_n = -1.20$.

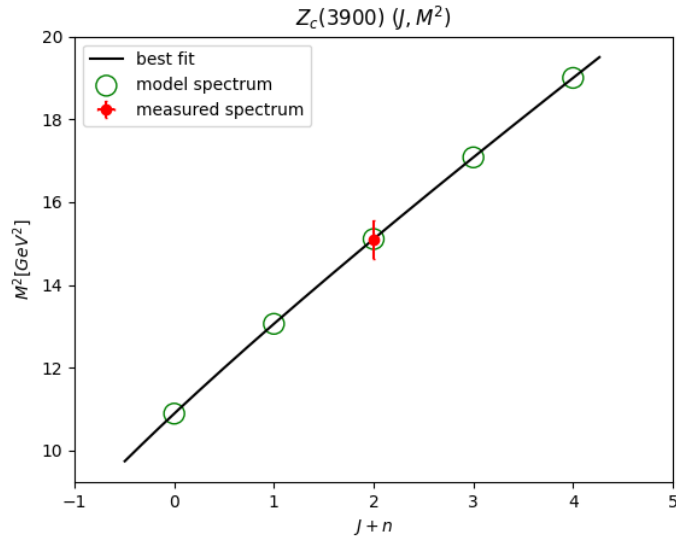


Figure 47: $Z_c(3900)$ (J, M^2) HMRT.

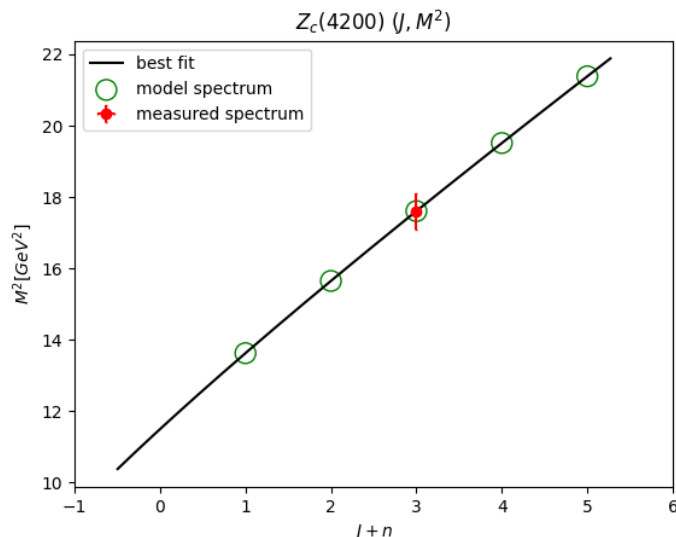


Figure 48: $Z_c(4200)$ (J, M^2) HMRT.

<i>State</i>	M [MeV]	Thry M [MeV]	J	Thry n	Thry $J + n$
		3512			1
		3797			2
$X(4050)^+$	4051	4051			3
		4283			4
		4499			5

Table 70: $X(4051)$ (J, M^2) HMRT.

<i>State</i>	M [MeV]	Thry M [MeV]	J	Thry n	Thry $J + n$
		3219			0
		3675			1
$X(4050)^+$	4051	4051			2
		4381			3
		4679			4

Table 71: $X(4051)$ (n, M^2) HMRT.

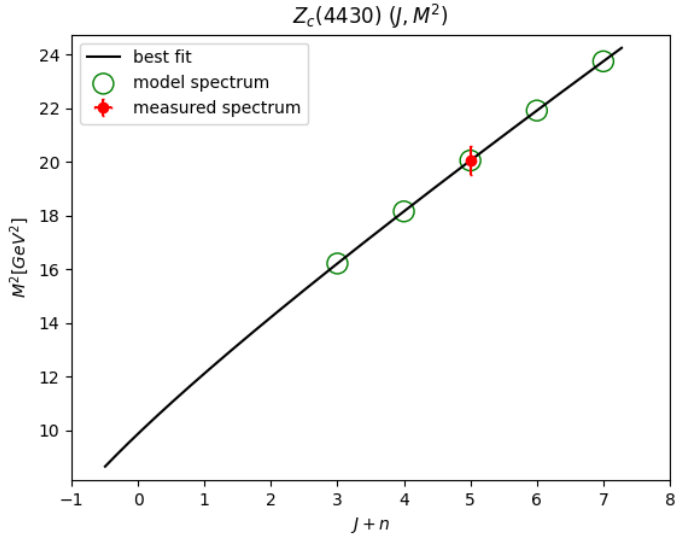


Figure 49: $Z_c(4430)$ (J, M^2) HMRT.

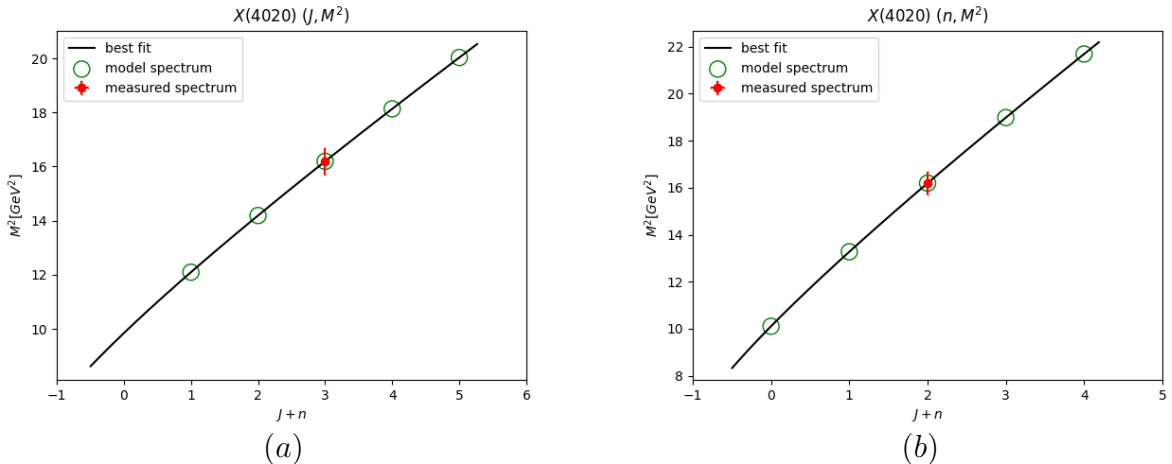


Figure 50: (a) is (J, M^2) $X(4020)$ MHRT, (b) (n, M^2) $X(4020)$ MHRT.

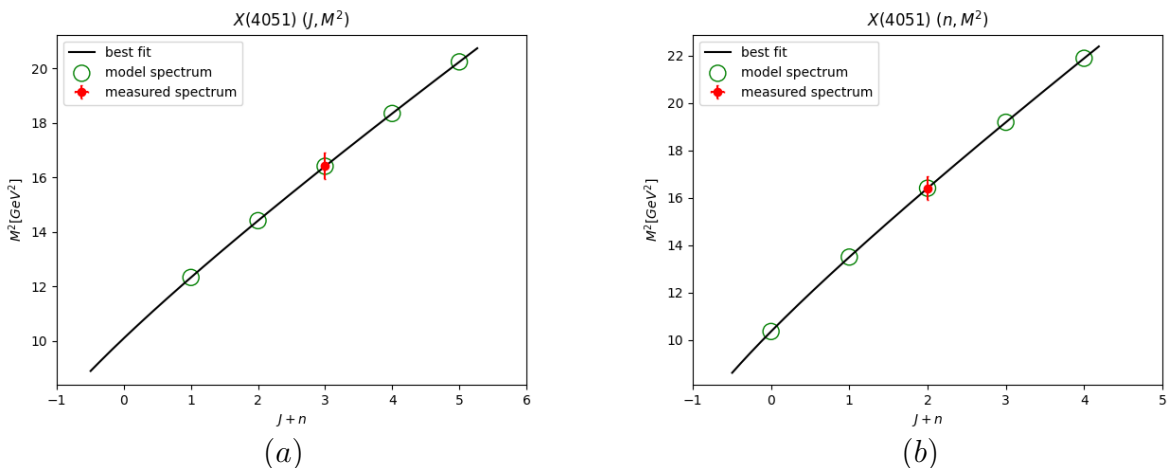


Figure 51: (a) is (J, M^2) $X(4051)$ MHRT, (b) (n, M^2) $X(4051)$ MHRT.

7.2.10.7 $X(4055)^{\pm}$

$X(4055)$ was observed in $X(4055) \rightarrow \pi^+ \psi(2S)$. Tables 72 and 73 are the built HMRT that includes the measured $X(4055)^{\pm}$ and 52 are the plot of these trajectories. These are consistent

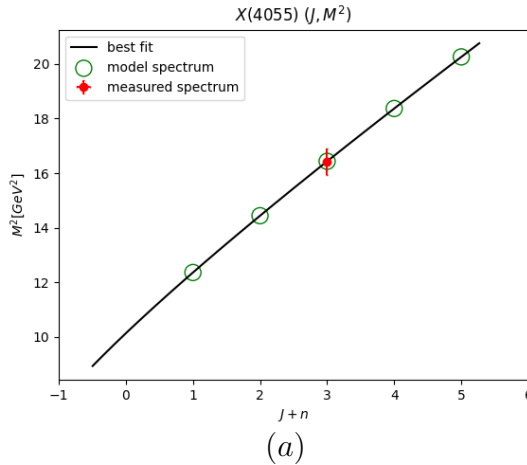
with tables 61 and 62. The intercept values are $a_J = -1.63$ and $a_n = -1.20$.

State	M [MeV]	Thry M [MeV]	J	Thry n	Thry $J + n$
		3516			1
		3800			2
$X(4055)^+$	4054	4054			3
		4286			4
		4501			5

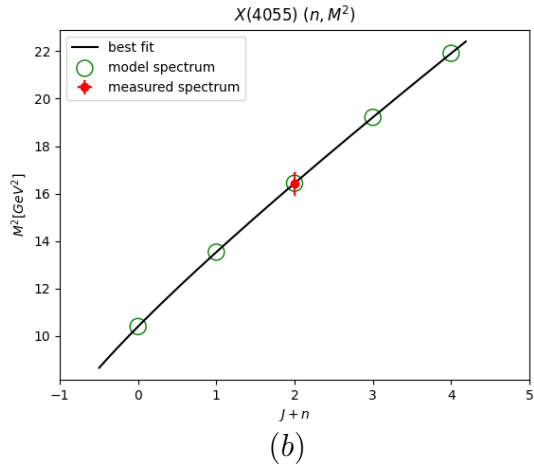
Table 72: $X(4055)$ (J, M^2) HMRT.

State	M [MeV]	Thry M [MeV]	J	Thry n	Thry $J + n$
		3224			0
		3678			1
$X(4055)^+$	4054	4054			2
		4383			3
		4681			4

Table 73: $X(4055)$ (n, M^2) HMRT.



(a)



(b)

Figure 52: (a) is (J, M^2) $X(4055)$ MHRT, (b) (n, M^2) $X(4055)$ MHRT.

7.2.10.8 $X(4100)^{\pm}$

$X(4100)$ was observed in $X(4100) \rightarrow \pi^- \eta(1S)$. Tables 74 and 75 are the built HMRT that includes the measured $X(4100)^{\pm}$ and 53 are the plot of these trajectories. These are consistent with tables 61 and 62. The intercept values are $a_J = -1.80$ and $a_n = -1.36$.

State	M [MeV]	Thry M [MeV]	J	Thry n	Thry $J + n$
		3568			1
		3846			2
$X(4100)^+$	4096	4096			3
		4325			4
		4537			5

Table 74: $X(4100)$ (J, M^2) HMRT.

State	M [MeV]	Thry M [MeV]	J	Thry n	Thry $J + n$
		3285			0
		3727			1
$X(4100)^+$	4096	4096			2
		4421			3
		4716			4

Table 75: $X(4100)$ (n, M^2) HMRT.

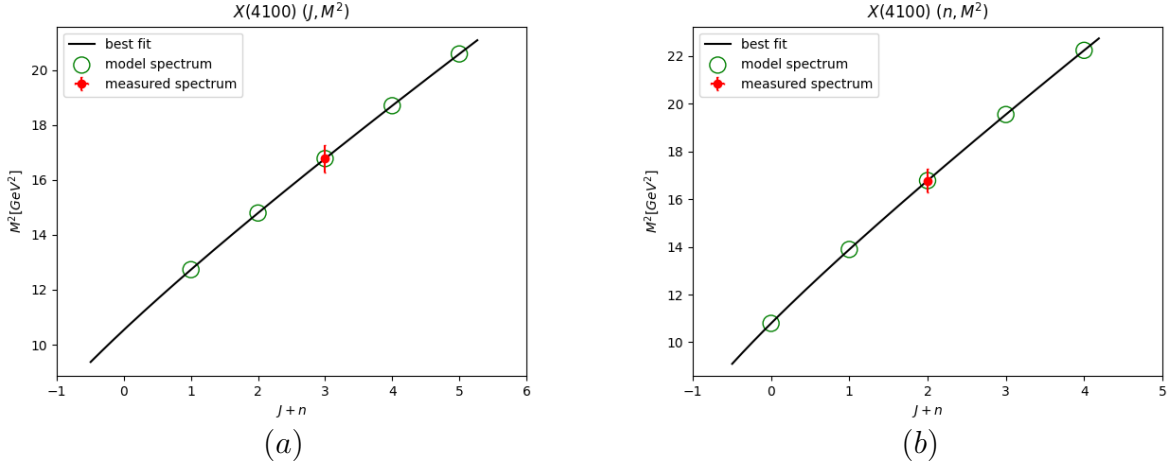


Figure 53: (a) is (J, M^2) $X(4100)$ MHRT, (b) (n, M^2) $X(4100)$ MHRT.

7.2.10.9 $R_{c0}(4240)^{\pm}$

$R_{c0}(4240)^{\pm}$ was observed in $R_{c0}(4240) \rightarrow \pi^- \psi(2S)$. Tables 76 and 77 are the built HMRT that includes the measured $R_{c0}(4240)^{\pm}$ and 54 are the plot of these trajectories. These are consistent with tables 61 and 62. The intercept values are $a_J = -2.42$ and $a_n = -1.75$.

State	M [MeV]	Thry M [MeV]	J	Thry n	Thry $J + n$
		3744			1
		4003			2
$R(4240)_{c0}$	4239	4239	0	3	3
		4457			4
		4662			5

Table 76: $R_{c0}(4240)$ (J, M^2) HMRT.

State	M [MeV]	Thry M [MeV]	J	Thry n	Thry $J + n$
		3486			0
		3891			1
$R(4240)_{c0}$	4239	4239	0	2	2
		4550			3
		4834			4

Table 77: $R_{c0}(4240)$ (n, M^2) HMRT.

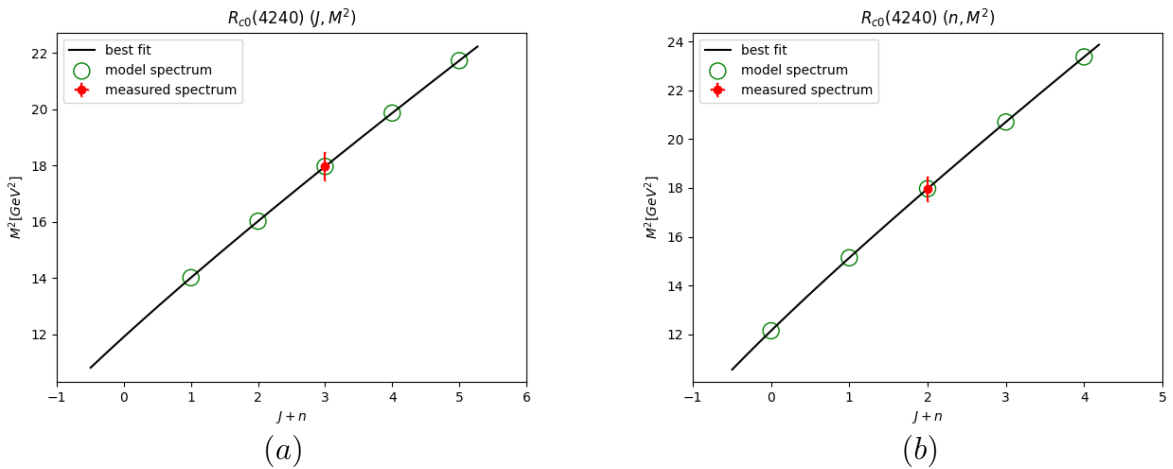


Figure 54: (a) is (J, M^2) $R_{c0}(4240)$ MHRT, (b) (n, M^2) $R_{c0}(4240)$ MHRT.

7.2.10.10 $X(4250)^{\pm}$

$X(4250)$ was observed in $X(4250) \rightarrow \pi^+ \chi(1P)$. Tables 78 and 79 are the built HMRT that includes the measured $X(4250)^{\pm}$ and 55 are the plot of these trajectories. These are consistent with tables 61 and 62. The intercept values are $a_J = -2.42$ and $a_n = -1.75$.

State	M [MeV]	Thry M [MeV]	J	Thry n	Thry $J+n$
		3744			1
		4003			2
$R(4240)_{c0}$	4239	4239	0	3	3
		4457			4
		4662			5

Table 78: $X(4250)$ (J, M^2) HMRT.

State	M [MeV]	Thry M [MeV]	J	Thry n	Thry $J+n$
		3486			0
		3891			1
$R(4240)_{c0}$	4239	4239	0	2	2
		4550			3
		4834			4

Table 79: $X(4250)$ (n, M^2) HMRT.

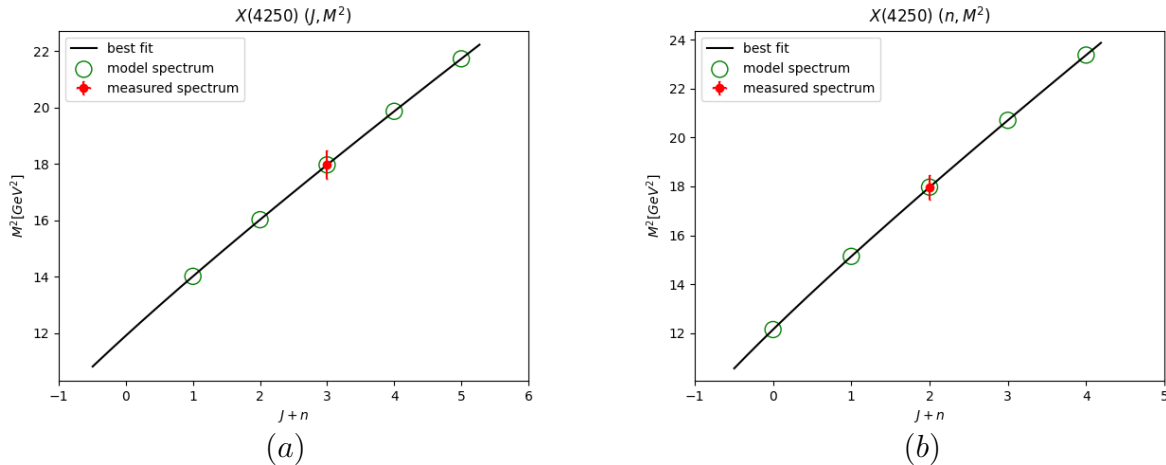


Figure 55: (a) is (J, M^2) $X(4250)$ MHRT, (b) (n, M^2) $X(4250)$ MHRT.

7.2.11 $T_{c\bar{c}u\bar{s}}$ or $T_{c\bar{c}d\bar{s}}$

For a tetraquarks with the quark content $T_{c\bar{c}u\bar{s}}$ (table 80). The candidate resonances are presented in table. We generated the predicted HMRTs for this quark content in tables 82 and 83, and the thresholds table 81 includes the predicted width. The HMRTs are also plotted in 56.

Candidate	Quarks Content	Selected Decay Channels	J^{PC}	Mass [MeV]	Width [MeV]	Ref.
$T_{\psi s1}^\theta(4000)^+$ also $Z_{cs}(4000)^+$	$c\bar{c}u\bar{s}$	$J/\psi K^+$ $D_s^+ \bar{D}^{*0}$ $D_s^{*+} \bar{D}^0$	1^+	$3980 - 4010$	$5 - 150$	
$T_{\psi s1}(4220)^+$ also $Z_{cs}(4220)^+$	$c\bar{c}u\bar{s}$	$J/\psi K^+$	1^+	4216^{+50}_{-40}	233^{+110}_{-90}	
$T_{\psi s1}^\theta(4000)^0$	$c\bar{c}d\bar{s}$	$J/\psi K_S^0$	1^+	3991^{+14}_{-20}	105^{+12+9}_{-10-17}	

Table 80: $T_{c\bar{u}u\bar{s}}$ or $T_{c\bar{d}u\bar{s}}$ tetraquark candidates.

Thry Width [MeV]	Mesons Pair	Meson Threshold [MeV]	Baryon Anti- baryon	Baryonic Threshold [MeV]	Genuine
47 – 79	$\eta_c(1S)K^+$	3478	$\Lambda_c^+\Xi_c^0$	4756	
29 – 59	$D_s^+ \bar{D}^0$	3833	$\Sigma_c^{++}\bar{\Xi}_c^-$ $\Xi_c^+ \bar{\Omega}_c^0$	4922 5163	*

Table 81: $T_{c\bar{c}u\bar{s}}$ thresholds.

J Spec	a_{T_J}	n Spec	a_{T_n}
4362 – 4488		4145 – 4282	
4587 – 4704		4489 – 4610	
4796 – 4906		4796 – 4906	
4993 – 5097		5076 – 5178	
5179 – 5278		5337 – 5432	
5356 – 5450		5580 – 5670	
5525 – 5616	-3.3 – -2.7	5811 – 5896	-2.0 – -1.6
5688 – 5776		6030 – 6111	
5845 – 5930		6240 – 6317	
5997 – 6079		6441 – 6515	
6144 – 6223		6634 – 6706	
6287 – 6364		6821 – 6891	

Table 82: $T_{c\bar{c}u\bar{s}}$ (J, M^2) predictions.

Table 83: $T_{c\bar{c}u\bar{s}}$ (n, M^2) predictions.

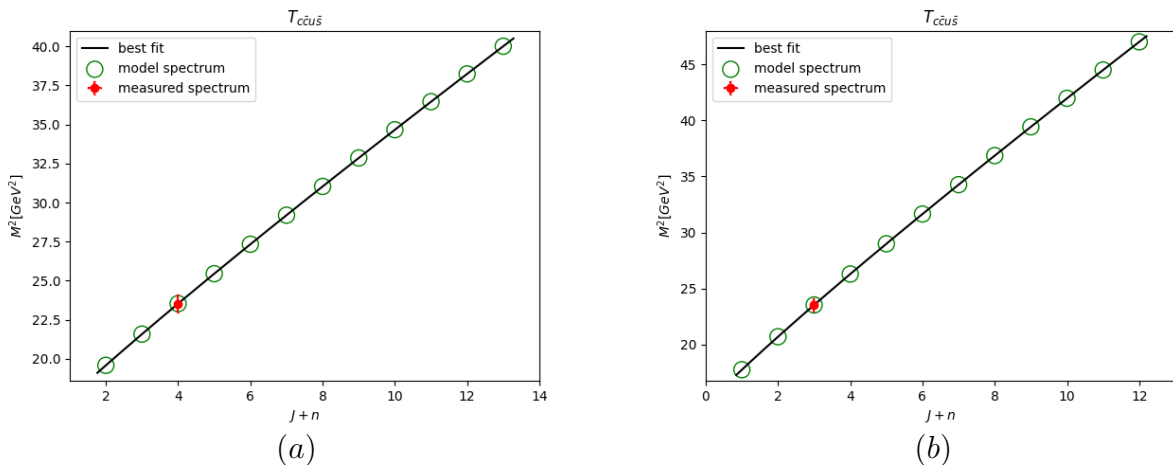


Figure 56: (a) is (J, M^2) $T_{c\bar{c}c\bar{u}}$ predicted HMRT, (b) (n, M^2) $T_{c\bar{c}c\bar{u}}$ predicted HMRT.

7.2.11.1 Z_{cs} (n, M^2) fit

For $J^{PC} = 1^+$, the best fit is with the fixed endpoint masses. The fits are shown in [Fig. 57] along with the predicted spectrum. The best fit parameters are: $\alpha'_{Z_{cs}} = 0.79$, $a_{Z_{cs}} = -2.98$.

χ^2_r	χ^2_{hish}	α'	a	m_1	m_2	Fit Type
0.00	0.00	0.74	-3.65	1.11	1.24	free fit
3.58	0.03	0.45	-1.08	1.12	1.47	fixed m_1, m_2 and α'
2.25	0.02	0.45	-1.95	1.11	1.11	fixed α'
0.00	0.00	0.79	-2.98	1.12	1.47	fixed m_1 and m_2

Table 84

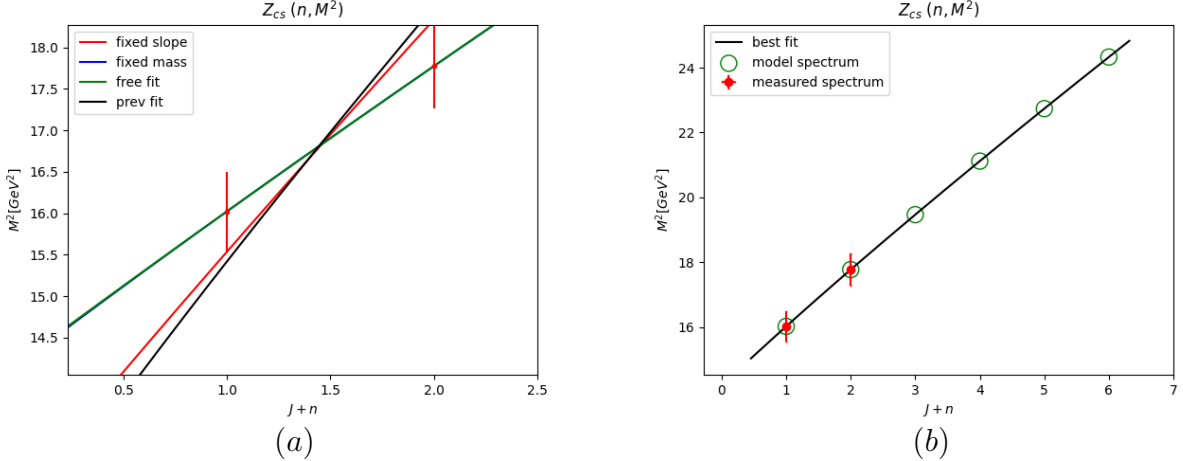


Figure 57: Z_{cs} with $J^P = 1^+$ HMRT. (a) Comparison between the fits, (b) Z_{cs} with fixed mass HMRT, which is the best fit.

State	M [MeV]	Thry M [MeV]	J	Thry n	Thry $J + n$
$Z(4000)_{cs1}^+$	4003	4003	1	0	1
$Z(4220)_{cs1}^+$	4216	4216	1	1	2
		4412			3
		4596			4
		4768			5
		4932			6

Table 85: Z_{cs} (n, M^2) HMRT.

7.2.12 $T_{\psi\phi}$ (quark content $c\bar{c}s\bar{s}$)

For tetraquarks with the quark content $T_{c\bar{c}s\bar{s}}$ The candidate resonances are presented in table 86. We generated the predicted HMRTs for this quark content in tables 88 and 89, and the thresholds table 87 includes the predicted width. The HMRTs are also plotted in 58.

Candidate	Quarks Content	Selected Decay Channels	J^{PC}	Mass [MeV]	Width [MeV]	Ref.

$X(3960)$	$c\bar{c}s\bar{s}$	$D_s^+ D_s^-$	0^{++}	$3956 \pm 5 \pm 10$	$43 \pm 13 \pm 8$	[95] another approach in [109]
$X(4140)$	$c\bar{c}s\bar{s}$	$J/\psi\phi$	1^{++}	4146.5 ± 3.0	19_{-5}^{+7}	[96]
$X(4274)$	$c\bar{c}s\bar{s}$	$J/\psi\phi$	1^{++}	4286_{-9}^{+8}	51 ± 7	[97]
$\chi_{c0}(4500)$	$c\bar{c}s\bar{s}$	$J/\psi\phi$	0^{++}	4474 ± 4	77_{-10}^{+12}	[97]
$\chi_{c1}(4685)$	$c\bar{c}s\bar{s}$	$J/\psi\phi$	1^{++}	4684_{-17}^{+15}	126 ± 40	[93]
$\chi_{c0}(4700)$	$c\bar{c}s\bar{s}$	$J/\psi\phi$	0^{++}	4694_{-5}^{+16}	87_{-10}^{+18}	[97]
$X(4350)^8$	$c\bar{c}s\bar{s}$	$J/\psi\phi$? [?] + ⁺	4351 ± 5	13_{-10}^{+18}	
$X(4630)$	$c\bar{c}s\bar{s}$	$J/\psi\phi$	1^{-+10}	4626_{-110}^{+24}	174_{-80}^{+140}	
$\psi(4360)$	$c\bar{c}s\bar{s}$	$J/\psi\eta$	1^{--}	4374 ± 7	118 ± 12	
$\psi(4660)$	$c\bar{c}s\bar{s}$	$\Lambda_c^+ \bar{\Lambda}_c^-$ $D_s^+ D_{s1}^-(2536)$ $D_s^+ D_{s2}^*(2573)$	1^{--}	4630 ± 6	72_{-12}^{+14}	

Table 86: $T_{c\bar{c}s\bar{s}}$ tetraquark candidates.

Thry Width [MeV]	Mesons Pair	Meson Threshold [MeV]	Baryon Anti-baryon	Baryonic Threshold [MeV]	Genuine
89 – 134	$D_s^+ D_s^-$	3936	$\Xi_c^+ \bar{\Xi}_c^-$	4936	
27 – 54	$\eta_c(1S)\phi(1020)$	4003	$\Xi_c^0 \bar{\Xi}_c^0$ $\Omega_c^0 \bar{\Omega}_c^0$	4940 5390	

Table 87: $T_{c\bar{c}s\bar{s}}$ thresholds.

J Spec	a_{T_J}	n Spec	a_{T_n}
4536 – 4664		4315 – 4454	
4765 – 4882		4666 – 4787	
4976 – 5086		4976 – 5086	
5174 – 5278		5258 – 5359	
5361 – 5459		5519 – 5613	
5538 – 5632		5763 – 5852	
5708 – 5798	-3.8 – -3.2	5993 – 6078	-2.7 – -2.3
5871 – 5958		6212 – 6293	
6028 – 6112		6421 – 6498	
6179 – 6260		6622 – 6696	
6326 – 6404		6814 – 6886	
6468 – 6545		7001 – 7070	

Table 88: $T_{c\bar{c}s\bar{s}}$ (J, M^2) predictions.

Table 89: $T_{c\bar{c}s\bar{s}}$ (n, M^2) predictions.

¹⁰ J^P needs confirmation.

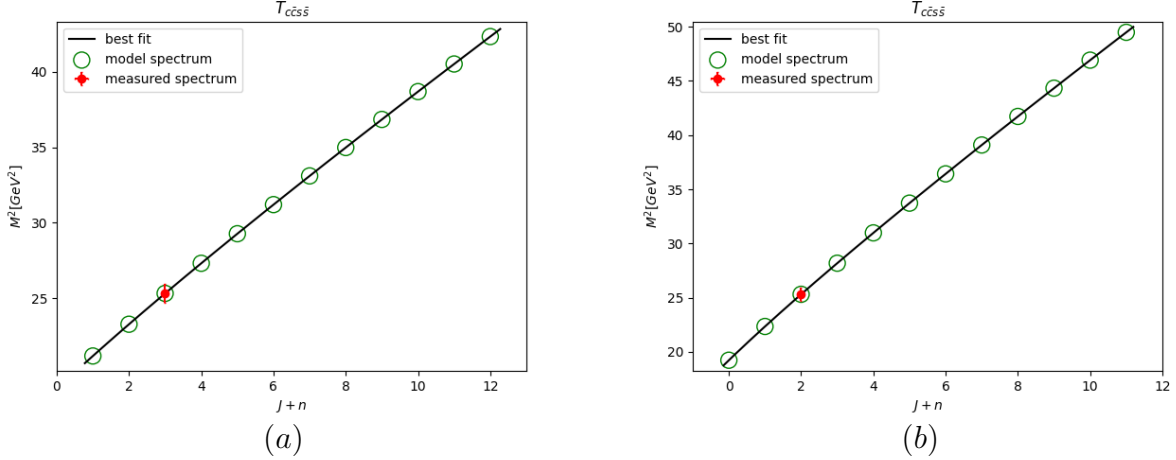


Figure 58: (a) is (J, M^2) $T_{c\bar{c}s\bar{s}}$ predicted HMRT, (b) (n, M^2) $T_{c\bar{c}s\bar{s}}$ predicted HMRT.

In [110]-[111] there were seven resonances observed that are tetraquark candidates with content $c\bar{c}s\bar{s}$. The decays in which these states were observed are $J/\psi\phi$ and D_sD_s .

We expect the natural decay of these states to be through a baryon-antibaryon pair for higher states that are above threshold. In this case, the annihilation threshold is ≈ 3940 which is slightly below $X(3960)$ found in [110], while the threshold for a decay through string tear is ≈ 4940 to $\Xi_c\bar{\Xi}_c$.

The fit of the data was done separately for $J^{PC} = 0^{++}$ and $J^{PC} = 1^{++}$ in the (n, M^2) plane. For each trajectory we fit the data four times - once with free parameters, another with fixed endpoint masses, one with fixed α' and at last we fixed both α' and the endpoint masses, letting only the intercept to change.

7.2.12.1 $T_{\psi\phi 0}$ (n, M^2) fit

For $J^{PC} = 0^{++}$, the best fit is with the fixed slope and endpoint masses, with $\chi_r^2 = 2.00$, but the spectrum prediction is similar for all fits. The fits are shown in [Fig. 59] along with the predicted spectrum.

χ_r^2	χ_{hish}^2	α'	a	m_1	m_2	Fit Type
2.09	0.01	0.67	-0.16	1.90	1.90	free fit
2.00	0.02	0.45	-1.55	1.47	1.47	fixed m_1, m_2 and α'
3.75	0.02	0.45	-1.16	1.56	1.56	fixed α'
3.89	0.02	0.43	-1.47	1.47	1.47	fixed m_1 and m_2

Table 90: $T_{\psi\phi 0}$ (n, M^2) fit results.

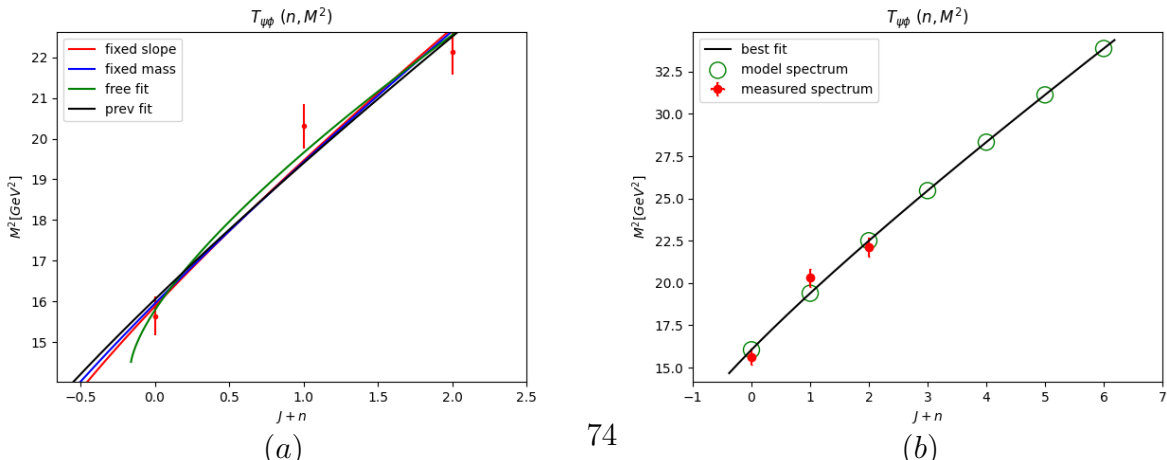


Figure 59: $T_{\psi\phi 0}$ with $J^{PC} = 0^{++}$ HMRT. (a) Comparison between the fits. (b) $T_{\psi\phi 0}$ with $J^{PC} = 1^{++}$.

State	M [MeV]	Thry M [MeV]	J	Thry n	Thry $J + n$
$X(3960)$	3955	3973	0	0	0
$X(4500)$	4506	4433	0	1	1
$X(4700)$	4704	4748	0	2	2
		5012			3
		5245			4
		5458			5
		5656			6

Table 91: $T_{\psi\phi}$ Regge trajectory.

7.2.12.2 $T_{\psi\phi 1}$ (n, M^2) fit

For $J^{PC} = 1^{++}$, the best fit is with the fixed masses and α' parameters with $\chi^2_r = 4.30$. The fits are shown in [Fig. 60]. The predicted spectrum is at 93.

χ^2_r	χ^2_{hish}	α'	a	m_1	m_2	Fit Type
4.38	0.02	0.48	-4.20	0.81	0.81	free fit
5.62	0.05	0.45	-0.53	1.47	1.47	fixed m_1, m_2 and α'
4.30	0.02	0.45	-5.71	0.35	0.35	fixed α'
4.69	0.02	0.64	-1.50	1.47	1.47	fixed m_1 and m_2

Table 92: $T_{\psi\phi 1}$ (n, M^2) fit results.

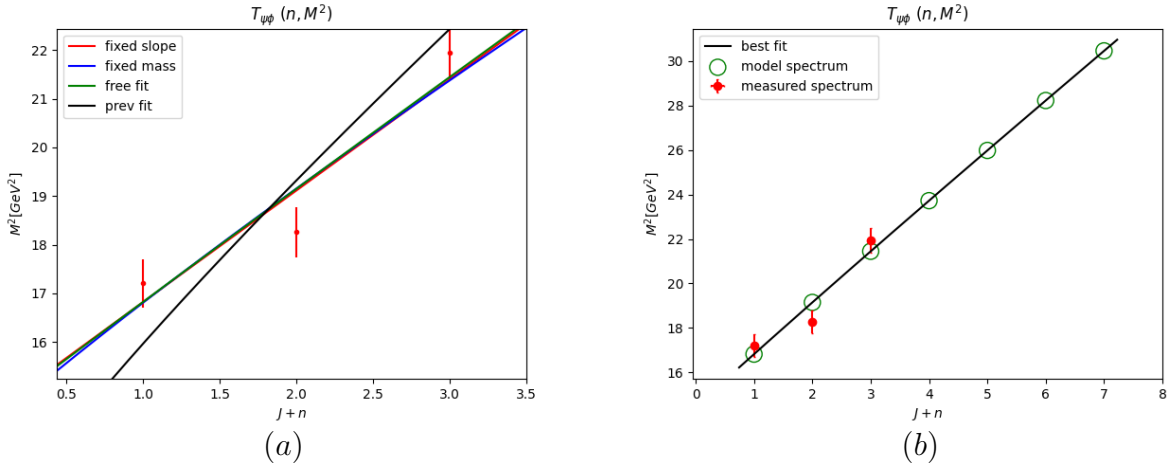


Figure 60: $T_{\psi\phi}$ with $J^{PC} = 1^{++}$ HMRT. (a) Comparison between the fits, (b) $T_{\psi\phi}$ with $J^{PC} = 1^{++}$ fixed fit HMRT which is the best fit.

State	M [MeV]	Thry M [MeV]	J	Thry n	Thry $J + n$
$X(4140)$	4148	3996	1	0	1
$X(4274)$	4273	4396	1	1	2

$X(4685)$	4684	4736	1	2	3
	5040			4	
	5317			5	
	5573			6	
	5814			7	

Table 93: $T_{\psi\phi}$ HMRT.

7.2.12.3 $X(4350)$ and $X(4630)$ (n, M^2) fit

For $J^{PC} = 1^{-+}$ ¹¹ the best fit is with the free parameters with $\chi_r^2 = 3.01$, but the spectrum prediction is similar for all fits. The fits are shown in [Fig. 61] along with the predicted spectrum.

χ_r^2	χ_{hish}^2	α'	a	m_1	m_2	Fit Type
0.00	0.00	0.44	-5.92	0.73	0.73	free fit
0.79	0.01	0.45	-2.31	1.47	1.47	fixed m_1, m_2 and α'
0.00	0.00	0.45	-5.69	0.80	0.80	fixed α'
0.00	0.00	0.57	-3.07	1.47	1.47	fixed m_1 and m_2

Table 94

State	M [MeV]	Thry M [MeV]	J	Thry n	Thry $J + n$
$X(4350)$	4351	4351	1	-1	0
$X(4630)$	4626	4626	1	0	1
		4883			2
		5126			3
		5356			4
		5575			5

Table 95: $X(4350)$, $X(4630)$ (n, M^2) HMRT.

7.2.12.4 ψ (n, M^2)

The candidates $\psi(4360)$ and $\psi(4660)$ were analysed in previous paper [10] as candidates on the same trajectory. In this paper, the $\psi(4660)$ and $X(4630)$ were considered as the same state. But it is now known that they have different quantum numbers. Hence, we separate their HMRTs in this paper. Also, we assumed that $X(4350)$ is on the same HMRT as the $X(4630)$ (section 7.2.12.3).

For $J^{PC} = 1^{--}$ the best fit is with the free parameters with $\chi_r^2 = 3.01$, but the spectrum prediction is similar for all fits. The fits are shown in [Fig. 61] along with the predicted spectrum.

χ_r^2	χ_{hish}^2	α'	a	m_1	m_2	Fit Type

¹¹We assume that the $X(4350)$ is with the same quantum numbers, although not all of them are known yet

0.00	0.00	0.53	-3.68	1.16	1.16	free fit
1.16	0.01	0.45	-1.35	1.47	1.47	fixed m_1, m_2 and α'
0.00	0.00	0.45	-6.24	0.47	0.47	fixed α'
0.03	0.00	0.57	-2.12	1.47	1.47	fixed m_1 and m_2

Table 96

State	M [MeV]	Thry M [MeV]	J	Thry n	Thry $J + n$
$\psi(4360)$	4372	4372	1	0	1
$\psi(4660)$	4630	4630	1	1	2
		4873			3
		5105			4
		5325			5
		5537			6

Table 97: $\psi(n, M^2)$ HMRT.

7.2.13 $T_{\psi\psi}$ (quark content $c\bar{c}c\bar{c}$)

In [24] the state $X(6900)$ was analysed in the context of the HISH model. This note relied on [112] where two additional resonance candidates at around 6.6GeV and 7.2GeV were observed. Now these candidates were observed in an additional note [113] with higher statistical significance. The states that we analyse in this section are listed in 98.

There are two measurements of $X(6600)$ and $X(6900)$, without quantum numbers. Not all of the states rely on the same trajectory. Hence, we fit the second, fourth and fifth in an HMRT.

Candidate	Quarks Content	Selected Decay Channels	J^{PC}	Mass [MeV]	Width [MeV]	Ref.
$T_{\psi\psi}(6600)$	$c\bar{c}c\bar{c}$	$J/\psi J/\psi$???	6630 ± 90	$350 \pm 11^{+110}_{-40}$	
$T_{\psi\psi}(6600)$	$c\bar{c}c\bar{c}$	$J/\psi J/\psi$???	$6552 \pm 10 \pm 12$	$124^{+32}_{-26} \pm 33$	
$T_{\psi\psi}(6900)$	$c\bar{c}c\bar{c}$	$J/\psi J/\psi$???	6886 ± 16	168 ± 80	
$T_{\psi\psi}(6900)$	$c\bar{c}c\bar{c}$	$J/\psi J/\psi$???	$6927 \pm 9 \pm 4$	$122^{+24}_{-21} \pm 18$	
$T_{\psi\psi}(7300)$	$c\bar{c}c\bar{c}$	$J/\psi J/\psi$???	$7287^{+20}_{-18} \pm 5$	$95^{+59}_{-40} \pm 19$	

Table 98: $T_{c\bar{c}c\bar{c}}$ tetraquark candidates.

Thry Width [MeV]	Mesons Pair	Meson Threshold [MeV]	Baryon Anti-baryon	Baryonic Threshold [MeV]	Genuine
6 – 21 29 – 58	$\eta_c(1S)\eta_c(1S)$	5968	$\Xi_{cc}^+\bar{\Xi}_{cc}^-$ $\Xi_{cc}^{++}\bar{\Xi}_{cc}^{--}$ $\Omega_{cc}^+\bar{\Omega}_{cc}^-$	7038 7244	*

Table 99: $T_{c\bar{c}c\bar{c}}$ thresholds.

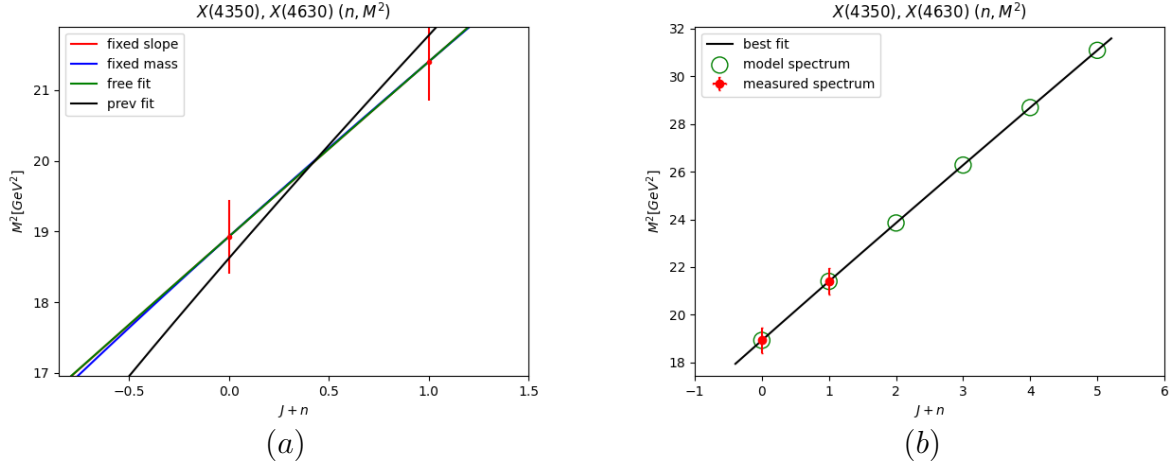


Figure 61: $X(4350)$ and $X(4630)$ with $J^{PC} = 1^{-+}$ HMRT. (a) Comparison between the fits, (b) $X(4350)$ and $X(4630)$ fixed slope fit HMRT which is the best fit.

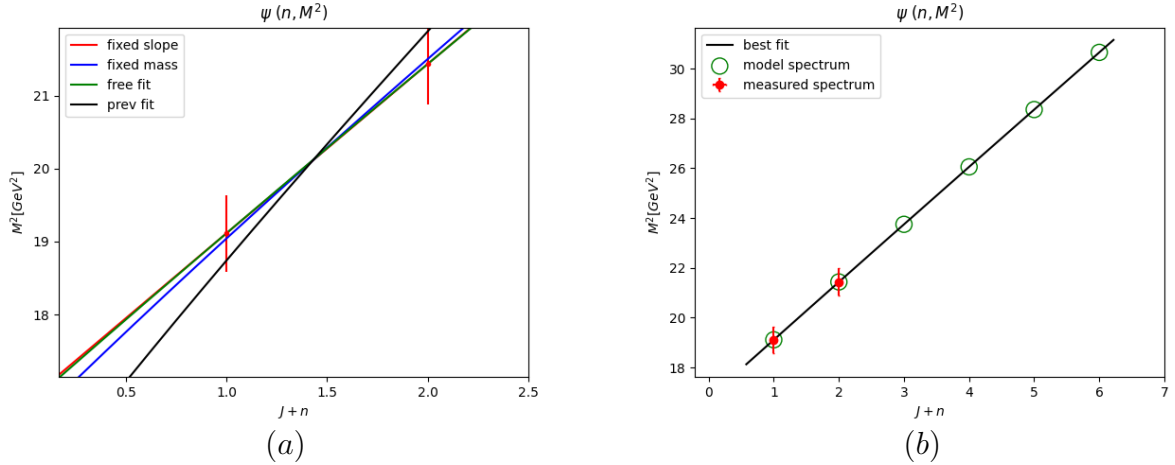


Figure 62: $X(4350)$ and $X(4630)$ with $J^{PC} = 1^{-+}$ HMRT. (a) Comparison between the fits, (b) $X(4350)$ and $X(4630)$ fixed slope fit HMRT which is the best fit.

J Spec	a_{T_j}
6768 – 6887	
6926 – 7040	
7078 – 7188	
7225 – 7331	
7366 – 7469	
7504 – 7604	
7637 – 7735	-5.9 – -5.1
7767 – 7862	
7894 – 7987	
8018 – 8108	
8139 – 8227	
8257 – 8344	

Table 100: $T_{c\bar{c}c\bar{c}}$ (J, M^2) predictions.

n Spec	a_{T_n}
6622 – 6745	
6857 – 6973	
7078 – 7188	
7288 – 7393	
7489 – 7589	
7681 – 7778	
7866 – 7959	
8045 – 8135	
8218 – 8305	
8385 – 8470	
8549 – 8631	
8707 – 8788	-4.2 – -3.7

Table 101: $T_{c\bar{c}c\bar{c}}$ (n, M^2) predictions.

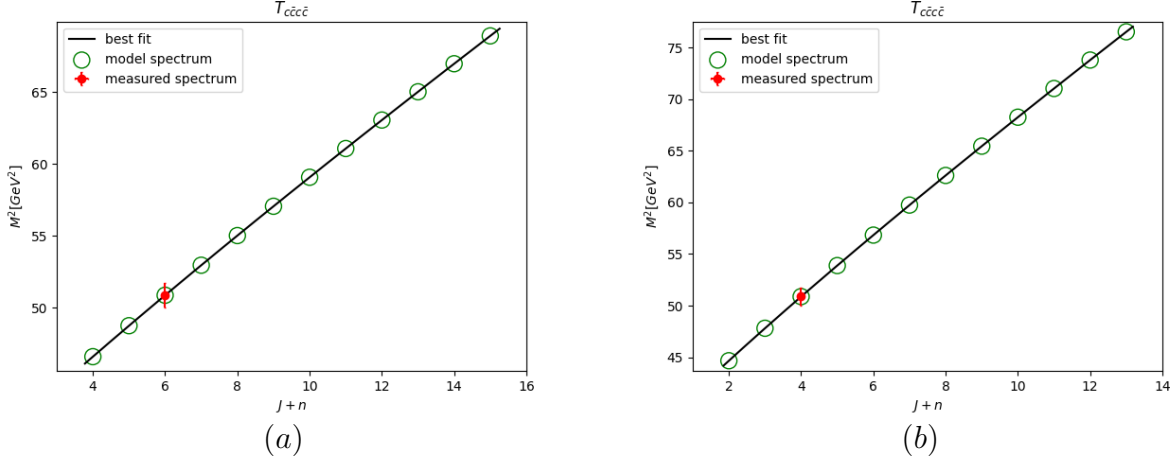


Figure 63: (a) is (J, M^2) $T_{c\bar{c}c\bar{c}}$ predicted HMRT, (b) (n, M^2) $T_{c\bar{c}c\bar{c}}$ predicted HMRT.

The decay channel in which these states were observed is $J/\psi J/\psi$. As before, we fit the data four times in the (n, M^2) plane with $\alpha' = 0.45$. For this trajectory, the mesons slope was too high for both planes.

The comparison between the different fits are shown in 64. The best fit, which is consistent with the universal description of the model is present in 64 on (b). The spectrum prediction is shown in 102.

χ_r^2	χ_{hish}^2	α'	a	m_1	m_2	Fit Type
0.12	0.00	0.21	-4.43	0.70	0.70	free fit
5.68	0.05	0.45	-2.93	2.22	2.22	fixed m_1 , m_2 and α'
3.05	0.01	0.45	1.00	2.78	2.78	fixed α'
0.84	0.00	0.31	-0.86	2.22	2.22	fixed m_1 and m_2

Table 102: $T_{\psi\psi}$ HMRT.

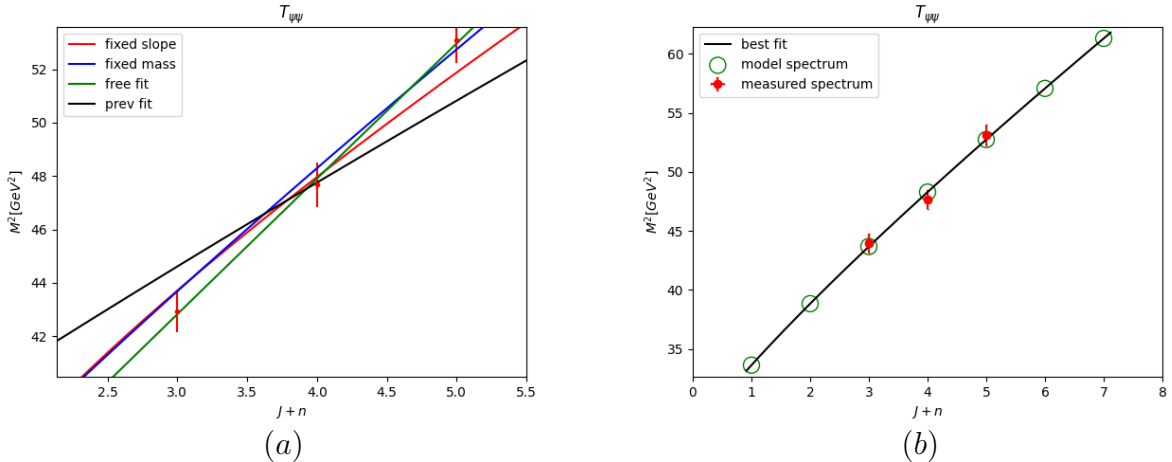


Figure 64: $X(6900)$ (n, M^2) HMRT. The graph in (a) shows the comparison between the fits, (b) $X(6900)$ fixed fit HMRT which is the best fit.

State	M [MeV]	Thry M [MeV]	J	Thry n	Thry $J + n$
		5800			1
		6232			2
$T(6600)_{\psi\psi 0}$	6630	6609			3
$T(6900)_{\psi\psi 0}$	6905	6950			4
$T(7300)_{\psi\psi 0}$	7287	7263			5
		7555			6
		7830			7

Table 103: $T_{\psi\psi}$ HMRT.

The decays width ratio:

$$\Gamma_{tear} \lesssim 31 \text{ MeV} \quad (60)$$

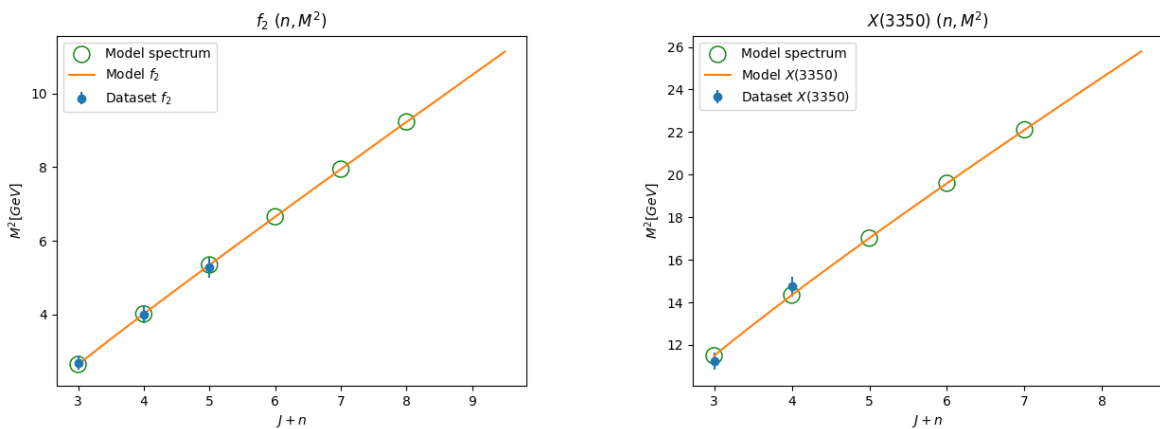
$$\Gamma_{annihilation} = 47 \text{ MeV} \quad (61)$$

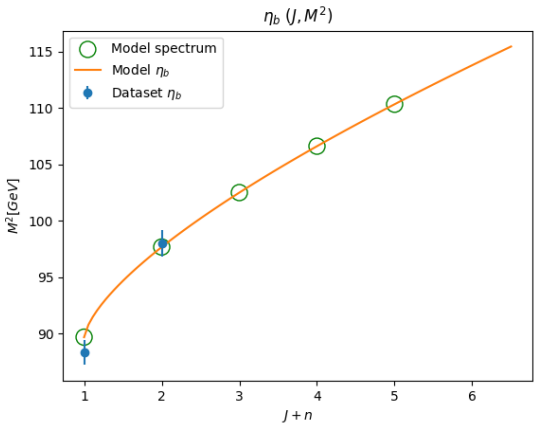
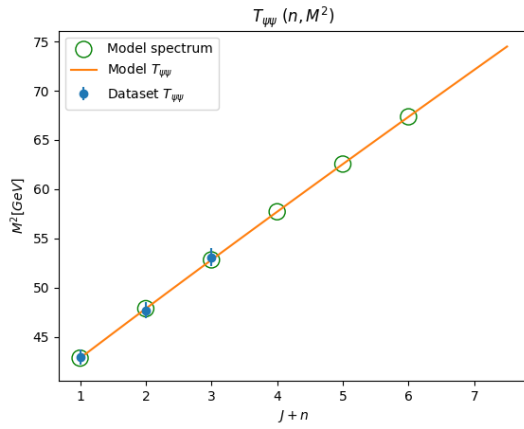
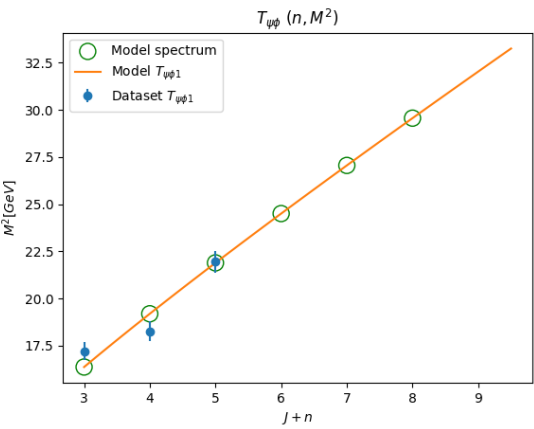
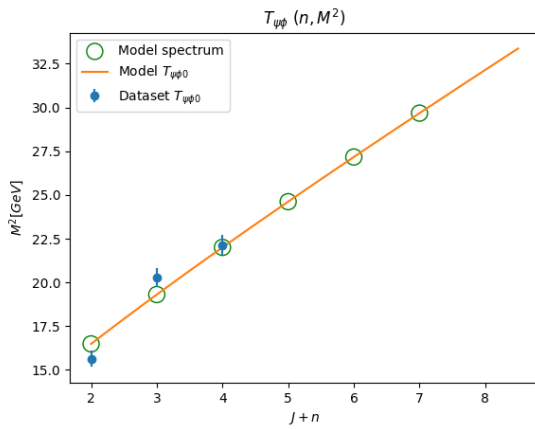
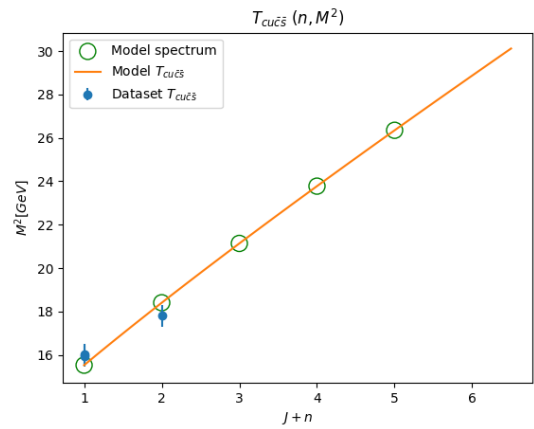
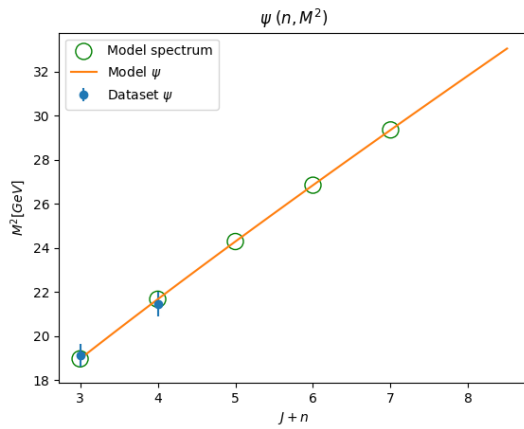
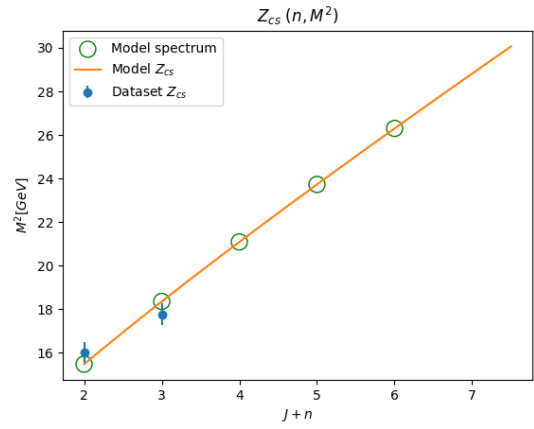
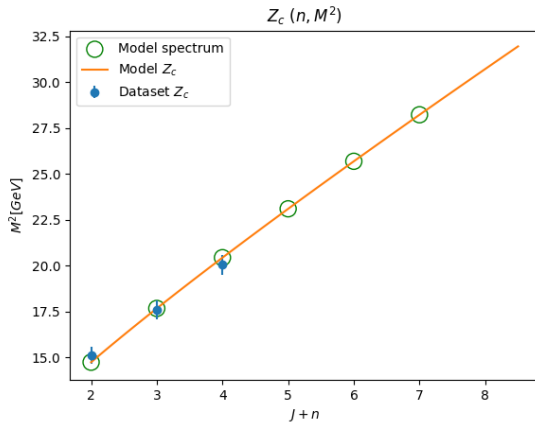
Adding the two widths, we get a result width - 78 MeV - which is a quite good approximation to the measured 95 MeV in [113]. Changing the A value used to 0.15 would give a closer result.

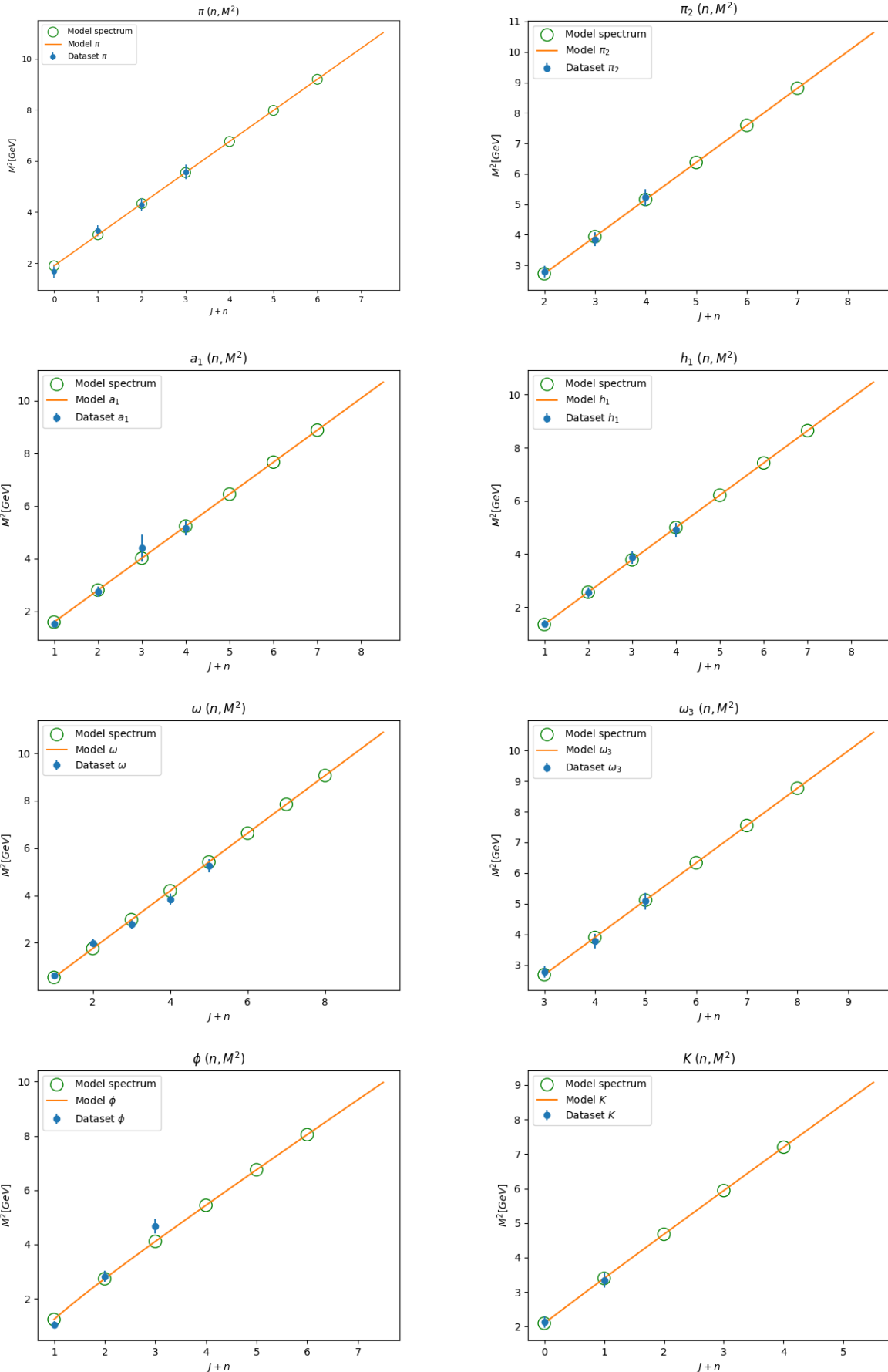
7.3 Tetraquarks and Mesons Global Fit

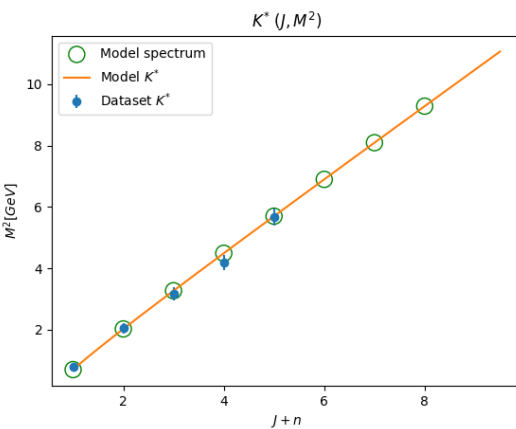
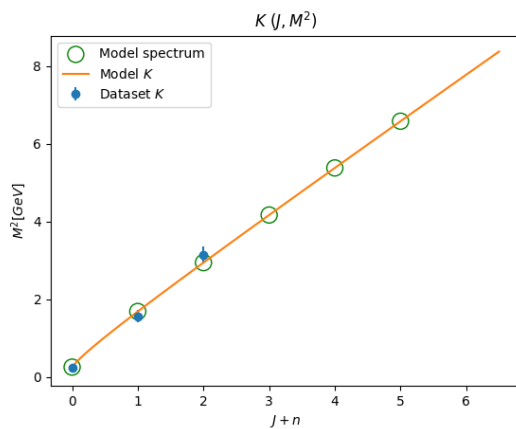
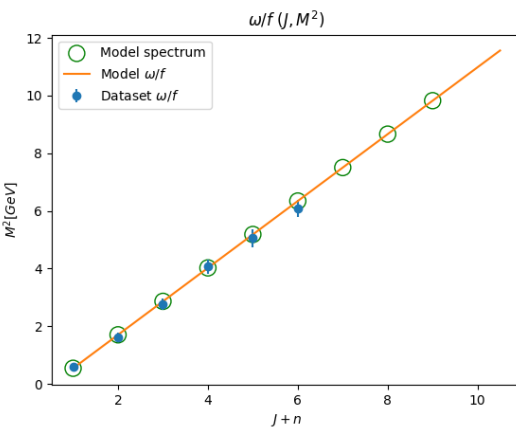
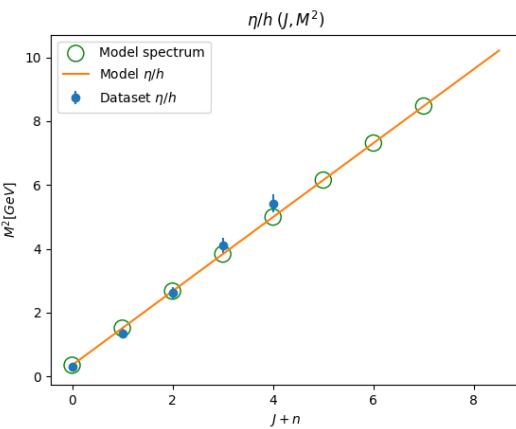
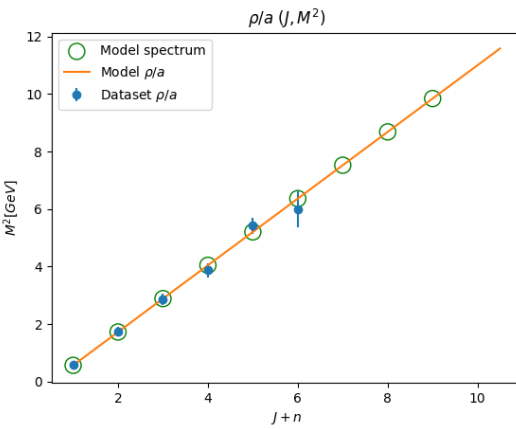
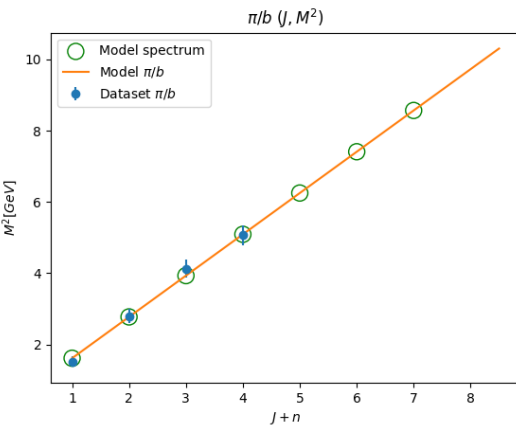
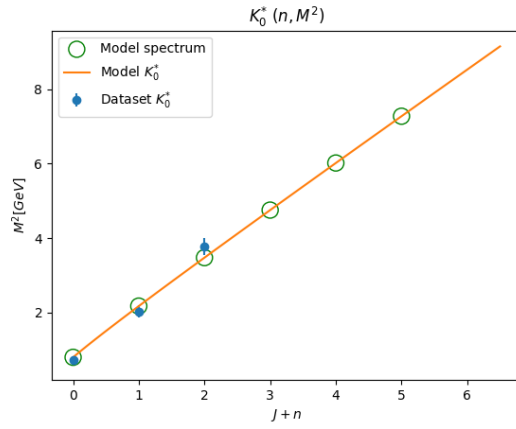
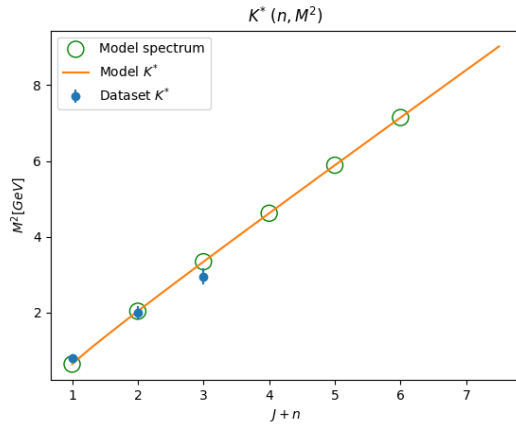
To conclude this section, we checked the coherency of our assumptions by fitting all tetraquarks and mesons data together, constraining the slopes of the heavy tetraquarks to be the same as that of the charmed and bottoms mesons.

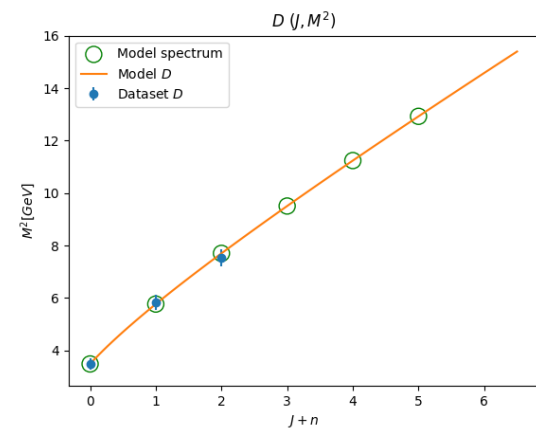
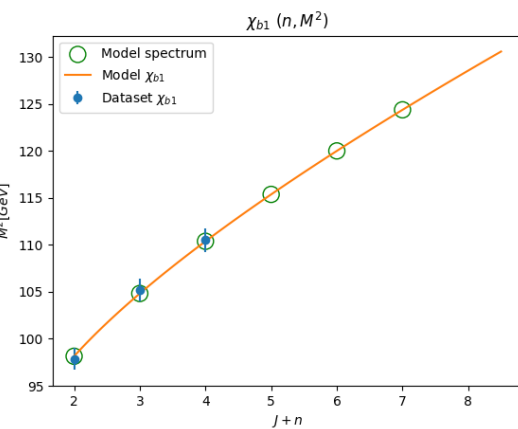
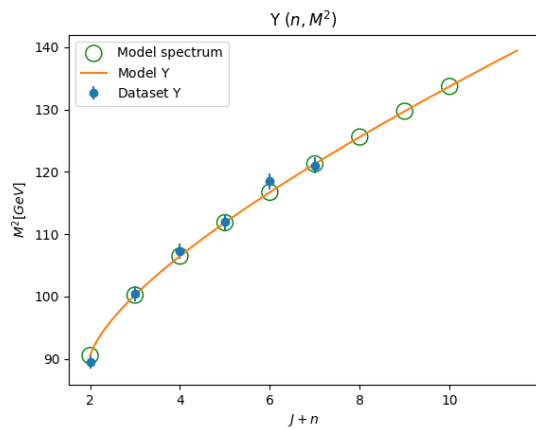
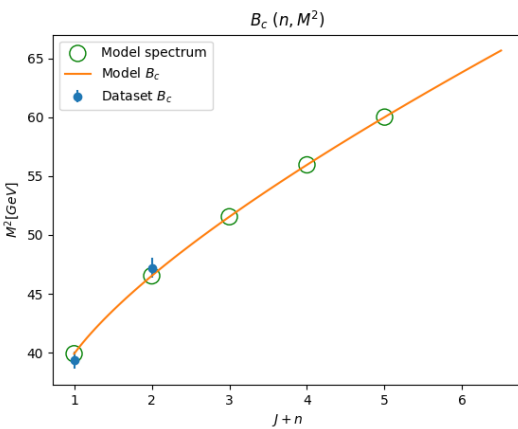
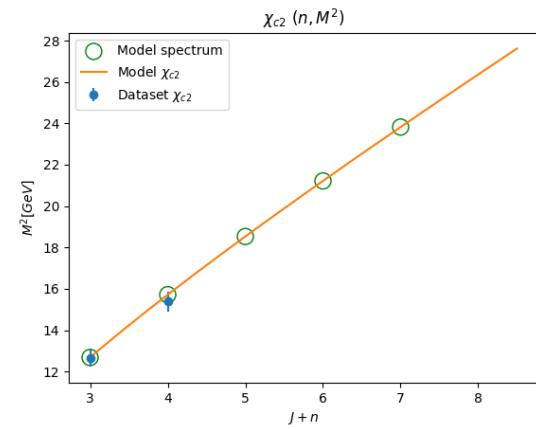
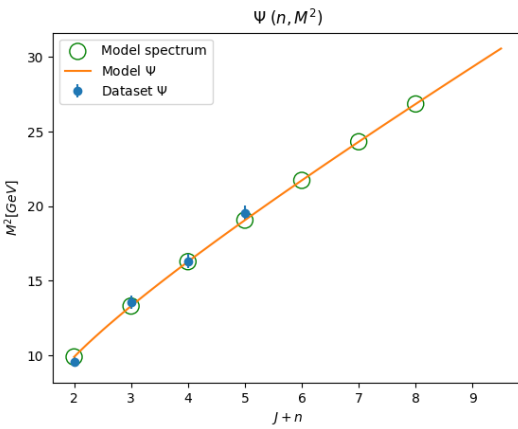
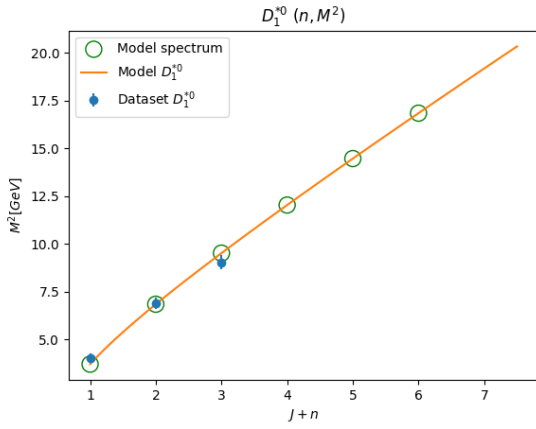
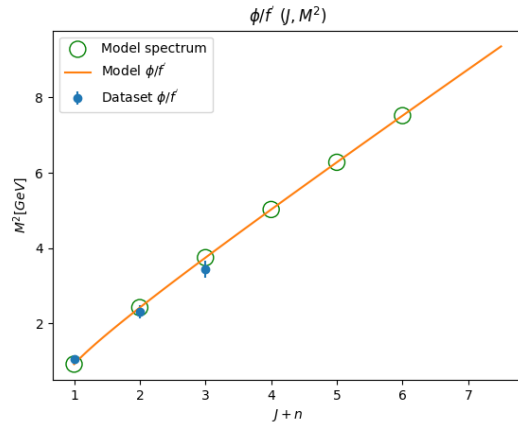
The results are of $\chi^2_r = 1.95$. The graphs are in the following figure 104, the fit results are in table 105.

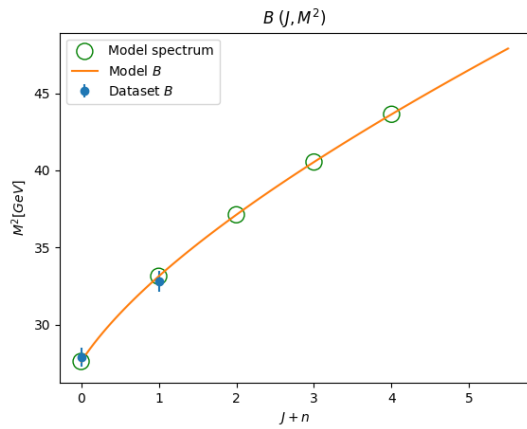
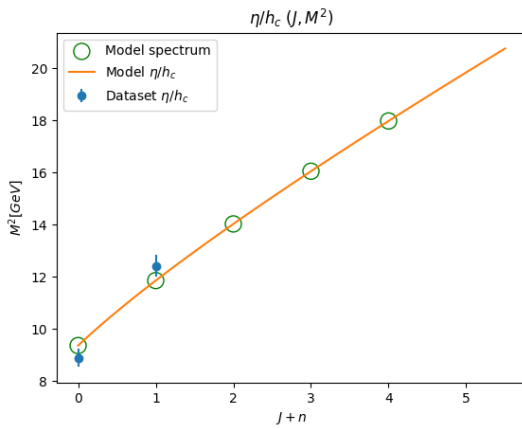
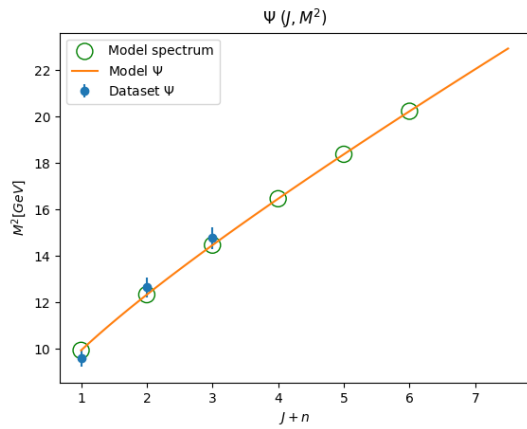
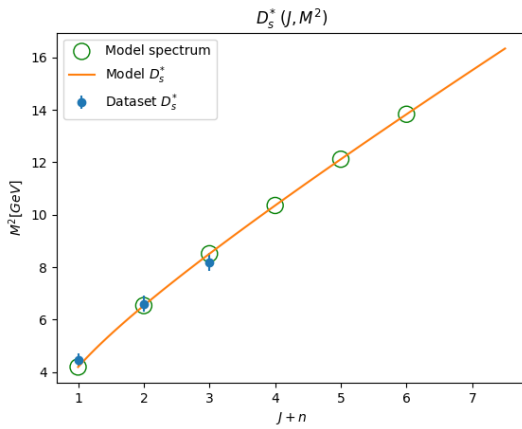
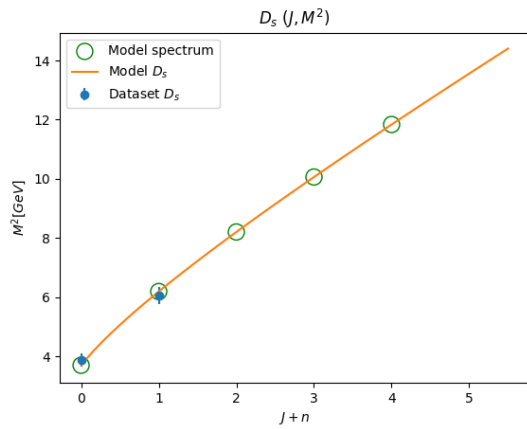
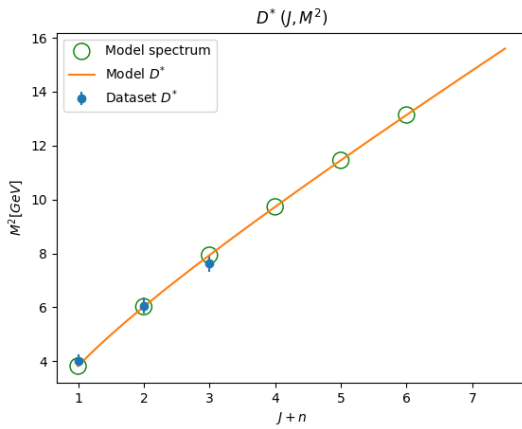
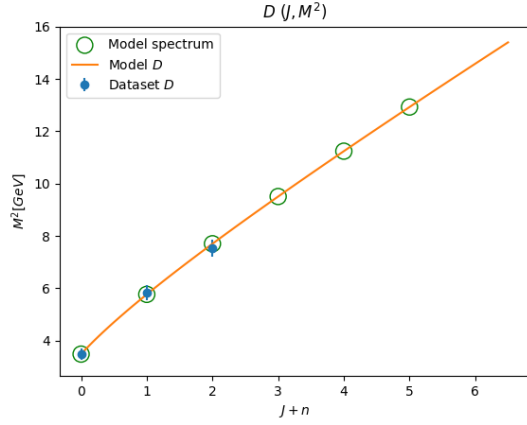
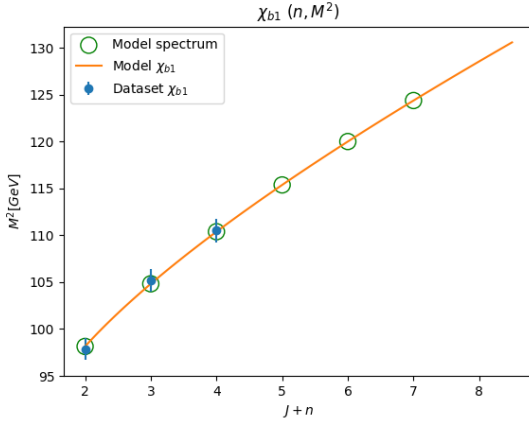


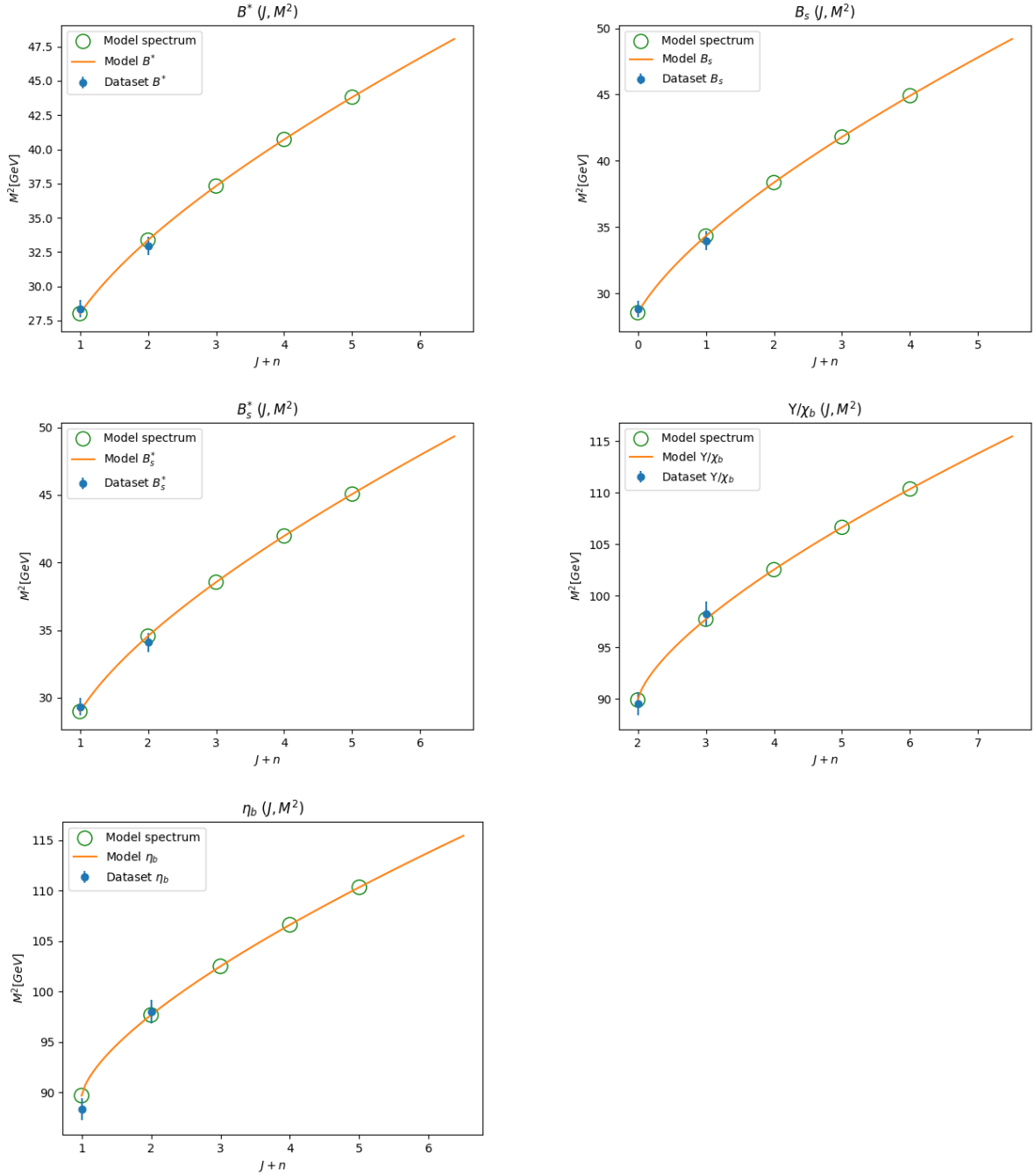












χ^2_r	$\alpha'_{J,L}$ [GeV $^{-2}$]	$\alpha'_{J,H}$ [GeV $^{-2}$]	$\alpha'_{n,L}$ [GeV $^{-2}$]	$\alpha'_{n,H}$ [GeV $^{-2}$]	$m_{u/d}$ [GeV]	m_s [GeV]	
1.95	0.86	0.65	0.83	0.48	0.011	0.36	
m_c [GeV]	m_b [GeV]	$\alpha_{T_{\psi\psi}}$	$m_{BV_{u/d,u/d}}$	$m_{BV_{s,u/d}}$	$m_{BV_{c,u/d}}$	$m_{BV_{c,s}}$	$m_{BV_{c,c}}$
1.27	4.73	0.23	0.93	0.35	1.32	1.31	1.53

Table 105: The parameters results from the tetraquarks and mesons global fit. We constraint the heavy slopes to equal in mesons and tetraquarks, aside from the $T_{c\bar{c}c\bar{c}}$, which clearly have a lower α' .

Traj.	$a_{n/J}$	Traj.	$a_{n/J}$ only	Traj.	$a_{n/J}$
π/b	$a_J = -0.38$	η_c/h_c	$a_J = -0.71$	ω_3	$a_n = 0.80$
ρ/a	$a_J = 0.52$	B	$a_J = -0.36$	ϕ	$a_n = 0.67$
η/h	$a_J = -0.30$	B^*	$a_J = 0.58$	K	$a_n = -1.29$
ω/f	$a_J = 0.53$	B_s	$a_J = -0.19$	K^*	$a_n = 0.75$
K	$a_J = -0.03$	B_s^*	$a_J = 0.75$	K_0^*	$a_n = -0.35$
K^*	$a_J = 0.70$	Υ/χ_b	$a_J = 1.97$	D_1^{*0}	$a_n = 0.65$
ϕ/f'	$a_J = 0.84$	η_b	$a_J = 1.00$	Ψ	$a_n = 1.38$
D	$a_J = -0.42$	π	$a_n = -1.56$	B_c	$a_n = 0.72$
D^*	$a_J = 0.45$	π_2	$a_n = -0.23$	χ_{c2}	$a_n = 1.58$
D_s	$a_J = -0.21$	a_1	$a_n = -0.29$	Υ	$a_n = 1.98$
D_s^*	$a_J = 0.62$	h_1	$a_n = -0.10$	χ_{b1}	$a_n = 1.26$
Ψ/χ_c	$a_J = 0.08$	ω	$a_n = 0.55$	f_2	$a_n = 1.72$
$X(3350)$	$a_n = 1.35$	Z_c	$a_n = 0.06$	Z_{cs}	$a_n = -0.18$
$\Psi(4630)$	$a_n = -0.41$	$T_{cu\bar{s}}$	$a_n = 0.06$	$T_{\psi\phi 0}$	$a_n = -0.54$
$T_{\psi\phi 1}$	$a_n = -4.47$	$T_{\psi\psi}$	$a_n = 1.53$		

Table 106: Mesons and tetraquarks global fits intercepts. a_J marks that the HMRT was done in the (J, M^2) plane. a_n is the intercept of a (n, M^2) HMRT.

7.4 Tetraquarks HMRTs predictions

The following table summarizes all the thresholds and predicted trajectories for all possible charm tetraquarks configurations. The thresholds were calculated for each possible product according to the HISH model through the annihilation and string tear mechanisms. The third mechanism that is mentioned in 4.3 is not calculated in the table.

The table predictions were calculated based on the mesons fit parameters. We assumed that the diquarks (and anti-diquarks) masses are the sum of masses of the two quarks. The slopes for each trajectory $((J, M^2)$ and (n, M^2)), was taken to be the heavy-slope from 1.

The 'Candidates' column contains the resonances that were already detected. We elaborate on all of these at the previous sub sections, including the decay channels through which they were observed. The 'Thry Width' column contains two values, one for the states at the (J, M^2) MHRT, and the second row is for the (n, M^2) MHRT. The 'Mesons Pair' and 'Meson Threshold' contains the mesons symbols and the threshold for their creation respectively (for example, in the first row of the table, $D^0\pi_d^0$ has a threshold of 2000, while $D^+\pi^-$ has threshold of 2010). The same applies for the 'Baryon-Antibaryon' and 'Baryonic Threshold' columns.

We calculated the 'J Spec' and 'n Spec' in the following steps:

- We first calculated the baryonic threshold and let it vary between $40 - 150 MeV$. This was done by looking at the available data that we collected, where the created tetraquarks candidates are above the baryonic threshold. We saw that this is the range of the distance from the threshold.
- The value for $J + n$ is calculated according to the number of states that are potentially on the trajectories between the mesonic and the baryonic thresholds. We calculated how many states are there, assuming the other parameters are similar to the mesons as explained above 7.4.

- We calculated the range of the baryonic spectrum accordingly.
- We derived the range of the spectrum for two states above, and two states below the expected $J + n$ of the baryonic threshold for each of the two spectra. For example, in the first row the in the 'J Spec' column, the $3264 - 3374$ is the range of the spectrum of the first state that we expect to decay to baryon-antibaryon pair. The $3526 - 3626$ is the first state above that should still decay to a baryonic pair and should have $J + n = 4$, whereas the $2972 - 3095$ should decay through annihilation only, and should have $J + n = 2$.
- When we weren't able to calculate the baryonic threshold (since the baryons weren't measured yet), we started from the mesonic threshold and calculated the trajectory from there up to 12 states.

The 'Genuine' column indicates whether the quark content is a *genuine* tetraquark or a *not obviously genuine*. This was decided as follows:

- If the content includes a light quark (u, d, s) and its counterpart, we assume its source could be a meson that decay through string tear. Thus this is *not obviously genuine* case. This is marked at the table as an empty cell.
- If the content include a heavy quark (c, b) and its counterpart, which is less likely to be a product of meson string break, it is likely to be genuine. This was marked with one *.
- ** means it is a pure tetraquark. These do not contain quark-antiquark pair of the same flavour.

Empty baryonic threshold means these baryons weren't found yet.

#	Candi-dates	J^{PC}	Quarks	Thry Width [MeV]	Mesons Pair	Meson Threshold [MeV]	Baryon Anti-baryon	Baryonic Threshold [MeV]	J Spec	n Spec	a_{T_j} a_{T_n}	Thry $J + n$	Gen-uine
1			$c\bar{u}u\bar{u}$	$79 - 118$ $30 - 61$	$D^0\pi_u^0$	2000	$\Lambda_c^+\bar{p}$ $\Xi_c^+\bar{\Sigma}^-$ $\Sigma_c^{++}\bar{\Delta}^{--}$	3224 3657 3686 3264 3374 3526 3626 3635 3731 3766 3858 3964 4051	2634 - 2779 2972 - 3095 3264 - 3374 3526 - 3626 3635 - 3731 3766 - 3858 3964 - 4051	2270 - 2448 2829 - 2961 3264 - 3374 3635 - 3731 3964 - 4051	-1.6--1.2 -1.2--0.92	3 2	
2	$X(3500)$ $X(3800)$	(0 or 1) ^{??} ???	$c\bar{d}d\bar{u}$	$79 - 118$ $30 - 61$	$D^0\pi_d^0$ $D^+\pi^-$	2000 2010	$\Lambda_c^+\bar{p}$ $\Sigma_c^0\bar{n}$ $\Xi_c^0\bar{\Lambda}^0$	3224 3394 3586 3264 3374 3526 3626 3635 3731 3766 3858 3964 4051	2634 - 2779 2972 - 3095 3264 - 3374 3526 - 3626 3635 - 3731 3766 - 3858 3964 - 4051	2270 - 2448 2829 - 2961 3264 - 3374 3635 - 3731 3964 - 4051	-1.6--1.2 -1.2--0.92	3 2	
3			$c\bar{d}u\bar{u}$	$78 - 117$ $31 - 61$	$D^+\pi_u^0$ $D^0\pi^+$	2005 2005	$\Lambda_c^+\bar{n}$ $\Sigma_c^+\bar{p}$ $\Xi_c^+\bar{\Lambda}^0$	3226 3392 3584 2974 - 3098 3266 - 3376 3528 - 3628 3767 - 3860 3226 3392 3584 3266 - 3376 3528 - 3628 3637 - 3733 3966 - 4053	2637 - 2782 2974 - 3098 3266 - 3376 3528 - 3628 3767 - 3860 2273 - 2451 2831 - 2963 3266 - 3376 3637 - 3733 3966 - 4053	-1.6--1.2 -1.2--0.93	3 2		
4			$c\bar{u}d\bar{u}$	$41 - 72$ $32 - 63$	$D^0\pi^-$	2005	$\Sigma_c^0\bar{p}$ $\Lambda_c^+\bar{\Delta}^{--}$ $\Xi_c^0\bar{\Sigma}^-$	3392 3518 3659 3160 - 3282 3432 - 3542 3679 - 3780 3908 - 4002 2854 - 2992 3160 - 3282 3432 - 3542 3679 - 3780 3908 - 4002	2537 - 2698 3029 - 3157 3432 - 3542 3783 - 3881 4098 - 4187 2273 - 2451 2831 - 2963 3266 - 3376 3637 - 3733 3966 - 4053	-2.3--1.8 -1.7--1.4	3 2	**	
5			$c\bar{d}d\bar{d}$	$78 - 117$ $31 - 61$	$D^+\pi_d^0$	2005	$\Lambda_c^+\bar{n}$ $\Xi_c^0\bar{\Sigma}^+$ $\Sigma_c^0\bar{\Delta}^+$	3226 3667 3686 2974 - 3098 3266 - 3376 3528 - 3628 3767 - 3860 3226 3667 3686 3266 - 3376 3528 - 3628 3637 - 3733 3966 - 4053	2637 - 2782 2974 - 3098 3266 - 3376 3528 - 3628 3767 - 3860 2273 - 2451 2831 - 2963 3266 - 3376 3637 - 3733 3966 - 4053	-1.6--1.2 -1.2--0.93	3 2		
6			$c\bar{d}u\bar{d}$	$40 - 71$ $32 - 63$	$D^+\pi^+$	2010	$\Sigma_c^{++}\bar{n}$ $\Lambda_c^+\bar{\Delta}^+$ $\Xi_c^+\bar{\Sigma}^+$	3394 3518 3665 3162 - 3284 3434 - 3544 3681 - 3782 3909 - 4004 2856 - 2994 3162 - 3284 3434 - 3544 3681 - 3782 3909 - 4004	2540 - 2701 3031 - 3160 3434 - 3544 3784 - 3883 4099 - 4189 2273 - 2451 2831 - 2963 3266 - 3376 3637 - 3733 3966 - 4053	-2.3--1.9 -1.7--1.4	3 2	**	

7	$X(2632)$???	$c\bar{s}u\bar{u}$	121 – 195 29 – 57	$D_s^+\pi_u^0$ D^0K^+	2103 2359	$\Lambda_c^+\bar{\Lambda}^0$ $\Sigma_c^+\bar{\Sigma}^-$ $\Xi_c^+\bar{\Xi}^0$	3402 3643 3783	2841 – 2983 3162 – 3284 3442 – 3552 3695 – 3796 3928 – 4021	2502 – 2672 3025 – 3155 3442 – 3552 3801 – 3898 4121 – 4209	-1.8–1.3 -1.3–1.0	3 2	
8			$c\bar{d}s\bar{s}$	121 – 195 29 – 57	$D_s^+\pi_d^0$ D^+K^0	2103 2368	$\Lambda_c^+\bar{\Lambda}^0$ $\Sigma_c^0\bar{\Sigma}^+$ $\Xi_c^0\bar{\Xi}^+$	3402 3651 3792	2841 – 2983 3162 – 3284 3442 – 3552 3695 – 3796 3928 – 4021	2502 – 2672 3025 – 3155 3442 – 3552 3801 – 3898 4121 – 4209	-1.8–1.3 -1.3–1.0	3 2	
9	$T_{c\bar{s}0}^a(2900)^0$	0?	$c\bar{s}d\bar{u}$	100 – 152 29 – 59	$D_s^+\pi^-$ D^0K^0	2108 2363	$\Lambda_c^+\bar{\Sigma}^-$ $\Sigma_c^0\bar{\Lambda}^0$ $\Xi_c^0\bar{\Xi}^0$	3475 3570 3785	2936 – 3075 3243 – 3365 3515 – 3625 3762 – 3863 3990 – 4084	2616 – 2780 3112 – 3240 3515 – 3625 3865 – 3963 4179 – 4269	-2.0–1.6 -1.5–1.2	3 2	**
10	$T_{cs1}(2900)^0$ $T_{c\bar{s}0}^a(2900)^{++}$	1– 0?	$c\bar{d}u\bar{s}$	98 – 147 29 – 59	$D_s^+\pi^+$ D^+K^+	2108 2364	$\Lambda_c^+\bar{\Sigma}^+$ $\Sigma_c^{++}\bar{\Lambda}^0$ $\Xi_c^+\bar{\Xi}^+$	3483 3570 3790	2946 – 3085 3252 – 3374 3523 – 3633 3769 – 3870 3996 – 4091	2628 – 2791 3121 – 3250 3523 – 3633 3872 – 3970 4186 – 4275	-2.1–1.6 -1.5–1.2	3 2	**
11			$c\bar{u}s\bar{u}$	127 – 208 27 – 54	D^0K^-	2359	$\Xi_c^0\bar{p}$ $\Xi_c^+\bar{\Delta}^{--}$ $\Omega_c^0\bar{\Sigma}^-$	3408 3700 3884	2793 – 2943 3147 – 3273 3448 – 3558 3715 – 3814 3957 – 4048	3448 – 3558 3825 – 3921 4157 – 4243 4457 – 4536 4734 – 4808	-2.2–1.8 -1.9–1.6	2 1	**
12	$T_{cs0}(2900)^0$	0 ⁺	$c\bar{d}s\bar{u}$	127 – 210 27 – 54	$D^0\bar{K}^0$ D^+K^-	2363 2364	$\Xi_c^+\bar{p}$ $\Xi_c^0\bar{n}$ $\Omega_c^0\bar{\Lambda}^0$	3406 3410 3811	2790 – 2941 3145 – 3270 3446 – 3556 3713 – 3812 3955 – 4047	3446 – 3556 3823 – 3919 4155 – 4241 4456 – 4535 4733 – 4806	-2.2–1.8 -1.9–1.6	2 1	**
13			$c\bar{d}s\bar{d}$	127 – 208 27 – 54	$D^+\bar{K}^0$	2368	$\Xi_c^+\bar{n}$ $\Xi_c^0\bar{\Delta}^+$ $\Omega_c^0\bar{\Sigma}^+$	3408 3702 3892	2793 – 2943 3147 – 3273 3448 – 3558 3715 – 3814 3957 – 4048	3448 – 3558 3825 – 3921 4157 – 4243 4457 – 4536 4734 – 4808	-2.2–1.8 -1.9–1.6	2 1	**
14			$c\bar{s}s\bar{u}$	178 – 330 25 – 51	$D_s^+K^-$ $D^0\phi(1020)$	2462 2884	$\Xi_c^0\bar{\Lambda}^0$ $\Xi_c^+\bar{\Sigma}^-$ $\Omega_c^0\bar{\Xi}^0$	3586 3657 4010	3004 – 3150 3338 – 3462 3626 – 3736 3883 – 3983 4118 – 4211	2636 – 2820 3197 – 3329 3626 – 3736 3990 – 4086 4313 – 4400	-1.3–0.91 -1.0–0.71	3 2	
15			$c\bar{s}u\bar{s}$	166 – 300 27 – 53	$D_s^+K^+$	2462	$\Lambda_c^+\bar{\Xi}^+$ $\Sigma_c^{++}\bar{\Xi}^0$ $\Xi_c^+\bar{\Omega}^+$	3608 3769 4140	3062 – 3203 3374 – 3497 3648 – 3758 3896 – 3996 4124 – 4217	2732 – 2901 3241 – 3371 3648 – 3758 3999 – 4097 4313 – 4402	-1.7–1.2 -1.2–0.94	3 2	**
16			$c\bar{s}d\bar{s}$	168 – 307 26 – 53	$D_s^+K^0$	2466	$\Lambda_c^+\bar{\Xi}^0$ $\Sigma_c^0\bar{\Xi}^+$ $\Xi_c^0\bar{\Omega}^+$	3601 3776 4142	3053 – 3194 3366 – 3489 3641 – 3751 3889 – 3990 4118 – 4211	2721 – 2891 3233 – 3363 3641 – 3751 3993 – 4090 4308 – 4396	-1.7–1.2 -1.2–0.92	3 2	**
17			$c\bar{d}s\bar{s}$	178 – 332 25 – 51	$D_s^+\bar{K}^0$ $D^+\phi(1020)$	2466 2889	$\Xi_c^+\bar{\Lambda}^0$ $\Xi_c^0\bar{\Sigma}^+$ $\Omega_c^0\bar{\Xi}^+$	3584 3667 4017	3001 – 3148 3336 – 3460 3624 – 3734 3881 – 3981 4117 – 4209	2632 – 2817 3194 – 3327 3624 – 3734 3988 – 4085 4311 – 4398	-1.3–0.9 -0.99–0.7	3 2	
18			$c\bar{s}s\bar{s}$	242 – 504 23 – 47	$D_s^+\phi(1020)$	2987	$\Xi_c^+\bar{\Xi}^0$ $\Xi_c^0\bar{\Xi}^+$ $\Omega_c^0\bar{\Omega}^+$	3783 3792 4367	3214 – 3360 3541 – 3665 3823 – 3933 4075 – 4175 4306 – 4399	3823 – 3933 4180 – 4277 4497 – 4585 4786 – 4866 5053 – 5128	-2.2–1.8 -1.9–1.6	2 1	
19			$c\bar{c}d\bar{d}$	24 – 51 32 – 64	$\eta_c(1S)\pi_d^0$ D^+D^-	3119 3740	$\Lambda_c^+\bar{\Lambda}_c^-$ $\Sigma_c^0\bar{\Sigma}_c^0$ $\Xi_c^0\bar{\Xi}_c^0$	4572 4908 4940	4182 – 4308 4404 – 4521 4612 – 4722 4808 – 4912 4993 – 5092	3969 – 4104 4308 – 4428 4612 – 4722 4891 – 4993 5151 – 5246	-2.7–2.2 -2.3–2.0	5 3	
20			$c\bar{c}u\bar{u}$	24 – 51 32 – 64	$\eta_c(1S)\pi_u^0$ $D^0\bar{D}^0$	3119 3730	$\Lambda_c^+\bar{\Lambda}_c^-$ $\Sigma_c^+\bar{\Sigma}_c^-$ $\Xi_c^+\bar{\Xi}_c^-$	4572 4908 4936	4182 – 4308 4404 – 4521 4612 – 4722 4808 – 4912 4993 – 5092	3969 – 4104 4308 – 4428 4612 – 4722 4891 – 4993 5151 – 5246	-2.7–2.2 -2.3–2.0	5 3	
21			$c\bar{c}u\bar{d}$	11 – 31 34 – 67	$\eta_c(1S)\pi^+$ $D^+\bar{D}^0$	3124 3735	$\Sigma_c^{++}\bar{\Lambda}_c^-$ $\Lambda_c^+\bar{\Sigma}_c^0$ $\Xi_c^+\bar{\Xi}_c^0$	4740 4740 4938	4373 – 4497 4583 – 4699 4780 – 4890 4967 – 5072 5145 – 5245	4174 – 4306 4491 – 4611 4780 – 4890 5047 – 5150 5297 – 5394	-2.6–2.0 -2.0–1.6	6 4	*

22	$Z_c(3900)$ $Z_c(4200)$ $Z_c(4430)$ $X(4020)$ $X(4051)$ $X(4055)$ $X(4100)$ $X(4240)$ $X(4250)$	1^{+-} 1^{+-} 1^{+-} $?^-$ $?^+$ $?^-$ $?^?$ 0^{--} $?^-$	$c\bar{c}d\bar{u}$	$11 - 31$ $34 - 67$	$\eta_c(1S)\pi^-$ $D^0 D^-$	3124 3735	$\Lambda_c^+ \bar{\Sigma}_c^{--}$ $\Sigma_c^0 \bar{\Lambda}_c^-$ $\Xi_c^0 \bar{\Xi}_c^-$	4740 4740 4938	$4373 - 4497$ $4583 - 4699$ $4780 - 4890$ $4967 - 5072$ $5145 - 5245$	$4174 - 4306$ $4491 - 4611$ $4780 - 4890$ $5047 - 5150$ $5297 - 5394$	$-2.6 - 2.0$ $-2.0 - 1.6$	6 4	*
23			$c\bar{c}s\bar{u}$	$47 - 79$ $29 - 59$	$\eta_c(1S)K^-$ $D^0 D_s^-$	3478 3833	$\Xi_c^0 \bar{\Lambda}_c^-$ $\Xi_c^+ \bar{\Sigma}_c^{--}$ $\Omega_c^0 \bar{\Xi}_c^-$	4756 4922 5163	$4362 - 4488$ $4587 - 4704$ $4796 - 4906$ $4993 - 5097$ $5179 - 5278$	$4145 - 4282$ $4489 - 4610$ $4796 - 4906$ $5076 - 5178$ $5337 - 5432$	$-3.3 - 2.7$ $-2.0 - 1.6$	4 3	*
24	$T_{\psi s1}^\theta(4000)^+$ $T_{\psi s1}(4220)^+$ $T_{\psi s1}^\theta(4000)^0$	1^+ 1^+ 1^+	$c\bar{c}u\bar{s}$	$47 - 79$ $29 - 59$	$\eta_c(1S)K^+$ $D_s^+ \bar{D}^0$	3478 3833	$\Lambda_c^+ \bar{\Xi}_c^0$ $\Sigma_c^{++} \bar{\Xi}_c^-$ $\Xi_c^+ \bar{\Omega}_c^0$	4756 4922 5163	$4362 - 4488$ $4587 - 4704$ $4796 - 4906$ $4993 - 5097$ $5179 - 5278$	$4145 - 4282$ $4489 - 4610$ $4796 - 4906$ $5076 - 5178$ $5337 - 5432$	$-3.3 - 2.7$ $-2.0 - 1.6$	4 3	*
25			$c\bar{c}d\bar{s}$	$47 - 80$ $29 - 59$	$\eta_c(1S)K^0$ $D_s^+ D^-$	3482 3838	$\Lambda_c^+ \bar{\Xi}_c^-$ $\Sigma_c^0 \bar{\Xi}_c^0$ $\Xi_c^0 \bar{\Omega}_c^0$	4754 4924 5165	$4359 - 4486$ $4585 - 4702$ $4794 - 4904$ $4991 - 5095$ $5177 - 5276$	$4142 - 4279$ $4487 - 4608$ $4794 - 4904$ $5075 - 5176$ $5335 - 5430$	$-3.2 - 2.7$ $-2.0 - 1.6$	4 3	*
26			$c\bar{c}s\bar{d}$	$47 - 80$ $29 - 59$	$\eta_c(1S)\bar{K}^0$ $D^+ D_s^-$	3482 3838	$\Xi_c^+ \bar{\Lambda}_c^-$ $\Xi_c^0 \bar{\Sigma}_c^0$ $\Omega_c^0 \bar{\Xi}_c^0$	4754 4924 5165	$4359 - 4486$ $4585 - 4702$ $4794 - 4904$ $4991 - 5095$ $5177 - 5276$	$4142 - 4279$ $4487 - 4608$ $4794 - 4904$ $5075 - 5176$ $5335 - 5430$	$-3.2 - 2.7$ $-2.0 - 1.6$	4 3	*
27			$c\bar{c}u\bar{u}$		$D^0 D^0$	3730	$\Xi_{cc}^+ \bar{p}$ $\Xi_{cc}^{++} \bar{\Delta}^{--}$ $\Omega_{cc}^+ \bar{\Sigma}^-$	4457 4854	$3981 - 4115$ $4253 - 4373$ $4497 - 4607$ $4721 - 4823$ $4930 - 5026$	$4497 - 4607$ $4816 - 4915$ $5105 - 5196$ $5372 - 5456$ $5621 - 5700$	$-3.7 - 3.3$ $-3.0 - 2.6$	2 1	**
28	$T_{cc}(3875)$??	$c\bar{c}\bar{d}\bar{u}$		$D^+ D^0$ $D^0 D^+$	3735 3735	$\Xi_{cc}^+ \bar{n}$ $\Xi_{cc}^{++} \bar{p}$ $\Omega_{cc}^+ \bar{\Lambda}^0$	4459 4560	$3983 - 4118$ $4255 - 4375$ $4499 - 4609$ $4723 - 4825$ $4932 - 5027$	$4499 - 4609$ $4818 - 4917$ $5107 - 5198$ $5373 - 5458$ $5622 - 5702$	$-3.7 - 3.3$ $-3.0 - 2.6$	2 1	**
29			$c\bar{d}cd\bar{d}$		$D^+ D^+$	3740	$\Xi_{cc}^{++} \bar{n}$ $\Xi_{cc}^{++} \bar{\Delta}^+$ $\Omega_{cc}^+ \bar{\Sigma}^+$	4562 4751	$4109 - 4241$ $4367 - 4487$ $4602 - 4712$ $4819 - 4921$ $5021 - 5118$	$3852 - 4000$ $4256 - 4381$ $4602 - 4712$ $4910 - 5010$ $5192 - 5284$	$-3.2 - 2.7$ $-2.3 - 2.0$	3 2	**
30			$c\bar{s}c\bar{u}$		$D_s^+ D^0$ $D^0 D_s^+$	3833 3833	$\Xi_{cc}^+ \bar{\Lambda}^0$ $\Xi_{cc}^{++} \bar{\Sigma}^-$ $\Omega_{cc}^+ \bar{\Xi}^0$	4635 4811	$4181 - 4314$ $4440 - 4560$ $4675 - 4785$ $4892 - 4994$ $5094 - 5191$	$3922 - 4071$ $4328 - 4453$ $4675 - 4785$ $4983 - 5083$ $5264 - 5356$	$-3.9 - 3.4$ $-2.1 - 1.8$	2	**
31			$c\bar{d}c\bar{s}$		$D^+ D_s^+$ $D_s^+ D^+$	3838 3838	$\Xi_{cc}^+ \bar{\Sigma}^+$ $\Xi_{cc}^{++} \bar{\Lambda}^0$ $\Omega_{cc}^+ \bar{\Xi}^+$	4716 4738	$4279 - 4410$ $4528 - 4647$ $4756 - 4866$ $4967 - 5070$ $5165 - 5262$	$4032 - 4178$ $4421 - 4544$ $4756 - 4866$ $5057 - 5157$ $5332 - 5425$	$-3.3 - 2.8$ $-2.4 - 2.0$	3 2	**
32	$X(3960)$ $X(4140)$ $X(4274)$ $\chi_{c0}(4500)$ $\chi_{c1}(4685)$ $\chi_{c0}(4700)$ $X(4350)$ $X(4630)$ $\psi(4360)$ $\psi(4660)$	0^{++} 1^{++} 1^{++} 0^{++} 1^{++} 0^{++} $?^+$ 1^{-+} 1^{--} 1^{--}	$c\bar{c}s\bar{s}$	$89 - 134$ $27 - 54$	$D_s^+ D_s^-$ $\eta_c(1S)\phi(1020)$	3936 4003	$\Xi_{cc}^+ \bar{\Xi}_c^-$ $\Xi_c^0 \bar{\Xi}_c^0$ $\Omega_c^0 \bar{\Omega}_c^0$	4936 4940 5390	$4536 - 4664$ $4765 - 4882$ $4976 - 5086$ $5174 - 5278$ $5361 - 5459$	$4315 - 4454$ $4666 - 4787$ $4976 - 5086$ $5258 - 5359$ $5519 - 5613$	$-3.8 - 3.2$ $-2.7 - 2.3$	3 2	
33			$c\bar{s}c\bar{s}$		$D_s^+ D_s^+$	3936	$\Xi_{cc}^+ \bar{\Xi}^+$ $\Xi_{cc}^{++} \bar{\Xi}^0$ $\Omega_{cc}^+ \bar{\Omega}^+$	4841 4937	$4401 - 4533$ $4652 - 4772$ $4881 - 4991$ $5093 - 5195$ $5291 - 5387$	$4151 - 4298$ $4544 - 4668$ $4881 - 4991$ $5182 - 5282$ $5457 - 5550$	$-2.9 - 2.4$ $-2.1 - 1.7$	3 2	**
34			$c\bar{c}c\bar{u}$	$13 - 33$ $29 - 59$	$\eta_c(1S)D^0$ $D^0 \eta_c(1S)$	4849 4849	$\Xi_{cc}^+ \bar{\Lambda}_c^-$ $\Xi_{cc}^{++} \bar{\Sigma}_c^{--}$ $\Omega_{cc}^+ \bar{\Xi}_c^-$	5805 6076	$5481 - 5602$ $5668 - 5783$ $5845 - 5955$ $6014 - 6120$ $6176 - 6278$	$5305 - 5434$ $5586 - 5704$ $5845 - 5955$ $6087 - 6191$ $6316 - 6414$	$-5.5 - 4.9$ $-3.6 - 3.2$	4 3	*

35			$c\bar{c}d\bar{d}$	8 – 24 30 – 61	$\eta_c(1S)D^+$ $D^+\eta_c(1S)$	4854 4854	$\Xi_{cc}^{++}\bar{\Lambda}_c^-$ $\Xi_{cc}^+\bar{\Sigma}_c^0$ $\Omega_{cc}^+\bar{\Xi}_c^0$	5908 5973	5595 – 5716 5776 – 5891 5948 – 6058 6113 – 6219 6271 – 6373	5425 – 5552 5696 – 5814 5948 – 6058 6184 – 6288 6407 – 6506	–5.2–4.5 –4.0–3.6	5 3	*
36			$c\bar{c}c\bar{s}$	26 – 53 27 – 55	$\eta_c(1S)D_s^+$ $D_s^+\eta_c(1S)$	4952 4952	$\Xi_{cc}^+\bar{\Xi}_c^0$ $\Xi_{cc}^+\bar{\Xi}_c^-$ $\Omega_{cc}^+\bar{\Omega}_c^0$	5989 6090	5664 – 5786 5851 – 5967 6029 – 6139 6198 – 6304 6360 – 6462	5487 – 5616 5769 – 5888 6029 – 6139 6271 – 6375 6499 – 6597	–5.1–4.4 –3.3–2.8	4 3	*
37	$T_{\psi\psi}(6600)$ $T_{\psi\psi}(6600)$ $T_{\psi\psi}(6900)$ $T_{\psi\psi}(6900)$ $T_{\psi\psi}(7300)$?? ?? ?? ?? ??	$c\bar{c}c\bar{c}$	6 – 21 29 – 58	$\eta_c(1S)\eta_c(1S)$	5968	$\Xi_{cc}^+\bar{\Xi}_{cc}^-$ $\Xi_{cc}^{++}\bar{\Xi}_{cc}--$ $\Omega_{cc}^+\bar{\Omega}_{cc}^-$	7038 7244	6768 – 6887 6926 – 7040 7078 – 7188 7225 – 7331 7366 – 7469	6622 – 6745 6857 – 6973 7078 – 7188 7288 – 7393 7489 – 7589	–5.9–5.1 –4.2–3.7	6 4	*
38			$c\bar{b}d\bar{d}$		$B_c^+\pi_d^0$ $D^+\bar{B}^0$	6409 7150	$\Xi_c^0\bar{\Xi}_b^+$ $\Sigma_c^0\bar{\Sigma}_b^+$ $\Lambda_c^+\bar{\Sigma}_b^0$	8267 8270	7986 – 8106 8150 – 8265 8307 – 8417 8457 – 8563 8602 – 8704	7833 – 7959 8078 – 8195 8307 – 8417 8522 – 8626 8726 – 8826	–2.6–1.8 –2.3–1.8	8 5	
39			$c\bar{b}u\bar{u}$		$B_c^+\pi_u^0$ D^0B^-	6409 7144	$\Xi_c^+\bar{\Xi}_b^0$ $\Sigma_c^+\bar{\Sigma}_b^-$ $\Lambda_c^+\bar{\Sigma}_b^0$	8260 8265	7978 – 8099 8143 – 8258 8300 – 8410 8451 – 8556 8595 – 8698	7825 – 7951 8071 – 8188 8300 – 8410 8516 – 8620 8720 – 8819	–2.5–1.8 –2.3–1.8	8 5	
40			$c\bar{b}d\bar{u}$		$B_c^+\pi^-$ $D^0\bar{B}^0$	6414 7145	$\Lambda_c^+\bar{\Sigma}^-$ $\Xi_c^0\bar{\Xi}_b^0$ $\Sigma_c^0\bar{\Sigma}_b^0$	8097 8262	7798 – 7920 7972 – 8088 8137 – 8247 8294 – 8400 8445 – 8546	7635 – 7764 7896 – 8014 8137 – 8247 8362 – 8466 8574 – 8672	–2.5–1.8 –1.5–1.1	7 5	**
41			$c\bar{b}u\bar{d}$		$B_c^+\pi^+$ D^+B^-	6414 7149	$\Lambda_c^+\bar{\Sigma}_b^+$ $\Xi_c^+\bar{\Xi}_b^+$ $\Sigma_c^+\bar{\Sigma}_b^0$	8102 8265	7804 – 7926 7977 – 8093 8142 – 8252 8299 – 8404 8450 – 8551	7641 – 7769 7902 – 8020 8142 – 8252 8367 – 8470 8579 – 8677	–2.5–1.8 –1.6–1.1	7 5	**
42			$c\bar{b}s\bar{u}$		$B_c^+K^-$ $D^0\bar{B}_s^0$	6768 7232	$\Xi_c^+\bar{\Sigma}_b^-$ $\Omega_c^0\bar{\Xi}_b^0$ $\Xi_c^0\bar{\Xi}_b^0$	8279 8487	7980 – 8102 8154 – 8270 8319 – 8429 8476 – 8581 8627 – 8728	7816 – 7945 8078 – 8196 8319 – 8429 8544 – 8647 8755 – 8853	–3.0–2.3 –2.2–1.7	6 4	**
43			$c\bar{b}u\bar{s}$		$B_c^+K^+$ $D_s^+B^-$	6768 7247	$\Lambda_c^+\bar{\Xi}_b^+$ $\Sigma_c^+\bar{\Xi}_b^0$ $\Xi_c^+\bar{\Omega}_b^+$	8083 8246 8514	7742 – 7868 7939 – 8056 8123 – 8233 8296 – 8400 8460 – 8559	7552 – 7688 7853 – 7974 8123 – 8233 8370 – 8472 8600 – 8695	–2.3–1.7 –2.1–1.6	5 3	**
44			$c\bar{b}s\bar{d}$		$B_c^+\bar{K}^0$ $D^+\bar{B}_s^0$	6772 7237	$\Xi_c^0\bar{\Sigma}_b^+$ $\Omega_c^0\bar{\Xi}_b^+$ $\Xi_c^+\bar{\Sigma}_b^0$	8286 8492	7988 – 8110 8161 – 8277 8326 – 8436 8483 – 8588 8633 – 8734	7824 – 7953 8086 – 8204 8326 – 8436 8550 – 8654 8762 – 8860	–3.0–2.3 –2.2–1.8	6 4	**
45			$c\bar{b}d\bar{s}$		$B_c^+K^0$ $D_s^+\bar{B}^0$	6772 7248	$\Lambda_c^+\bar{\Xi}_b^0$ $\Sigma_c^0\bar{\Xi}_b^+$ $\Xi_c^0\bar{\Omega}_b^+$	8078 8251 8516	7736 – 7862 7934 – 8051 8118 – 8228 8291 – 8395 8456 – 8555	7545 – 7682 7848 – 7969 8118 – 8228 8365 – 8467 8595 – 8691	–2.3–1.7 –2.1–1.6	5 3	**
46			$b\bar{u}c\bar{u}$		B^+D^0	7144	$\Xi_{bc}^+\bar{\Delta}^{--}$ $\Xi_{bc}^0\bar{\Xi}_c^0$ $\Omega_{bc}^0\bar{\Sigma}^-$		7154 – 7194 7449 – 7482 7702 – 7732 7928 – 7955 8135 – 8159 8326 – 8349 8506 – 8528 8676 – 8697 8838 – 8857 8992 – 9011 9141 – 9159 9284 – 9301	7154 – 7194 7565 – 7597 7904 – 7931 8200 – 8224 8467 – 8489 8713 – 8733 8942 – 8961 9157 – 9175 9361 – 9378 9556 – 9572 9742 – 9758 9921 – 9937	–2.3–2.1 –1.6–1.5		**

47		$b\bar{c}u$		$B^0 D^0$ $B^+ D^+$	7145 7149	$\Xi_{bc}^+\bar{p}$ $\Xi_{bc}^0\bar{n}$ $\Omega_{bc}^0\Lambda^0$		7155 – 7195 7450 – 7483 7703 – 7732 7929 – 7956 8135 – 8160 8327 – 8350 8507 – 8528 8677 – 8697 8838 – 8858 8993 – 9012 9141 – 9159 9284 – 9302	7155 – 7195 7566 – 7598 7905 – 7932 8201 – 8225 8468 – 8490 8713 – 8734 8942 – 8961 9157 – 9175 9361 – 9379 9556 – 9573 9743 – 9758 9922 – 9937	-2.3–2.1 -1.6–1.5	**
48		$b\bar{c}d\bar{d}$		$B^0 D^+$	7150	$\Xi_{bc}^+\bar{n}$ $\Xi_{bc}^0\Delta^+$ $\Omega_{bc}^0\Sigma^+$		7160 – 7200 7454 – 7487 7706 – 7736 7932 – 7959 8138 – 8163 8330 – 8353 8509 – 8531 8679 – 8700 8841 – 8860 8995 – 9014 9143 – 9162 9286 – 9304	7160 – 7200 7570 – 7602 7908 – 7935 8204 – 8228 8470 – 8493 8716 – 8736 8944 – 8964 9160 – 9178 9364 – 9381 9558 – 9575 9744 – 9760 9924 – 9939	-2.3–2.1 -1.6–1.5	**
49		$b\bar{s}c\bar{u}$		$B_s^0 D^0$ $B^+ D_s^+$	7232 7247	$\Xi_{bc}^+\bar{\Sigma}^-$ $\Xi_{bc}^0\bar{\Lambda}^0$ $\Omega_{bc}^0\bar{\Xi}^0$		7242 – 7282 7537 – 7570 7789 – 7818 8014 – 8040 8219 – 8244 8410 – 8433 8589 – 8610 8758 – 8778 8918 – 8938 9072 – 9091 9220 – 9238 9362 – 9380	7242 – 7282 7653 – 7684 7990 – 8017 8284 – 8308 8550 – 8572 8794 – 8814 9022 – 9041 9236 – 9254 9439 – 9456 9633 – 9649 9818 – 9834 9997 – 10012	-2.0–1.9 -1.4–1.3	**
50		$b\bar{c}s\bar{s}$		$B_s^0 D^+$ $B^0 D_s^+$	7237 7248	$\Xi_{bc}^+\bar{\Lambda}^0$ $\Xi_{bc}^0\Sigma^+$ $\Omega_{bc}^0\Xi^+$		7247 – 7287 7541 – 7574 7792 – 7822 8017 – 8044 8222 – 8247 8413 – 8436 8591 – 8613 8760 – 8781 8921 – 8940 9075 – 9093 9222 – 9240 9364 – 9382	7247 – 7287 7657 – 7688 7993 – 8020 8287 – 8311 8553 – 8574 8797 – 8817 9024 – 9043 9238 – 9256 9441 – 9458 9635 – 9651 9820 – 9836 9999 – 10014	-2.0–1.9 -1.4–1.3	**
51		$c\bar{b}s\bar{s}$		$B_c^+ \phi(1020)$ $D_s^+ \bar{B}_s^0$	7293 7335	$\Xi_c^+\bar{\Xi}_b^0$ $\Xi_c^0\bar{\Xi}_b^+$ $\Omega_c^0\bar{\Omega}_b^+$	8260 8267 8741	7915 – 8042 8115 – 8232 8300 – 8410 8474 – 8578 8638 – 8737	7722 – 7860 8028 – 8150 8300 – 8410 8548 – 8649 8778 – 8873	-2.8–2.2 -2.7–2.3	4 2
52		$b\bar{s}c\bar{s}$		$B_s^0 D_s^+$	7335	$\Xi_{bc}^+\bar{\Xi}^0$ $\Xi_{bc}^0\bar{\Xi}^+$ $\Omega_{bc}^0\bar{\Omega}^+$		7345 – 7385 7649 – 7682 7906 – 7934 8132 – 8158 8339 – 8362 8529 – 8551 8708 – 8729 8877 – 8896 9037 – 9056 9191 – 9209 9338 – 9355 9480 – 9496	7345 – 7385 7768 – 7798 8108 – 8134 8404 – 8427 8669 – 8690 8913 – 8933 9140 – 9158 9354 – 9371 9556 – 9573 9749 – 9765 9934 – 9949 10112 – 10126	-1.6–1.5 -1.1–1.0	**

53		$b\bar{c}c\bar{u}$		$\bar{B}_c^- D^0$ $B^+ \eta_c(1S)$	8139 8263	$\Xi_{bc}^+ \bar{\Sigma}_c^{--}$ $\Xi_{bc}^0 \bar{\Lambda}_c^-$ $\Omega_{bc}^0 \bar{\Xi}_c^-$		8149 – 8189 8372 – 8408 8575 – 8608 8763 – 8794 8939 – 8968 9105 – 9132 9262 – 9289 9413 – 9439 9558 – 9583 9698 – 9722 9833 – 9856 9964 – 9986	8149 – 8189 8465 – 8499 8743 – 8774 8995 – 9023 9228 – 9255 9446 – 9471 9652 – 9676 9848 – 9870 10035 – 10057 10215 – 10235 10387 – 10408 10555 – 10574	-3.4–3.2 -2.3–2.2	*	
54		$c\bar{b}u\bar{c}$		$B_c^+ \bar{D}^0$ $\eta_c(1S)B^-$	8139 8263	$\Sigma_c^{++} \bar{\Xi}_{bc}^-$ $\Lambda_c^+ \bar{\Xi}_{bc}^0$ $\Xi_c^+ \bar{\Omega}_{bc}^0$		8149 – 8189 8372 – 8408 8575 – 8608 8763 – 8794 8939 – 8968 9105 – 9132 9262 – 9289 9413 – 9439 9558 – 9583 9698 – 9722 9833 – 9856 9964 – 9986	8149 – 8189 8465 – 8499 8743 – 8774 8995 – 9023 9228 – 9255 9446 – 9471 9652 – 9676 9848 – 9870 10035 – 10057 10215 – 10235 10387 – 10408 10555 – 10574	-3.4–3.2 -2.3–2.2	*	
55		$c\bar{b}c\bar{u}$		$B_c^+ D^0$ $D^0 B_c^+$	8139 8139	$\Xi_{cc}^{++} \bar{\Sigma}_b^-$ $\Xi_{cc}^+ \bar{\Sigma}_b^0$ $\Omega_{cc}^+ \bar{\Xi}_b^-$	9433	9198 – 9316 9338 – 9451 9473 – 9583 9604 – 9711 9731 – 9835	9069 – 9191 9276 – 9392 9473 – 9583 9661 – 9766 9841 – 9942	-5.9–5.1 -3.9–3.4	7 5	**
56		$c\bar{b}d\bar{c}$		$B_c^+ D^-$ $\eta_c(1S)\bar{B}^0$	8144 8264	$\Lambda_c^+ \bar{\Xi}_{bc}^-$ $\Sigma_c^0 \bar{\Xi}_{bc}^0$ $\Xi_c^0 \bar{\Omega}_{bc}^0$		8154 – 8194 8377 – 8413 8579 – 8612 8767 – 8798 8942 – 8971 9108 – 9136 9266 – 9292 9417 – 9442 9561 – 9586 9701 – 9724 9836 – 9859 9967 – 9989	8154 – 8194 8469 – 8504 8746 – 8778 8998 – 9027 9231 – 9258 9449 – 9474 9655 – 9679 9851 – 9873 10038 – 10059 10217 – 10238 10390 – 10410 10557 – 10576	-3.4–3.2 -2.4–2.2	*	
57		$b\bar{c}c\bar{d}$		$\bar{B}_c^- D^+$ $B^0 \eta_c(1S)$	8144 8264	$\Xi_{bc}^+ \bar{\Lambda}_c^-$ $\Xi_{bc}^0 \bar{\Sigma}_c^0$ $\Omega_{bc}^0 \bar{\Xi}_c^-$		8154 – 8194 8377 – 8413 8579 – 8612 8767 – 8798 8942 – 8971 9108 – 9136 9266 – 9292 9417 – 9442 9561 – 9586 9701 – 9724 9836 – 9859 9967 – 9989	8154 – 8194 8469 – 8504 8746 – 8778 8998 – 9027 9231 – 9258 9449 – 9474 9655 – 9679 9851 – 9873 10038 – 10059 10217 – 10238 10390 – 10410 10557 – 10576	-3.4–3.2 -2.4–2.2	*	
58		$c\bar{b}c\bar{d}$		$B_c^+ D^+$ $D^+ B_c^+$	8144 8144	$\Xi_{cc}^{++} \bar{\Sigma}_b^+$ $\Xi_{cc}^{++} \bar{\Sigma}_b^0$ $\Omega_{cc}^+ \bar{\Xi}_b^+$	9335	9093 – 9211 9236 – 9350 9375 – 9485 9509 – 9615 9639 – 9742	8960 – 9082 9173 – 9289 9375 – 9485 9567 – 9672 9751 – 9852	-5.2–4.3 -4.4–3.8	7 4	**
59		$c\bar{b}s\bar{c}$		$B_c^+ D_s^-$ $\eta_c(1S)\bar{B}_s^0$	8242 8351	$\Xi_c^+ \bar{\Xi}_{bc}^-$ $\Xi_c^0 \bar{\Xi}_{bc}^0$ $\Omega_c^0 \bar{\Omega}_{bc}^0$		8252 – 8292 8488 – 8523 8699 – 8731 8892 – 8922 9072 – 9099 9240 – 9266 9400 – 9425 9553 – 9577 9699 – 9722 9840 – 9862 9976 – 9997 10107 – 10128	8252 – 8292 8584 – 8618 8871 – 8901 9129 – 9156 9365 – 9391 9586 – 9609 9793 – 9816 9990 – 10012 10178 – 10199 10358 – 10378 10532 – 10550 10699 – 10717	-2.6–2.4 -1.8–1.7	*	

60		$b\bar{c}c\bar{s}$		$\bar{B}_c^- D_s^+$ $B_s^0 \eta_c(1S)$	8242 8351	$\Xi_{bc}^+ \bar{\Xi}_{bc}^-$ $\Xi_{bc}^0 \bar{\Xi}_{bc}^0$ $\Omega_{bc}^0 \bar{\Omega}_c^0$		8252 – 8292 8488 – 8523 8699 – 8731 8892 – 8922 9072 – 9099 9240 – 9266 9400 – 9425 9553 – 9577 9699 – 9722 9840 – 9862 9976 – 9997 10107 – 10128	8252 – 8292 8584 – 8618 8871 – 8901 9129 – 9156 9365 – 9391 9586 – 9609 9793 – 9816 9990 – 10012 10178 – 10199 10358 – 10378 10532 – 10550 10699 – 10717	-2.6 – -2.4 -1.8 – -1.7	*	
61		$c\bar{b}c\bar{s}$		$B_c^+ D_s^+$ $D_s^+ B_c^+$	8242 8242	$\Xi_{cc}^+ \bar{\Xi}_b^+$ $\Xi_{cc}^+ \bar{\Xi}_b^0$ $\Omega_{cc}^+ \bar{\Omega}_b^+$	9316 9414	9045 – 9166 9204 – 9319 9356 – 9466 9501 – 9607 9641 – 9743	8896 – 9023 9134 – 9252 9356 – 9466 9564 – 9668 9761 – 9860	-4.6 – -3.9 -2.7 – -2.1	5 4	**
62		$c\bar{b}c\bar{c}$		$B_c^+ \eta_c(1S)$ $\eta_c(1S) B_c^+$	9258 9258	$\Xi_{cc}^{++} \bar{\Xi}_{bc}^-$ $\Xi_{cc}^+ \bar{\Xi}_b^0$ $\Omega_{cc}^+ \bar{\Omega}_{bc}^0$		9268 – 9308 9456 – 9493 9631 – 9666 9795 – 9828 9951 – 9982 10099 – 10129 10241 – 10270 10378 – 10406 10510 – 10537 10638 – 10664 10762 – 10787 10883 – 10907	9268 – 9308 9535 – 9571 9777 – 9810 10001 – 10032 10210 – 10239 10408 – 10435 10596 – 10622 10776 – 10801 10949 – 10973 11115 – 11138 11276 – 11299 11432 – 11454	-4.2 – -4.0 -2.9 – -2.8	*	
63		$b\bar{b}c\bar{u}$		$\eta_b(1S) D^0$ $B^+ B_c^+$	11264 11553	$\Xi_{bc}^+ \bar{\Sigma}_b^-$ $\Xi_{bc}^0 \bar{\Sigma}_b^0$ $\Omega_{bc}^0 \bar{\Xi}_b^0$		11274 – 11314 11473 – 11508 11651 – 11683 11815 – 11845 11969 – 11997 12114 – 12141 12252 – 12277 12384 – 12409 12511 – 12535 12634 – 12657 12753 – 12775 12868 – 12890	11274 – 11314 11554 – 11588 11798 – 11828 12018 – 12046 12222 – 12248 12413 – 12437 12593 – 12617 12766 – 12788 12931 – 12952 13089 – 13110 13243 – 13263 13391 – 13411	-2.5 – -2.3 -1.7 – -1.6	*	
64		$b\bar{b}c\bar{d}$		$\eta_b(1S) D^+$ $B^0 B_c^+$	11269 11554	$\Xi_{bc}^+ \bar{\Sigma}_b^0$ $\Xi_{bc}^0 \bar{\Sigma}_b^+$ $\Omega_{bc}^0 \bar{\Xi}_b^+$		11279 – 11319 11477 – 11513 11655 – 11687 11819 – 11849 11972 – 12001 12117 – 12144 12255 – 12281 12387 – 12412 12514 – 12538 12637 – 12660 12755 – 12778 12871 – 12892	11279 – 11319 11558 – 11592 11801 – 11832 12021 – 12049 12225 – 12251 12416 – 12440 12596 – 12619 12768 – 12791 12933 – 12955 13092 – 13113 13245 – 13265 13394 – 13413	-2.5 – -2.3 -1.7 – -1.6	*	
65		$b\bar{b}c\bar{s}$		$\eta_b(1S) D_s^+$ $B_s^0 B_c^+$	11367 11641	$\Xi_{bc}^+ \bar{\Xi}_b^0$ $\Xi_{bc}^0 \bar{\Xi}_b^+$ $\Omega_{bc}^0 \bar{\Omega}_b^+$		11377 – 11417 11608 – 11641 11805 – 11834 11981 – 12008 12144 – 12169 12296 – 12319 12440 – 12462 12576 – 12598 12707 – 12728 12833 – 12853 12955 – 12974 13073 – 13091	11377 – 11417 11699 – 11730 11963 – 11990 12196 – 12220 12408 – 12431 12606 – 12627 12792 – 12812 12968 – 12987 13136 – 13155 13298 – 13315 13454 – 13470 13604 – 13620	-1.4 – -1.3 -0.98 – -0.87	*	

66		$c\bar{u}b\bar{b}$		$B_c^+ B^-$	11553	$\Sigma_c^{++}\Xi_{bb}^0$ $\Lambda_c^+\Xi_{bb}^+$ $\Xi_c^+\Omega_{bb}^+$		11563 – 11603 11795 – 11830 12002 – 12034 12191 – 12221 12367 – 12395 12532 – 12558 12688 – 12713 12837 – 12860 12979 – 13001 13116 – 13137 13247 – 13268 13375 – 13395	11563 – 11603 11890 – 11923 12171 – 12201 12423 – 12450 12654 – 12679 12869 – 12892 13071 – 13093 13262 – 13283 13444 – 13464 13618 – 13637 13786 – 13804 13948 – 13965	-2.7–2.6 -1.9–1.8	**
67		$c\bar{d}b\bar{b}$		$B_c^+ \bar{B}^0$	11554	$\Lambda_c^+\Xi_{bb}^0$ $\Sigma_c^0\Xi_{bb}^+$ $\Xi_c^0\Omega_{bb}^+$		11564 – 11604 11796 – 11831 12003 – 12035 12192 – 12222 12368 – 12395 12533 – 12559 12689 – 12713 12837 – 12861 12979 – 13002 13116 – 13138 13248 – 13269 13375 – 13396	11564 – 11604 11891 – 11924 12172 – 12202 12424 – 12451 12655 – 12680 12869 – 12893 13071 – 13093 13262 – 13283 13444 – 13464 13619 – 13638 13786 – 13805 13948 – 13966	-2.7–2.6 -1.9–1.8	**
68		$c\bar{s}b\bar{b}$		$B_c^+ \bar{B}_s^0$	11641	$\Xi_c^+\Xi_{bb}^0$ $\Xi_c^0\Xi_{bb}^+$ $\Omega_c^0\Omega_{bb}^+$		11651 – 11691 11902 – 11936 12120 – 12150 12316 – 12343 12496 – 12521 12664 – 12688 12822 – 12845 12973 – 12995 13117 – 13137 13254 – 13274 13387 – 13406 13515 – 13534	11651 – 11691 12002 – 12034 12295 – 12322 12553 – 12578 12788 – 12811 13005 – 13027 13209 – 13229 13401 – 13421 13584 – 13603 13759 – 13777 13927 – 13944 14089 – 14106	-1.9–1.8 -1.3–1.2	**
69		$b\bar{b}c\bar{c}$		$\eta_b(1S)\eta_c(1S)$ $\bar{B}_c^- B_c^+$	12383 12548	$\Xi_{bc}^+\Xi_{bc}^-$ $\Xi_{bc}^0\Xi_{bc}^0$ $\Omega_{bc}^0\Omega_{bc}^0$		12393 – 12433 12580 – 12616 12749 – 12782 12905 – 12936 13052 – 13081 13191 – 13218 13323 – 13349 13450 – 13475 13572 – 13597 13691 – 13714 13805 – 13828 13916 – 13939	12393 – 12433 12657 – 12691 12888 – 12919 13099 – 13127 13294 – 13321 13478 – 13503 13652 – 13676 13818 – 13841 13977 – 13999 14131 – 14152 14279 – 14300 14423 – 14443	-2.7–2.5 -1.9–1.7	*
70		$c\bar{b}c\bar{b}$		$B_c^+ B_c^+$	12548	$\Xi_{cc}^{++}\Xi_{bb}^0$ $\Xi_{cc}^+\Xi_{bb}^+$ $\Omega_{cc}^+\Omega_{bb}^+$		12558 – 12598 12762 – 12798 12946 – 12979 13116 – 13147 13276 – 13304 13426 – 13453 13569 – 13595 13706 – 13731 13838 – 13862 13965 – 13988 14087 – 14110 14207 – 14228	12558 – 12598 12846 – 12880 13098 – 13129 13327 – 13355 13538 – 13564 13736 – 13761 13923 – 13946 14101 – 14123 14271 – 14293 14435 – 14456 14593 – 14613 14745 – 14765	-2.9–2.7 -2.0–1.9	**
71		$b\bar{b}c\bar{b}$		$\eta_b(1S)B_c^+$	15673	$\Xi_{bc}^+\Xi_{bb}^0$ $\Xi_{bc}^0\Xi_{bb}^+$ $\Omega_{bc}^0\Omega_{bb}^+$		15683 – 15723 15894 – 15927 16074 – 16103 16235 – 16262 16384 – 16409 16523 – 16547 16655 – 16677 16781 – 16802 16901 – 16921 17016 – 17036 17128 – 17147 17236 – 17255	15683 – 15723 15977 – 16008 16218 – 16245 16432 – 16456 16626 – 16649 16808 – 16829 16978 – 16998 17140 – 17159 17295 – 17313 17444 – 17461 17587 – 17604 17726 – 17742	-1.4–1.3 -0.99–0.87	*

Table 107: Tetraquark predicted configurations and thresholds.

7.4.1 Detailed Predictions for Genuine and Semi-Genuine Tetraquarks

In the following sections we present the graphs and extended predicted spectra of each of the genuine and semi-genuine tetraquarks configurations that haven't been analysed yet in section 7.2.

7.4.2 $T_{c\bar{u}d\bar{u}}$

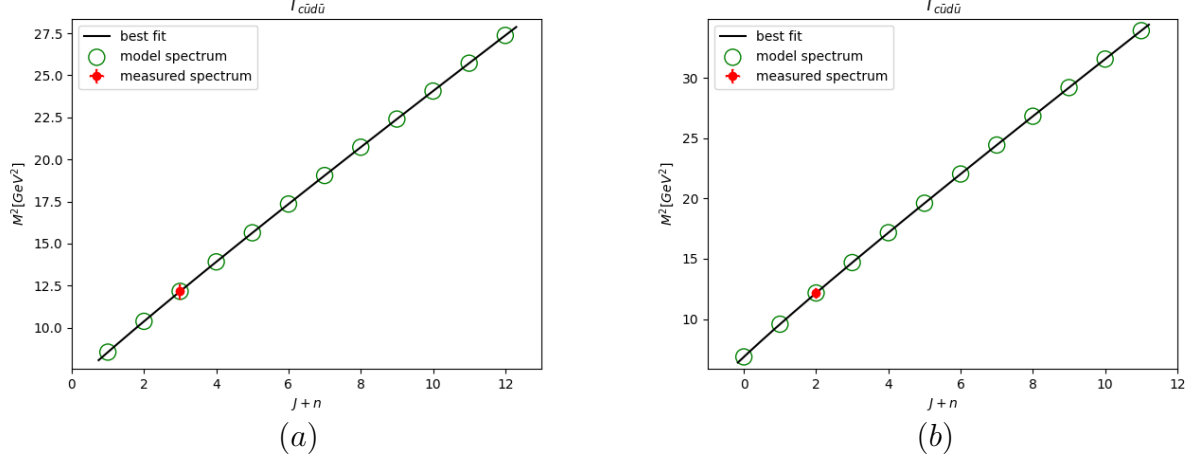


Figure 65: (a) is (J, M^2) $T_{c\bar{u}d\bar{u}}$ HMRT, (b) (n, M^2) $T_{c\bar{u}d\bar{u}}$ HMRT.

J Spec	a_{T_j}
2854 – 2992	
3160 – 3282	
3432 – 3542	
3679 – 3780	
3908 – 4002	
4121 – 4210	
4322 – 4406	-2.3 – -1.8
4513 – 4593	
4695 – 4771	
4869 – 4942	
5036 – 5107	
5198 – 5266	

Table 108: $T_{c\bar{u}d\bar{u}}$ (J, M^2) predictions.

n Spec	a_{T_n}
2537 – 2698	
3029 – 3157	
3432 – 3542	
3783 – 3881	
4098 – 4187	
4387 – 4469	
4655 – 4732	-1.7 – -1.4
4907 – 4979	
5144 – 5214	
5371 – 5437	
5587 – 5650	
5794 – 5855	

Table 109: $T_{c\bar{u}d\bar{u}}$ (n, M^2) predictions.

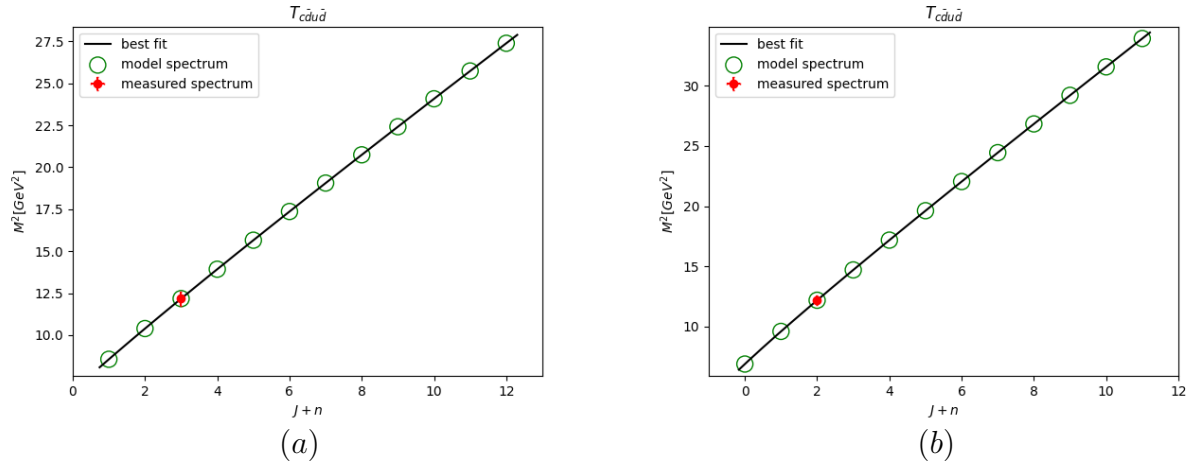


Figure 66: (a) is (J, M^2) $T_{cd\bar{u}\bar{d}}$ HMRT, (b) (n, M^2) $T_{cd\bar{u}\bar{d}}$ HMRT.

7.4.3 $T_{cd\bar{u}\bar{d}}$

J Spec	a_{T_j}
2856 – 2994	
3162 – 3284	
3434 – 3544	
3681 – 3782	
3909 – 4004	
4122 – 4211	
4323 – 4408	-2.3–-1.9
4514 – 4594	
4696 – 4773	
4870 – 4944	
5038 – 5108	
5199 – 5267	

Table 110: $T_{cd\bar{u}\bar{d}}$ (J, M^2) predictions.

n Spec	a_{T_n}
2540 – 2701	
3031 – 3160	
3434 – 3544	
3784 – 3883	
4099 – 4189	
4388 – 4471	
4656 – 4734	-1.7–-1.4
4908 – 4981	
5146 – 5215	
5372 – 5438	
5588 – 5651	
5795 – 5856	

Table 111: $T_{cd\bar{u}\bar{d}}$ (n, M^2) predictions.

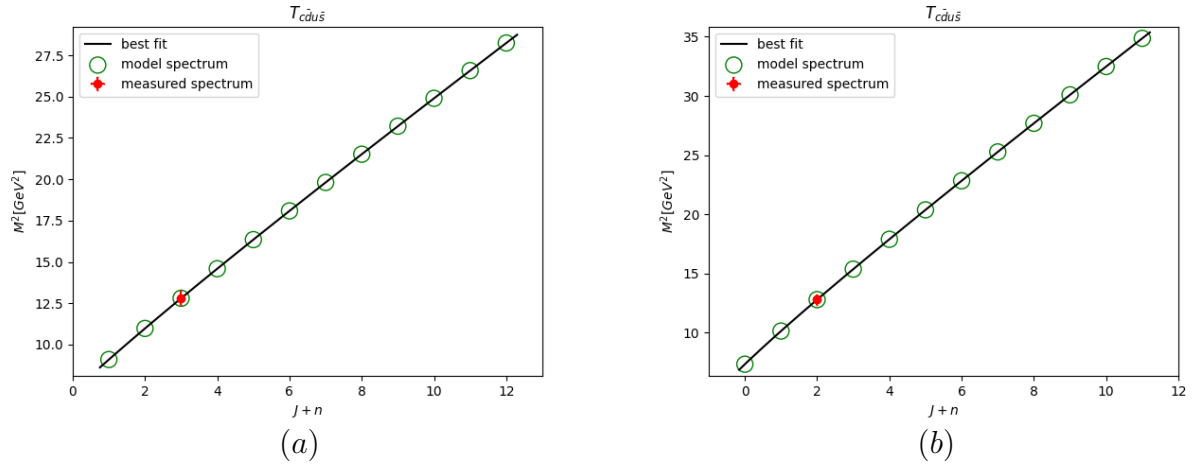


Figure 67: (a) is (J, M^2) $T_{cdus\bar{s}}$ HMRT, (b) (n, M^2) $T_{cdus\bar{s}}$ HMRT.

7.4.4 $T_{cdus\bar{s}}$

J Spec	a_{T_j}
2946 – 3085	
3252 – 3374	
3523 – 3633	
3769 – 3870	
3996 – 4091	
4209 – 4298	
4409 – 4493	
4599 – 4679	
4780 – 4856	
4953 – 5027	
5120 – 5191	
5281 – 5349	-2.1–-1.6

Table 112: $T_{cdus\bar{s}}$ (J, M^2) predictions.

n Spec	a_{T_n}
2628 – 2791	
3121 – 3250	
3523 – 3633	
3872 – 3970	
4186 – 4275	
4473 – 4556	
4740 – 4818	
4991 – 5064	
5228 – 5297	
5453 – 5519	
5668 – 5731	
5874 – 5935	-1.5–-1.2

Table 113: $T_{cdus\bar{s}}$ (n, M^2) predictions.

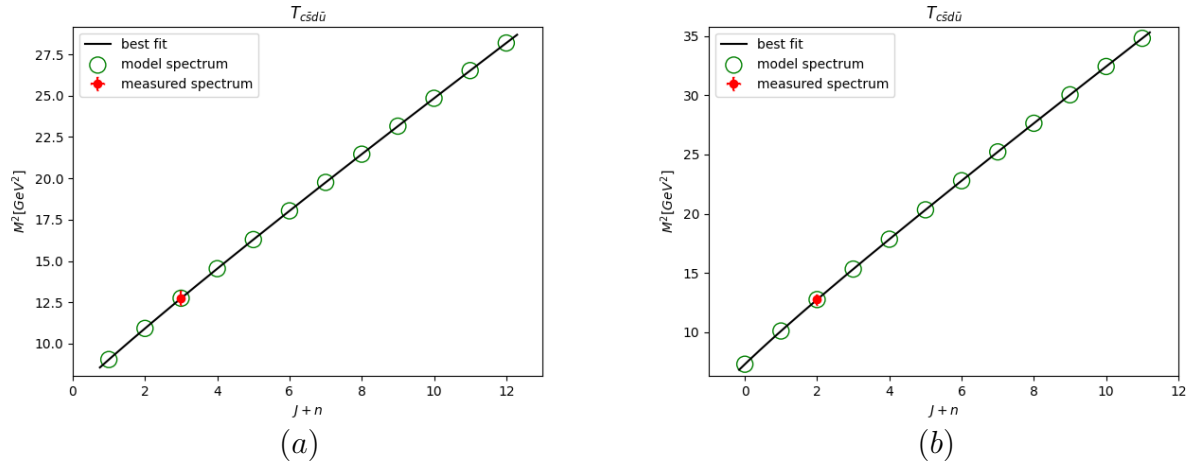


Figure 68: (a) is (J, M^2) $T_{c\bar{s}d\bar{u}}$ HMRT, (b) (n, M^2) $T_{c\bar{s}d\bar{u}}$ HMRT.

7.4.5 $T_{c\bar{s}d\bar{u}}$

J Spec	a_{T_j}
2936 – 3075	
3243 – 3365	
3515 – 3625	
3762 – 3863	
3990 – 4084	
4202 – 4291	
4403 – 4487	-2.0 – -1.6
4593 – 4673	
4774 – 4851	
4948 – 5021	
5115 – 5185	
5276 – 5344	

Table 114: $T_{c\bar{s}d\bar{u}}$ (J, M^2) predictions.

n Spec	a_{T_n}
2616 – 2780	
3112 – 3240	
3515 – 3625	
3865 – 3963	
4179 – 4269	
4467 – 4550	
4735 – 4812	-1.5 – -1.2
4986 – 5058	
5223 – 5292	
5448 – 5514	
5663 – 5726	
5870 – 5931	

Table 115: $T_{c\bar{s}d\bar{u}}$ (n, M^2) predictions.

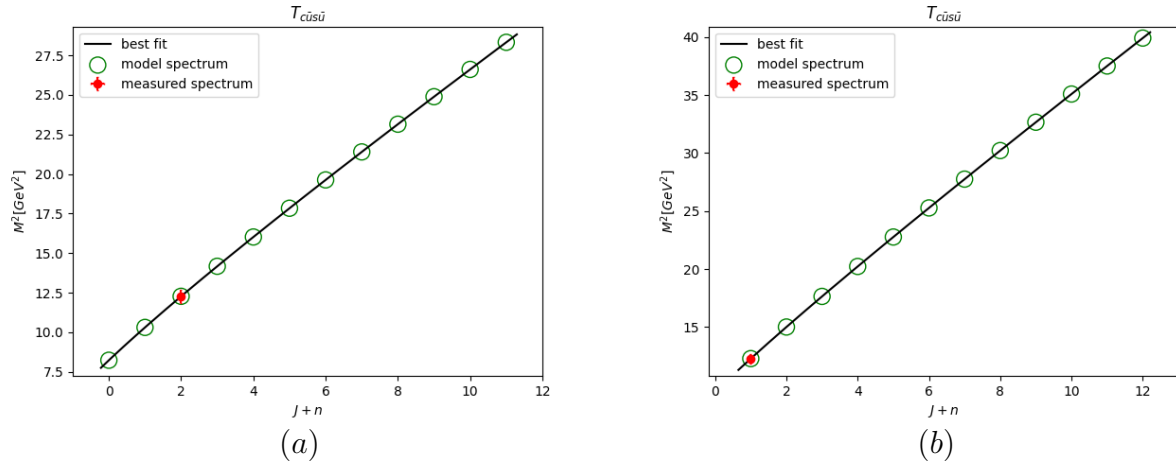


Figure 69: (a) is (J, M^2) $T_{c\bar{u}s\bar{u}}$ HMRT, (b) (n, M^2) $T_{c\bar{u}s\bar{u}}$ HMRT.

7.4.6 $T_{c\bar{u}s\bar{u}}$

J Spec	a_{T_j}
2793 – 2943	
3147 – 3273	
3448 – 3558	
3715 – 3814	
3957 – 4048	
4181 – 4266	
4390 – 4471	
4588 – 4664	
4775 – 4848	
4954 – 5023	
5125 – 5192	
5290 – 5354	-2.2–-1.8

Table 116: $T_{c\bar{u}s\bar{u}}$ (J, M^2) predictions.

n Spec	a_{T_n}
3448 – 3558	
3825 – 3921	
4157 – 4243	
4457 – 4536	
4734 – 4808	
4993 – 5062	
5236 – 5301	
5466 – 5528	
5686 – 5745	
5896 – 5953	
6098 – 6152	-1.9–-1.6
6292 – 6345	

Table 117: $T_{c\bar{u}s\bar{u}}$ (n, M^2) predictions.

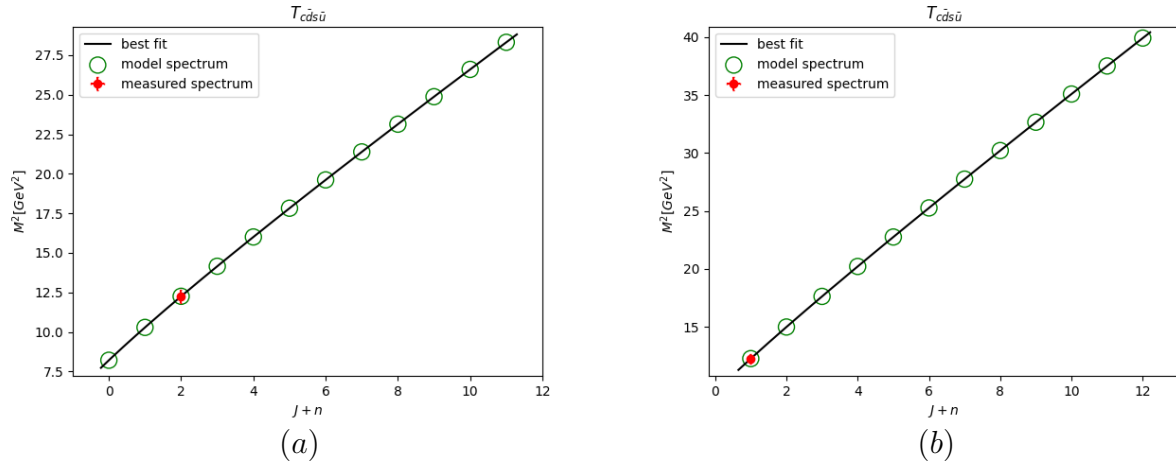


Figure 70: (a) is (J, M^2) $T_{cds\bar{u}}$ HMRT, (b) (n, M^2) $T_{cds\bar{u}}$ HMRT.

7.4.7 $T_{cds\bar{u}}$

J Spec	a_{T_j}
2790 – 2941	
3145 – 3270	
3446 – 3556	
3713 – 3812	
3955 – 4047	
4179 – 4265	
4389 – 4469	
4587 – 4663	
4774 – 4846	
4953 – 5022	
5124 – 5191	
5289 – 5353	-2.2–-1.8

Table 118: $T_{cds\bar{u}}$ (J, M^2) predictions.

n Spec	a_{T_n}
3446 – 3556	
3823 – 3919	
4155 – 4241	
4456 – 4535	
4733 – 4806	
4992 – 5060	
5235 – 5300	
5465 – 5527	
5685 – 5744	
5895 – 5952	
6097 – 6151	-1.9–-1.6
6291 – 6344	

Table 119: $T_{cds\bar{u}}$ (n, M^2) predictions.

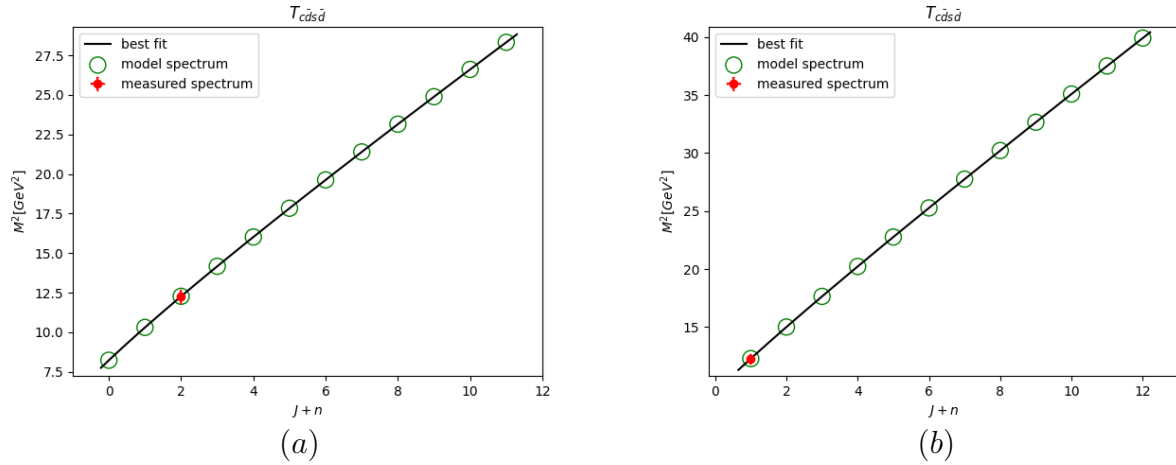


Figure 71: (a) is (J, M^2) $T_{cd\bar{s}d}$ HMRT, (b) (n, M^2) $T_{cd\bar{s}d}$ HMRT.

7.4.8 $T_{cd\bar{s}d}$

J Spec	a_{T_j}
2793 – 2943	
3147 – 3273	
3448 – 3558	
3715 – 3814	
3957 – 4048	
4181 – 4266	-2.2–-1.8
4390 – 4471	
4588 – 4664	
4775 – 4848	
4954 – 5023	
5125 – 5192	
5290 – 5354	

Table 120: $T_{cd\bar{s}d}$ (J, M^2) predictions.

n Spec	a_{T_n}
3448 – 3558	
3825 – 3921	
4157 – 4243	
4457 – 4536	
4734 – 4808	
4993 – 5062	
5236 – 5301	-1.9–-1.6
5466 – 5528	
5686 – 5745	
5896 – 5953	
6098 – 6152	
6292 – 6345	

Table 121: $T_{cd\bar{s}d}$ (n, M^2) predictions.

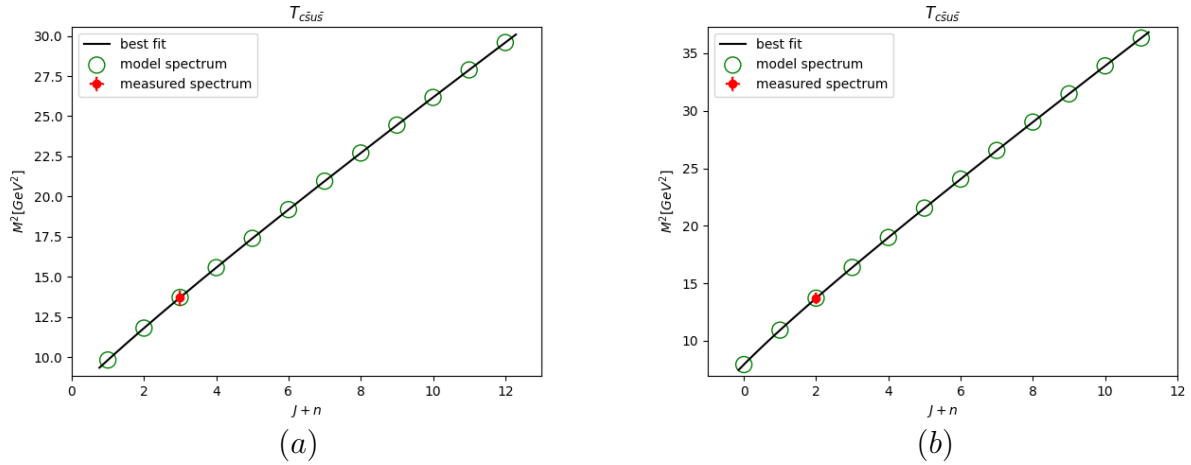


Figure 72: (a) is (J, M^2) $T_{c\bar{s}u\bar{s}}$ HMRT, (b) (n, M^2) $T_{c\bar{s}u\bar{s}}$ HMRT.

7.4.9 $T_{c\bar{s}u\bar{s}}$

J Spec	a_{T_j}
3062 – 3203	
3374 – 3497	
3648 – 3758	
3896 – 3996	
4124 – 4217	
4336 – 4424	-1.7--1.2
4536 – 4619	
4726 – 4805	
4906 – 4982	
5079 – 5152	
5246 – 5316	
5406 – 5473	

Table 122: $T_{c\bar{s}u\bar{s}}$ (J, M^2) predictions.

n Spec	a_{T_n}
2732 – 2901	
3241 – 3371	
3648 – 3758	
3999 – 4097	
4313 – 4402	
4600 – 4682	-1.2--0.94
4867 – 4944	
5117 – 5189	
5353 – 5421	
5577 – 5643	
5792 – 5854	
5997 – 6057	

Table 123: $T_{c\bar{s}u\bar{s}}$ (n, M^2) predictions.

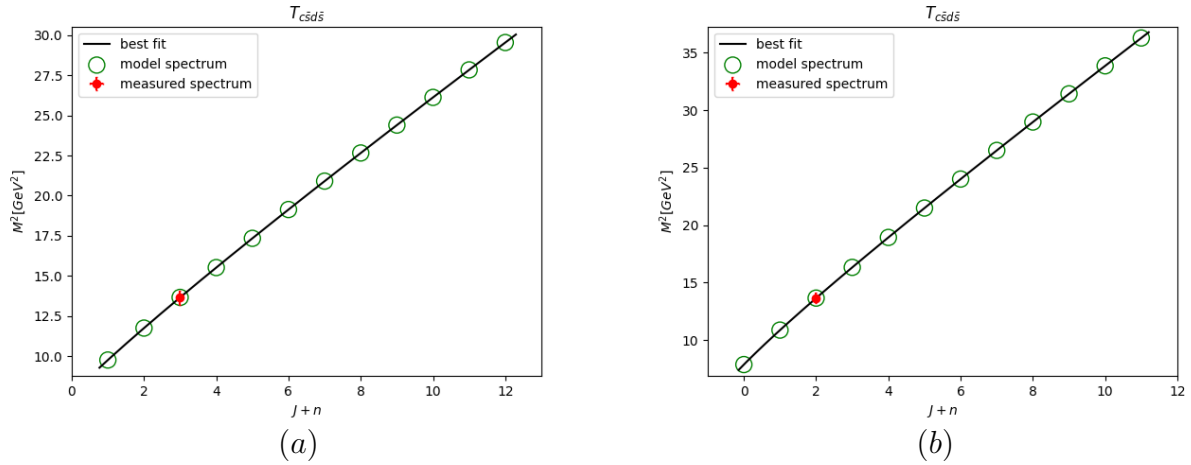


Figure 73: (a) is (J, M^2) $T_{c\bar{s}d\bar{s}}$ HMRT, (b) (n, M^2) $T_{c\bar{s}d\bar{s}}$ HMRT.

7.4.10 $T_{c\bar{s}d\bar{s}}$

J Spec	a_{T_j}
3053 – 3194	
3366 – 3489	
3641 – 3751	
3889 – 3990	
4118 – 4211	
4331 – 4419	-1.7--1.2
4531 – 4614	
4721 – 4800	
4902 – 4977	
5075 – 5147	
5241 – 5311	
5401 – 5469	

Table 124: $T_{c\bar{s}d\bar{s}}$ (J, M^2) predictions.

n Spec	a_{T_n}
2721 – 2891	
3233 – 3363	
3641 – 3751	
3993 – 4090	
4308 – 4396	
4595 – 4677	-1.2--0.92
4862 – 4939	
5112 – 5184	
5349 – 5417	
5573 – 5638	
5788 – 5850	
5994 – 6054	

Table 125: $T_{c\bar{s}d\bar{s}}$ (n, M^2) predictions.

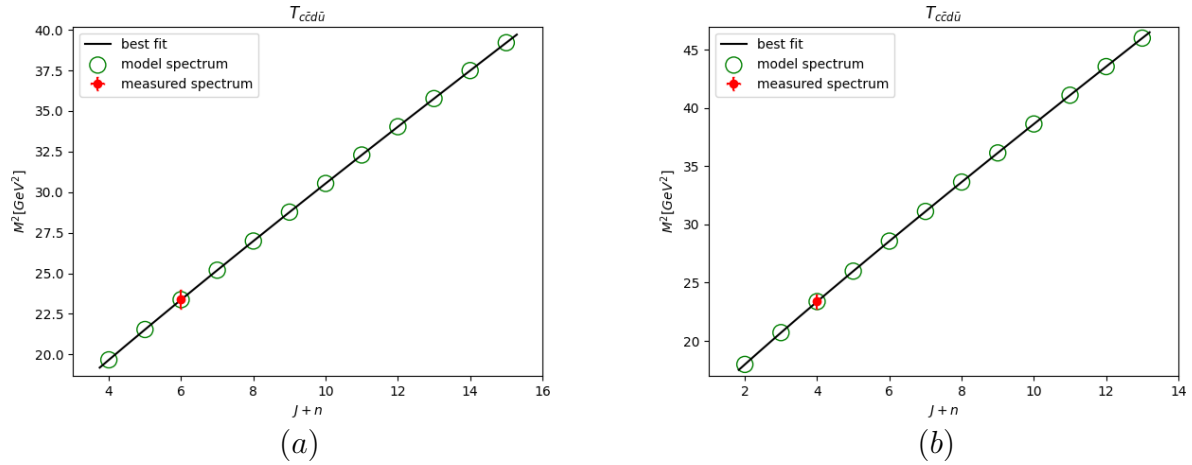


Figure 74: (a) is (J, M^2) $T_{c\bar{c}d\bar{u}}$ HMRT, (b) (n, M^2) $T_{c\bar{c}d\bar{u}}$ HMRT.

7.4.11 $T_{c\bar{c}d\bar{u}}$

J Spec	a_{T_j}
4373 – 4497	
4583 – 4699	
4780 – 4890	
4967 – 5072	
5145 – 5245	
5316 – 5412	
5480 – 5572	-2.6–-2.0
5638 – 5727	
5790 – 5877	
5938 – 6023	
6082 – 6164	
6222 – 6301	

Table 126: $T_{c\bar{c}d\bar{u}}$ (J, M^2) predictions.

n Spec	a_{T_n}
4174 – 4306	
4491 – 4611	
4780 – 4890	
5047 – 5150	
5297 – 5394	
5533 – 5625	
5757 – 5844	-2.0–-1.6
5971 – 6054	
6176 – 6256	
6373 – 6450	
6563 – 6638	
6747 – 6819	

Table 127: $T_{c\bar{c}d\bar{u}}$ (n, M^2) predictions.

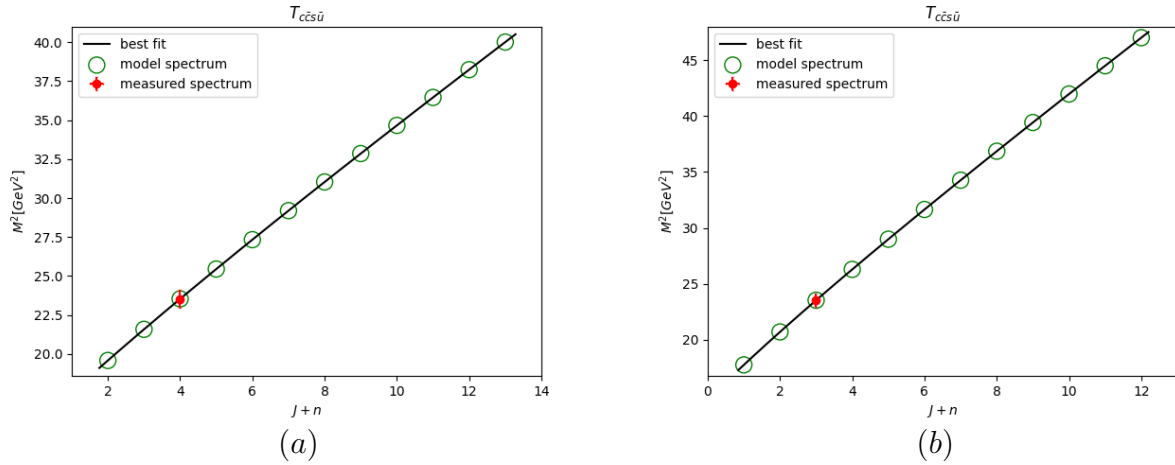


Figure 75: (a) is (J, M^2) $T_{c\bar{c}s\bar{u}}$ HMRT, (b) (n, M^2) $T_{c\bar{c}s\bar{u}}$ HMRT.

7.4.12 $T_{c\bar{c}s\bar{u}}$

J Spec	a_{T_j}
4362 – 4488	
4587 – 4704	
4796 – 4906	
4993 – 5097	
5179 – 5278	
5356 – 5450	
5525 – 5616	
5688 – 5776	
5845 – 5930	
5997 – 6079	
6144 – 6223	
6287 – 6364	
	-3.3–-2.7

Table 128: $T_{c\bar{c}s\bar{u}}$ (J, M^2) predictions.

n Spec	a_{T_n}
4145 – 4282	
4489 – 4610	
4796 – 4906	
5076 – 5178	
5337 – 5432	
5580 – 5670	
5811 – 5896	
6030 – 6111	
6240 – 6317	
6441 – 6515	
6634 – 6706	
6821 – 6891	
	-2.0–-1.6

Table 129: $T_{c\bar{c}s\bar{u}}$ (n, M^2) predictions.

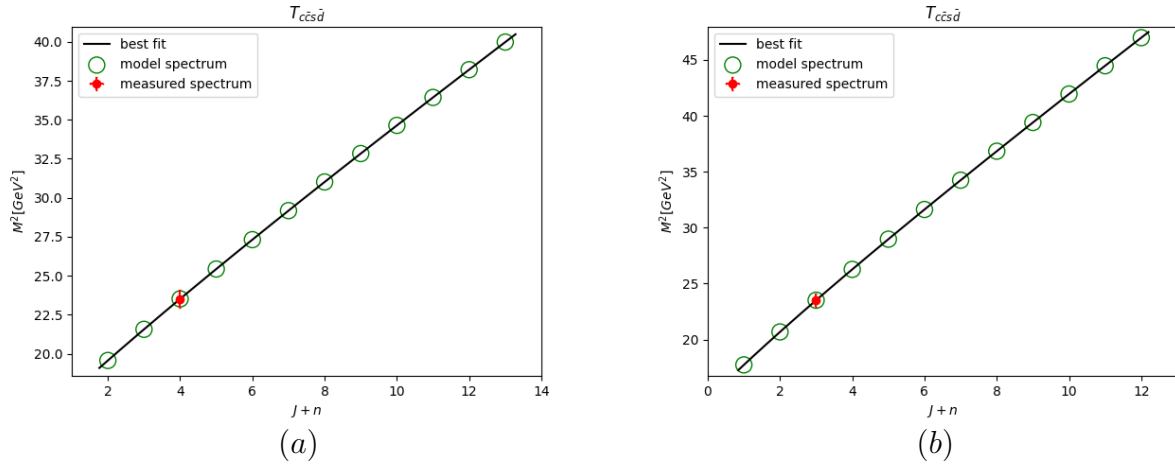


Figure 76: (a) is (J, M^2) $T_{c\bar{c}s\bar{d}}$ HMRT, (b) (n, M^2) $T_{c\bar{c}s\bar{d}}$ HMRT.

7.4.13 $T_{c\bar{c}s\bar{d}}$

J Spec	a_{T_j}
4359 – 4486	
4585 – 4702	
4794 – 4904	
4991 – 5095	
5177 – 5276	
5354 – 5449	
5524 – 5615	
5687 – 5774	
5844 – 5928	
5996 – 6077	
6143 – 6222	
6285 – 6362	
	-3.2--2.7

Table 130: $T_{c\bar{c}s\bar{d}}$ (J, M^2) predictions.

n Spec	a_{T_n}
4142 – 4279	
4487 – 4608	
4794 – 4904	
5075 – 5176	
5335 – 5430	
5579 – 5668	
5809 – 5894	
6029 – 6110	
6238 – 6316	
6439 – 6514	
6633 – 6705	
6820 – 6889	
	-2.0--1.6

Table 131: $T_{c\bar{c}s\bar{d}}$ (n, M^2) predictions.

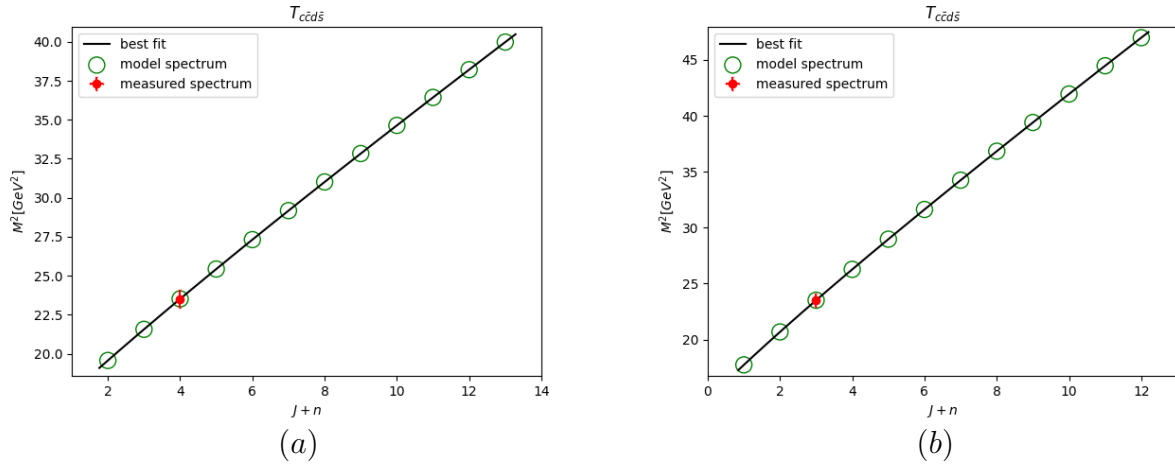


Figure 77: (a) is (J, M^2) $T_{c\bar{c}d\bar{s}}$ HMRT, (b) (n, M^2) $T_{c\bar{c}d\bar{s}}$ HMRT.

7.4.14 $T_{c\bar{c}d\bar{s}}$

J Spec	a_{T_j}
4359 – 4486	
4585 – 4702	
4794 – 4904	
4991 – 5095	
5177 – 5276	
5354 – 5449	
5524 – 5615	
5687 – 5774	
5844 – 5928	
5996 – 6077	
6143 – 6222	
6285 – 6362	
	-3.2--2.7

Table 132: $T_{c\bar{c}d\bar{s}}$ (J, M^2) predictions.

n Spec	a_{T_n}
4142 – 4279	
4487 – 4608	
4794 – 4904	
5075 – 5176	
5335 – 5430	
5579 – 5668	
5809 – 5894	
6029 – 6110	
6238 – 6316	
6439 – 6514	
6633 – 6705	
6820 – 6889	
	-2.0--1.6

Table 133: $T_{c\bar{c}d\bar{s}}$ (n, M^2) predictions.

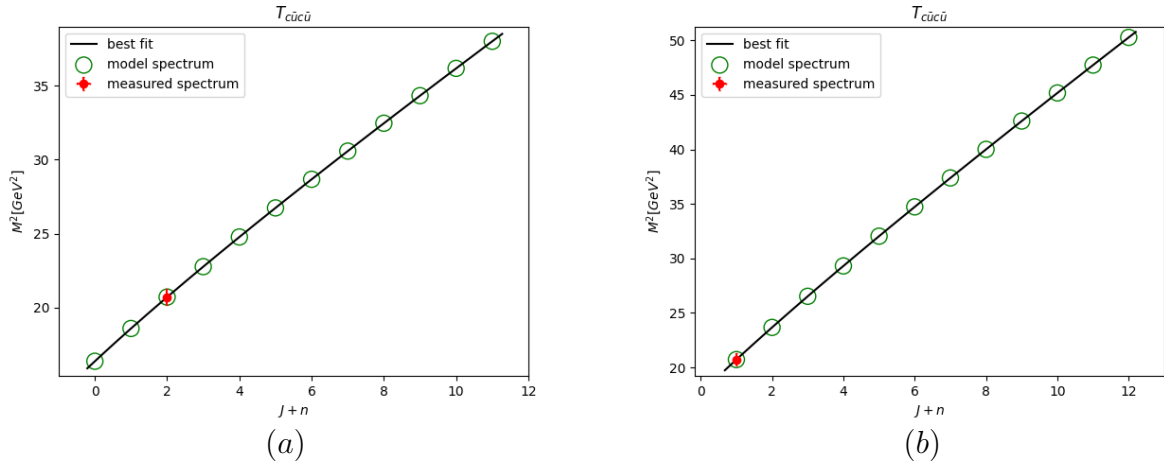


Figure 78: (a) is (J, M^2) $T_{c\bar{u}c\bar{u}}$ HMRT, (b) (n, M^2) $T_{c\bar{u}c\bar{u}}$ HMRT.

7.4.15 $T_{c\bar{c}c\bar{c}}$

J Spec	a_{T_j}
3981 – 4115	
4253 – 4373	
4497 – 4607	
4721 – 4823	
4930 – 5026	
5126 – 5217	
5312 – 5398	
5489 – 5571	
5658 – 5737	
5820 – 5896	
5977 – 6050	
6128 – 6199	
	-3.7--3.3

Table 134: $T_{c\bar{u}c\bar{u}}$ (J, M^2) predictions.

Spec	n	a_{T_n}
4497 – 4607		
4816 – 4915		
5105 – 5196		
5372 – 5456		
5621 – 5700		
5856 – 5931		
6078 – 6150		
6291 – 6359		
6494 – 6560		
6690 – 6753		
6879 – 6940		
7061 – 7121		

Table 135: $T_{c\bar{c}c\bar{c}}$ (n, M^2) predictions.

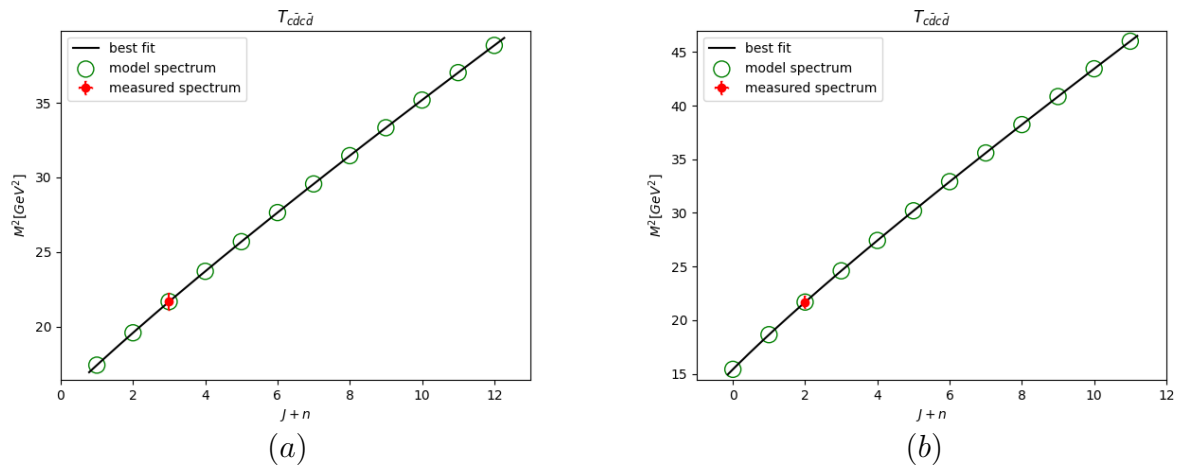


Figure 79: (a) is (J, M^2) $T_{c\bar{c}d\bar{d}}$ HMRT, (b) (n, M^2) $T_{c\bar{c}d\bar{d}}$ HMRT.

7.4.16 $T_{c\bar{c}d\bar{d}}$

J Spec	a_{T_j}
4109 – 4241	
4367 – 4487	
4602 – 4712	
4819 – 4921	
5021 – 5118	
5212 – 5304	
5394 – 5481	
5567 – 5651	
5733 – 5814	
5893 – 5970	
6047 – 6122	
6196 – 6269	
	-3.2–-2.7

Table 136: $T_{c\bar{c}d\bar{d}}$ (J, M^2) predictions.

n Spec	a_{T_n}
3852 – 4000	
4256 – 4381	
4602 – 4712	
4910 – 5010	
5192 – 5284	
5453 – 5539	
5697 – 5778	
5928 – 6004	
6147 – 6220	
6356 – 6427	
6557 – 6625	
6751 – 6816	
	-2.3–-2.0

Table 137: $T_{c\bar{c}d\bar{d}}$ (n, M^2) predictions.

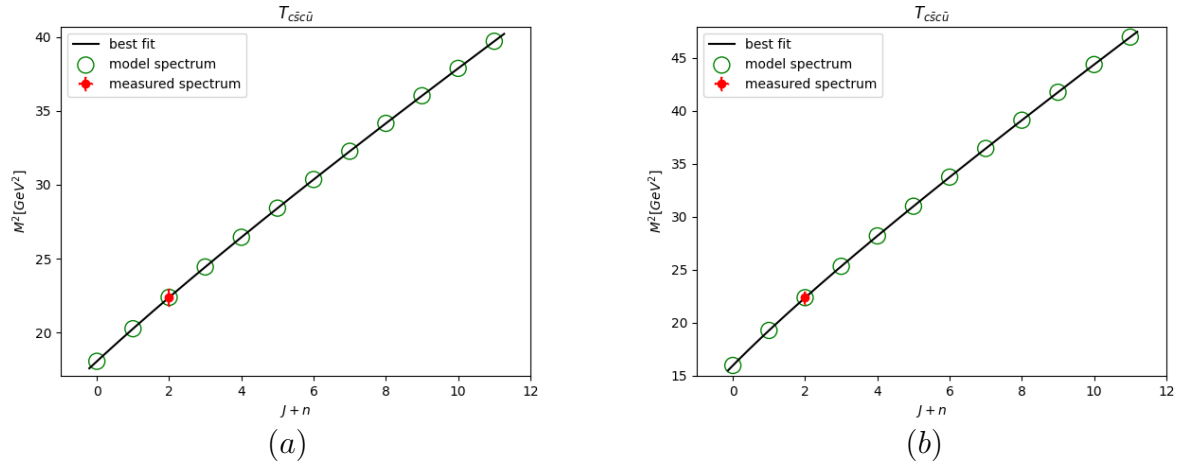


Figure 80: (a) is (J, M^2) $T_{c\bar{s}c\bar{u}}$ HMRT, (b) (n, M^2) $T_{c\bar{s}c\bar{u}}$ HMRT.

7.4.17 $T_{c\bar{s}c\bar{u}}$

J Spec	a_{T_j}
4181 – 4314	
4440 – 4560	
4675 – 4785	
4892 – 4994	
5094 – 5191	
5285 – 5377	
5466 – 5553	-3.9 – -3.4
5639 – 5723	
5805 – 5885	
5964 – 6041	
6118 – 6193	
6267 – 6339	

Table 138: $T_{c\bar{s}c\bar{u}}$ (J, M^2) predictions.

n Spec	a_{T_n}
3922 – 4071	
4328 – 4453	
4675 – 4785	
4983 – 5083	
5264 – 5356	
5525 – 5611	
5769 – 5849	-2.1 – -1.8
5999 – 6076	
6218 – 6291	
6427 – 6497	
6627 – 6694	
6820 – 6885	

Table 139: $T_{c\bar{s}c\bar{u}}$ (n, M^2) predictions.

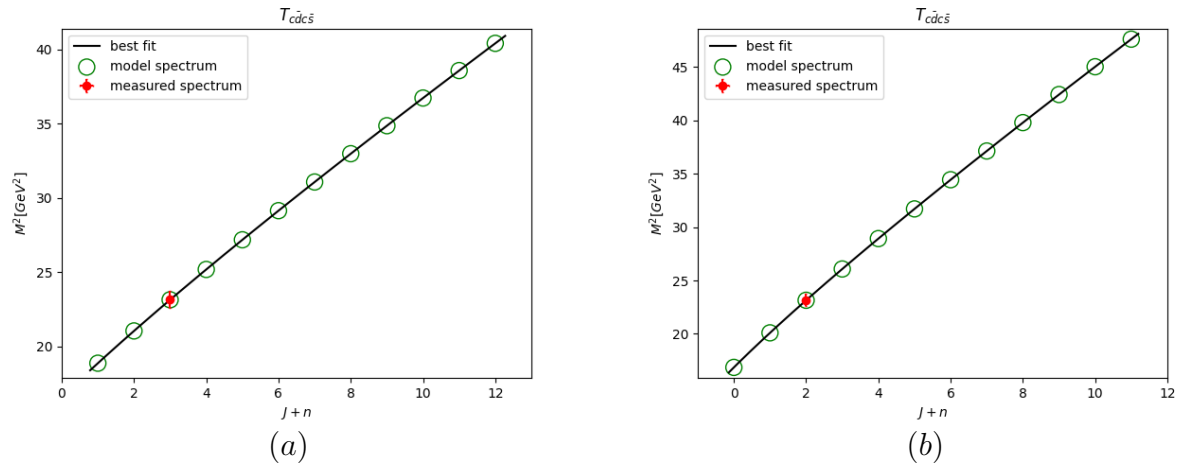


Figure 81: (a) is (J, M^2) $T_{c\bar{d}c\bar{s}}$ HMRT, (b) (n, M^2) $T_{c\bar{d}c\bar{s}}$ HMRT.

7.4.18 $T_{c\bar{d}c\bar{s}}$

J Spec	a_{T_j}
4279 – 4410	
4528 – 4647	
4756 – 4866	
4967 – 5070	
5165 – 5262	
5352 – 5445	
5530 – 5618	
5700 – 5785	
5864 – 5945	
6021 – 6099	
6173 – 6249	
6320 – 6393	
	-3.3 – -2.8

Table 140: $T_{c\bar{d}c\bar{s}}$ (J, M^2) predictions.

n Spec	a_{T_n}
4032 – 4178	
4421 – 4544	
4756 – 4866	
5057 – 5157	
5332 – 5425	
5588 – 5675	
5828 – 5910	
6055 – 6133	
6271 – 6346	
6478 – 6549	
6676 – 6745	
6868 – 6934	
	-2.4 – -2.0

Table 141: $T_{c\bar{d}c\bar{s}}$ (n, M^2) predictions.

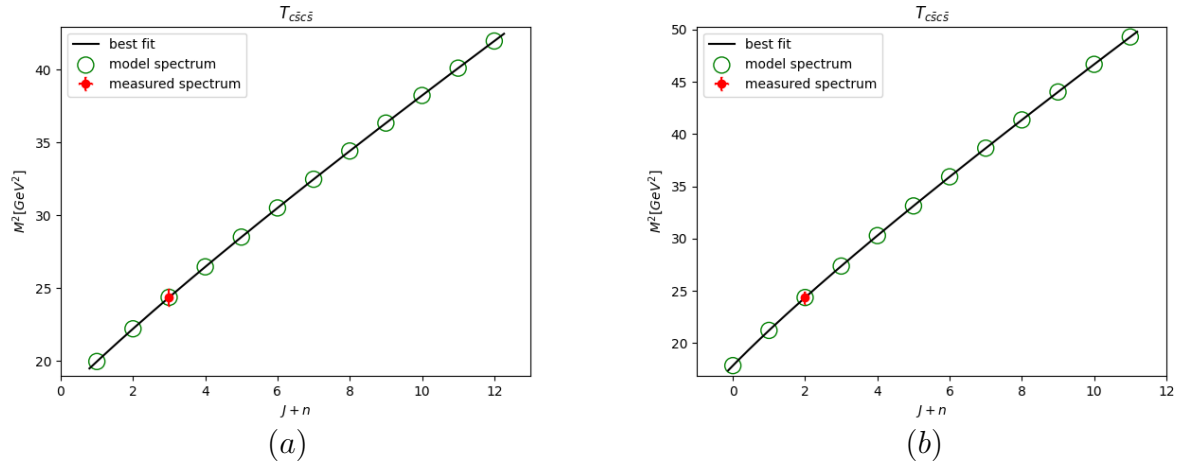


Figure 82: (a) is (J, M^2) $T_{c\bar{s}c\bar{s}}$ HMRT, (b) (n, M^2) $T_{c\bar{s}c\bar{s}}$ HMRT.

7.4.19 $T_{c\bar{s}c\bar{s}}$

J Spec	a_{T_j}
4401 – 4533	
4652 – 4772	
4881 – 4991	
5093 – 5195	
5291 – 5387	
5477 – 5569	
5655 – 5743	-2.9 – -2.4
5825 – 5909	
5988 – 6068	
6144 – 6222	
6296 – 6371	
6442 – 6515	

Table 142: $T_{c\bar{s}c\bar{s}}$ (J, M^2) predictions.

n Spec	a_{T_n}
4151 – 4298	
4544 – 4668	
4881 – 4991	
5182 – 5282	
5457 – 5550	
5712 – 5799	
5952 – 6033	-2.1 – -1.7
6178 – 6256	
6394 – 6468	
6600 – 6671	
6797 – 6866	
6988 – 7054	

Table 143: $T_{c\bar{s}c\bar{s}}$ (n, M^2) predictions.

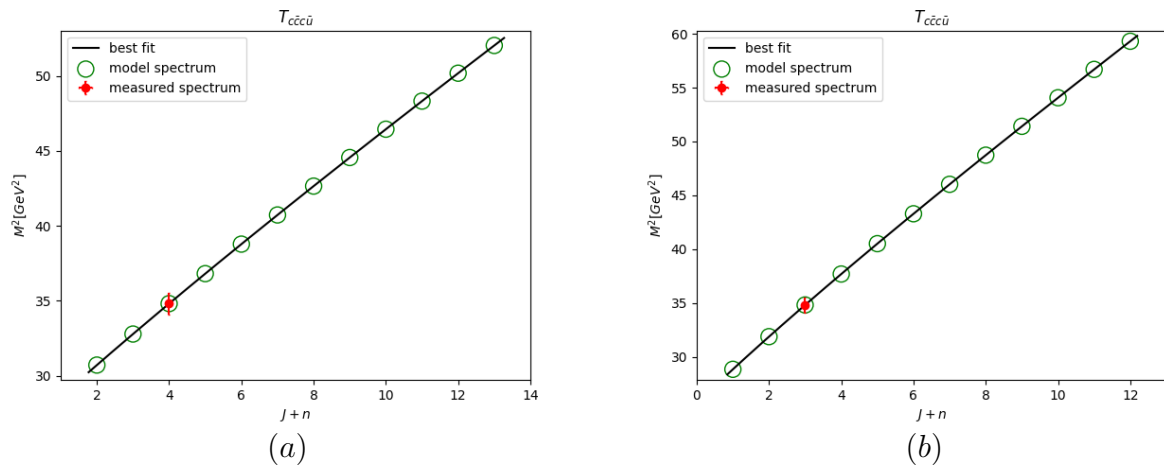


Figure 83: (a) is (J, M^2) $T_{c\bar{c}c\bar{u}}$ HMRT, (b) (n, M^2) $T_{c\bar{c}c\bar{u}}$ HMRT.

7.4.20 $T_{c\bar{c}c\bar{u}}$

J Spec	a_{T_j}
5481 – 5602	
5668 – 5783	
5845 – 5955	
6014 – 6120	
6176 – 6278	
6333 – 6430	
6483 – 6578	
6629 – 6721	
6770 – 6859	
6908 – 6994	
7041 – 7126	
7172 – 7254	
	-5.5 – -4.9

Table 144: $T_{c\bar{c}c\bar{u}}$ (J, M^2) predictions.

n Spec	a_{T_n}
5305 – 5434	
5586 – 5704	
5845 – 5955	
6087 – 6191	
6316 – 6414	
6532 – 6626	
6739 – 6829	
6938 – 7024	
7129 – 7212	
7313 – 7393	
7491 – 7569	
7664 – 7740	
	-3.6 – -3.2

Table 145: $T_{c\bar{c}c\bar{u}}$ (n, M^2) predictions.

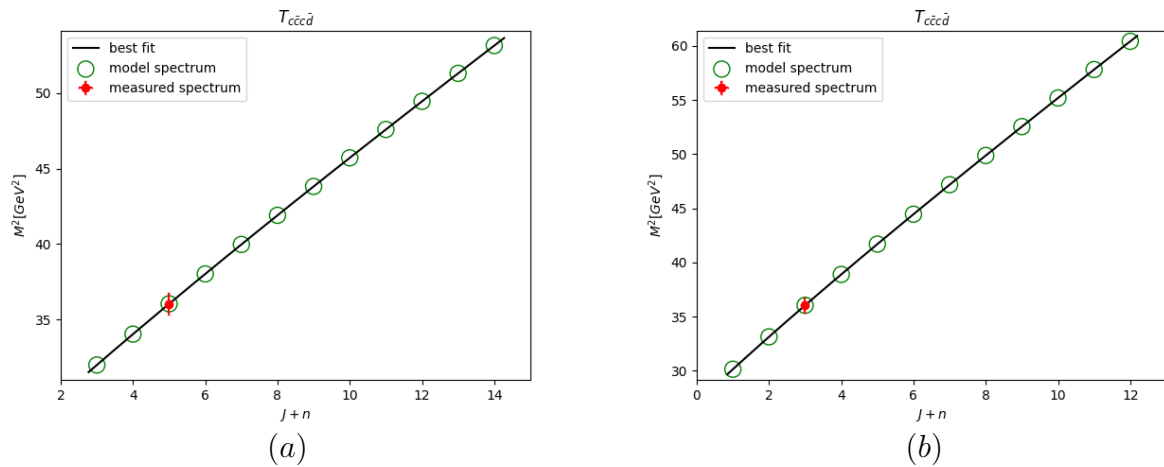


Figure 84: (a) is (J, M^2) $T_{c\bar{c}cd}$ HMRT, (b) (n, M^2) $T_{c\bar{c}cd}$ HMRT.

7.4.21 $T_{c\bar{c}cd}$

J Spec	a_{T_j}
5595 – 5716	
5776 – 5891	
5948 – 6058	
6113 – 6219	
6271 – 6373	
6424 – 6522	
6572 – 6667	
6715 – 6807	
6854 – 6944	
6989 – 7076	
7120 – 7206	
7249 – 7332	-5.2–-4.5

Table 146: $T_{c\bar{c}cd}$ (J, M^2) predictions.

n Spec	a_{T_n}
5425 – 5552	
5696 – 5814	
5948 – 6058	
6184 – 6288	
6407 – 6506	
6620 – 6714	
6823 – 6914	-4.0–-3.6
7018 – 7105	
7206 – 7290	
7388 – 7469	
7564 – 7643	
7735 – 7811	

Table 147: $T_{c\bar{c}cd}$ (n, M^2) predictions.

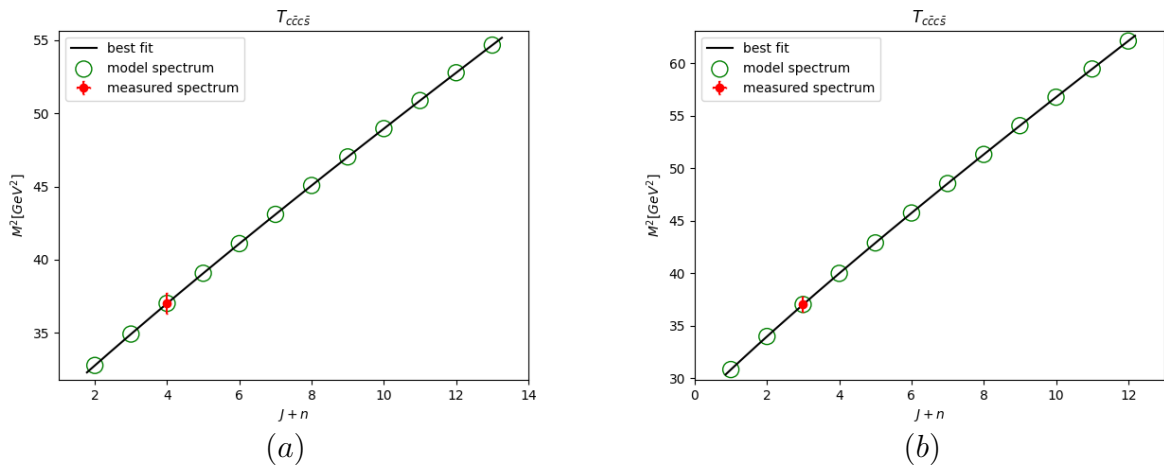


Figure 85: (a) is (J, M^2) $T_{c\bar{c}c\bar{s}}$ HMRT, (b) (n, M^2) $T_{c\bar{c}c\bar{s}}$ HMRT.

7.4.22 $T_{c\bar{c}c\bar{s}}$

J Spec	a_{T_j}
5664 – 5786	
5851 – 5967	
6029 – 6139	
6198 – 6304	
6360 – 6462	
6516 – 6614	
6667 – 6761	
6812 – 6903	
6953 – 7042	
7090 – 7176	
7223 – 7307	
7353 – 7435	
	-5.1--4.4

Table 148: $T_{c\bar{c}c\bar{s}}$ (J, M^2) predictions.

n Spec	a_{T_n}
5487 – 5616	
5769 – 5888	
6029 – 6139	
6271 – 6375	
6499 – 6597	
6716 – 6809	
6922 – 7011	
7120 – 7206	
7310 – 7393	
7493 – 7573	
7671 – 7748	
7843 – 7918	
	–3.3 – 2.8

Table 149: $T_{c\bar{c}c\bar{s}}$ (n, M^2) predictions.

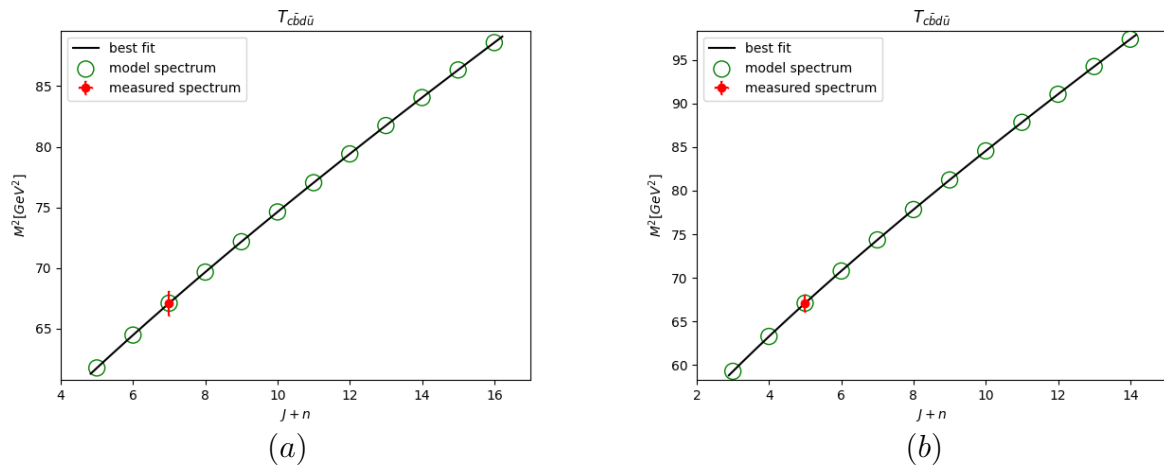


Figure 86: (a) is (J, M^2) $T_{c\bar{b}d\bar{u}}$ HMRT, (b) (n, M^2) $T_{c\bar{b}d\bar{u}}$ HMRT.

7.4.23 $T_{c\bar{b}d\bar{u}}$

J Spec	a_{T_j}
7798 – 7920	
7972 – 8088	
8137 – 8247	
8294 – 8400	
8445 – 8546	
8590 – 8688	
8730 – 8825	
8866 – 8958	
8997 – 9086	
9125 – 9212	
9250 – 9334	
9371 – 9454	
	-2.5–-1.8

Table 150: $T_{c\bar{b}d\bar{u}}$ (J, M^2) predictions.

n Spec	a_{T_n}
7635 – 7764	
7896 – 8014	
8137 – 8247	
8362 – 8466	
8574 – 8672	
8776 – 8869	
8968 – 9058	
9153 – 9239	
9331 – 9414	
9503 – 9583	
9669 – 9747	
9830 – 9906	
	-1.5–-1.1

Table 151: $T_{c\bar{b}d\bar{u}}$ (n, M^2) predictions.

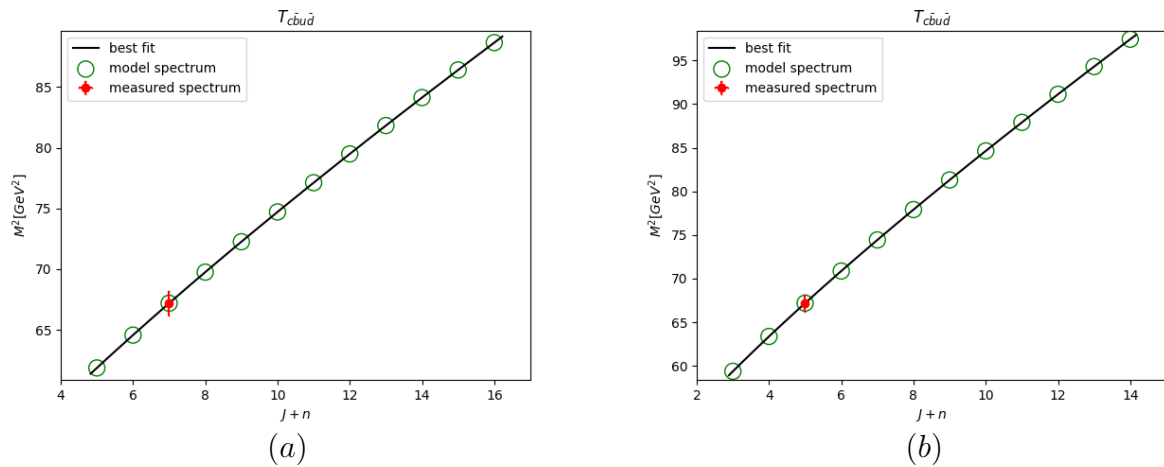


Figure 87: (a) is (J, M^2) T_{cbud} HMRT, (b) (n, M^2) T_{cbud} HMRT.

7.4.24 T_{cbud}

J Spec	a_{T_j}
7804 – 7926	
7977 – 8093	
8142 – 8252	
8299 – 8404	
8450 – 8551	
8595 – 8692	
8734 – 8829	
8870 – 8962	
9001 – 9091	
9129 – 9216	
9253 – 9338	
9375 – 9457	-2.5–-1.8

Table 152: T_{cbud} (J, M^2) predictions.

n Spec	a_{T_n}
7641 – 7769	
7902 – 8020	
8142 – 8252	
8367 – 8470	
8579 – 8677	
8780 – 8874	
8972 – 9062	-1.6–-1.1
9157 – 9243	
9335 – 9418	
9506 – 9587	
9672 – 9751	
9834 – 9910	

Table 153: T_{cbud} (n, M^2) predictions.

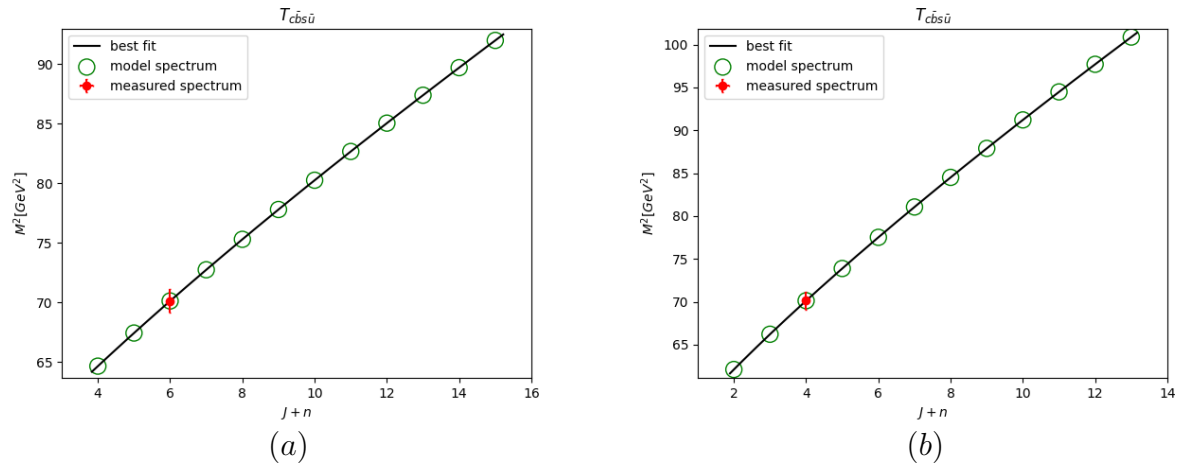


Figure 88: (a) is (J, M^2) $T_{\bar{c}\bar{b}s\bar{u}}$ HMRT, (b) (n, M^2) $T_{\bar{c}\bar{b}s\bar{u}}$ HMRT.

7.4.25 $T_{c\bar{b}s\bar{u}}$

J Spec	a_{T_j}
7980 – 8102	
8154 – 8270	
8319 – 8429	
8476 – 8581	
8627 – 8728	
8771 – 8869	
8911 – 9005	
9046 – 9137	
9177 – 9266	
9304 – 9391	
9428 – 9512	
9549 – 9631	
	-3.0--2.3

Table 154: $T_{c\bar{b}s\bar{u}}$ (J, M^2) predictions.

n Spec	a_{T_n}
7816 – 7945	
8078 – 8196	
8319 – 8429	
8544 – 8647	
8755 – 8853	
8956 – 9050	
9148 – 9238	
9332 – 9418	
9509 – 9592	
9680 – 9760	
9845 – 9923	
10006 – 10081	–2.2 – 1.7

Table 155: $T_{c\bar{b}s\bar{u}}$ (n, M^2) predictions.

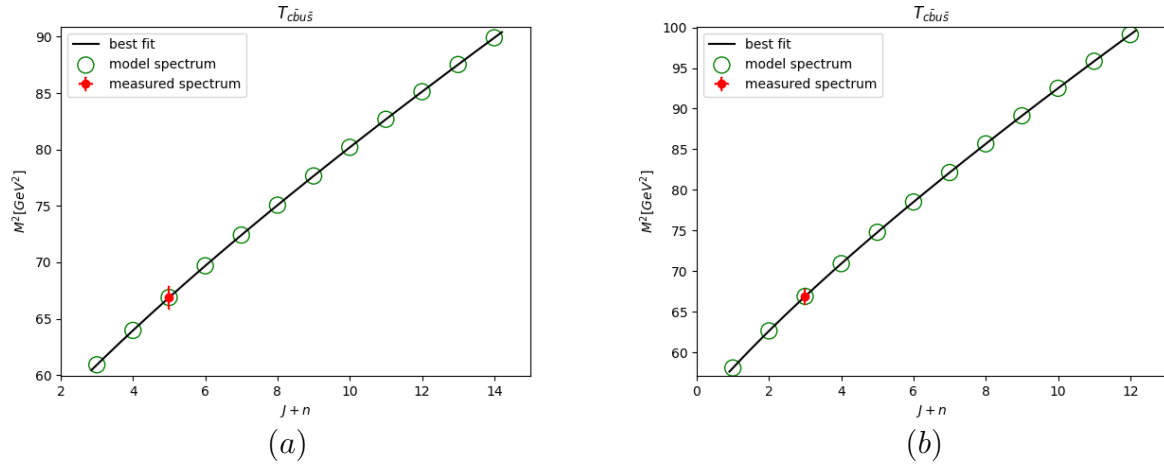


Figure 89: (a) is (J, M^2) $T_{c\bar{b}u\bar{s}}$ HMRT, (b) (n, M^2) $T_{c\bar{b}u\bar{s}}$ HMRT.

7.4.26 $T_{c\bar{b}u\bar{s}}$

J Spec	a_{T_j}
7742 – 7868	
7939 – 8056	
8123 – 8233	
8296 – 8400	
8460 – 8559	
8617 – 8712	
8767 – 8858	-2.3 – -1.7
8911 – 8999	
9050 – 9136	
9185 – 9268	
9316 – 9396	
9443 – 9521	

Table 156: $T_{c\bar{b}u\bar{s}}$ (J, M^2) predictions.

n Spec	a_{T_n}
7552 – 7688	
7853 – 7974	
8123 – 8233	
8370 – 8472	
8600 – 8695	
8815 – 8906	
9020 – 9106	-2.1 – -1.6
9214 – 9297	
9401 – 9480	
9580 – 9656	
9753 – 9827	
9920 – 9992	

Table 157: $T_{c\bar{b}u\bar{s}}$ (n, M^2) predictions.

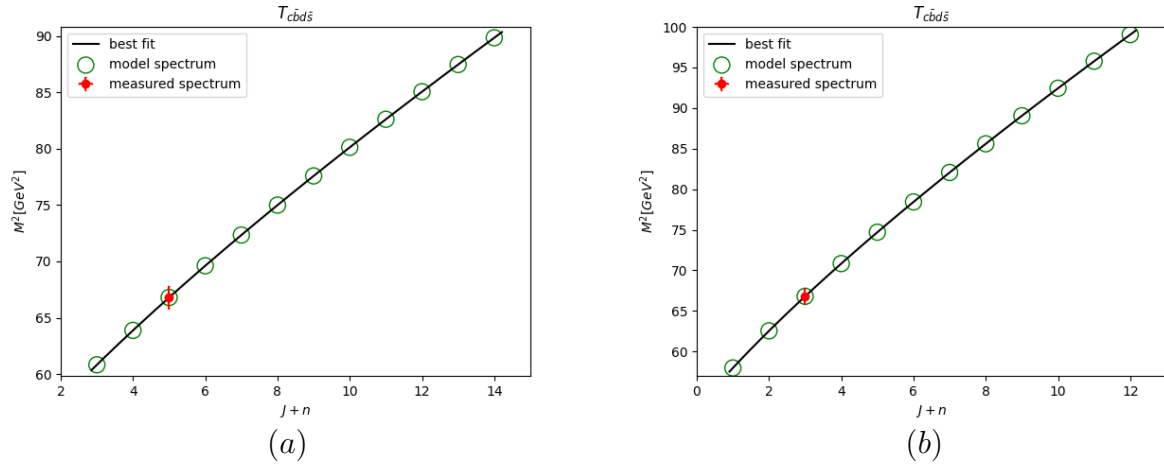


Figure 90: (a) is (J, M^2) $T_{c\bar{b}d\bar{s}}$ HMRT, (b) (n, M^2) $T_{c\bar{b}d\bar{s}}$ HMRT.

7.4.27 $T_{c\bar{b}d\bar{s}}$

J Spec	a_{T_j}
7736 – 7862	
7934 – 8051	
8118 – 8228	
8291 – 8395	
8456 – 8555	
8612 – 8707	
8763 – 8854	-2.3 – -1.7
8907 – 8995	
9046 – 9132	
9181 – 9264	
9312 – 9392	
9439 – 9518	

Table 158: $T_{c\bar{b}d\bar{s}}$ (J, M^2) predictions.

n Spec	a_{T_n}
7545 – 7682	
7848 – 7969	
8118 – 8228	
8365 – 8467	
8595 – 8691	
8811 – 8902	
9016 – 9102	-2.1 – -1.6
9211 – 9293	
9397 – 9476	
9577 – 9653	
9750 – 9823	
9917 – 9988	

Table 159: $T_{c\bar{b}d\bar{s}}$ (n, M^2) predictions.

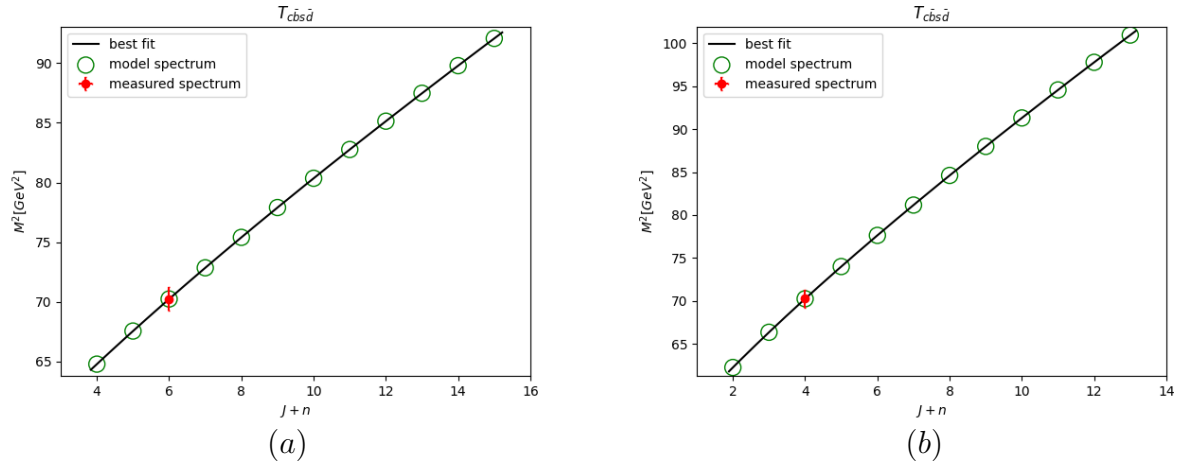


Figure 91: (a) is (J, M^2) $T_{c\bar{b}s\bar{d}}$ HMRT, (b) (n, M^2) $T_{c\bar{b}s\bar{d}}$ HMRT.

7.4.28 $T_{c\bar{b}s\bar{d}}$

J Spec	a_{T_j}
7988 – 8110	
8161 – 8277	
8326 – 8436	
8483 – 8588	
8633 – 8734	
8777 – 8875	
8917 – 9011	
9052 – 9143	
9183 – 9272	
9310 – 9396	
9433 – 9518	
9554 – 9637	
–3.0–2.3	

Table 160: $T_{c\bar{b}s\bar{d}}$ (J, M^2) predictions.

n Spec	a_{T_n}
7824 – 7953	
8086 – 8204	
8326 – 8436	
8550 – 8654	
8762 – 8860	
8962 – 9056	
9154 – 9243	
9338 – 9424	
9514 – 9597	
9685 – 9765	
9850 – 9928	
10011 – 10086	
–2.2–1.8	

Table 161: $T_{c\bar{b}s\bar{d}}$ (n, M^2) predictions.

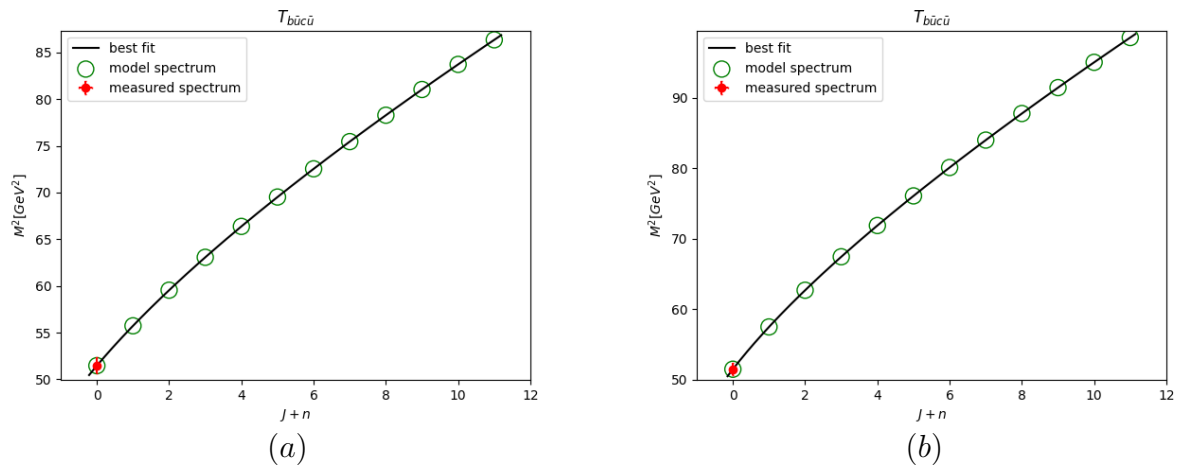


Figure 92: (a) is (J, M^2) $T_{b\bar{u}c\bar{u}}$ HMRT, (b) (n, M^2) $T_{b\bar{u}c\bar{u}}$ HMRT.

7.4.29 $T_{b\bar{u}c\bar{u}}$

J Spec	a_{T_j}
7154 – 7194	
7449 – 7482	
7702 – 7732	
7928 – 7955	
8135 – 8159	
8326 – 8349	
8506 – 8528	
8676 – 8697	
8838 – 8857	
8992 – 9011	
9141 – 9159	
9284 – 9301	
	-2.3–-2.1

Table 162: $T_{b\bar{u}c\bar{u}}$ (J, M^2) predictions.

n Spec	a_{T_n}
7154 – 7194	
7565 – 7597	
7904 – 7931	
8200 – 8224	
8467 – 8489	
8713 – 8733	
8942 – 8961	
9157 – 9175	
9361 – 9378	
9556 – 9572	
9742 – 9758	
9921 – 9937	
	-1.6–-1.5

Table 163: $T_{b\bar{u}c\bar{u}}$ (n, M^2) predictions.

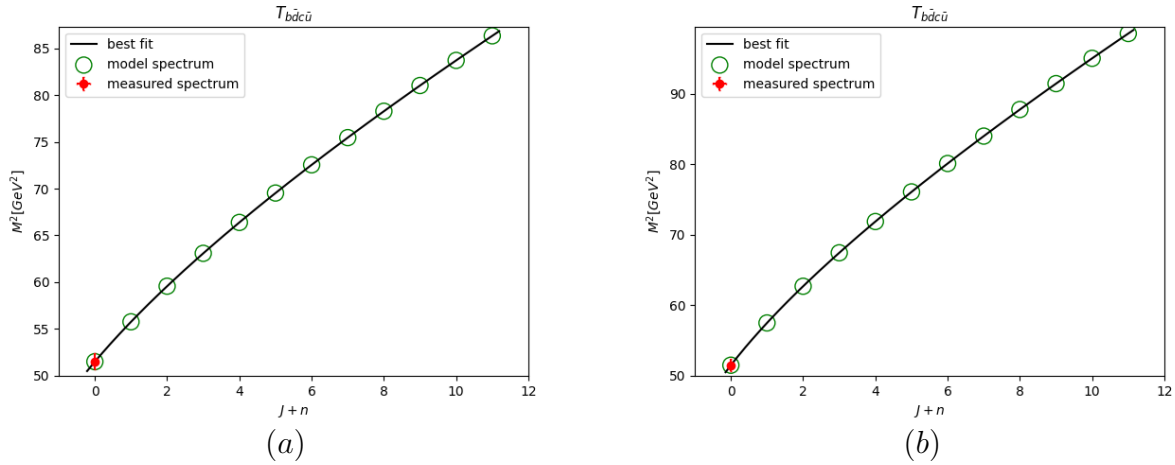


Figure 93: (a) is (J, M^2) $T_{b\bar{d}c\bar{u}}$ HMRT, (b) (n, M^2) $T_{b\bar{d}c\bar{u}}$ HMRT.

7.4.30 $T_{b\bar{d}c\bar{u}}$

J Spec	a_{T_j}
7155 – 7195	
7450 – 7483	
7703 – 7732	
7929 – 7956	
8135 – 8160	
8327 – 8350	
8507 – 8528	
8677 – 8697	
8838 – 8858	
8993 – 9012	
9141 – 9159	
9284 – 9302	
	-2.3--2.1

Table 164: $T_{b\bar{d}c\bar{u}}$ (J, M^2) predictions.

n Spec	a_{T_n}
7155 – 7195	
7566 – 7598	
7905 – 7932	
8201 – 8225	
8468 – 8490	
8713 – 8734	
8942 – 8961	–1.6
9157 – 9175	–1.5
9361 – 9379	
9556 – 9573	
9743 – 9758	
9922 – 9937	

Table 165: $T_{b\bar{d}c\bar{u}}$ (n, M^2) predictions.

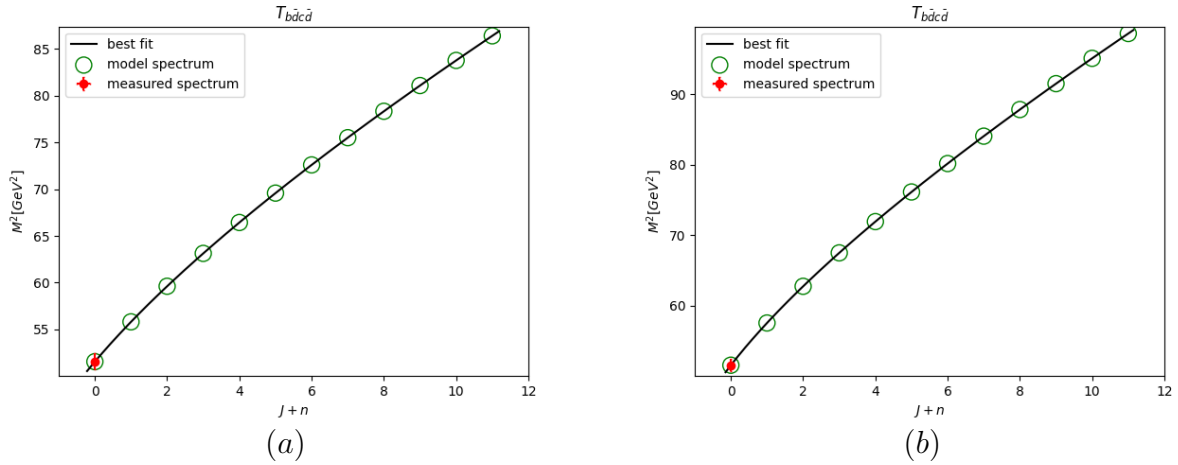


Figure 94: (a) is (J, M^2) $T_{b\bar{d}c\bar{d}}$ HMRT, (b) (n, M^2) $T_{b\bar{d}c\bar{d}}$ HMRT.

7.4.31 $T_{b\bar{d}c\bar{d}}$

J Spec	a_{T_j}
7160 – 7200	
7454 – 7487	
7706 – 7736	
7932 – 7959	
8138 – 8163	
8330 – 8353	
8509 – 8531	
8679 – 8700	
8841 – 8860	
8995 – 9014	
9143 – 9162	
9286 – 9304	
	-2.3 – -2.1

Table 166: $T_{b\bar{d}c\bar{d}}$ (J, M^2) predictions.

n Spec	a_{T_n}
7160 – 7200	
7570 – 7602	
7908 – 7935	
8204 – 8228	
8470 – 8493	
8716 – 8736	
8944 – 8964	
9160 – 9178	
9364 – 9381	
9558 – 9575	
9744 – 9760	
9924 – 9939	
	-1.6 – -1.5

Table 167: $T_{b\bar{d}c\bar{d}}$ (n, M^2) predictions.

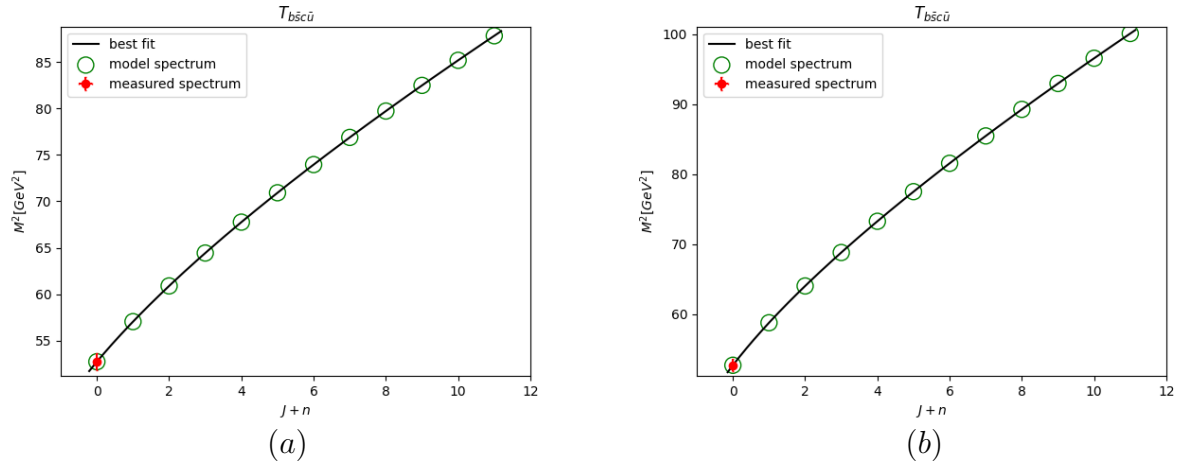


Figure 95: (a) is (J, M^2) $T_{b\bar{s}c\bar{u}}$ HMRT, (b) (n, M^2) $T_{b\bar{s}c\bar{u}}$ HMRT.

7.4.32 $T_{b\bar{s}c\bar{u}}$

J Spec	a_{T_j}
7242 – 7282	
7537 – 7570	
7789 – 7818	
8014 – 8040	
8219 – 8244	
8410 – 8433	
8589 – 8610	
8758 – 8778	
8918 – 8938	
9072 – 9091	
9220 – 9238	
9362 – 9380	
	-2.0--1.9

Table 168: $T_{b\bar{s}c\bar{u}}$ (J, M^2) predictions.

n Spec	a_{T_n}
7242 – 7282	
7653 – 7684	
7990 – 8017	
8284 – 8308	
8550 – 8572	
8794 – 8814	
9022 – 9041	
9236 – 9254	
9439 – 9456	
9633 – 9649	
9818 – 9834	
9997 – 10012	
	-1.4--1.3

Table 169: $T_{b\bar{s}c\bar{u}}$ (n, M^2) predictions.

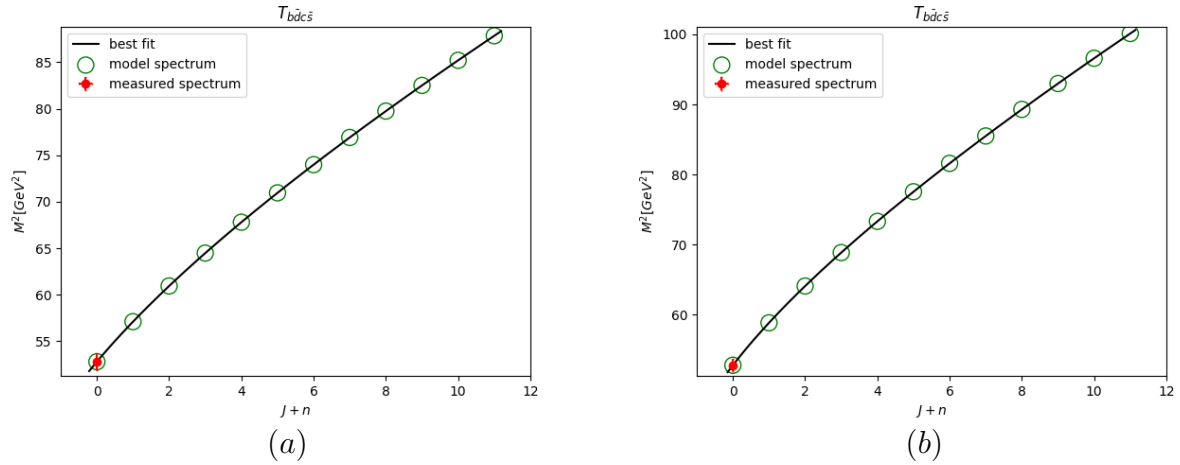


Figure 96: (a) is (J, M^2) $T_{b\bar{d}c\bar{s}}$ HMRT, (b) (n, M^2) $T_{b\bar{d}c\bar{s}}$ HMRT.

7.4.33 $T_{b\bar{d}c\bar{s}}$

J Spec	a_{T_j}
7247 – 7287	
7541 – 7574	
7792 – 7822	
8017 – 8044	
8222 – 8247	
8413 – 8436	
8591 – 8613	-2.0–-1.9
8760 – 8781	
8921 – 8940	
9075 – 9093	
9222 – 9240	
9364 – 9382	

Table 170: $T_{b\bar{d}c\bar{s}}$ (J, M^2) predictions.

n Spec	a_{T_n}
7247 – 7287	
7657 – 7688	
7993 – 8020	
8287 – 8311	
8553 – 8574	
8797 – 8817	
9024 – 9043	-1.4–-1.3
9238 – 9256	
9441 – 9458	
9635 – 9651	
9820 – 9836	
9999 – 10014	

Table 171: $T_{b\bar{d}c\bar{s}}$ (n, M^2) predictions.

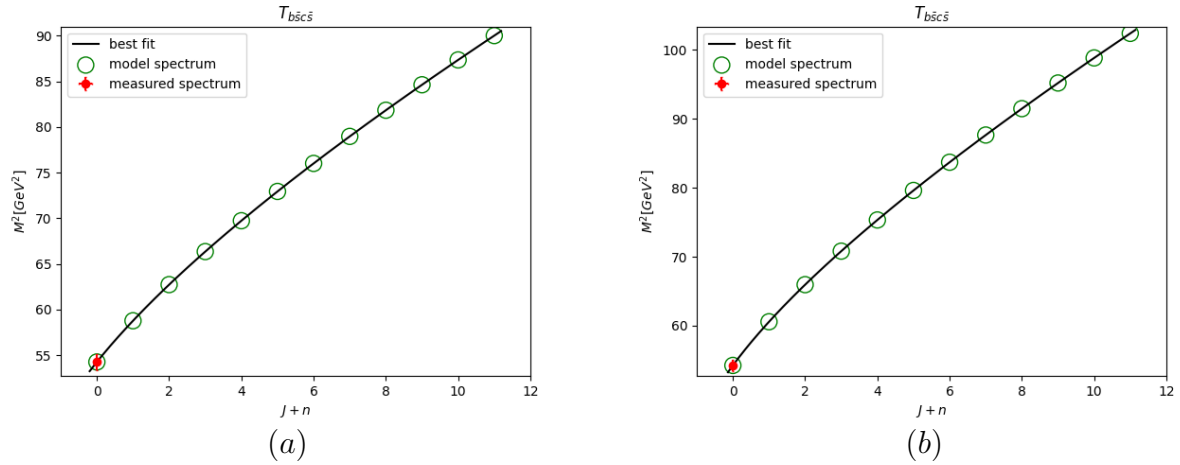


Figure 97: (a) is (J, M^2) $T_{b\bar{s}c\bar{s}}$ HMRT, (b) (n, M^2) $T_{b\bar{s}c\bar{s}}$ HMRT.

7.4.34 $T_{b\bar{s}c\bar{s}}$

J Spec	a_{T_j}
7345 – 7385	
7649 – 7682	
7906 – 7934	
8132 – 8158	
8339 – 8362	
8529 – 8551	
8708 – 8729	
8877 – 8896	
9037 – 9056	
9191 – 9209	
9338 – 9355	
9480 – 9496	
	-1.6--1.5

Table 172: $T_{b\bar{s}c\bar{s}}$ (J, M^2) predictions.

n Spec	a_{T_n}
7345 – 7385	
7768 – 7798	
8108 – 8134	
8404 – 8427	
8669 – 8690	
8913 – 8933	
9140 – 9158	
9354 – 9371	
9556 – 9573	
9749 – 9765	
9934 – 9949	
10112 – 10126	-1.1--1.0

Table 173: $T_{b\bar{s}c\bar{s}}$ (n, M^2) predictions.

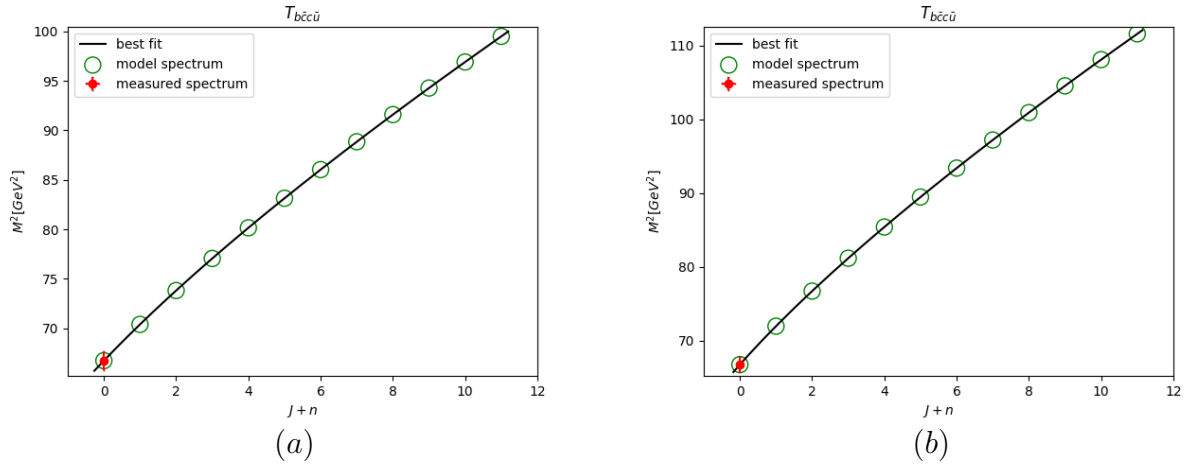


Figure 98: (a) is (J, M^2) $T_{b\bar{c}c\bar{u}}$ HMRT, (b) (n, M^2) $T_{b\bar{c}c\bar{u}}$ HMRT.

7.4.35 $T_{b\bar{c}c\bar{u}}$

J Spec	a_{T_j}
8149 – 8189	
8372 – 8408	
8575 – 8608	
8763 – 8794	
8939 – 8968	
9105 – 9132	
9262 – 9289	
9413 – 9439	
9558 – 9583	
9698 – 9722	
9833 – 9856	
9964 – 9986	
	-3.4–-3.2

Table 174: $T_{b\bar{c}c\bar{u}}$ (J, M^2) predictions.

n Spec	a_{T_n}
8149 – 8189	
8465 – 8499	
8743 – 8774	
8995 – 9023	
9228 – 9255	
9446 – 9471	
9652 – 9676	
9848 – 9870	
10035 – 10057	
10215 – 10235	
10387 – 10408	
10555 – 10574	
	-2.3–-2.2

Table 175: $T_{b\bar{c}c\bar{u}}$ (n, M^2) predictions.

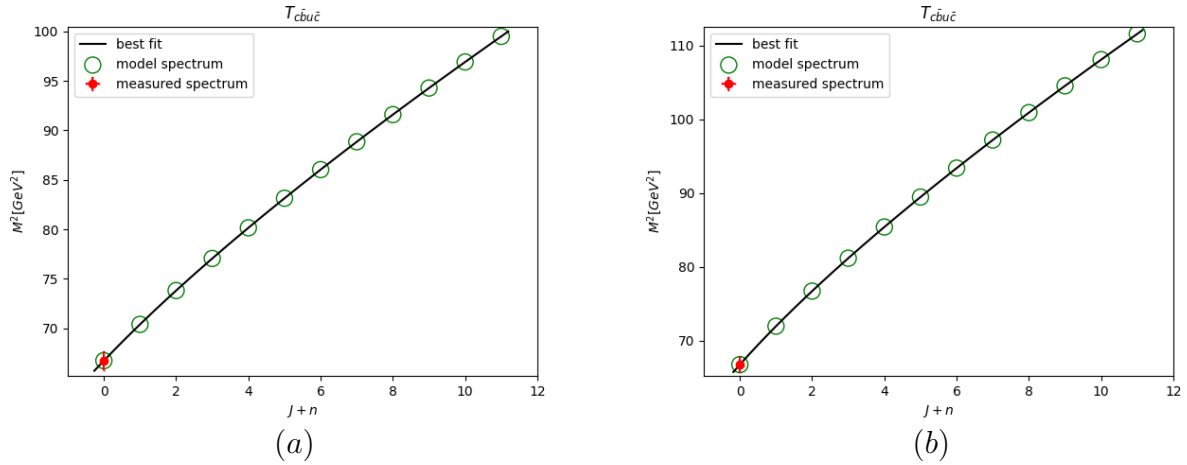


Figure 99: (a) is (J, M^2) $T_{c\bar{b}u\bar{c}}$ HMRT, (b) (n, M^2) $T_{c\bar{b}u\bar{c}}$ HMRT.

7.4.36 $T_{c\bar{b}u\bar{c}}$

J Spec	a_{T_j}
8149 – 8189	
8372 – 8408	
8575 – 8608	
8763 – 8794	
8939 – 8968	
9105 – 9132	
9262 – 9289	
9413 – 9439	
9558 – 9583	
9698 – 9722	
9833 – 9856	
9964 – 9986	
	-3.4–-3.2

Table 176: $T_{c\bar{b}u\bar{c}}$ (J, M^2) predictions.

n Spec	a_{T_n}
8149 – 8189	
8465 – 8499	
8743 – 8774	
8995 – 9023	
9228 – 9255	
9446 – 9471	
9652 – 9676	
9848 – 9870	
10035 – 10057	
10215 – 10235	
10387 – 10408	
10555 – 10574	
	-2.3–-2.2

Table 177: $T_{c\bar{b}u\bar{c}}$ (n, M^2) predictions.

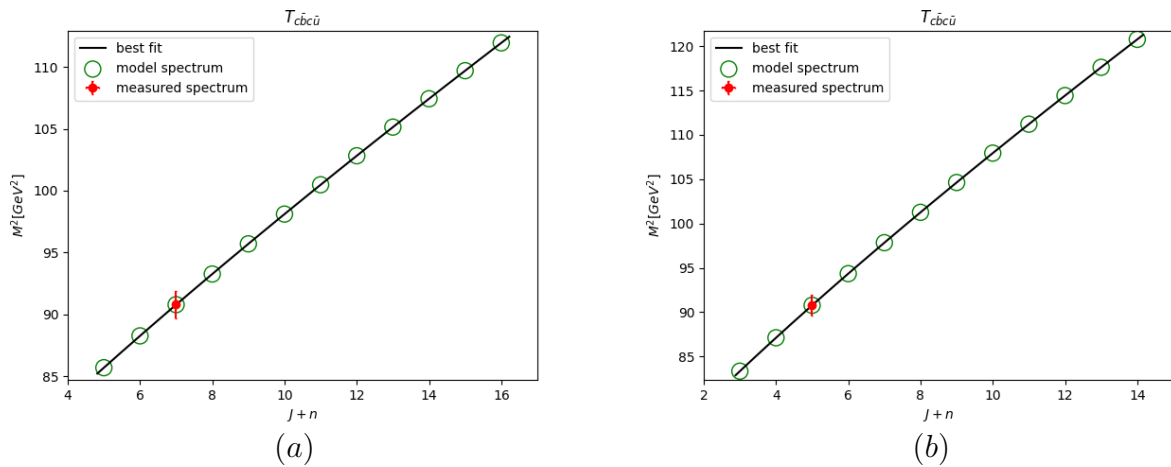


Figure 100: (a) is (J, M^2) $T_{c\bar{b}c\bar{u}}$ HMRT, (b) (n, M^2) $T_{c\bar{b}c\bar{u}}$ HMRT.

7.4.37 $T_{c\bar{b}c\bar{u}}$

J Spec	a_{T_j}
9198 – 9316	
9338 – 9451	
9473 – 9583	
9604 – 9711	
9731 – 9835	
9854 – 9955	
9975 – 10073	-5.9 – -5.1
10092 – 10188	
10207 – 10301	
10319 – 10411	
10429 – 10519	
10536 – 10625	

Table 178: $T_{c\bar{b}c\bar{u}}$ (J, M^2) predictions.

n Spec	a_{T_n}
9069 – 9191	
9276 – 9392	
9473 – 9583	
9661 – 9766	
9841 – 9942	
10014 – 10112	
10181 – 10276	
10343 – 10435	
10501 – 10590	
10654 – 10740	
10803 – 10887	
10948 – 11031	
	–3.9–3.4

Table 179: $T_{c\bar{b}c\bar{u}}$ (n, M^2) predictions.

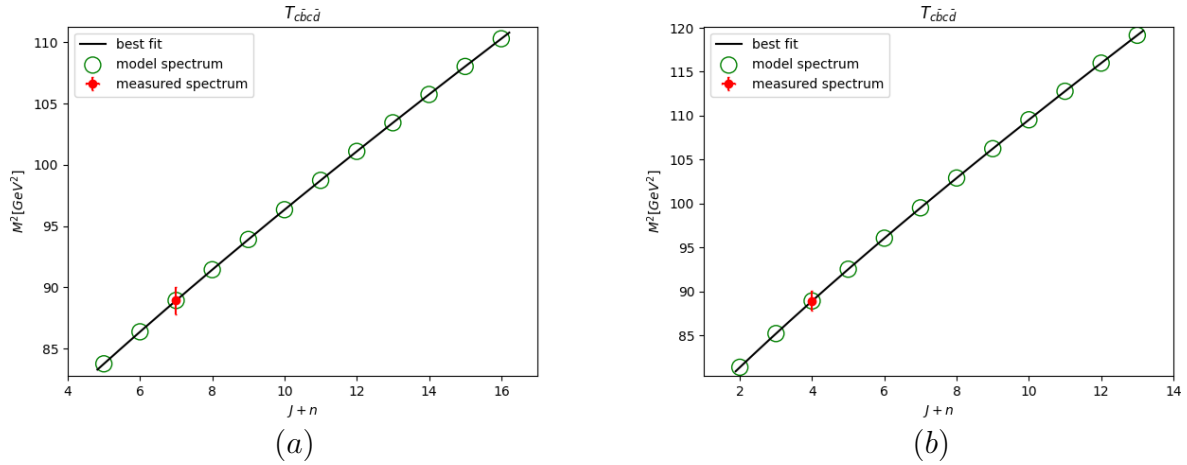


Figure 101: (a) is (J, M^2) $T_{c\bar{b}c\bar{d}}$ HMRT, (b) (n, M^2) $T_{c\bar{b}c\bar{d}}$ HMRT.

7.4.38 $T_{c\bar{b}c\bar{d}}$

J Spec	a_{T_j}
9093 – 9211	
9236 – 9350	
9375 – 9485	
9509 – 9615	
9639 – 9742	
9765 – 9865	
9887 – 9985	
10007 – 10102	
10123 – 10217	
10237 – 10329	
10349 – 10438	
10458 – 10546	
	-5.2–-4.3

Table 180: $T_{c\bar{b}c\bar{d}}$ (J, M^2) predictions.

n Spec	a_{T_n}
8960 – 9082	
9173 – 9289	
9375 – 9485	
9567 – 9672	
9751 – 9852	
9927 – 10025	
10098 – 10192	
10262 – 10353	
10422 – 10510	
10577 – 10663	
10728 – 10812	
10875 – 10957	
	-4.4–-3.8

Table 181: $T_{c\bar{b}c\bar{d}}$ (n, M^2) predictions.

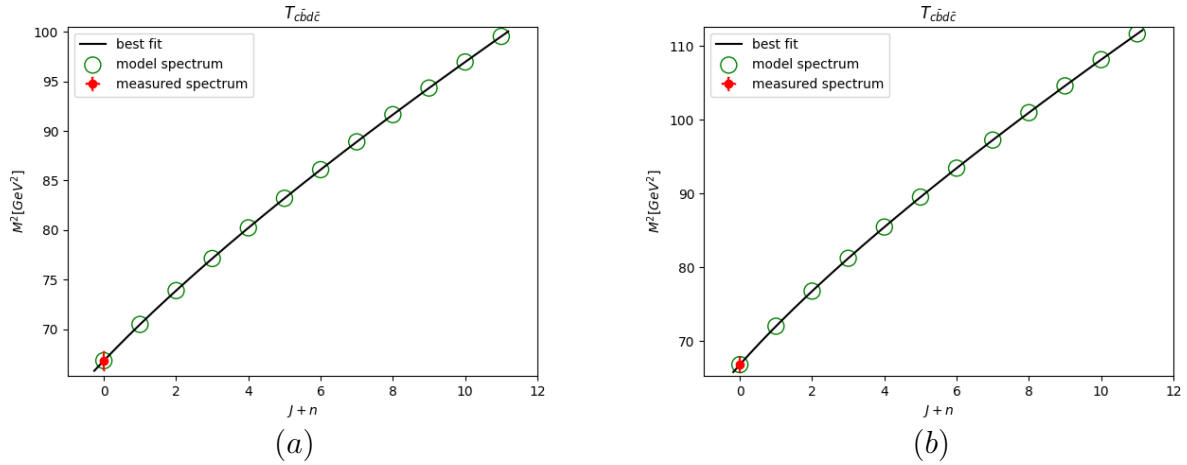


Figure 102: (a) is (J, M^2) $T_{c\bar{b}d\bar{c}}$ HMRT, (b) (n, M^2) $T_{c\bar{b}d\bar{c}}$ HMRT.

7.4.39 $T_{c\bar{b}d\bar{c}}$

J Spec	a_{T_j}
8154 – 8194	
8377 – 8413	
8579 – 8612	
8767 – 8798	
8942 – 8971	
9108 – 9136	
9266 – 9292	
9417 – 9442	
9561 – 9586	
9701 – 9724	
9836 – 9859	
9967 – 9989	
	-3.4–-3.2

Table 182: $T_{c\bar{b}d\bar{c}}$ (J, M^2) predictions.

n Spec	a_{T_n}
8154 – 8194	
8469 – 8504	
8746 – 8778	
8998 – 9027	
9231 – 9258	
9449 – 9474	
9655 – 9679	
9851 – 9873	
10038 – 10059	
10217 – 10238	
10390 – 10410	
10557 – 10576	
	-2.4–-2.2

Table 183: $T_{c\bar{b}d\bar{c}}$ (n, M^2) predictions.

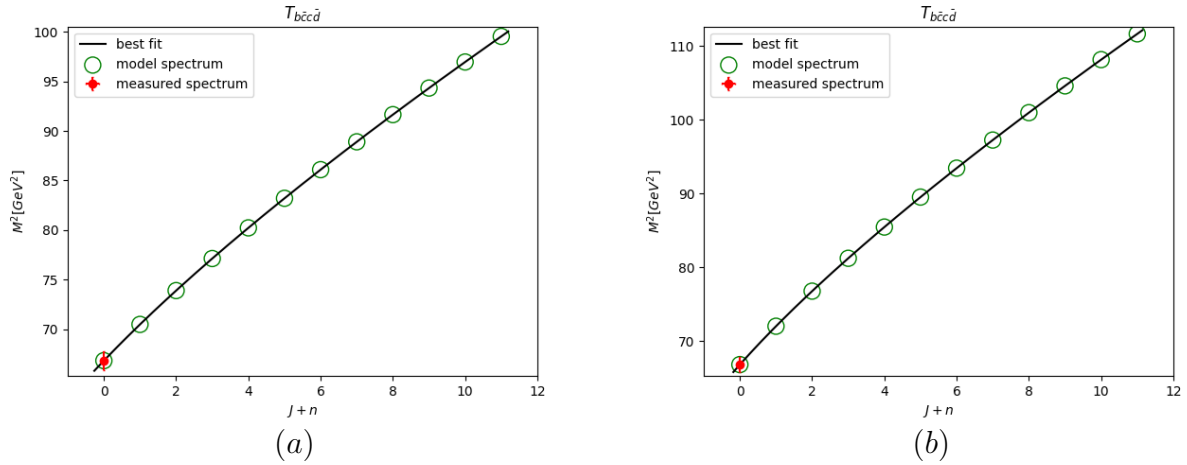


Figure 103: (a) is (J, M^2) $T_{b\bar{c}c\bar{d}}$ HMRT, (b) (n, M^2) $T_{b\bar{c}c\bar{d}}$ HMRT.

7.4.40 $T_{b\bar{c}c\bar{d}}$

J Spec	a_{T_j}
8154 – 8194	
8377 – 8413	
8579 – 8612	
8767 – 8798	
8942 – 8971	
9108 – 9136	
9266 – 9292	
9417 – 9442	
9561 – 9586	
9701 – 9724	
9836 – 9859	
9967 – 9989	
	-3.4–-3.2

Table 184: $T_{b\bar{c}c\bar{d}}$ (J, M^2) predictions.

n Spec	a_{T_n}
8154 – 8194	
8469 – 8504	
8746 – 8778	
8998 – 9027	
9231 – 9258	
9449 – 9474	
9655 – 9679	
9851 – 9873	
10038 – 10059	
10217 – 10238	
10390 – 10410	
10557 – 10576	
	-2.4–-2.2

Table 185: $T_{b\bar{c}c\bar{d}}$ (n, M^2) predictions.

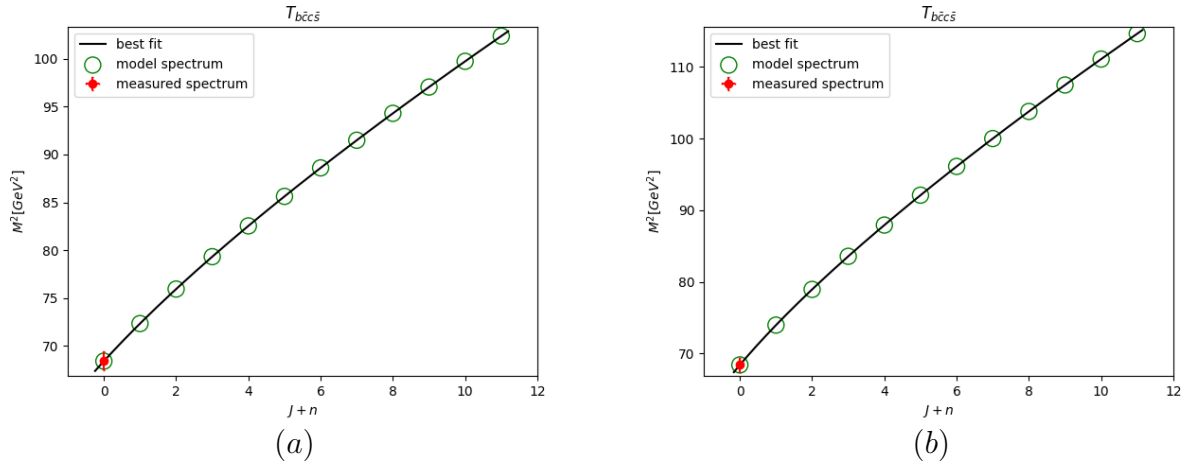


Figure 104: (a) is (J, M^2) $T_{b\bar{c}c\bar{s}}$ HMRT, (b) (n, M^2) $T_{b\bar{c}c\bar{s}}$ HMRT.

7.4.41 $T_{b\bar{c}c\bar{s}}$

J Spec	a_{T_j}
8252 – 8292	
8488 – 8523	
8699 – 8731	
8892 – 8922	
9072 – 9099	
9240 – 9266	
9400 – 9425	
9553 – 9577	
9699 – 9722	
9840 – 9862	
9976 – 9997	
10107 – 10128	-2.6–-2.4

Table 186: $T_{b\bar{c}c\bar{s}}$ (J, M^2) predictions.

n Spec	a_{T_n}
8252 – 8292	
8584 – 8618	
8871 – 8901	
9129 – 9156	
9365 – 9391	
9586 – 9609	
9793 – 9816	-1.8–-1.7
9990 – 10012	
10178 – 10199	
10358 – 10378	
10532 – 10550	
10699 – 10717	

Table 187: $T_{b\bar{c}c\bar{s}}$ (n, M^2) predictions.

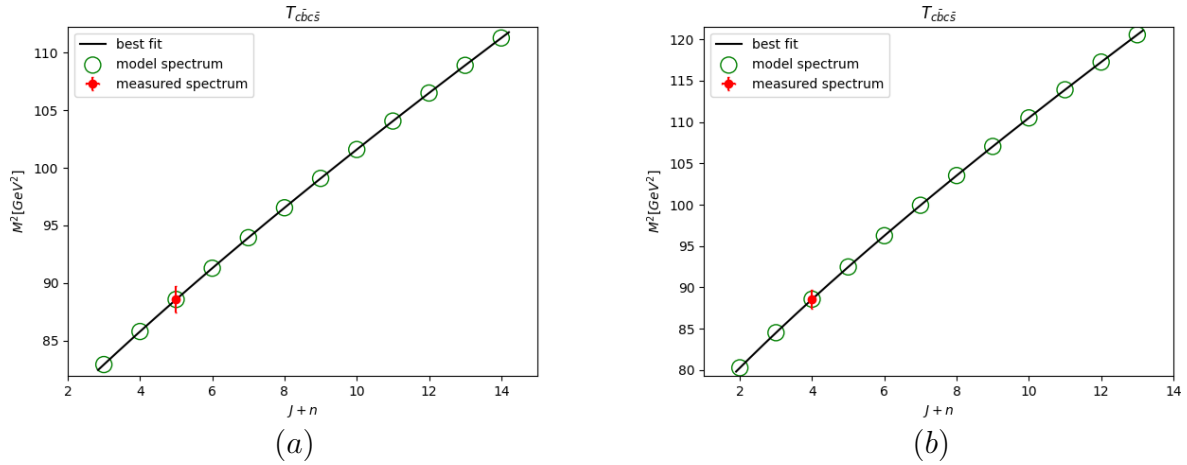


Figure 105: (a) is (J, M^2) $T_{c\bar{b}c\bar{s}}$ HMRT, (b) (n, M^2) $T_{c\bar{b}c\bar{s}}$ HMRT.

7.4.42 $T_{c\bar{b}c\bar{s}}$

J Spec	a_{T_j}
9045 – 9166	
9204 – 9319	
9356 – 9466	
9501 – 9607	
9641 – 9743	
9776 – 9875	
9907 – 10002	
10033 – 10126	
10156 – 10247	
10276 – 10364	
10393 – 10479	
10507 – 10592	
	-4.6–-3.9

Table 188: $T_{c\bar{b}c\bar{s}}$ (J, M^2) predictions.

n Spec	a_{T_n}
8896 – 9023	
9134 – 9252	
9356 – 9466	
9564 – 9668	
9761 – 9860	
9949 – 10044	
10129 – 10220	
10302 – 10390	
10470 – 10555	
10631 – 10714	
10788 – 10868	
10941 – 11019	
	-2.7–-2.1

Table 189: $T_{c\bar{b}c\bar{s}}$ (n, M^2) predictions.

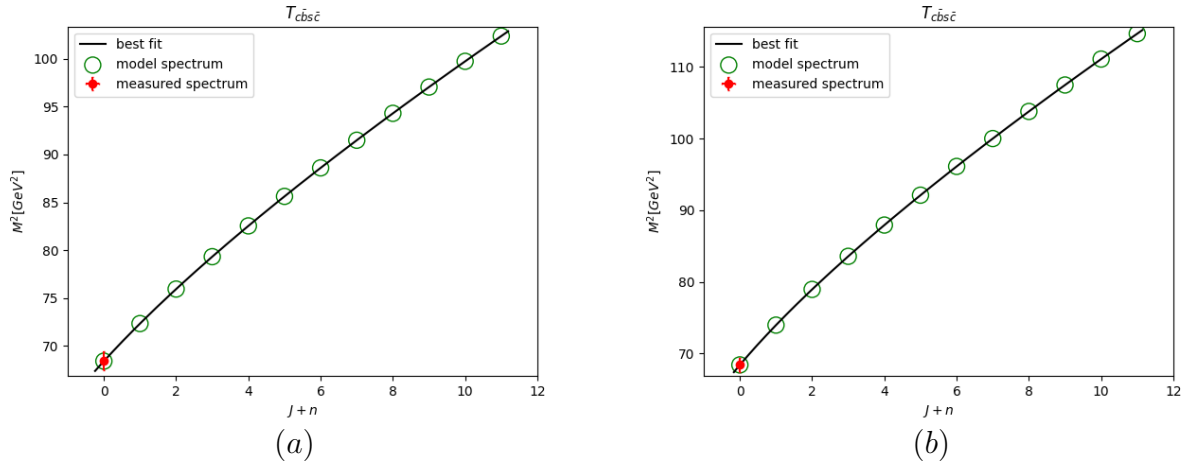


Figure 106: (a) is (J, M^2) $T_{c\bar{b}s\bar{c}}$ HMRT, (b) (n, M^2) $T_{c\bar{b}s\bar{c}}$ HMRT.

7.4.43 $T_{c\bar{b}s\bar{c}}$

J Spec	a_{T_j}
8252 – 8292	
8488 – 8523	
8699 – 8731	
8892 – 8922	
9072 – 9099	
9240 – 9266	
9400 – 9425	
9553 – 9577	
9699 – 9722	
9840 – 9862	
9976 – 9997	
10107 – 10128	-2.6–-2.4

Table 190: $T_{c\bar{b}s\bar{c}}$ (J, M^2) predictions.

n Spec	a_{T_n}
8252 – 8292	
8584 – 8618	
8871 – 8901	
9129 – 9156	
9365 – 9391	
9586 – 9609	
9793 – 9816	-1.8–-1.7
9990 – 10012	
10178 – 10199	
10358 – 10378	
10532 – 10550	
10699 – 10717	

Table 191: $T_{c\bar{b}s\bar{c}}$ (n, M^2) predictions.

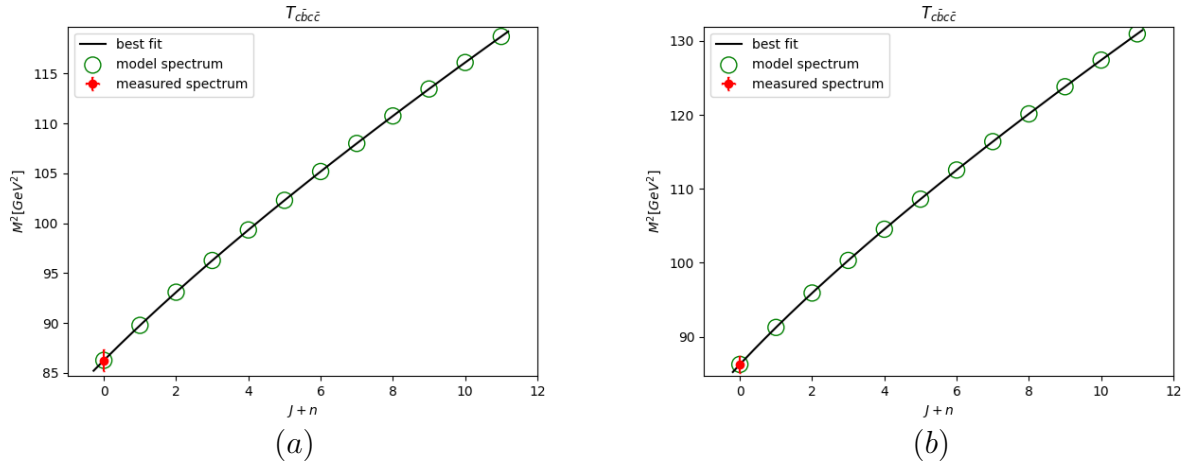


Figure 107: (a) is (J, M^2) $T_{c\bar{b}c\bar{c}}$ HMRT, (b) (n, M^2) $T_{c\bar{b}c\bar{c}}$ HMRT.

7.4.44 $T_{c\bar{b}c\bar{c}}$

J Spec	a_{T_j}
9268 – 9308	
9456 – 9493	
9631 – 9666	
9795 – 9828	
9951 – 9982	
10099 – 10129	
10241 – 10270	
10378 – 10406	
10510 – 10537	
10638 – 10664	
10762 – 10787	
10883 – 10907	
–4.2–4.0	

Table 192: $T_{c\bar{b}c\bar{c}}$ (J, M^2) predictions.

n Spec	a_{T_n}
9268 – 9308	
9535 – 9571	
9777 – 9810	
10001 – 10032	
10210 – 10239	
10408 – 10435	
10596 – 10622	
10776 – 10801	
10949 – 10973	
11115 – 11138	
11276 – 11299	
11432 – 11454	
–2.9–2.8	

Table 193: $T_{c\bar{b}c\bar{c}}$ (n, M^2) predictions.

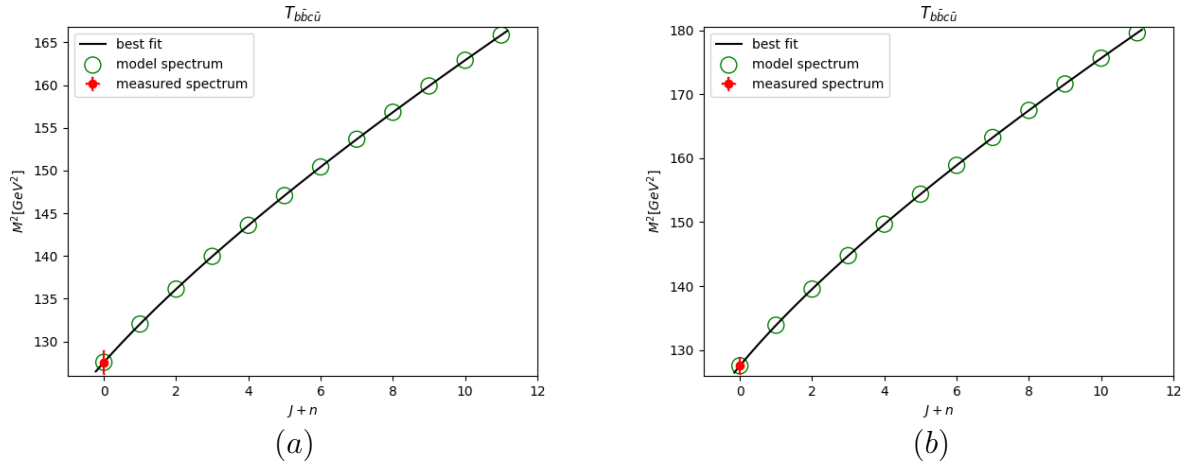


Figure 108: (a) is (J, M^2) $T_{b\bar{b}c\bar{u}}$ HMRT, (b) (n, M^2) $T_{b\bar{b}c\bar{u}}$ HMRT.

7.4.45 $T_{b\bar{b}c\bar{u}}$

J Spec	a_{T_j}
11274 – 11314	
11473 – 11508	
11651 – 11683	
11815 – 11845	
11969 – 11997	
12114 – 12141	
12252 – 12277	
12384 – 12409	
12511 – 12535	
12634 – 12657	
12753 – 12775	
12868 – 12890	
	-2.5--2.3

Table 194: $T_{b\bar{b}c\bar{u}}$ (J, M^2) predictions.

n Spec	a_{T_n}
11274 – 11314	
11554 – 11588	
11798 – 11828	
12018 – 12046	
12222 – 12248	
12413 – 12437	
12593 – 12617	
12766 – 12788	
12931 – 12952	
13089 – 13110	
13243 – 13263	
13391 – 13411	
	-1.7--1.6

Table 195: $T_{b\bar{b}c\bar{u}}$ (n, M^2) predictions.

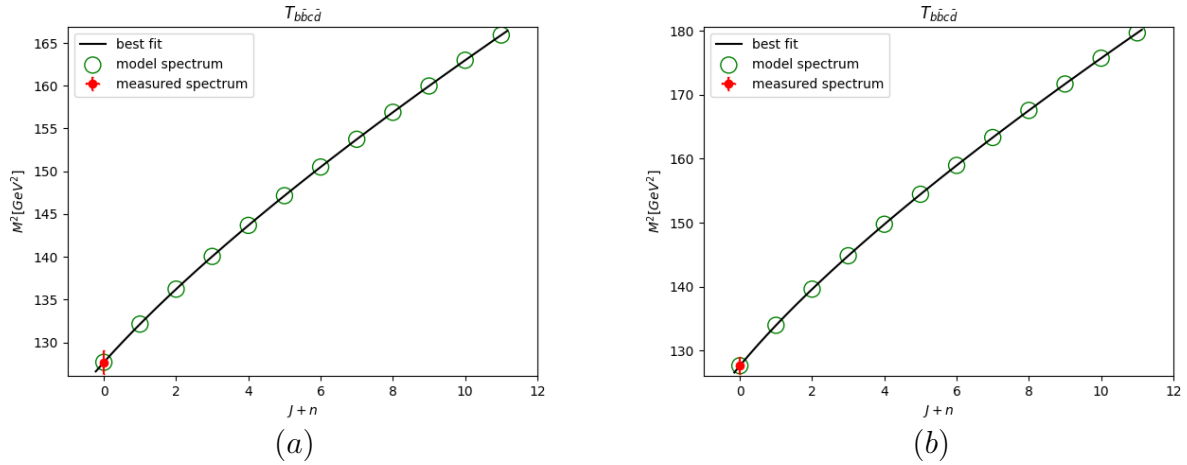


Figure 109: (a) is (J, M^2) $T_{bb\bar{c}\bar{d}}$ HMRT, (b) (n, M^2) $T_{bb\bar{c}\bar{d}}$ HMRT.

7.4.46 $T_{bb\bar{c}\bar{d}}$

J Spec	a_{T_j}
11279 – 11319	
11477 – 11513	
11655 – 11687	
11819 – 11849	
11972 – 12001	
12117 – 12144	
12255 – 12281	
12387 – 12412	
12514 – 12538	
12637 – 12660	
12755 – 12778	
12871 – 12892	
	-2.5--2.3

Table 196: $T_{bb\bar{c}\bar{d}}$ (J, M^2) predictions.

n Spec	a_{T_n}
11279 – 11319	
11558 – 11592	
11801 – 11832	
12021 – 12049	
12225 – 12251	
12416 – 12440	
12596 – 12619	
12768 – 12791	
12933 – 12955	
13092 – 13113	
13245 – 13265	
13394 – 13413	
	-1.7--1.6

Table 197: $T_{bb\bar{c}\bar{d}}$ (n, M^2) predictions.

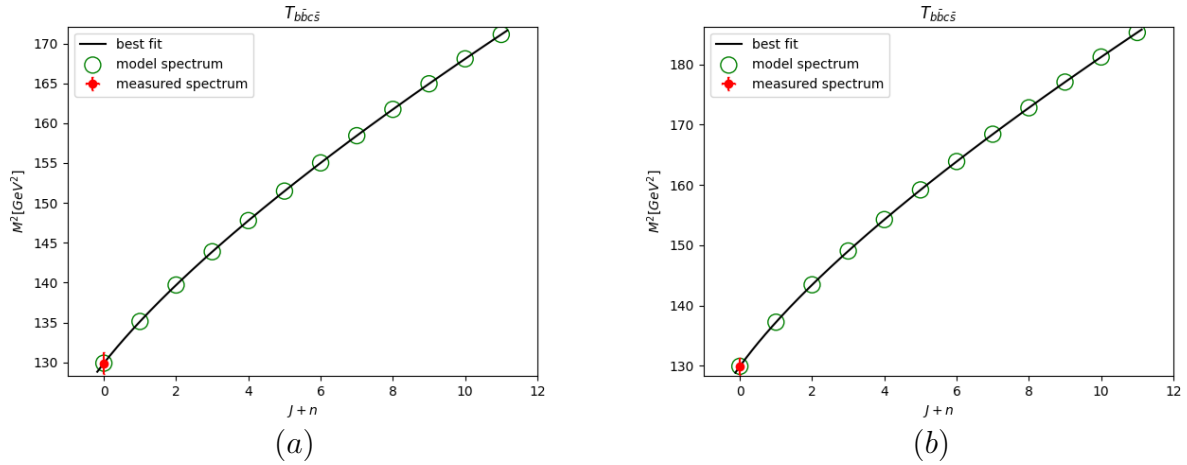


Figure 110: (a) is (J, M^2) $T_{b\bar{b}c\bar{s}}$ HMRT, (b) (n, M^2) $T_{b\bar{b}c\bar{s}}$ HMRT.

7.4.47 $T_{b\bar{b}c\bar{s}}$

J Spec	a_{T_j}
11377 – 11417	
11608 – 11641	
11805 – 11834	
11981 – 12008	
12144 – 12169	
12296 – 12319	
12440 – 12462	
12576 – 12598	
12707 – 12728	
12833 – 12853	
12955 – 12974	
13073 – 13091	
	-1.4 – -1.3

Table 198: $T_{b\bar{b}c\bar{s}}$ (J, M^2) predictions.

n Spec	a_{T_n}
11377 – 11417	
11699 – 11730	
11963 – 11990	
12196 – 12220	
12408 – 12431	
12606 – 12627	
12792 – 12812	-0.98 – -0.87
12968 – 12987	
13136 – 13155	
13298 – 13315	
13454 – 13470	
13604 – 13620	

Table 199: $T_{b\bar{b}c\bar{s}}$ (n, M^2) predictions.

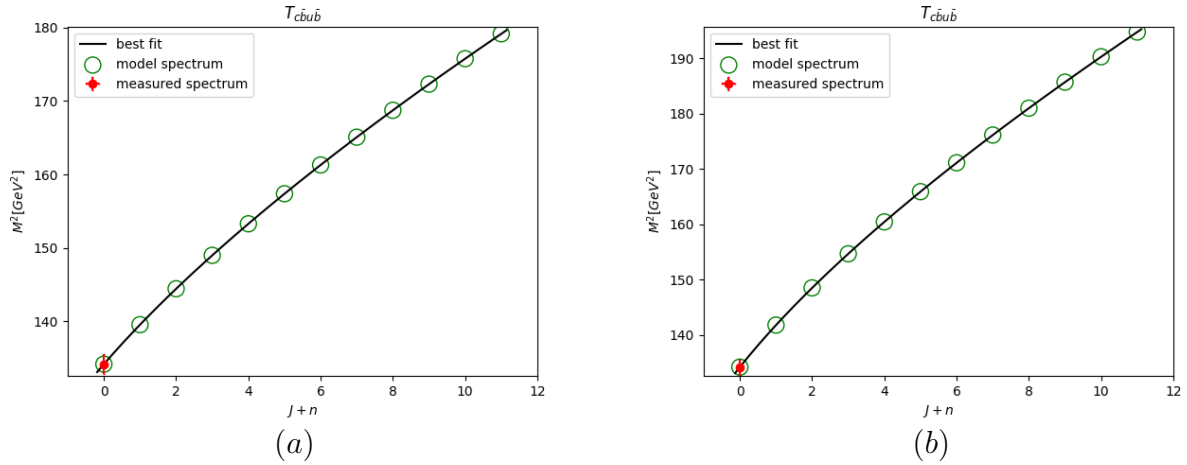


Figure 111: (a) is (J, M^2) $T_{c\bar{b}u\bar{b}}$ HMRT, (b) (n, M^2) $T_{c\bar{b}u\bar{b}}$ HMRT.

7.4.48 $T_{c\bar{b}u\bar{b}}$

J Spec	a_{T_j}
11563 – 11603	
11795 – 11830	
12002 – 12034	
12191 – 12221	
12367 – 12395	
12532 – 12558	
12688 – 12713	–2.7
12837 – 12860	–2.6
12979 – 13001	
13116 – 13137	
13247 – 13268	
13375 – 13395	

Table 200: $T_{c\bar{b}u\bar{b}}$ (J, M^2) predictions.

n Spec	a_{T_n}
11563 – 11603	
11890 – 11923	
12171 – 12201	
12423 – 12450	
12654 – 12679	
12869 – 12892	
13071 – 13093	
13262 – 13283	
13444 – 13464	
13618 – 13637	
13786 – 13804	
13948 – 13965	
	–1.9–1.8

Table 201: $T_{c\bar{b}u\bar{b}}$ (n, M^2) predictions.

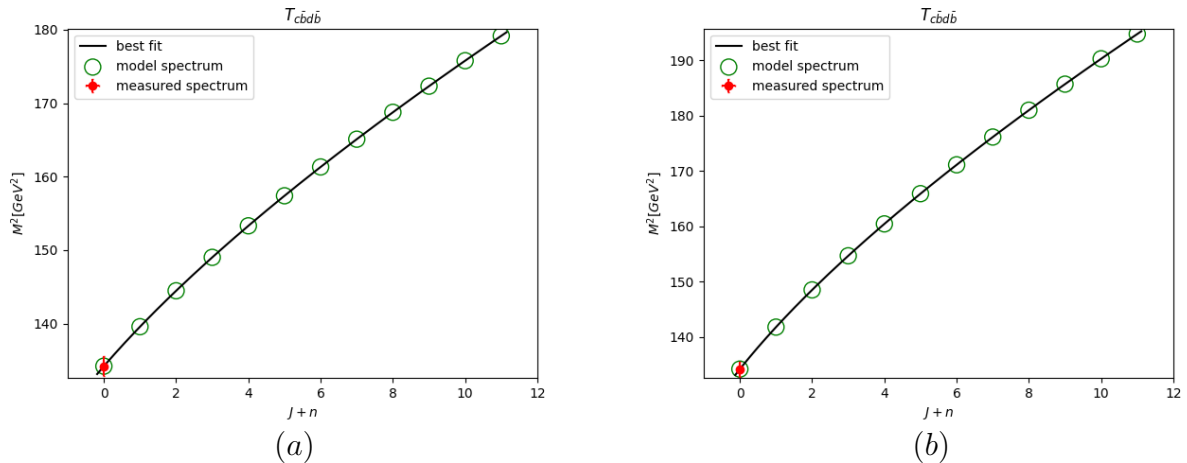


Figure 112: (a) is (J, M^2) $T_{c\bar{b}d\bar{b}}$ HMRT, (b) (n, M^2) $T_{c\bar{b}d\bar{b}}$ HMRT.

7.4.49 $T_{c\bar{b}d\bar{b}}$

J Spec	a_{T_j}
11564 – 11604	
11796 – 11831	
12003 – 12035	
12192 – 12222	
12368 – 12395	
12533 – 12559	
12689 – 12713	
12837 – 12861	
12979 – 13002	
13116 – 13138	
13248 – 13269	
13375 – 13396	
	-2.7 – -2.6

Table 202: $T_{c\bar{b}d\bar{b}}$ (J, M^2) predictions.

n Spec	a_{T_n}
11564 – 11604	
11891 – 11924	
12172 – 12202	
12424 – 12451	
12655 – 12680	
12869 – 12893	
13071 – 13093	–1.9
13262 – 13283	–1.8
13444 – 13464	
13619 – 13638	
13786 – 13805	
13948 – 13966	

Table 203: $T_{c\bar{b}d\bar{b}}$ (n, M^2) predictions.

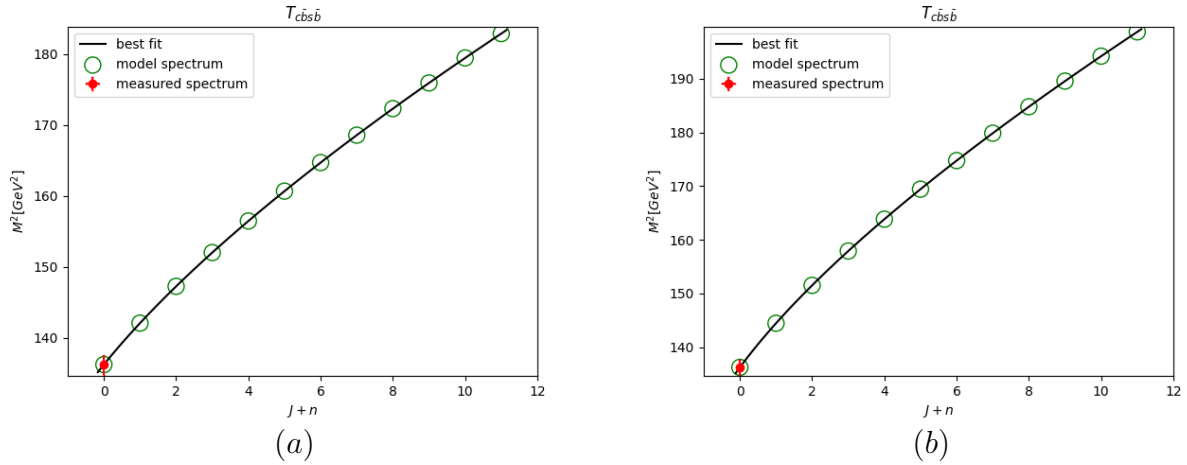


Figure 113: (a) is (J, M^2) $T_{c\bar{b}s\bar{b}}$ HMRT, (b) (n, M^2) $T_{c\bar{b}s\bar{b}}$ HMRT.

7.4.50 $T_{c\bar{b}s\bar{b}}$

J Spec	a_{T_j}
11651 – 11691	
11902 – 11936	
12120 – 12150	
12316 – 12343	
12496 – 12521	
12664 – 12688	
12822 – 12845	
12973 – 12995	
13117 – 13137	
13254 – 13274	
13387 – 13406	
13515 – 13534	
–1.9–1.8	

Table 204: $T_{c\bar{b}s\bar{b}}$ (J, M^2) predictions.

n Spec	a_{T_n}
11651 – 11691	
12002 – 12034	
12295 – 12322	
12553 – 12578	
12788 – 12811	
13005 – 13027	
13209 – 13229	
13401 – 13421	
13584 – 13603	
13759 – 13777	
13927 – 13944	
14089 – 14106	
–1.3–1.2	

Table 205: $T_{c\bar{b}s\bar{b}}$ (n, M^2) predictions.

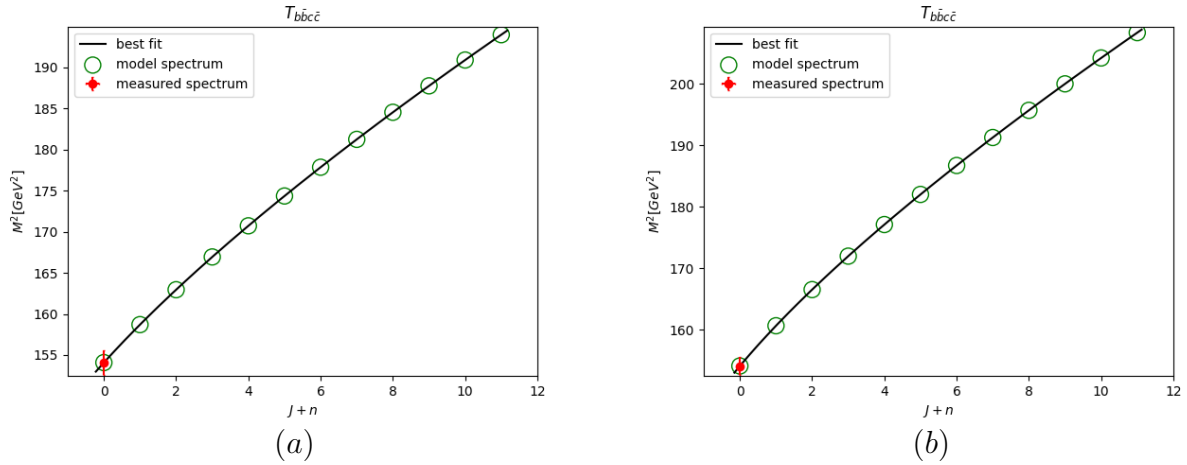


Figure 114: (a) is (J, M^2) $T_{b\bar{b}c\bar{c}}$ HMRT, (b) (n, M^2) $T_{b\bar{b}c\bar{c}}$ HMRT.

7.4.51 $T_{b\bar{b}c\bar{c}}$

J Spec	a_{T_j}
12393 – 12433	
12580 – 12616	
12749 – 12782	
12905 – 12936	
13052 – 13081	
13191 – 13218	-2.7–-2.5
13323 – 13349	
13450 – 13475	
13572 – 13597	
13691 – 13714	
13805 – 13828	
13916 – 13939	

Table 206: $T_{b\bar{b}c\bar{c}}$ (J, M^2) predictions.

n Spec	a_{T_n}
12393 – 12433	
12657 – 12691	
12888 – 12919	
13099 – 13127	
13294 – 13321	
13478 – 13503	-1.9–-1.7
13652 – 13676	
13818 – 13841	
13977 – 13999	
14131 – 14152	
14279 – 14300	
14423 – 14443	

Table 207: $T_{b\bar{b}c\bar{c}}$ (n, M^2) predictions.

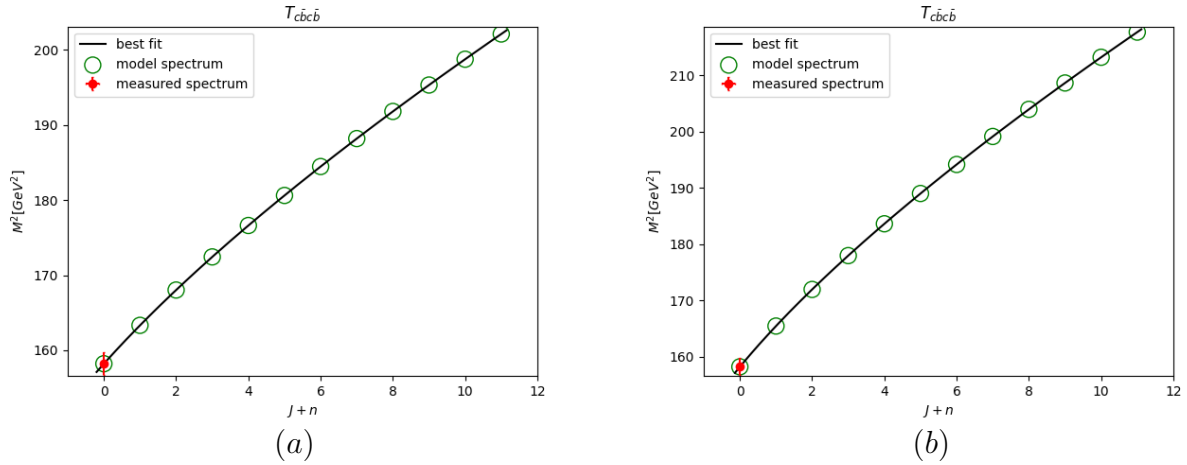


Figure 115: (a) is (J, M^2) $T_{c\bar{b}c\bar{b}}$ HMRT, (b) (n, M^2) $T_{c\bar{b}c\bar{b}}$ HMRT.

7.4.52 $T_{c\bar{b}c\bar{b}}$

J Spec	a_{T_j}
12558 – 12598	
12762 – 12798	
12946 – 12979	
13116 – 13147	
13276 – 13304	
13426 – 13453	
13569 – 13595	
13706 – 13731	
13838 – 13862	
13965 – 13988	
14087 – 14110	
14207 – 14228	
–2.9–2.7	

Table 208: $T_{c\bar{b}c\bar{b}}$ (J, M^2) predictions.

n Spec	a_{T_n}
12558 – 12598	
12846 – 12880	
13098 – 13129	
13327 – 13355	
13538 – 13564	
13736 – 13761	
13923 – 13946	
14101 – 14123	
14271 – 14293	
14435 – 14456	
14593 – 14613	
14745 – 14765	
–2.0–1.9	

Table 209: $T_{c\bar{b}c\bar{b}}$ (n, M^2) predictions.

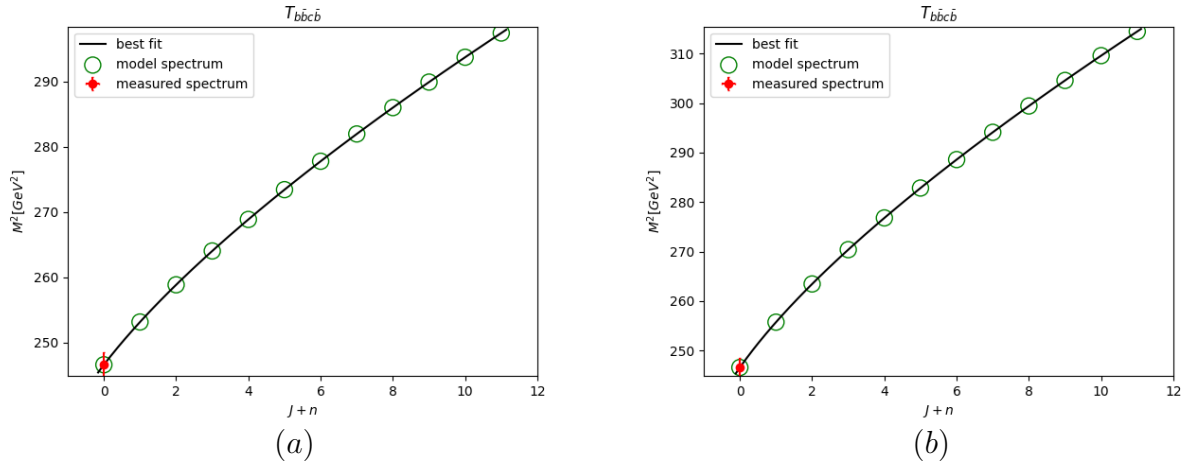


Figure 116: (a) is (J, M^2) $T_{bb\bar{c}\bar{b}}$ HMRT, (b) (n, M^2) $T_{bb\bar{c}\bar{b}}$ HMRT.

7.4.53 $T_{bb\bar{c}\bar{b}}$

J Spec	a_{T_j}
15683 – 15723	
15894 – 15927	
16074 – 16103	
16235 – 16262	
16384 – 16409	
16523 – 16547	-1.4 – -1.3
16655 – 16677	
16781 – 16802	
16901 – 16921	
17016 – 17036	
17128 – 17147	
17236 – 17255	

Table 210: $T_{bb\bar{c}\bar{b}}$ (J, M^2) predictions.

n Spec	a_{T_n}
15683 – 15723	
15977 – 16008	
16218 – 16245	
16432 – 16456	
16626 – 16649	
16808 – 16829	-0.99 – -0.87
16978 – 16998	
17140 – 17159	
17295 – 17313	
17444 – 17461	
17587 – 17604	
17726 – 17742	

Table 211: $T_{bb\bar{c}\bar{b}}$ (n, M^2) predictions.

7.5 Pentaquarks Candidates

Candidate	Quarks Content	Decay Channel	J^P	Mass [MeV]	Width [MeV]	Ref.
$P_\psi^N(4312)^+$ or $P_c(4312)^+$	$c\bar{c}uud$	$J/\psi p$	$1/2^?$	$4311.9 \pm 0.7^{+6.8}_{-0.6}$	$9.8 \pm 2.7^{+3.7}_{-4.5}$	[114]
$P_\psi^N(4380)^+$ or $P_c(4380)^+$	$c\bar{c}uud$	$J/\psi p$	$3/2^?$ or $5/2^?$	$4380 \pm 8 \pm 29$	$205 \pm 18 \pm 86$	[114]

$P_\psi^N(4450)^+$ or $P_c(4450)^+$ ¹²	$c\bar{c}uud$	$J/\psi p$	$3/2^?$ or $5/2^?$	$4449.8 \pm 1.7 \pm 2.5$	$39 \pm 5 \pm 19$	[114]
$P_\psi^N(4457)^+$ or $P_c(4457)^+$ ¹²	$c\bar{c}uud$	$J/\psi p$	$3/2^?$ or $5/2^?$	$4457.3 \pm 0.6^{+4.1}_{-1.7}$	$6.4 \pm 2.0^{+5.7}_{-1.9}$	[114], [115]
$P_\psi^N(4440)^+$ or $P_c(4440)^+$ ¹²	$c\bar{c}uud$	$J/\psi p$	$3/2^?$ or $5/2^?$	$4440.3 \pm 1.3^{+4.1}_{-4.7}$	$20.6 \pm 4.9^{+8.7}_{-10.1}$	[114]
$P_{\psi s}^\Lambda(4338)^0$	$c\bar{c}uud$	$J/\psi \Lambda$	$1/2^-$	$4338.2 \pm 0.7 \pm 0.4$	$7.0 \pm 1.2 \pm 1.3$	[116] another approach in [117]

Table 212: Pentaquarks candidates summary. These states were analysed in detail in this paper and compared with the pentaquarks predicted HMRTs described at 223.

7.6 $P_\psi^{N^+}$ (quark content $c\bar{c}uud$)

The pentaquark candidates were observed in [114] and in [115]. The state $P_c(4380)$ requires further confirmation and is not included in the analysis of [115]. This state does not fit the trajectory. The decay channel in which these states were observed is $J/\psi p$ which is compatible with the annihilation mechanism.

7.6.1 $P_\psi^{N^+}$ baryonic configuration fit

For the baryonic configuration, the fit that we got is displayed in figure 213, alongside with the best fit. The spectrum for the best fit is in table 214.

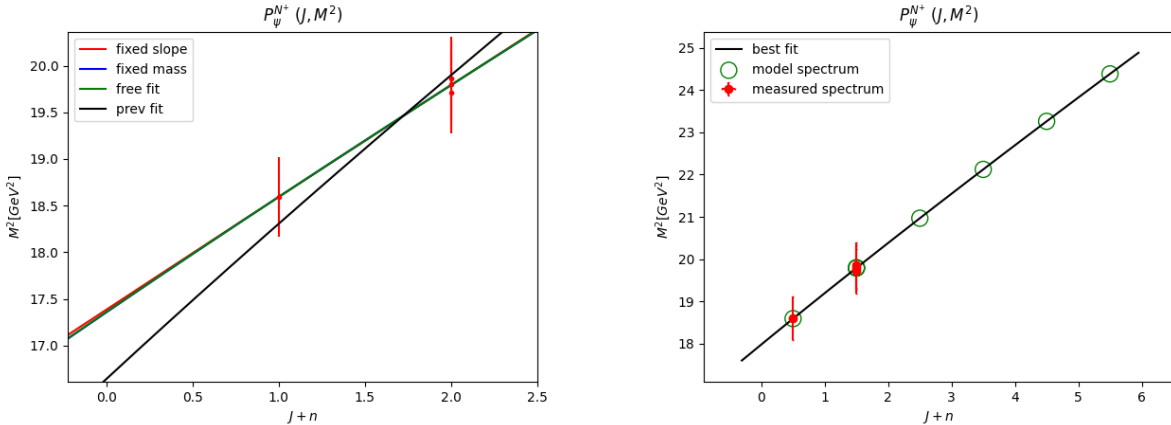


Table 213: On the left - $P_\psi^{N^+}$ all fits, on the right is the best fit.

State	M [MeV]	Thry M [MeV]	J	Thry n	Thry $J+n$

¹²This state was resolved in [115] to two other resonances.

$P(4312)_{\psi 0}^{N^+}$	4312	4312	0	0	0
$P(4440)_{\psi 0}^{N^+}$	4440	4449	0	1	2
$P(4450)_{\psi 0}^{N^+}$	4450	4449	0	1	2
$P(4457)_{\psi 0}^{N^+}$	4457	4449	0	1	2
		4579			2
		4703			4
		4823			4
		4938			6

Table 214: $P_\psi^{N^+} (J, M^2)$ HMRT.

7.6.2 $P_\psi^{N^+}$ tetraquark-like configuration fit

For the tetraquark-like configuration, the fit that we got is displayed in figure 215, alongside with the best fit. The spectrum for the best fit is in table 216.

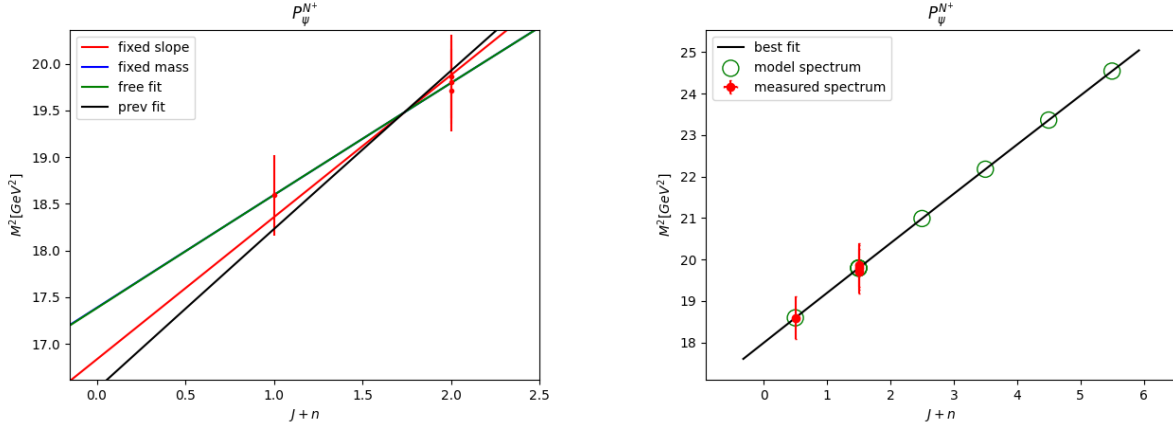


Table 215: On the left - $P_\psi^{N^+}$ all fits, on the right is the best fit.

State	M [MeV]	Thry M [MeV]	J	Thry n	Thry $J + n$
$P(4312)_{\psi 0}^{N^+}$	4312	4312	0	0	0
$P(4440)_{\psi 0}^{N^+}$	4440	4449	0	1	2
$P(4450)_{\psi 0}^{N^+}$	4450	4449	0	1	2
$P(4457)_{\psi 0}^{N^+}$	4457	4449	0	1	2
		4581			2
		4709			4
		4833			4
		4954			6

Table 216: $P_\psi^{N^+}$ HMRT.

7.7 $P_{c\bar{c}sud}$

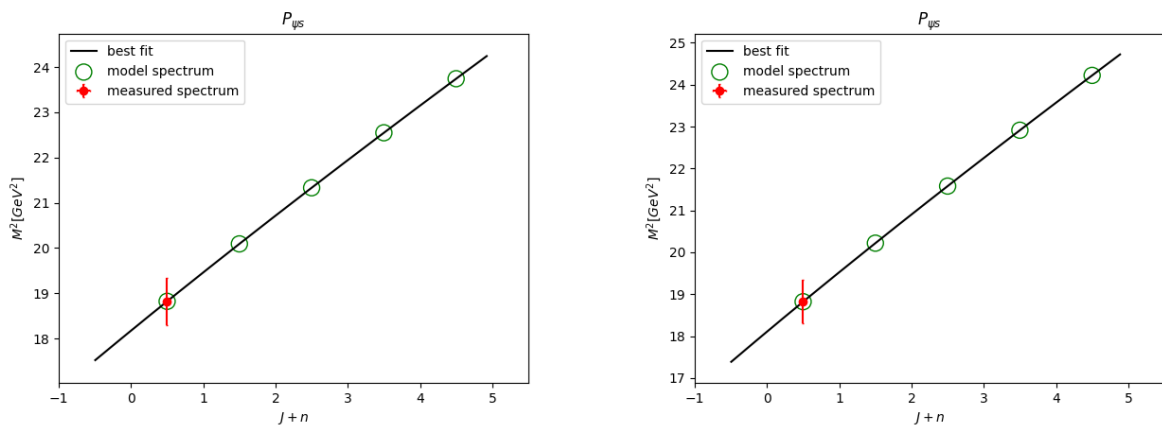
This state was observed in [116]. In this section we built the trajectories for both baryonic and tetraquark configurations.

7.7.1 $P_{c\bar{c}sud}$ baryon configuration HMRTs

<i>State</i>	M [MeV]	Thry M [MeV]	J	Thry n	Thry $J + n$	<i>State</i>	M [MeV]	Thry M [MeV]	J	Thry n	Thry $J + n$
$P(4338)_{\psi s0}^0$	4338	4338			0	$P(4338)_{\psi s0}^0$	4338	4338			0
		4482			2				4496		2
		4619			2				4645		2
		4748			4				4787		4
		4873			4				4922		4

Table 217: $P_{\psi s}^\Lambda(J, M^2)$ HMRT.

Table 218: $P_{\psi s}^\Lambda(n, M^2)$ HMRT.

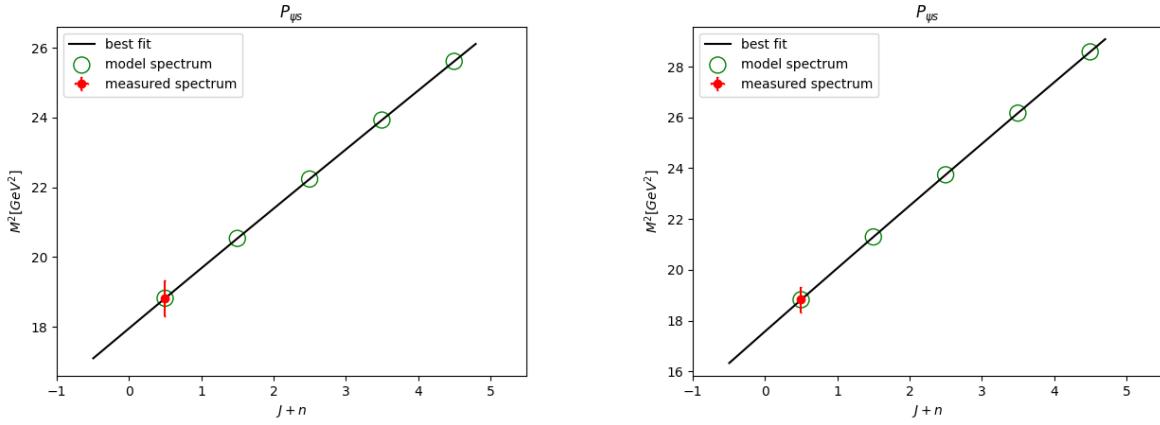


7.7.2 $P_{c\bar{c}sud}$ tetra configuration fit

<i>State</i>	M [MeV]	Thry M [MeV]	J	Thry n	Thry $J + n$	<i>State</i>	M [MeV]	Thry M [MeV]	J	Thry n	Thry $J + n$
$P(4338)_{\psi s0}^0$	4338	4338			0	$P(4338)_{\psi s0}^0$	4338	4338			0
		4532			2				4614		2
		4716			2				4872		2
		4892			4				5116		4
		5061			4				5346		4

Table 220: $P_{\psi s}^\Lambda(J, M^2)$ HMRT.

Table 221: $P_{\psi s}^\Lambda(n, M^2)$ HMRT.



7.8 Pentaquarks HMRTs Predictions

The following table summarizes all the thresholds and predicted trajectories for all possible charm pentaquarks configurations. The thresholds were calculated for each possible product according to the HISH model through the annihilation mechanisms. This is because in the case of pentaquarks, there is not yet any observed state that matches the string-tear mechanism.

The 'Candidates' column contains the resonances that were already detected. We elaborate on all of these at the following sub sections, including the decay channels through which they were observed.

The table spectrum predictions were calculated based on the mesons and baryons fit parameters. We assumed that the endpoint masses are the sum of masses of the quarks (or antiquarks). We calculated four spectrum ranges - the first two ('J Spec Baryon' and 'n Spec Baryon') are based on the pentaquarks baryon configuration as described in 21. For these spectra we used the baryons charm slopes. For the second two ('J Spec Tetra' and 'n Spec Tetra') are based on the tetraquark-like configuration as described in 23. The slopes for the latter are the mesonic slopes for heavy mesons for each plane as summarized at 1.

We did assume that the first 21 configuration is allowed only when there is quark that is of the same flavor as the antiquark. Therefore the 'baryonic' spectrum is not calculated for all pentaquarks.

We calculated the 'J Spec (Baryon)' and 'n Spec (Baryon)' in the following steps:

- We first calculated the annihilation threshold and let it vary between $175 - 275 \text{ MeV}$ above the threshold. This was done by looking at the available data that we collected, where the created pentaquarks candidates are above the annihilation threshold.
- We assumed that this is the first resonance on the trajectory, so we set $J + n = 0$.
- Since we do not know the arrangement of the quarks within the endpoints, we went over all the possible arrangement.
- For each arrangement, we calculated the endpoint masses and deduced the spectrum using the baryons slope of the plane (J or n).
- The final spectrum range for each plane was taken to be between the minimum and maximum of all the possible arrangements.
- We derived the range of the spectrum for four more states that were above the lowest mass.

We calculated the 'J Spec (Tetra)' and 'n Spec (Tetra)' in the following steps:

- We first calculated the annihilation threshold and let it vary between $175 - 275\text{ MeV}$ above the threshold. This was done by looking at the available data that we collected, where the created pentaquarks candidates are above the annihilation threshold.
- We assumed that this is the first resonance on the trajectory, so we set $J + n = 0$.
- Since we do not know the arrangement of the quarks within the endpoints, we went over all the possible arrangement.
- We assumed that the antiquark is always around the center of mass, so it does not contribute to the $J + n$ (its β is close to 0). This means that it can be treated as part of the energy of the string itself, and not as part of the endpoint masses.
- For each arrangement, we calculated the endpoint masses and deduced the spectrum using the heavy mesons slope of the plane (J or n).
- The final spectrum range for each plane was taken to be between the minimum and maximum of all the possible arrangements.
- We derived the range of the spectrum for four more states that were above the lowest mass.

The 'Genuine' column indicates whether the quark content is a pure pentaquark or not. This was decided as follows:

- If the content includes a light quark (u, d, s) and its counterpart, we assume its source could be a meson that decay through string tear. This is marked at the table as an empty cell.
- If the content include a heavy quark (c, b) and its counterpart, which is less likely to be a product of meson string break, it is likely to be genuine. This was marked with one *.
- ** means it is a pure pentaquark. These does not contain quark-antiquark pair of the same flavour.

Empty spectrum/threshold, means these baryons weren't found yet, therefore we couldn't predict the HMRTs.

#	Name.	Quarks	Baryon-Meson	Baryon Meson Threshold [MeV]	J Spec (Baryon)	n Spec (Baryon)	J Spec (Tetra)	n Spec (Tetra)	Genuine
1	$P_{\pi_c^0 \pi_u^+}^{A_c^+}$ $P_{\pi_c^- \pi_d^+}^{A_c^+}$ $P_{D^0}^{\Sigma_c^+}$	$u\bar{u}cd\bar{u}$	$\Lambda_c^+ \pi_u^0$ $\Sigma_c^{++} \pi^-$ pD^0	2421 2594 2803	2596 – 2696 2836 – 2925 3051 – 3132 3247 – 3322 3430 – 3500	2596 – 2696 2818 – 2908 3019 – 3101 3203 – 3279 3374 – 3446	2596 – 2696 2939 – 3024 3235 – 3310 3500 – 3568 3742 – 3804	2596 – 2696 3076 – 3156 3472 – 3541 3818 – 3879 4130 – 4186	
2	$P_{\pi_d^0 \pi_c^+}^{A_c^+}$ $P_{D^+}^{\Sigma_c^0}$ $P_{D^+}^{\pi_c^+}$	$d\bar{d}cd\bar{u}$	$\Lambda_c^+ \pi_d^0$ $\Sigma_c^0 \pi_c^+$ nD^+	2421 2594 2810	2596 – 2696 2836 – 2925 3051 – 3132 3247 – 3322 3430 – 3500	2596 – 2696 2818 – 2908 3019 – 3101 3203 – 3279 3374 – 3446	2596 – 2696 2939 – 3024 3235 – 3310 3500 – 3568 3742 – 3804	2596 – 2696 3076 – 3156 3472 – 3541 3818 – 3879 4130 – 4186	
3	$P_{\pi_u^0 \pi_c^+}^{A_c^+}$ $P_{D^0}^{\Sigma_c^0}$ $P_{D^0}^{\pi_u^0}$	$d\bar{u}cd\bar{u}$	$\Lambda_c^+ \pi^-$ $\Sigma_c^0 \pi_u^0$ nD^0	2426 2589 2805	2601 – 2701 2840 – 2929 3055 – 3136 3251 – 3326 3433 – 3503	2601 – 2701 2823 – 2912 3023 – 3105 3207 – 3283 3378 – 3449	2601 – 2701 2944 – 3028 3239 – 3314 3503 – 3571 3745 – 3808	2601 – 2701 3080 – 3160 3475 – 3544 3821 – 3882 4133 – 4189	

4	$P_{\pi^+}^{\Lambda_c^+}$ $P_{\pi^0}^{\Sigma_c^0}$ $P_{D^+}^{\Xi_c^0}$	$u\bar{d}cd u$	$\Lambda_c^+ \pi^+$ $\Sigma_c^0 \pi_d^0$ $p D^+$	2426 2589 2808	2601 – 2701 2840 – 2929 3055 – 3136 3251 – 3326 3433 – 3503	2601 – 2701 2823 – 2912 3023 – 3105 3207 – 3283 3378 – 3449	2601 – 2701 2944 – 3028 3239 – 3314 3503 – 3571 3745 – 3808	2601 – 2701 3080 – 3160 3475 – 3544 3821 – 3882 4133 – 4189	
5	$P_{\pi^0}^{\Sigma_c^0}$ $P_{\pi_d^0}^{\Delta^-}$ $P_{D^+}^{\Delta^-}$	$d\bar{d}cd d$	$\Sigma_c^0 \pi_d^0$ $\Delta^- D^+$	2589 3102	2764 – 2864 2986 – 3076 3188 – 3271 3374 – 3452 3548 – 3621	2764 – 2864 2969 – 3060 3157 – 3242 3332 – 3411 3495 – 3570	2764 – 2864 3082 – 3169 3362 – 3440 3615 – 3687 3848 – 3915	2764 – 2864 3211 – 3293 3588 – 3660 3922 – 3987 4225 – 4285	
6	$P_{\pi_u^0}^{\Sigma_c^{++}}$ $P_{D^0}^{\Delta^{++}}$	$u\bar{u}cu u$	$\Sigma_c^{++} \pi_u^0$ $\Delta^{++} D^0$	2589 3097	2764 – 2864 2986 – 3076 3188 – 3271 3374 – 3452 3548 – 3621	2764 – 2864 2969 – 3060 3157 – 3242 3332 – 3411 3495 – 3570	2764 – 2864 3082 – 3169 3362 – 3440 3615 – 3687 3848 – 3915	2764 – 2864 3211 – 3293 3588 – 3660 3922 – 3987 4225 – 4285	
7	$P_{\pi^-}^{\Sigma_c^0}$ $P_{D^0}^{\Delta^-}$	$d\bar{u}cd d$	$\Sigma_c^0 \pi^-$ $\Delta^- D^0$	2594 3097	2769 – 2869 2990 – 3081 3192 – 3275 3378 – 3456 3552 – 3625	2769 – 2869 2974 – 3065 3161 – 3246 3336 – 3415 3499 – 3573	2769 – 2869 3087 – 3174 3366 – 3444 3619 – 3690 3852 – 3918	2769 – 2869 3215 – 3297 3592 – 3664 3925 – 3990 4228 – 4288	**
8	$P_{\pi^+}^{\Sigma_c^{++}}$ $P_{D^+}^{\Delta^{++}}$	$u\bar{d}cu u$	$\Sigma_c^{++} \pi^+$ $\Delta^{++} D^+$	2594 3102	2769 – 2869 2990 – 3081 3192 – 3275 3378 – 3456 3552 – 3625	2769 – 2869 2974 – 3065 3161 – 3246 3336 – 3415 3499 – 3573	2769 – 2869 3087 – 3174 3366 – 3444 3619 – 3690 3852 – 3918	2769 – 2869 3215 – 3297 3592 – 3664 3925 – 3990 4228 – 4288	**
9	$P_{\pi_d^0}^{\Xi_c^+}$ $P_{\pi_c^0}^{\Xi_c^0}$ $P_{\pi_c^+}^{\Lambda_c^+}$ $P_{K^0}^{\Lambda_c^+}$ $P_{D^+}^{\Lambda_0^0}$	$d\bar{d}cs u$	$\Xi_c^+ \pi_d^0$ $\Xi_c^0 \pi^+$ $\Lambda_c^+ \bar{K}^0$ $\Lambda^0 D^+$	2603 2610 2784 2986	2778 – 2878 2998 – 3089 3199 – 3283 3385 – 3463 3558 – 3632	2778 – 2878 2982 – 3073 3169 – 3254 3343 – 3422 3506 – 3580	2778 – 2878 3108 – 3193 3394 – 3470 3651 – 3721 3887 – 3952	2778 – 2878 3239 – 3320 3624 – 3694 3962 – 4025 4268 – 4325	
10	$P_{\pi_c^0}^{\Xi_c^+}$ $P_{\Sigma_c^0}^{\Sigma_c^{++}}$ $P_{K^0}^{\Sigma_c^+}$ $P_{D^0}^{\Sigma_c^+}$	$u\bar{u}cs u$	$\Xi_c^+ \pi_u^0$ $\Sigma_c^{++} K^-$ $\Sigma^+ D^0$	2603 2948 3054	2778 – 2878 2998 – 3089 3199 – 3283 3385 – 3463 3558 – 3632	2778 – 2878 2982 – 3073 3169 – 3254 3343 – 3422 3506 – 3580	2778 – 2878 3135 – 3218 3437 – 3510 3705 – 3770 3948 – 4008	2778 – 2878 3275 – 3352 3677 – 3742 4025 – 4083 4337 – 4390	
11	$P_{\pi_u^0}^{\Xi_c^0}$ $P_{\pi_c^0}^{\Xi_c^+}$ $P_{\pi_c^-}^{\Lambda_c^+}$ $P_{K^0}^{\Lambda_c^+}$ $P_{D^0}^{\Lambda_0^0}$	$u\bar{u}cd s$	$\Xi_c^0 \pi_u^0$ $\Xi_c^+ \pi^-$ $\Lambda_c^+ K^-$ $\Lambda^0 D^0$	2605 2608 2780 2981	2780 – 2880 2963 – 3057 3136 – 3225 3300 – 3384 3456 – 3537	2780 – 2880 2950 – 3044 3110 – 3200 3262 – 3348 3408 – 3490	2780 – 2880 3109 – 3195 3396 – 3472 3653 – 3722 3889 – 3953	2780 – 2880 3241 – 3322 3625 – 3695 3963 – 4026 4269 – 4326	
12	$P_{\pi_d^0}^{\Xi_c^0}$ $P_{\Sigma_c^0}^{\Sigma_c^0}$ $P_{K^0}^{\Sigma_c^0}$ $P_{D^+}^{\Sigma_c^0}$	$d\bar{d}cd s$	$\Xi_c^0 \pi_d^0$ $\Sigma_c^0 \bar{K}^0$ $\Sigma^- D^+$	2605 2952 3067	2780 – 2880 3000 – 3091 3201 – 3284 3386 – 3464 3560 – 3633	2780 – 2880 2984 – 3075 3171 – 3255 3344 – 3423 3507 – 3582	2780 – 2880 3109 – 3195 3396 – 3472 3653 – 3722 3889 – 3953	2780 – 2880 3241 – 3322 3625 – 3695 3963 – 4026 4269 – 4326	
13	$P_{\pi_c^0}^{\Xi_c^+}$ $P_{\Sigma_c^0}^{\Sigma_c^{++}}$ $P_{K^0}^{\Sigma_c^+}$ $P_{D^+}^{\Sigma_c^+}$	$u\bar{d}cs u$	$\Xi_c^+ \pi^+$ $\Sigma_c^{++} \bar{K}^0$ $\Sigma^+ D^+$	2608 2952 3059	2783 – 2883 3003 – 3094 3203 – 3287 3389 – 3467 3562 – 3635	2783 – 2883 2987 – 3078 3173 – 3258 3347 – 3426 3509 – 3584	2783 – 2883 3139 – 3222 3441 – 3513 3708 – 3773 3951 – 4011	2783 – 2883 3278 – 3356 3680 – 3746 4028 – 4086 4340 – 4393	**
14	$P_{\pi_c^0}^{\Xi_c^0}$ $P_{\Sigma_c^0}^{\Sigma_c^0}$ $P_{K^0}^{\Sigma_c^0}$ $P_{D^0}^{\Sigma_c^0}$	$d\bar{u}cd s$	$\Xi_c^0 \pi^-$ $\Sigma_c^0 K^-$ $\Sigma^- D^0$	2610 2948 3062	2785 – 2885 3005 – 3095 3205 – 3289 3390 – 3468 3564 – 3637	2785 – 2885 2988 – 3080 3175 – 3259 3348 – 3427 3511 – 3586	2785 – 2885 3114 – 3199 3399 – 3476 3656 – 3726 3892 – 3956	2785 – 2885 3245 – 3326 3629 – 3699 3966 – 4029 4272 – 4329	**
15	$P_{K^0}^{\Lambda_c^+}$ $P_{D^+}^{\Lambda_c^+}$ $P_{K^0}^{\Sigma_c^{++}}$	$u\bar{s}cd u$	$\Lambda_c^+ K^+$ $p D_s^+$ $\Sigma_c^{++} K^0$	2780 2906 2952	2955 – 3055 3167 – 3258 3361 – 3445 3541 – 3620 3710 – 3784	2955 – 3055 3151 – 3243 3331 – 3417 3500 – 3580 3658 – 3734	2955 – 3055 3249 – 3338 3512 – 3593 3753 – 3828 3976 – 4046	2955 – 3055 3369 – 3454 3727 – 3802 4048 – 4116 4340 – 4403	**
16	$P_{K^0}^{\Lambda_c^+}$ $P_{D^+}^n$ $P_{K^+}^{\Sigma_c^0}$	$d\bar{s}cd u$	$\Lambda_c^+ K^0$ $n D_s^+$ $\Sigma_c^0 K^+$	2784 2908 2948	2959 – 3059 3170 – 3262 3364 – 3448 3544 – 3623 3713 – 3787	2959 – 3059 3155 – 3246 3335 – 3420 3503 – 3583 3661 – 3737	2959 – 3059 3253 – 3341 3516 – 3596 3756 – 3831 3979 – 4049	2959 – 3059 3373 – 3458 3730 – 3805 4050 – 4118 4343 – 4406	**
17	$P_{D^+}^p$ $P_{D^-}^{\Delta^{++}}$	$u\bar{c}du u$	$p \bar{D}^0$ $\Delta^{++} D^-$	2803 3102	2978 – 3078 3180 – 3272 3367 – 3453 3542 – 3623 3707 – 3783	2978 – 3078 3165 – 3258 3339 – 3426 3502 – 3584 3657 – 3734	2978 – 3078 3226 – 3319 3457 – 3543 3673 – 3754 3876 – 3954	2978 – 3078 3331 – 3420 3649 – 3731 3942 – 4018 4215 – 4286	**

18	$P_{D^-}^n$ $P_{D^-}^{B^0}$	$u\bar{c}ddu$	$n\bar{D}^0$ pD^-	2805 2808	2980 – 3080 3183 – 3275 3370 – 3456 3545 – 3626 3710 – 3787	2980 – 3080 3168 – 3260 3342 – 3429 3506 – 3587 3660 – 3738	2980 – 3080 3228 – 3321 3458 – 3545 3674 – 3756 3878 – 3955	2980 – 3080 3332 – 3422 3651 – 3733 3944 – 4020 4216 – 4287	**
19	$P_{D^-}^n$ $P_{D^-}^{\Delta^-}$ $P_{D^0}^{\Delta^0}$	$d\bar{c}ddu$	nD^- $\Delta^- \bar{D}^0$	2810 3097	2985 – 3085 3188 – 3280 3375 – 3460 3549 – 3630 3714 – 3790	2985 – 3085 3172 – 3265 3346 – 3433 3510 – 3591 3664 – 3742	2985 – 3085 3233 – 3325 3463 – 3549 3678 – 3760 3882 – 3959	2985 – 3085 3337 – 3427 3655 – 3737 3947 – 4024 4220 – 4291	**
20	$P_{\pi_u^0}^{\Omega_c^0}$ $P_{\Xi_d^0}^{\Xi_c^0}$ $P_{K^-}^{\Xi_c^0}$ $P_{D^+}^{\Xi_c^0}$	$d\bar{d}css$	$\Omega_c^0 \pi_d^0$ $\Xi_c^0 K_0^0$ $\Xi^- D^+$	2830 2968 3192	3005 – 3105 3205 – 3297 3390 – 3477 3564 – 3645 3727 – 3804	3005 – 3105 3190 – 3283 3362 – 3449 3524 – 3606 3677 – 3755	3005 – 3105 3339 – 3424 3627 – 3702 3884 – 3952 4119 – 4182	3005 – 3105 3472 – 3551 3857 – 3925 4193 – 4255 4497 – 4553	
21	$P_{\pi_u^0}^{\Omega_c^0}$ $P_{\Xi_c^+}^{\Xi_c^+}$ $P_{K^-}^{\Xi_c^+}$ $P_{D^0}^{\Xi_c^+}$	$u\bar{u}css$	$\Omega_c^0 \pi_u^0$ $\Xi_c^+ K^-$ $\Xi^0 D^0$	2830	3005 – 3105 3205 – 3297 3390 – 3477 3564 – 3645 3727 – 3804	3005 – 3105 3190 – 3283 3362 – 3449 3524 – 3606 3677 – 3755	3005 – 3105 3339 – 3424 3627 – 3702 3884 – 3952 4119 – 4182	3005 – 3105 3472 – 3551 3857 – 3925 4193 – 4255 4497 – 4553	
22	$P_{\pi_u^0}^{\Omega_c^0}$ $P_{\Xi_c^0}^{\Xi_c^0}$ $P_{K^-}^{\Xi_c^-}$ $P_{D^0}^{\Xi_c^-}$	$d\bar{u}css$	$\Omega_c^0 \pi^-$ $\Xi_c^0 K^-$ $\Xi^- D^0$	2835 2964 3187	3010 – 3110 3210 – 3302 3395 – 3481 3568 – 3649 3731 – 3808	3010 – 3110 3195 – 3288 3367 – 3454 3528 – 3611 3681 – 3759	3010 – 3110 3343 – 3428 3631 – 3705 3887 – 3955 4122 – 4185	3010 – 3110 3476 – 3555 3860 – 3929 4196 – 4258 4500 – 4556	**
23	$P_{\pi_c^+}^{\Omega_c^0}$ $P_{\Xi_c^+}^{\Xi_c^+}$ $P_{K^-}^{\Xi_c^0}$ $P_{D^+}^{\Xi_c^0}$	$u\bar{d}css$	$\Omega_c^0 \pi^+$ $\Xi_c^+ \bar{K}^0$ $\Xi^0 D^+$	2835 2966 3185	3010 – 3110 3210 – 3302 3395 – 3481 3568 – 3649 3731 – 3808	3010 – 3110 3195 – 3288 3367 – 3454 3528 – 3611 3681 – 3759	3010 – 3110 3343 – 3428 3631 – 3705 3887 – 3955 4122 – 4185	3010 – 3110 3476 – 3555 3860 – 3929 4196 – 4258 4500 – 4556	**
24	$P_{D_s^-}^p$ $P_{D_s^0}^{\Lambda^0}$ $P_{D^-}^{\Sigma^+}$ $P_{D^-}^{\Sigma^+}$	$s\bar{c}duu$	pD_s^- $\Lambda^0 \bar{D}^0$ $\Sigma^+ D^-$	2906 2981 3059	3081 – 3181 3276 – 3368 3457 – 3544 3627 – 3709 3787 – 3865	3081 – 3181 3261 – 3354 3430 – 3517 3588 – 3671 3738 – 3817	3081 – 3181 3327 – 3420 3556 – 3643 3770 – 3852 3973 – 4050	3081 – 3181 3431 – 3521 3747 – 3829 4038 – 4114 4309 – 4380	**
25	$P_{D_s^-}^n$ $P_{D_s^0}^{\Lambda^0}$ $P_{D^-}^{\Sigma^-}$ $P_{D^0}^{\Sigma^-}$	$s\bar{c}ddu$	nD_s^- $\Lambda^0 D^-$ $\Sigma^- \bar{D}^0$	2908 2986 3062	3083 – 3183 3278 – 3370 3459 – 3545 3628 – 3710 3789 – 3867	3083 – 3183 3263 – 3356 3431 – 3519 3590 – 3673 3740 – 3819	3083 – 3183 3329 – 3422 3558 – 3644 3772 – 3854 3974 – 4052	3083 – 3183 3433 – 3522 3749 – 3831 4040 – 4116 4310 – 4382	**
26	$P_{K_c^+}^{\Sigma_c^{++}}$ $P_{D_s^+}^{\Delta^{++}}$ $P_{D_s^+}^{\Delta^{++}}$	$u\bar{s}cuu$	$\Sigma_c^{++} K^+$ $\Delta^{++} D_s^+$	2948 3200	3123 – 3223 3320 – 3413 3503 – 3589 3674 – 3755 3836 – 3913	3123 – 3223 3306 – 3398 3475 – 3563 3635 – 3718 3786 – 3865	3123 – 3223 3399 – 3489 3649 – 3731 3879 – 3956 4094 – 4166	3123 – 3223 3512 – 3599 3854 – 3932 4163 – 4234 4447 – 4513	**
27	$P_{K_c^0}^{\Sigma_c^0}$ $P_{D_s^+}^{\Delta^-}$ $P_{D_s^+}^{\Delta^-}$	$d\bar{s}cd$	$\Sigma_c^0 K^0$ $\Delta^- D_s^+$	2952 3200	3127 – 3227 3324 – 3416 3506 – 3593 3677 – 3759 3839 – 3916	3127 – 3227 3309 – 3402 3479 – 3566 3639 – 3721 3790 – 3868	3127 – 3227 3402 – 3492 3652 – 3735 3882 – 3959 4097 – 4169	3127 – 3227 3516 – 3603 3857 – 3935 4166 – 4237 4450 – 4515	**
28	$P_{\Xi_c^+}^{\Xi_c^+}$ $P_{D_s^+}^{\Sigma_c^+}$ $P_{D_s^+}^{\Delta^+}$ $P_{\phi(1020)}^{\Sigma_c^+}$	$u\bar{s}csu$	$\Xi_c^+ K^+$ $\Sigma^+ D_s^+$ $\Sigma_c^{++} \phi(1020)$	2962 3157 3473	3137 – 3237 3333 – 3426 3515 – 3601 3685 – 3767 3846 – 3924	3137 – 3237 3319 – 3411 3488 – 3575 3647 – 3729 3797 – 3876	3137 – 3237 3439 – 3527 3706 – 3785 3949 – 4022 4174 – 4242	3137 – 3237 3561 – 3645 3923 – 3997 4245 – 4312 4539 – 4600	
29	$P_{K_c^+}^{\Xi_c^0}$ $P_{\Xi_c^0}^{\Xi_c^+}$ $P_{K_c^0}^{\Xi_c^0}$ $P_{D_s^+}^{\Lambda^0}$ $P_{D_s^+}^{\Lambda^+}$ $P_{\phi(1020)}^{\Lambda_c^+}$	$u\bar{s}cds$	$\Xi_c^0 K^+$ $\Xi_c^+ K^0$ $\Lambda^0 D_s^+$ $\Lambda_c^+ \phi(1020)$	2964 2966 3084 3305	3139 – 3239 3335 – 3427 3517 – 3603 3687 – 3769 3848 – 3925	3139 – 3239 3320 – 3413 3489 – 3577 3648 – 3731 3799 – 3878	3139 – 3239 3422 – 3511 3677 – 3758 3911 – 3986 4129 – 4199	3139 – 3239 3538 – 3624 3886 – 3962 4198 – 4268 4485 – 4549	
30	$P_{K_c^0}^{\Xi_c^0}$ $P_{D_s^+}^{\Sigma_c^-}$ $P_{\phi(1020)}^{\Sigma_c^0}$	$d\bar{s}cds$	$\Xi_c^0 K^0$ $\Sigma^- D_s^+$ $\Sigma_c^0 \phi(1020)$	2968 3165 3473	3143 – 3243 3339 – 3431 3520 – 3607 3690 – 3772 3851 – 3928	3143 – 3243 3324 – 3417 3493 – 3580 3652 – 3734 3802 – 3881	3143 – 3243 3425 – 3515 3680 – 3762 3914 – 3990 4131 – 4202	3143 – 3243 3542 – 3627 3889 – 3965 4201 – 4270 4487 – 4552	
31	$P_{\bar{D}^0}^{\Xi_c^+}$ $P_{D_s^-}^{\Delta^{++}}$ $P_{D_s^-}^{\Delta^{++}}$	$u\bar{c}suu$	$\Sigma^+ \bar{D}^0$ $\Delta^{++} D_s^-$	3054 3200	3229 – 3329 3413 – 3507 3586 – 3674 3748 – 3832 3903 – 3983	3229 – 3329 3399 – 3493 3559 – 3648 3711 – 3796 3856 – 3937	3229 – 3329 3464 – 3558 3684 – 3772 3891 – 3974 4088 – 4167	3229 – 3329 3564 – 3654 3869 – 3952 4151 – 4229 4415 – 4488	**

32	$P_{D_s^-}^{\Sigma^-}$ $P_{D_s^-}^{\Delta^-}$	$d\bar{c}dds$	$\Sigma^- D^-$ $\Delta^- D_s^-$	3067 3200	3242 – 3342 3425 – 3519 3597 – 3685 3759 – 3843 3913 – 3993	3242 – 3342 3411 – 3505 3571 – 3660 3722 – 3807 3866 – 3947	3242 – 3342 3477 – 3570 3696 – 3783 3902 – 3985 4098 – 4177	3242 – 3342 3576 – 3666 3880 – 3963 4161 – 4239 4424 – 4497	**
33	$P_{D_s^-}^{A^0}$ $P_{\Xi^0 \bar{D}}^{D^-}$ $P_{\Xi^- \bar{D}^0}^{\Xi^-}$	$s\bar{c}dsu$	$\Lambda^0 D_s^-$ $\Xi^0 D^-$ $\Xi^- \bar{D}^0$	3084 3185 3187	3259 – 3359 3441 – 3535 3612 – 3700 3773 – 3857 3927 – 4007	3259 – 3359 3427 – 3521 3586 – 3675 3736 – 3821 3880 – 3961	3259 – 3359 3498 – 3591 3720 – 3807 3929 – 4012 4127 – 4206	3259 – 3359 3599 – 3689 3907 – 3990 4191 – 4268 4456 – 4529	**
34	$P_{D_s^0}^{\Delta^{++}}$	$u\bar{c}uuu$	$\Delta^{++} \bar{D}^0$	3097	3272 – 3372 3453 – 3546 3622 – 3711 3783 – 3867 3935 – 4016	3272 – 3372 3439 – 3533 3597 – 3686 3746 – 3831 3889 – 3970	3272 – 3372 3499 – 3593 3713 – 3801 3915 – 3999 4107 – 4187	3272 – 3372 3596 – 3687 3893 – 3977 4169 – 4248 4427 – 4502	**
35	$P_{D_s^-}^{\Delta^-}$	$d\bar{c}ddd$	$\Delta^- D^-$	3102	3277 – 3377 3458 – 3552 3628 – 3716 3788 – 3872 3941 – 4021	3277 – 3377 3444 – 3538 3602 – 3691 3752 – 3837 3894 – 3976	3277 – 3377 3504 – 3598 3717 – 3806 3919 – 4003 4111 – 4191	3277 – 3377 3600 – 3692 3897 – 3981 4173 – 4252 4431 – 4505	**
36	$P_{D_s^-}^{\Sigma^+}$ $P_{\Xi^0 \bar{D}}^{\Xi^+}$ $P_{\Xi^- \bar{D}^0}^{\Xi^-}$	$s\bar{c}suu$	$\Sigma^+ D_s^-$ $\Xi^0 \bar{D}^0$	3157 3180	3332 – 3432 3509 – 3603 3676 – 3765 3834 – 3919 3985 – 4066	3332 – 3432 3496 – 3590 3651 – 3741 3798 – 3884 3939 – 4021	3332 – 3432 3566 – 3659 3784 – 3871 3989 – 4072 4184 – 4263	3332 – 3432 3664 – 3755 3967 – 4051 4247 – 4325 4509 – 4582	**
37	$P_{D_s^-}^{\Sigma^-}$ $P_{D_s^-}^{\Xi^-}$	$s\bar{c}dds$	$\Sigma^- D_s^-$ $\Xi^- D^-$	3165 3192	3340 – 3440 3517 – 3611 3683 – 3772 3841 – 3926 3991 – 4072	3340 – 3440 3504 – 3598 3658 – 3748 3805 – 3891 3945 – 4028	3340 – 3440 3577 – 3670 3799 – 3886 4006 – 4089 4203 – 4282	3340 – 3440 3677 – 3768 3984 – 4067 4267 – 4344 4531 – 4603	**
38	$P_{K_s^0}^{\Omega_c^0}$ $P_{D_s^0}^{\Omega_c^0}$	$s\bar{u}css$	$\Omega_c^0 K^-$ $\Omega^- D^0$	3189 3537	3364 – 3464 3539 – 3633 3704 – 3793 3860 – 3945 4009 – 4091	3364 – 3464 3526 – 3620 3679 – 3769 3824 – 3910 3964 – 4046	3364 – 3464 3669 – 3755 3936 – 4014 4178 – 4250 4401 – 4468	3364 – 3464 3791 – 3874 4152 – 4224 4472 – 4537 4763 – 4823	**
39	$P_{K_s^0}^{\Omega_c^0}$ $P_{D_s^0}^{\Xi_c^0}$ $P_{\Xi_c^0 \phi(1020)}^{\Xi_c^+}$	$u\bar{s}css$	$\Omega_c^0 K^+$ $\Xi^0 D_s^+$ $\Xi_c^+ \phi(1020)$	3189 3283 3487	3364 – 3464 3544 – 3637 3713 – 3801 3872 – 3956 4024 – 4104	3364 – 3464 3530 – 3624 3687 – 3776 3836 – 3921 3978 – 4059	3364 – 3464 3649 – 3737 3904 – 3985 4137 – 4212 4354 – 4424	3364 – 3464 3765 – 3850 4112 – 4187 4423 – 4492 4708 – 4771	
40	$P_{K_s^0}^{\Omega_c^0}$ $P_{D_s^0}^{\Xi_c^0}$ $P_{\Xi_c^0 \phi(1020)}^{\Xi_c^+}$	$d\bar{s}css$	$\Omega_c^0 K^0$ $\Xi^- D_s^+$ $\Xi_c^0 \phi(1020)$	3193 3290 3489	3368 – 3468 3548 – 3641 3716 – 3805 3875 – 3960 4027 – 4107	3368 – 3468 3534 – 3628 3691 – 3780 3839 – 3924 3981 – 4062	3368 – 3468 3652 – 3741 3907 – 3988 4140 – 4215 4357 – 4427	3368 – 3468 3768 – 3853 4115 – 4191 4426 – 4494 4710 – 4774	
41	$P_{K_s^0}^{\Omega_c^0}$ $P_{D_s^0}^{\Omega_c^0}$	$s\bar{d}css$	$\Omega_c^0 \bar{K}^0$ $\Omega^- D^+$	3193 3542	3368 – 3468 3543 – 3637 3707 – 3796 3864 – 3948 4013 – 4094	3368 – 3468 3529 – 3624 3682 – 3772 3828 – 3914 3967 – 4049	3368 – 3468 3672 – 3759 3939 – 4017 4181 – 4253 4404 – 4470	3368 – 3468 3795 – 3877 4155 – 4227 4475 – 4540 4765 – 4825	**
42	$P_{D_s^-}^{\Xi^0}$ $P_{D_s^-}^{\Omega_c^0}$	$s\bar{c}ssu$	$\Xi^0 D_s^-$ $\Omega^- \bar{D}^0$	3283 3537	3458 – 3558 3628 – 3722 3788 – 3878 3941 – 4027 4087 – 4169	3458 – 3558 3615 – 3710 3764 – 3854 3906 – 3993 4042 – 4126	3458 – 3558 3692 – 3785 3911 – 3998 4117 – 4199 4311 – 4390	3458 – 3558 3791 – 3882 4094 – 4177 4374 – 4451 4636 – 4708	**
43	$P_{D_s^-}^{\Xi^-}$ $P_{D_s^-}^{\Omega_c^0}$	$s\bar{c}cdss$	$\Xi^- D_s^-$ $\Omega^- D^-$	3290 3542	3465 – 3565 3634 – 3728 3794 – 3884 3946 – 4032 4091 – 4174	3465 – 3565 3621 – 3716 3770 – 3860 3911 – 3998 4047 – 4130	3465 – 3565 3699 – 3792 3917 – 4004 4122 – 4205 4317 – 4395	3465 – 3565 3798 – 3888 4100 – 4183 4380 – 4457 4641 – 4713	**
44	$P_{D_s^-}^{\Omega^-}$	$s\bar{c}sss$	$\Omega^- D_s^-$	3640	3815 – 3915 3982 – 4076 4139 – 4229 4289 – 4374 4432 – 4514	3815 – 3915 3969 – 4064 4115 – 4205 4254 – 4341 4388 – 4471	3815 – 3915 4034 – 4128 4240 – 4329 4435 – 4519 4620 – 4701	3815 – 3915 4127 – 4218 4414 – 4498 4680 – 4759 4930 – 5005	**
45	$P_{D_s^0}^{\Omega^-}$ $P_{\Omega_c^0 \phi(1020)}^{\Omega_c^0}$	$c\bar{s}sss$	$\Omega^- D_s^+$ $\Omega_c^0 \phi(1020)$	3640 3714	3815 – 3915 3969 – 4065 4117 – 4208 4258 – 4346 4394 – 4479	3815 – 3915 3958 – 4053 4094 – 4186 4226 – 4314 4352 – 4438	3815 – 3915 4068 – 4159 4299 – 4383 4514 – 4593 4716 – 4790	3815 – 3915 4173 – 4261 4491 – 4570 4780 – 4853 5048 – 5116	
46	$P_{\pi^0}^{\Xi_{cc}^+}$ $P_{\pi^+}^{\Xi_{cc}^0}$ $P_{\pi^-}^{\Lambda_c^+}$ $P_{D^0}^{\Lambda_c^+}$	$u\bar{u}cccd$	$\Xi_{cc}^+ \pi_u^0$ $\Xi_{cc}^0 \pi^-$ $\Lambda_c^+ D^0$	3654 3762 4151	3829 – 3929 3964 – 4061 4095 – 4188 4221 – 4312 4344 – 4433	3829 – 3929 3954 – 4051 4075 – 4169 4192 – 4284 4307 – 4396	3829 – 3929 4119 – 4207 4377 – 4456 4610 – 4683 4826 – 4894	3829 – 3929 4237 – 4320 4585 – 4659 4895 – 4962 5178 – 5239	

47	$P_{\pi_d^0}^{\Xi_{cc}^+}$ $P_{D^+}^{\Sigma_c^0}$	$d\bar{d}ccd$	$\Xi_{cc}^+ \pi_d^0$ $\Sigma_c^0 D^+$	3654 4324	3829 – 3929 3980 – 4075 4124 – 4215 4262 – 4350 4395 – 4481	3829 – 3929 3968 – 4064 4102 – 4194 4230 – 4319 4354 – 4441	3829 – 3929 4080 – 4171 4310 – 4394 4524 – 4603 4724 – 4799	3829 – 3929 4185 – 4272 4501 – 4580 4789 – 4862 5055 – 5123	
48	$P_{\pi_d^0}^{\Xi_{cc}^+}$ $P_{\pi_d^0}^{\Xi_{cc}^+}$ $P_{D^+}^{\Sigma_c^0}$ $P_{D^+}^{\Lambda_c^+}$	$u\bar{d}ccd$	$\Xi_{cc}^+ \pi^+$ $\Xi_{cc}^+ \pi_d^0$ $\Lambda_c^+ D^+$	3659 3757 4156	3834 – 3934 3984 – 4080 4128 – 4220 4266 – 4355 4400 – 4485	3834 – 3934 3973 – 4069 4106 – 4199 4235 – 4324 4359 – 4445	3834 – 3934 4124 – 4211 4380 – 4460 4614 – 4687 4830 – 4898	3834 – 3934 4241 – 4325 4589 – 4662 4899 – 4965 5181 – 5242	
49	$P_{\pi_d^0}^{\Xi_{cc}^+}$ $P_{D^0}^{\Sigma_c^0}$	$d\bar{u}ccd$	$\Xi_{cc}^+ \pi^-$ $\Sigma_c^0 D^0$	3659 4319	3834 – 3934 3984 – 4080 4128 – 4220 4266 – 4355 4400 – 4485	3834 – 3934 3973 – 4069 4106 – 4199 4235 – 4324 4359 – 4445	3834 – 3934 4085 – 4176 4314 – 4399 4528 – 4607 4728 – 4803	3834 – 3934 4189 – 4277 4505 – 4584 4792 – 4866 5059 – 5127	**
50	$P_{\pi_u^0}^{\Xi_{cc}^{++}}$ $P_{D^0}^{\Sigma_c^{++}}$ $P_{D^0}^{\Sigma_c^c}$	$u\bar{u}ccu$	$\Xi_{cc}^{++} \pi_u^0$ $\Sigma_c^{++} D^0$	3757 4319	3932 – 4032 4078 – 4174 4218 – 4310 4353 – 4442 4483 – 4569	3932 – 4032 4067 – 4163 4197 – 4290 4322 – 4412 4443 – 4530	3932 – 4032 4210 – 4298 4458 – 4539 4685 – 4760 4896 – 4966	3932 – 4032 4323 – 4408 4661 – 4736 4964 – 5032 5241 – 5304	
51	$P_{\pi_c^+}^{\Xi_{cc}^{++}}$ $P_{D^+}^{\Sigma_c^{++}}$ $P_{D^+}^{\Sigma_c^c}$	$u\bar{d}ccu$	$\Xi_{cc}^{++} \pi^+$ $\Sigma_c^{++} D^+$	3762 4324	3937 – 4037 4083 – 4179 4223 – 4315 4357 – 4447 4488 – 4574	3937 – 4037 4072 – 4168 4201 – 4294 4327 – 4416 4448 – 4535	3937 – 4037 4214 – 4303 4462 – 4543 4689 – 4764 4900 – 4970	3937 – 4037 4327 – 4412 4665 – 4740 4967 – 5036 5244 – 5307	**
52	$P_{\eta_c(1S)}^p$ $P_{D^0}^{\Lambda_c^+}$ $P_{D^-}^{\Sigma_c^{++}}$ $P_{D^-}^{\Sigma_c^c}$	$c\bar{c}duu$	$p\eta_c(1S)$ $\Lambda_c^+ \bar{D}^0$ $\Sigma_c^{++} D^-$	3922 4151 4324	4097 – 4197 4255 – 4349 4404 – 4495 4547 – 4634 4684 – 4767	4097 – 4197 4243 – 4338 4381 – 4473 4514 – 4602 4642 – 4726	4097 – 4197 4299 – 4394 4491 – 4581 4674 – 4760 4849 – 4932	4097 – 4197 4386 – 4478 4654 – 4741 4906 – 4988 5144 – 5221	*
53	$P_{\eta_c(1S)}^n$ $P_{D^-}^{\Lambda_c^+}$ $P_{D^0}^{\Sigma_c^0}$ $P_{D^0}^{\Sigma_c^c}$	$c\bar{c}ddu$	$n\eta_c(1S)$ $\Lambda_c^+ D^-$ $\Sigma_c^0 \bar{D}^0$	3924 4156 4319	4099 – 4199 4256 – 4351 4406 – 4497 4549 – 4636 4686 – 4769	4099 – 4199 4245 – 4340 4383 – 4474 4516 – 4604 4644 – 4728	4099 – 4199 4301 – 4396 4493 – 4583 4676 – 4762 4851 – 4933	4099 – 4199 4388 – 4480 4656 – 4742 4908 – 4989 5145 – 5223	*
54	$P_{K_c^0}^{\Xi_{cc}^+}$ $P_{D^0}^{\Xi_c^0}$ $P_{\Omega_c^0}^{\Xi_c^0}$ $P_{\pi^-}^{\Xi_c^+}$	$s\bar{u}ccd$	$\Xi_{cc}^+ K^-$ $\Xi_c^0 D^0$ $\Omega_{cc}^+ \pi^-$	4013 4335	4188 – 4288 4324 – 4420 4455 – 4548 4582 – 4672 4705 – 4793	4188 – 4288 4314 – 4410 4435 – 4529 4553 – 4644 4667 – 4756	4188 – 4288 4427 – 4519 4647 – 4732 4853 – 4933 5046 – 5122	4188 – 4288 4527 – 4616 4830 – 4911 5108 – 5183 5366 – 5436	**
55	$P_{K_c^0}^{\Xi_{cc}^+}$ $P_{K_c^0}^{\Xi_{cc}^+}$ $P_{D_s^+}^{\Lambda_c^+}$ $P_{D_s^+}^{\Lambda_c^+}$	$u\bar{s}ccd$	$\Xi_{cc}^+ K^+$ $\Xi_{cc}^+ K^0$ $\Lambda_c^+ D_s^+$	4013 4120 4254	4188 – 4288 4327 – 4423 4460 – 4553 4589 – 4679 4713 – 4801	4188 – 4288 4316 – 4412 4439 – 4533 4559 – 4650 4675 – 4763	4188 – 4288 4438 – 4529 4667 – 4751 4880 – 4958 5079 – 5153	4188 – 4288 4542 – 4630 4857 – 4936 5142 – 5215 5407 – 5474	**
56	$P_{K_c^0}^{\Xi_{cc}^+}$ $P_{D_s^+}^{\Sigma_c^0}$ $P_{D_s^+}^{\Sigma_c^c}$	$d\bar{s}ccd$	$\Xi_{cc}^+ K^0$ $\Sigma_c^0 D_s^+$	4017 4422	4192 – 4292 4330 – 4427 4464 – 4557 4592 – 4682 4717 – 4804	4192 – 4292 4320 – 4416 4443 – 4537 4563 – 4653 4679 – 4767	4192 – 4292 4414 – 4507 4621 – 4708 4816 – 4899 5001 – 5080	4192 – 4292 4507 – 4598 4795 – 4878 5061 – 5139 5310 – 5383	**
57	$P_{K_c^0}^{\Xi_{cc}^+}$ $P_{D_s^+}^{\Xi_c^0}$ $P_{\Omega_c^0}^{\Xi_c^0}$ $P_{\pi_d^0}^{\Xi_c^+}$	$s\bar{d}ccd$	$\Xi_{cc}^+ \bar{K}^0$ $\Xi_c^0 D^+$ $\Omega_{cc}^+ \pi_d^0$	4017 4340	4192 – 4292 4328 – 4424 4459 – 4552 4586 – 4676 4709 – 4796	4192 – 4292 4317 – 4414 4439 – 4533 4557 – 4648 4671 – 4759	4192 – 4292 4431 – 4522 4651 – 4736 4856 – 4936 5049 – 5125	4192 – 4292 4531 – 4619 4834 – 4914 5111 – 5186 5369 – 5439	
58	$P_{\eta_c(1S)}^{\Lambda^0}$ $P_{D_s^+}^{\Lambda_c^+}$ $P_{D_s^+}^{\Lambda_c^+}$ $P_{D_s^+}^{\Xi_c^0}$ $P_{D_s^+}^{\Xi_c^+}$	$c\bar{c}dsu$	$\Lambda^0 \eta_c(1S)$ $\Lambda_c^+ D_s^-$ $\Xi_c^0 \bar{D}^0$ $\Xi_c^+ D^-$	4100 4254 4335 4338	4275 – 4375 4424 – 4519 4566 – 4657 4702 – 4790 4833 – 4918	4275 – 4375 4412 – 4508 4544 – 4636 4671 – 4760 4793 – 4879	4275 – 4375 4472 – 4567 4658 – 4749 4837 – 4924 5008 – 5091	4275 – 4375 4556 – 4649 4817 – 4905 5064 – 5146 5297 – 5375	*
59	$P_{K_c^0}^{\Xi_{cc}^+}$ $P_{D_s^+}^{\Sigma_c^0}$ $P_{D_s^+}^{\Sigma_c^c}$	$u\bar{s}ccu$	$\Xi_{cc}^{++} K^+$ $\Sigma_c^{++} D_s^+$	4116 4422	4291 – 4391 4426 – 4522 4556 – 4649 4681 – 4772 4803 – 4891	4291 – 4391 4415 – 4512 4536 – 4630 4652 – 4744 4766 – 4855	4291 – 4391 4532 – 4624 4754 – 4839 4960 – 5040 5155 – 5230	4291 – 4391 4633 – 4721 4938 – 5019 5217 – 5292 5476 – 5546	**
60	$P_{K_c^0}^{\Xi_{cc}^+}$ $P_{D_s^+}^{\Xi_c^0}$ $P_{D_s^+}^{\Xi_c^+}$ $P_{\pi_u^0}^{\Omega_{cc}^0}$	$s\bar{u}ccu$	$\Xi_{cc}^{++} K^-$ $\Xi_c^+ D^0$ $\Omega_{cc}^+ \pi_u^0$	4116 4333	4291 – 4391 4412 – 4509 4530 – 4625 4645 – 4737 4757 – 4847	4291 – 4391 4403 – 4500 4512 – 4607 4618 – 4711 4722 – 4813	4291 – 4391 4522 – 4614 4735 – 4821 4935 – 5016 5124 – 5201	4291 – 4391 4618 – 4708 4913 – 4995 5185 – 5261 5438 – 5509	

61	$P_{\bar{K}^0}^{\Xi_{cc}^{++}}$ $P_{\Xi_c^+}^{\Xi_c^+}$ $P_{D_s^+}^{\Omega_{cc}^+}$ $P_{\pi^+}^{\Xi_{cc}^+}$	$s\bar{d}cu$	$\Xi_{cc}^{++}\bar{K}^0$ $\Xi_c^+ D^+$ $\Omega_{cc}^+ \pi^+$	4120 4338	4295 – 4395 4427 – 4524 4555 – 4649 4679 – 4770 4799 – 4887	4295 – 4395 4417 – 4514 4525 – 4618 4738 – 4825 4650 – 4742 4938 – 5020 4762 – 4851	4295 – 4395 4622 – 4711 4917 – 4999 5188 – 5264 5127 – 5204 5441 – 5512	**	
62	$P_{\eta_c(1S)}^{\Sigma^+}$ $P_{\Xi_c^0}^{\Xi_c^+}$ $P_{D_s^-}^{\Sigma_c^+}$ $P_{D_s^-}^{\Sigma_c^0}$	$c\bar{c}suu$	$\Sigma^+ \eta_c(1S)$ $\Xi_c^+ \bar{D}^0$ $\Sigma_c^+ D_s^-$	4173 4333 4422	4348 – 4448 4493 – 4589 4632 – 4724 4766 – 4855 4895 – 4981	4348 – 4448 4482 – 4578 4611 – 4704 4735 – 4825 4856 – 4942	4348 – 4448 4548 – 4642 4737 – 4827 4918 – 5004 5090 – 5173	*	
63	$P_{\eta_c(1S)}^{\Sigma^+}$ $P_{\Xi_c^0}^{\Xi_c^0}$ $P_{D_s^-}^{\Sigma_c^0}$ $P_{D_s^-}^{\Sigma_c^+}$	$c\bar{c}dds$	$\Sigma^- \eta_c(1S)$ $\Xi_c^0 D^-$ $\Sigma_c^0 D_s^-$	4181 4340 4422	4356 – 4456 4501 – 4597 4640 – 4732 4773 – 4862 4902 – 4988	4356 – 4456 4490 – 4586 4619 – 4711 4743 – 4832 4862 – 4949	4356 – 4456 4548 – 4644 4732 – 4823 4907 – 4994 5075 – 5159	*	
64	$P_{\eta_c(1S)}^{\Delta^{++}}$ $P_{\Sigma_c^0}^{\Sigma_c^+}$ $P_{\bar{D}^0}^{\Sigma_c^+}$	$c\bar{c}uuu$	$\Delta^{++} \eta_c(1S)$ $\Sigma_c^+ \bar{D}^0$	4216 4319	4391 – 4491 4534 – 4630 4672 – 4764 4804 – 4893 4932 – 5018	4391 – 4491 4524 – 4620 4651 – 4744 4774 – 4863 4893 – 4979	4391 – 4491 4578 – 4674 4757 – 4849 4929 – 5017 5094 – 5179	*	
65	$P_{\eta_c(1S)}^{\Delta^-}$ $P_{\Sigma_c^0}^{\Sigma_c^0}$ $P_{D^-}^{\Sigma_c^0}$	$c\bar{c}ddd$	$\Delta^- \eta_c(1S)$ $\Sigma_c^0 D^-$	4216 4324	4391 – 4491 4534 – 4630 4672 – 4764 4804 – 4893 4932 – 5018	4391 – 4491 4524 – 4620 4651 – 4744 4774 – 4863 4893 – 4979	4391 – 4491 4578 – 4674 4757 – 4849 4929 – 5017 5094 – 5179	*	
66	$P_{\eta_c(1S)}^{\Xi^0}$ $P_{\Xi_c^0}^{\Xi_c^+}$ $P_{D_s^-}^{\Omega_c^0}$ $P_{\bar{D}^0}^{\Omega_c^0}$	$c\bar{c}ssu$	$\Xi^0 \eta_c(1S)$ $\Xi_c^+ D_s^-$ $\Omega_c^0 \bar{D}^0$	4299 4436 4560	4474 – 4574 4614 – 4710 4748 – 4841 4878 – 4967 5003 – 5090	4474 – 4574 4603 – 4700 4728 – 4821 4848 – 4938 5036 – 5122	4474 – 4574 4671 – 4765 4857 – 4948 5036 – 5122 5206 – 5289	*	
67	$P_{\eta_c(1S)}^{\Xi^-}$ $P_{\Xi_c^0}^{\Xi_c^0}$ $P_{D_s^-}^{\Omega_c^0}$ $P_{D^-}^{\Omega_c^0}$	$c\bar{c}dss$	$\Xi^- \eta_c(1S)$ $\Xi_c^0 D_s^-$ $\Omega_c^0 D^-$	4306 4438 4565	4481 – 4581 4621 – 4717 4755 – 4847 4884 – 4973 5009 – 5096	4481 – 4581 4610 – 4706 4734 – 4827 4854 – 4944 4971 – 5058	4481 – 4581 4677 – 4772 4864 – 4954 5042 – 5128 5212 – 5295	*	
68	$P_{\Xi_c^0}^{\Xi_c^+}$ $P_{\Xi_c^0}^{\Xi_c^+}$ $P_{\phi(1020)}^{\Xi_c^+}$ $P_{K^+}^{\Omega_{cc}^+}$	$c\bar{s}csu$	$\Xi_c^+ D_s^+$ $\Xi_{cc}^{++} \phi(1020)$ $\Omega_{cc}^+ K^+$	4436 4641	4611 – 4711 4735 – 4832 4855 – 4950 4972 – 5064 5086 – 5176	4611 – 4711 4726 – 4823 4837 – 4932 4945 – 5038 5051 – 5142	4611 – 4711 4819 – 4913 5014 – 5103 5199 – 5283 5375 – 5456		
69	$P_{\Xi_c^0}^{\Xi_c^0}$ $P_{\Xi_c^0}^{\Xi_c^+}$ $P_{\phi(1020)}^{\Xi_c^+}$ $P_{K^0}^{\Omega_{cc}^+}$	$c\bar{s}cds$	$\Xi_c^0 D_s^+$ $\Xi_{cc}^+ \phi(1020)$ $\Omega_{cc}^+ K^0$	4438 4538	4613 – 4713 4737 – 4834 4857 – 4952 4974 – 5066 5088 – 5178	4613 – 4713 4727 – 4825 4839 – 4934 4947 – 5040 5053 – 5143	4613 – 4713 4821 – 4914 5016 – 5105 5201 – 5285 5377 – 5458		
70	$P_{D_s^0}^{\Omega_c^0}$ $P_{K^-}^{\Omega_{cc}^+}$	$c\bar{u}css$	$\Omega_c^0 D^0$ $\Omega_{cc}^+ K^-$	4560	4735 – 4835 4854 – 4951 4969 – 5064 5082 – 5174 5191 – 5282	4735 – 4835 4845 – 4942 4951 – 5047 5056 – 5149 5158 – 5249	4735 – 4835 4948 – 5042 5148 – 5236 5336 – 5419 5515 – 5594	4735 – 4835 5038 – 5129 5316 – 5399 5573 – 5651 5813 – 5887	**
71	$P_{D_s^+}^{\Omega_c^0}$ $P_{K^0}^{\Omega_{cc}^+}$	$c\bar{d}css$	$\Omega_c^0 D^+$ $\Omega_{cc}^+ \bar{K}^0$	4565	4740 – 4840 4858 – 4956 4974 – 5069 5086 – 5179 5196 – 5286	4740 – 4840 4849 – 4947 4956 – 5051 5060 – 5153 5162 – 5253	4740 – 4840 4953 – 5046 5152 – 5240 5340 – 5423 5519 – 5598	4740 – 4840 5043 – 5134 5320 – 5404 5576 – 5655 5817 – 5891	**
72	$P_{\eta_c(1S)}^{\Omega^-}$ $P_{D_s^-}^{\Omega_c^0}$	$c\bar{c}sss$	$\Omega^- \eta_c(1S)$ $\Omega_c^0 D_s^-$	4656 4663	4831 – 4931 4958 – 5054 5080 – 5174 5199 – 5290 5315 – 5404	4831 – 4931 4948 – 5045 5062 – 5156 5172 – 5264 5279 – 5369	4831 – 4931 5016 – 5111 5192 – 5283 5361 – 5449 5524 – 5608	4831 – 4931 5095 – 5189 5343 – 5431 5576 – 5660 5799 – 5878	*
73	$P_{D_s^+}^{\Omega_c^0}$ $P_{\phi(1020)}^{\Omega_{cc}^+}$	$c\bar{s}css$	$\Omega_c^0 D_s^+$ $\Omega_{cc}^+ \phi(1020)$	4663	4838 – 4938 4956 – 5053 5070 – 5165 5181 – 5274 5290 – 5381	4838 – 4938 4946 – 5044 5052 – 5148 5156 – 5249 5257 – 5348	4838 – 4938 5044 – 5138 5238 – 5327 5422 – 5506 5597 – 5677	4838 – 4938 5132 – 5223 5402 – 5487 5653 – 5733 5890 – 5965	
74	$P_{\eta_c(1S)}^{\Lambda_c^+}$ $P_{\Xi_c^0}^{\Xi_c^+}$ $P_{D_s^-}^{\Omega_{cc}^+}$ $P_{D_s^-}^{\Xi_{cc}^+}$	$c\bar{c}cds$	$\Lambda_c^+ \eta_c(1S)$ $\Xi_{cc}^+ \bar{D}^0$ $\Xi_{cc}^{++} D^-$	5270 5384 5492	5445 – 5545 5547 – 5645 5647 – 5743 5745 – 5839 5841 – 5934	5445 – 5545 5539 – 5637 5632 – 5728 5722 – 5817 5811 – 5905	5445 – 5545 5616 – 5712 5780 – 5872 5938 – 6027 6091 – 6177	5445 – 5545 5690 – 5784 5921 – 6010 6140 – 6226 6350 – 6432	*
75	$P_{\Xi_c^0}^{\Xi_c^+}$ $P_{\Omega_{cc}^+}^{\Omega_{cc}^+}$ $P_{\pi^-}^{\Xi_{cc}^+}$	$c\bar{u}ccd$	$\Xi_{cc}^+ D^0$ $\Omega_{ccc}^{++} \pi^-$	5384	5559 – 5659 5659 – 5757 5756 – 5853 5852 – 5947 5946 – 6040	5559 – 5659 5651 – 5749 5741 – 5838 5830 – 5925 5917 – 6011	5559 – 5659 5742 – 5837 5916 – 6006 6082 – 6169 6241 – 6325	5559 – 5659 5820 – 5913 6064 – 6151 6293 – 6376 6511 – 6590	**

76	$P_{D_c^+ \eta_c(1S)}^{\Xi_c^+}$	$d\bar{c}cd$	$\Xi_c^+ D^-$ $\Sigma_c^0 \eta_c(1S)$	5389 5438	5564 – 5664 5664 – 5762 5761 – 5858 5857 – 5952 5952 – 6045	5564 – 5664 5656 – 5754 5746 – 5843 5835 – 5930 5922 – 6016	5564 – 5664 5719 – 5816 5869 – 5963 6015 – 6106 6156 – 6245	5564 – 5664 5786 – 5882 5999 – 6090 6203 – 6291 6399 – 6484	*
77	$P_{D_c^+ \pi_d^0}^{\Xi_c^+}$ $P_{\Omega_c^{++} \pi_d^0}^{\Omega_c^{++}}$	$c\bar{d}cd$	$\Xi_c^+ D^+$ $\Omega_c^{++} \pi_d^0$	5389	5564 – 5664 5664 – 5762 5761 – 5857 5857 – 5952 5951 – 6044	5564 – 5664 5656 – 5754 5746 – 5843 5835 – 5930 5922 – 6016	5564 – 5664 5746 – 5842 5920 – 6011 6086 – 6173 6246 – 6329	5564 – 5664 5825 – 5918 6068 – 6156 6297 – 6380 6515 – 6594	
78	$P_{\eta_c(1S)}^{\Sigma_c^{++}}$ $P_{\bar{D}_s^0}^{\Xi_c^{++}}$	$c\bar{c}cuu$	$\Sigma_c^{++} \eta_c(1S)$ $\Xi_c^{++} \bar{D}^0$	5438 5487	5613 – 5713 5718 – 5816 5821 – 5917 5922 – 6016 6021 – 6113	5613 – 5713 5710 – 5808 5805 – 5902 5899 – 5993 5991 – 6083	5613 – 5713 5777 – 5873 5935 – 6028 6088 – 6178 6236 – 6323	5613 – 5713 5848 – 5943 6071 – 6161 6284 – 6370 6488 – 6571	*
79	$P_{\eta_c(1S)}^{\Xi_c^+}$ $P_{\bar{D}_s^0}^{\Xi_c^{++}}$ $P_{\bar{D}^0}^{\Omega_c^{++}}$	$c\bar{c}csu$	$\Xi_c^+ \eta_c(1S)$ $\Xi_c^{++} D_s^-$ $\Omega_c^+ \bar{D}^0$	5452 5590	5627 – 5727 5732 – 5830 5835 – 5931 5935 – 6029 6034 – 6126	5627 – 5727 5724 – 5822 5819 – 5915 5912 – 6006 6003 – 6096	5627 – 5727 5786 – 5883 5940 – 6033 6089 – 6179 6233 – 6321	5627 – 5727 5855 – 5950 6072 – 6163 6280 – 6367 6479 – 6563	*
80	$P_{\eta_c(1S)}^{\Xi_c^0}$ $P_{\bar{D}_s^0}^{\Xi_c^+}$ $P_{\bar{D}^0}^{\Omega_c^{++}}$	$c\bar{c}cds$	$\Xi_c^0 \eta_c(1S)$ $\Xi_c^+ D_s^-$ $\Omega_c^+ D^-$	5454 5487	5629 – 5729 5727 – 5826 5824 – 5920 5919 – 6014 6012 – 6105	5629 – 5729 5720 – 5818 5809 – 5906 5897 – 5992 5983 – 6077	5629 – 5729 5788 – 5885 5942 – 6035 6090 – 6181 6235 – 6322	5629 – 5729 5857 – 5952 6074 – 6165 6282 – 6369 6481 – 6565	*
81	$P_{\eta_c(1S)}^{\Xi_c^+}$ $P_{K_0^0}^{\Xi_c^{++}}$ $P_{K_0^0}^{\Omega_c^{++}}$	$c\bar{s}ccd$	$\Xi_c^+ D_s^+$ $\Omega_c^{++} K^0$	5487	5662 – 5762 5761 – 5859 5858 – 5954 5953 – 6047 6046 – 6139	5662 – 5762 5753 – 5851 5843 – 5939 5931 – 6026 6017 – 6111	5662 – 5762 5840 – 5935 6009 – 6100 6172 – 6259 6328 – 6412	5662 – 5762 5916 – 6009 6154 – 6242 6379 – 6462 6592 – 6672	**
82	$P_{\bar{D}_s^0}^{\Xi_c^{++}}$ $P_{\pi_u^0}^{\Omega_c^{++}}$	$c\bar{u}ccu$	$\Xi_c^{++} D^0$ $\Omega_c^{++} \pi_u^0$	5487	5662 – 5762 5760 – 5858 5856 – 5952 5950 – 6045 6042 – 6136	5662 – 5762 5752 – 5850 5841 – 5937 5928 – 6023 6014 – 6107	5662 – 5762 5840 – 5935 6009 – 6100 6172 – 6259 6328 – 6412	5662 – 5762 5916 – 6009 6154 – 6242 6379 – 6462 6592 – 6672	
83	$P_{\bar{D}_s^0}^{\Xi_c^{++}}$ $P_{\pi^+}^{\Omega_c^{++}}$ $P_{K_0^+}^{\Omega_c^{++}}$	$c\bar{d}ccu$	$\Xi_c^{++} D^+$ $\Omega_c^{++} \pi^+$	5492	5667 – 5767 5765 – 5863 5860 – 5957 5954 – 6049 6047 – 6140	5667 – 5767 5757 – 5855 5846 – 5942 5933 – 6028 6018 – 6112	5667 – 5767 5844 – 5940 6014 – 6105 6176 – 6264 6332 – 6417	5667 – 5767 5921 – 6014 6158 – 6246 6383 – 6467 6596 – 6676	**
84	$P_{\bar{D}_s^0}^{\Xi_c^{++}}$ $P_{K_0^+}^{\Omega_c^{++}}$ $P_{K_0^+}^{\Omega_c^{++}}$	$c\bar{s}ccu$	$\Xi_c^{++} D_s^+$ $\Omega_c^{++} K^+$	5590	5765 – 5865 5862 – 5960 5957 – 6053 6050 – 6145 6142 – 6235	5765 – 5865 5854 – 5953 5942 – 6039 6029 – 6124 6114 – 6208	5765 – 5865 5938 – 6033 6103 – 6195 6262 – 6350 6415 – 6500	5765 – 5865 6012 – 6106 6245 – 6333 6465 – 6549 6675 – 6756	**
85	$P_{\eta_c(1S)}^{\Omega_c^0}$ $P_{D_s^-}^{\Omega_c^+}$	$c\bar{c}css$	$\Omega_c^0 \eta_c(1S)$ $\Omega_c^+ D_s^-$	5679	5854 – 5954 5954 – 6052 6052 – 6149 6149 – 6243 6243 – 6336	5854 – 5954 5946 – 6045 6037 – 6134 6126 – 6221 6214 – 6307	5854 – 5954 6011 – 6108 6163 – 6257 6311 – 6401 6453 – 6541	5854 – 5954 6080 – 6175 6294 – 6385 6500 – 6587 6697 – 6781	*
86	$P_{\eta_c(1S)}^{\Xi_c^+}$ $P_{D^-}^{\Omega_c^{++}}$	$c\bar{c}cd$	$\Xi_c^+ \eta_c(1S)$ $\Omega_c^{++} D^-$	6503	6678 – 6778 6760 – 6859 6841 – 6938 6921 – 7017 7000 – 7095	6678 – 6778 6754 – 6852 6828 – 6926 6902 – 6999 6975 – 7071	6678 – 6778 6818 – 6915 6954 – 7049 7087 – 7179 7216 – 7306	6678 – 6778 6879 – 6975 7072 – 7164 7258 – 7348 7438 – 7525	*
87	$P_{\eta_c(1S)}^{\Xi_c^{++}}$ $P_{\bar{D}_s^0}^{\Omega_c^{++}}$	$c\bar{c}ccu$	$\Xi_c^{++} \eta_c(1S)$ $\Omega_c^{++} \bar{D}^0$	6606	6781 – 6881 6865 – 6964 6949 – 7046 7031 – 7127 7112 – 7207	6781 – 6881 6859 – 6958 6936 – 7033 7012 – 7108 7087 – 7182	6781 – 6881 6918 – 7015 7051 – 7146 7182 – 7274 7309 – 7399	6781 – 6881 6978 – 7074 7167 – 7260 7350 – 7440 7527 – 7614	*
88	$P_{B_c^+}^p$ $P_{B_c^+}^{\Lambda_c^+}$ $P_{B_c^+}^{\Sigma_c^0}$ $P_{\bar{B}^0}^{\Sigma_c^0}$	$c\bar{b}duu$	pB_c^+ $\Lambda_c^+ B^-$ $\Sigma_c^+ \bar{B}^0$	7212 7565 7734	7387 – 7487 7509 – 7605 7626 – 7719 7739 – 7830 7849 – 7937	7387 – 7487 7499 – 7596 7608 – 7702 7713 – 7804 7815 – 7904	7387 – 7487 7494 – 7593 7600 – 7697 7705 – 7800 7807 – 7902	7387 – 7487 7542 – 7640 7693 – 7789 7841 – 7935 7987 – 8079	**
89	$P_{B_c^+}^p$ $P_{B_c^+}^{\Sigma_c^0}$ $P_{D^0}^{\Sigma_c^0}$	$b\bar{c}duu$	$p\bar{B}_c^-$ $\Sigma_c^+ D^-$ $\Sigma_b^0 \bar{D}^0$	7212 7681	7387 – 7487 7461 – 7560 7534 – 7632 7606 – 7703 7677 – 7773	7387 – 7487 7455 – 7554 7522 – 7620 7589 – 7686 7655 – 7751	7387 – 7487 7563 – 7658 7731 – 7821 7891 – 7977 8044 – 8127	7387 – 7487 7639 – 7732 7873 – 7960 8094 – 8176 8303 – 8381	**
90	$P_{B_c^+}^n$ $P_{B_c^+}^{\Lambda_c^+}$ $P_{B_c^+}^{\Sigma_c^0}$ $P_{B^-}^{\Sigma_c^0}$	$c\bar{b}ddu$	nB_c^+ $\Lambda_c^+ \bar{B}^0$ $\Sigma_c^0 B^-$	7214 7566 7733	7389 – 7489 7511 – 7607 7628 – 7721 7741 – 7831 7851 – 7939	7389 – 7489 7501 – 7598 7610 – 7703 7715 – 7806 7817 – 7906	7389 – 7489 7496 – 7595 7602 – 7699 7706 – 7802 7809 – 7904	7389 – 7489 7544 – 7641 7695 – 7791 7843 – 7937 7988 – 8081	**

91	$P_{\bar{B}_c^-}^n$ $P_{\Sigma_b^-}^n$ $P_{\bar{D}_s^0}^n$ $P_{D^-}^n$	$b\bar{c}ddu$	$n\bar{B}_c^-$ $\Sigma^- \bar{D}^0$ $\Sigma_b^0 D^-$	7214 7681	7389 – 7489 7463 – 7562 7536 – 7634 7608 – 7705 7679 – 7775	7389 – 7489 7457 – 7556 7524 – 7622 7591 – 7688 7657 – 7753	7389 – 7489 7565 – 7660 7732 – 7823 7892 – 7979 8046 – 8129	7389 – 7489 7641 – 7733 7875 – 7962 8095 – 8178 8304 – 8383	**
92	$P_{B_c^+}^{\Lambda^0}$ $P_{\bar{B}_s^0}^{\Lambda_c^+}$ $P_{\bar{D}_s^0}^{\Xi_c^+}$ $P_{\Xi_c^0}^{B_c^0}$ $P_{B_c^0}^{\Xi_c^-}$ $P_{\Xi_c^-}^{B_s^-}$	$c\bar{b}dsu$	$\Lambda^0 B_c^+$ $\Lambda_c^+ \bar{B}_s^0$ $\Xi_c^+ \bar{B}^0$ $\Xi_c^0 B^-$	7390 7653 7748 7749	7565 – 7665 7680 – 7777 7792 – 7886 7900 – 7992 8006 – 8095	7565 – 7665 7672 – 7769 7775 – 7869 7875 – 7967 7973 – 8063	7565 – 7665 7671 – 7769 7775 – 7872 7877 – 7973 7978 – 8073	7565 – 7665 7717 – 7815 7866 – 7962 8012 – 8106 8155 – 8247	**
93	$P_{\bar{B}_c^-}^{\Lambda^0}$ $P_{\Xi_b^0}^{B_c^-}$ $P_{D^-}^{\Xi_b^-}$ $P_{\bar{D}_s^0}^{\Sigma_b^-}$ $P_{D_s^-}^{\Sigma_b^0}$	$b\bar{c}dsu$	$\Lambda^0 \bar{B}_c^-$ $\Xi_b^0 D^-$ $\Xi_b^- \bar{D}^0$ $\Sigma_b^0 D_s^-$	7390 7662 7662	7565 – 7665 7637 – 7736 7708 – 7806 7778 – 7876 7848 – 7944	7565 – 7665 7631 – 7730 7697 – 7795 7762 – 7859 7827 – 7923	7565 – 7665 7735 – 7831 7898 – 7989 8053 – 8141 8203 – 8287	7565 – 7665 7809 – 7902 8036 – 8124 8252 – 8335 8456 – 8535	**
94	$P_{\bar{B}_c^-}^{\Sigma^+}$ $P_{\Xi_b^0}^{B_c^-}$ $P_{D^-}^{\Sigma_b^+}$ $P_{D_s^-}^{\Sigma_b^0}$	$b\bar{c}suu$	$\Sigma^+ \bar{B}_c^-$ $\Xi_b^0 \bar{D}^0$ $\Sigma_b^+ D_s^-$	7463 7657 7779	7638 – 7738 7764 – 7860 7884 – 7977 8000 – 8089 8112 – 8199	7638 – 7738 7754 – 7850 7866 – 7959 7974 – 8063 8078 – 8165	7638 – 7738 7818 – 7912 7988 – 8078 8150 – 8236 8305 – 8388	7638 – 7738 7894 – 7987 8132 – 8219 8355 – 8437 8567 – 8644	**
95	$P_{B_c^+}^{\Sigma^+}$ $P_{\Xi_c^+}^{B_c^-}$ $P_{\Xi_c^-}^{B_s^+}$ $P_{B_s^0}^{\Sigma_c^+}$	$c\bar{b}suu$	$\Sigma^+ B_c^+$ $\Xi_c^+ B^-$ $\Sigma_c^{++} \bar{B}_s^0$	7463 7747 7821	7638 – 7738 7751 – 7848 7861 – 7955 7967 – 8059 8070 – 8160	7638 – 7738 7742 – 7839 7844 – 7938 7942 – 8035 8039 – 8129	7638 – 7738 7744 – 7842 7848 – 7945 7951 – 8047 8052 – 8147	7638 – 7738 7790 – 7888 7940 – 8035 8086 – 8180 8229 – 8321	**
96	$P_{\bar{B}_c^-}^{\Sigma^-}$ $P_{\Xi_b^0}^{B_c^-}$ $P_{D^-}^{\Sigma_b^-}$ $P_{D_s^-}^{\Sigma_b^0}$	$b\bar{c}dds$	$\Sigma^- \bar{B}_c^-$ $\Xi_b^- D^-$ $\Sigma_b^- D_s^-$	7471 7667 7784	7646 – 7746 7717 – 7816 7787 – 7886 7857 – 7954 7926 – 8023	7646 – 7746 7712 – 7811 7777 – 7875 7841 – 7938 7905 – 8001	7646 – 7746 7813 – 7908 7972 – 8063 8124 – 8212 8271 – 8356	7646 – 7746 7884 – 7978 8108 – 8196 8319 – 8403 8520 – 8600	**
97	$P_{B_c^+}^{\Sigma^-}$ $P_{\Xi_c^0}^{B_c^-}$ $P_{\bar{B}_s^0}^{\Sigma_c^0}$ $P_{B_s^-}^{\Sigma_b^0}$	$c\bar{b}dds$	$\Sigma^- B_c^+$ $\Xi_c^0 \bar{B}^0$ $\Sigma_c^0 \bar{B}_s^0$	7471 7750 7821	7646 – 7746 7759 – 7856 7868 – 7962 7974 – 8066 8078 – 8167	7646 – 7746 7750 – 7847 7851 – 7946 7950 – 8042 8046 – 8136	7646 – 7746 7750 – 7849 7853 – 7950 7955 – 8051 8055 – 8149	7646 – 7746 7796 – 7894 7943 – 8039 8088 – 8182 8229 – 8322	**
98	$P_{B_c^+}^{\Delta^-}$ $P_{\Sigma_c^0}^{B_c^-}$ $P_{\bar{B}_s^0}^{\Sigma_c^0}$	$c\bar{b}ddd$	$\Delta^- B_c^+$ $\Sigma_c^0 \bar{B}^0$	7506 7734	7681 – 7781 7793 – 7890 7901 – 7995 8006 – 8098 8109 – 8198	7681 – 7781 7784 – 7881 7884 – 7979 7982 – 8074 8077 – 8167	7681 – 7781 7784 – 7883 7886 – 7983 7986 – 8082 8085 – 8180	7681 – 7781 7830 – 7928 7975 – 8071 8118 – 8212 8258 – 8351	**
99	$P_{\bar{B}_c^-}^{\Delta^-}$ $P_{\Sigma_b^-}^{B_c^-}$	$b\bar{c}ddd$	$\Delta^- \bar{B}_c^-$ $\Sigma_b^- D^-$	7506 7686	7681 – 7781 7752 – 7851 7822 – 7920 7891 – 7988 7960 – 8056	7681 – 7781 7746 – 7845 7811 – 7909 7875 – 7972 7939 – 8035	7681 – 7781 7843 – 7939 7998 – 8090 8148 – 8236 8292 – 8377	7681 – 7781 7913 – 8007 8131 – 8220 8339 – 8423 8536 – 8618	**
100	$P_{\bar{B}_c^-}^{\Delta^{++}}$ $P_{\Sigma_b^+}^{B_c^-}$ $P_{\bar{D}_s^0}^{\Sigma_c^0}$	$b\bar{c}uuu$	$\Delta^{++} \bar{B}_c^-$ $\Sigma_b^+ \bar{D}^0$	7506 7676	7681 – 7781 7805 – 7901 7924 – 8016 8039 – 8128 8149 – 8236	7681 – 7781 7795 – 7892 7906 – 7999 8012 – 8102 8115 – 8203	7681 – 7781 7843 – 7939 7998 – 8090 8148 – 8236 8292 – 8377	7681 – 7781 7913 – 8007 8131 – 8220 8339 – 8423 8536 – 8618	**
101	$P_{B_c^+}^{\Delta^{++}}$ $P_{\Sigma_c^0}^{B_c^+}$ $P_{B_c^-}^{\Sigma_c^0}$	$c\bar{b}uuu$	$\Delta^{++} B_c^+$ $\Sigma_c^0 B^-$	7506 7733	7681 – 7781 7793 – 7890 7901 – 7995 8006 – 8098 8109 – 8198	7681 – 7781 7784 – 7881 7884 – 7979 7982 – 8074 8077 – 8167	7681 – 7781 7784 – 7883 7886 – 7983 7986 – 8082 8085 – 8180	7681 – 7781 7830 – 7928 7975 – 8071 8118 – 8212 8258 – 8351	**
102	$P_{B_c^+}^{A^+}$ $P_{\Sigma_b^0}^{B_c^+}$ $P_{D^0}^{B_c^-}$ $P_{\Xi_{bc}^+}^{\Xi_{bc}^-}$ $P_{\pi_{bc}^-}^{\pi_{bc}^0}$ $P_{\pi_u^0}^{\Xi_{bc}^0}$	$b\bar{c}udu$	$\Lambda_c^+ B^+$ $\Sigma_b^0 D^0$ $\Xi_{bc}^+ \pi^-$ $\Xi_{bc}^0 \pi_u^0$	7565	7740 – 7840 7808 – 7907 7875 – 7973 7941 – 8039 8007 – 8104	7740 – 7840 7802 – 7902 7864 – 7963 7926 – 8024 7987 – 8084	7740 – 7840 7963 – 8054 8167 – 8251 8356 – 8435 8534 – 8609	7740 – 7840 8055 – 8143 8336 – 8415 8591 – 8665 8828 – 8897	
103	$P_{B_c^+}^{A^+}$ $P_{\Sigma_b^0}^{B_c^+}$ $P_{D^+}^{B_c^-}$ $P_{\Xi_{bc}^+}^{\Xi_{bc}^-}$ $P_{\pi_d^0}^{\pi_u^0}$ $P_{\Xi_{bc}^0}^{\Xi_{bc}^0}$	$b\bar{c}udu$	$\Lambda_c^+ B^0$ $\Sigma_b^0 D^+$ $\Xi_{bc}^+ \pi_d^0$ $\Xi_{bc}^0 \pi^+$	7566	7741 – 7841 7809 – 7908 7876 – 7974 7942 – 8040 8008 – 8105	7741 – 7841 7803 – 7903 7865 – 7964 7927 – 8025 7988 – 8085	7741 – 7841 7963 – 8055 8167 – 8252 8357 – 8436 8535 – 8610	7741 – 7841 8056 – 8144 8336 – 8416 8592 – 8666 8829 – 8897	

104	$P_{B_c^+}^{\Xi^0}$ $P_{B_c^0}^{\Xi^-}$ $P_{B_c^-}^{\Omega^0}$ $P_{B_c^-}^{\Omega^-}$	$c\bar{b}ssu$	$\Xi^0 B_c^+$ $\Xi_c^+ \bar{B}_s^0$ $\Omega_c^0 B^-$	7589 7835 7974	7764 – 7864 7873 – 7970 7979 – 8074 8082 – 8175 8183 – 8273	7764 – 7864 7865 – 7962 7963 – 8058 8059 – 8151 8152 – 8243	7764 – 7864 7869 – 7967 7972 – 8069 8074 – 8169 8174 – 8269	7764 – 7864 7915 – 8013 8062 – 8158 8207 – 8301 8349 – 8442	**
105	$P_{\bar{B}_c^-}^{\Xi^0}$ $P_{\bar{B}_c^0}^{\Xi^-}$ $P_{\bar{D}_s^-}^{\Omega^0}$ $P_{\bar{D}_s^-}^{\Omega^-}$	$b\bar{c}ssu$	$\Xi^0 \bar{B}_c^-$ $\Xi_b^0 D_s^-$ $\Omega_b^- \bar{D}^0$	7589 7760 7911	7764 – 7864 7885 – 7981 8001 – 8094 8113 – 8203 8221 – 8309	7764 – 7864 7875 – 7972 7983 – 8076 8087 – 8178 8188 – 8276	7764 – 7864 7940 – 8035 8108 – 8198 8267 – 8354 8420 – 8503	7764 – 7864 8016 – 8108 8250 – 8337 8470 – 8552 8678 – 8756	**
106	$P_{B_c^+}^{\Xi^-}$ $P_{B_c^0}^{\Xi^0}$ $P_{B_c^-}^{\Omega^0}$ $P_{B_c^-}^{\Omega^-}$	$c\bar{b}dss$	$\Xi^- B_c^+$ $\Xi_c^0 \bar{B}_s^0$ $\Omega_c^0 \bar{B}^0$	7596 7837 7975	7771 – 7871 7880 – 7977 7986 – 8080 8089 – 8181 8189 – 8279	7771 – 7871 7872 – 7969 7970 – 8065 8065 – 8158 8158 – 8249	7771 – 7871 7876 – 7974 7979 – 8076 8080 – 8176 8181 – 8275	7771 – 7871 7922 – 8020 8069 – 8165 8214 – 8308 8356 – 8448	**
107	$P_{\bar{B}_c^-}^{\Xi^-}$ $P_{\bar{B}_c^0}^{\Xi^0}$ $P_{\bar{D}_s^-}^{\Omega^0}$ $P_{\bar{D}_s^-}^{\Omega^-}$	$b\bar{c}dss$	$\Xi^- \bar{B}_c^-$ $\Xi_b^0 D_s^-$ $\Omega_b^- D^-$	7596 7765 7916	7771 – 7871 7841 – 7940 7910 – 8008 7979 – 8076 8047 – 8143	7771 – 7871 7835 – 7935 7899 – 7998 7963 – 8060 8026 – 8122	7771 – 7871 7937 – 8032 8095 – 8187 8247 – 8335 8394 – 8479	7771 – 7871 8008 – 8102 8231 – 8319 8441 – 8525 8642 – 8722	**
108	$P_{B_c^0}^{\Lambda^+}$ $P_{\Sigma_b^0}^{\Sigma^0}$ $P_{D_s^+}^{\Xi^0}$ $P_{\Xi_{bc}^0}^{\Xi^0}$ $P_{K^0}^{\Omega^0}$ $P_{K_{bc}^0}^{\Xi^0}$	$b\bar{s}cds$	$\Lambda^+ B_s^0$ $\Sigma_0^0 D_s^+$ $\Xi_b^+ K^0$ $\Xi_{bc}^0 K^+$	7653	7828 – 7928 7901 – 8000 7974 – 8072 8046 – 8143 8117 – 8213	7828 – 7928 7896 – 7995 7963 – 8061 8029 – 8126 8095 – 8191	7828 – 7928 8043 – 8135 8241 – 8326 8426 – 8506 8600 – 8676	7828 – 7928 8133 – 8221 8406 – 8487 8656 – 8731 8888 – 8958	**
109	$P_{D^0}^{\Xi_b^-}$ $P_{\Xi_c^+}^{\Xi^0}$ $P_{B_c^+}^{\Xi^-}$ $P_{\Xi_{bc}^0}^{\Xi^0}$ $P_{K_c^0}^{\Omega^0}$ $P_{\pi_u^0}^{\Xi^0}$	$c\bar{u}bsu$	$\Xi_b^0 D^0$ $\Xi_c^+ B^+$ $\Xi_b^+ K^-$ $\Omega_{bc}^0 \pi_u^0$	7657 7747	7832 – 7932 7900 – 7999 7967 – 8065 8033 – 8131 8099 – 8196	7832 – 7932 7894 – 7994 7956 – 8055 8018 – 8116 8079 – 8176	7832 – 7932 8053 – 8144 8255 – 8340 8444 – 8523 8620 – 8695	7832 – 7932 8145 – 8233 8423 – 8503 8677 – 8751 8912 – 8981	
110	$P_{D_c^+}^{\Xi_b^-}$ $P_{\Xi_c^+}^{\Xi^0}$ $P_{B_c^0}^{\Xi^-}$ $P_{\Xi_{bc}^0}^{\Xi^0}$ $P_{\bar{K}_c^0}^{\Omega^0}$ $P_{\pi_c^+}^{\Xi^0}$	$c\bar{d}bsu$	$\Xi_b^0 D^+$ $\Xi_c^+ B^0$ $\Xi_b^+ \bar{K}^0$ $\Omega_{bc}^0 \pi^+$	7662 7748	7837 – 7937 7905 – 8004 7972 – 8070 8038 – 8136 8104 – 8201	7837 – 7937 7899 – 7999 7961 – 8060 8023 – 8121 8084 – 8181	7837 – 7937 8057 – 8149 8260 – 8344 8448 – 8527 8624 – 8699	7837 – 7937 8149 – 8237 8427 – 8507 8681 – 8754 8916 – 8985	**
111	$P_{D_c^0}^{\Xi_b^-}$ $P_{\Xi_c^0}^{\Xi^0}$ $P_{B_c^+}^{\Xi^0}$ $P_{\Xi_{bc}^0}^{\Xi^-}$ $P_{\pi_c^-}^{\Xi^0}$ $P_{K_c^-}^{\Xi^0}$	$c\bar{u}bds$	$\Xi_b^0 D^0$ $\Xi_c^0 B^+$ $\Omega_{bc}^0 \pi^-$ $\Xi_{bc}^0 K^-$	7662 7749	7837 – 7937 7905 – 8004 7972 – 8070 8038 – 8136 8104 – 8201	7837 – 7937 7899 – 7999 7961 – 8060 8023 – 8121 8084 – 8181	7837 – 7937 8057 – 8149 8260 – 8344 8448 – 8527 8624 – 8699	7837 – 7937 8149 – 8237 8427 – 8507 8681 – 8754 8916 – 8985	**
112	$P_{D_c^+}^{\Xi_b^-}$ $P_{\Xi_c^0}^{\Xi^0}$ $P_{B_c^0}^{\Xi^0}$ $P_{\Xi_{bc}^0}^{\Xi^0}$ $P_{\pi_c^0}^{\Xi^0}$ $P_{\bar{K}_c^0}^{\Xi^0}$	$c\bar{d}bds$	$\Xi_b^0 D^+$ $\Xi_c^0 B^0$ $\Omega_{bc}^0 \pi_u^0$ $\Xi_{bc}^0 K^0$	7667 7750	7842 – 7942 7909 – 8008 7975 – 8073 8041 – 8138 8106 – 8203	7842 – 7942 7904 – 8003 7965 – 8063 8026 – 8123 8086 – 8183	7842 – 7942 8062 – 8153 8264 – 8348 8451 – 8531 8628 – 8703	7842 – 7942 8154 – 8242 8431 – 8511 8684 – 8758 8919 – 8988	
113	$P_{D_c^0}^{\Sigma_b^+}$ $P_{\Sigma_c^++}^{\Sigma^0}$ $P_{B_c^+}^{\Xi_c^+}$ $P_{\Xi_{bc}^0}^{\Xi^+}$ $P_{\pi_u^0}^{\Xi^0}$	$c\bar{u}buu$	$\Sigma_b^+ D^0$ $\Sigma_c^{++} B^+$ $\Xi_{bc}^+ \pi_u^0$	7676 7733	7851 – 7951 7918 – 8017 7984 – 8082 8050 – 8147 8115 – 8212	7851 – 7951 7913 – 8012 7974 – 8072 8034 – 8132 8095 – 8192	7851 – 7951 8022 – 8117 8184 – 8275 8340 – 8427 8489 – 8572	7851 – 7951 8095 – 8188 8323 – 8410 8537 – 8620 8740 – 8819	
114	$P_{D_c^0}^{\Sigma_b^-}$ $P_{\Sigma_c^0}^{\Sigma^0}$ $P_{B_c^+}^{\Xi_c^+}$ $P_{\Xi_{bc}^0}^{\Xi^+}$ $P_{\pi_u^0}^{\Xi^0}$	$c\bar{u}bdd$	$\Sigma_b^- D^0$ $\Sigma_c^0 B^+$ $\Xi_{bc}^0 \pi^-$	7681 7733	7856 – 7956 7928 – 8027 7999 – 8097 8069 – 8166 8138 – 8235	7856 – 7956 7922 – 8021 7988 – 8086 8053 – 8150 8117 – 8213	7856 – 7956 8068 – 8160 8265 – 8350 8448 – 8529 8621 – 8698	7856 – 7956 8157 – 8246 8428 – 8509 8677 – 8752 8908 – 8978	**
115	$P_{D_c^+}^{\Sigma_b^+}$ $P_{\Sigma_c^++}^{\Sigma^0}$ $P_{B_c^0}^{\Xi_c^+}$ $P_{\Xi_{bc}^0}^{\Xi^+}$ $P_{\pi_c^+}^{\Xi^0}$	$c\bar{d}buu$	$\Sigma_b^+ D^+$ $\Sigma_c^{++} B^0$ $\Xi_{bc}^+ \pi^+$	7681 7734	7856 – 7956 7928 – 8027 7999 – 8097 8069 – 8166 8138 – 8235	7856 – 7956 7922 – 8021 7988 – 8086 8053 – 8150 8117 – 8213	7856 – 7956 8027 – 8122 8189 – 8280 8344 – 8431 8493 – 8576	7856 – 7956 8100 – 8193 8327 – 8414 8541 – 8624 8744 – 8823	**
116	$P_{D_c^0}^{\Sigma_b^-}$ $P_{\Sigma_c^0}^{\Sigma^0}$ $P_{B_c^0}^{\Xi_c^+}$ $P_{\Xi_{bc}^0}^{\Xi^+}$ $P_{\pi_d^0}^{\Xi^0}$	$c\bar{d}bdd$	$\Sigma_b^- D^+$ $\Sigma_c^0 B^0$ $\Xi_{bc}^0 \pi_d^0$	7686 7734	7861 – 7961 7928 – 8027 7994 – 8092 8059 – 8157 8124 – 8221	7861 – 7961 7923 – 8022 7984 – 8082 8044 – 8142 8104 – 8201	7861 – 7961 8073 – 8165 8269 – 8355 8452 – 8533 8625 – 8701	7861 – 7961 8162 – 8251 8432 – 8514 8680 – 8756 8911 – 8982	

117	$P_{D_s^+}^{\Xi_b^0}$ $P_{\Xi_c^0}^{B_s^0}$ $P_{\phi(1020)}^{\Xi_{bc}^0}$ $P_{K^+}^{\Omega_{bc}^0}$	$c\bar{s}bsu$	$\Xi_b^0 D_s^+$ $\Xi_c^+ B_s^0$ $\Xi_{bc}^+ \phi(1020)$ $\Omega_{bc}^0 K^+$	7760 7835	7935 – 8035 8007 – 8106 8079 – 8177 8150 – 8247 8220 – 8316	7935 – 8035 8002 – 8101 8068 – 8166 8133 – 8230 8198 – 8294	7935 – 8035 8147 – 8239 8342 – 8428 8525 – 8606 8698 – 8774	7935 – 8035 8236 – 8325 8505 – 8587 8753 – 8828 8983 – 9054	
118	$P_{D_s^+}^{\Xi_b^-}$ $P_{\Xi_c^0}^{B_s^0}$ $P_{\phi(1020)}^{\Xi_{bc}^0}$ $P_{K^0}^{\Xi_{bc}^0}$	$c\bar{s}bds$	$\Xi_b^- D_s^+$ $\Xi_c^0 B_s^0$ $\Omega_{bc}^0 K^0$ $\Xi_{bc}^0 \phi(1020)$	7765 7837	7940 – 8040 8012 – 8111 8084 – 8182 8155 – 8252 8225 – 8321	7940 – 8040 8007 – 8106 8073 – 8171 8138 – 8235 8203 – 8299	7940 – 8040 8151 – 8243 8347 – 8432 8529 – 8610 8701 – 8778	7940 – 8040 8240 – 8329 8509 – 8591 8757 – 8832 8987 – 9057	
119	$P_{D_s^+}^{\Sigma_b^+}$ $P_{\Sigma_c^0}^{B_s^0}$ $P_{\Xi_{bc}^0}^{B_s^0}$ $P_{K^+}^{\Xi_{bc}^0}$	$c\bar{s}buu$	$\Sigma_b^+ D_s^+$ $\Sigma_c^+ B_s^0$ $\Xi_{bc}^+ K^+$	7779 7821	7954 – 8054 8026 – 8125 8097 – 8195 8168 – 8265 8238 – 8334	7954 – 8054 8021 – 8120 8086 – 8185 8152 – 8249 8216 – 8313	7954 – 8054 8120 – 8215 8278 – 8369 8429 – 8517 8575 – 8659	7954 – 8054 8191 – 8284 8413 – 8501 8622 – 8706 8822 – 8901	**
120	$P_{D_s^+}^{\Sigma_b^0}$ $P_{\Sigma_c^0}^{B_s^0}$ $P_{\Xi_{bc}^0}^{B_s^0}$ $P_{K^0}^{\Xi_{bc}^0}$	$c\bar{s}bdd$	$\Sigma_b^- D_s^+$ $\Sigma_c^0 B_s^0$ $\Xi_{bc}^0 K^0$	7784 7821	7959 – 8059 8031 – 8130 8102 – 8200 8173 – 8270 8243 – 8339	7959 – 8059 8025 – 8125 8091 – 8189 8157 – 8254 8221 – 8318	7959 – 8059 8163 – 8256 8353 – 8440 8531 – 8613 8700 – 8778	7959 – 8059 8249 – 8339 8512 – 8594 8754 – 8831 8981 – 9053	**
121	$P_{D^0}^{\Omega_b^-}$ $P_{B_s^0}^{\Omega_b^0}$ $P_{\Xi_{bc}^0}^{B_s^0}$ $P_{K^-}^{\Omega_{bc}^0}$	$c\bar{u}bss$	$\Omega_b^- D^0$ $\Omega_b^0 B^+$ $\Omega_{bc}^0 K^-$	7911 7974	8086 – 8186 8152 – 8251 8217 – 8315 8281 – 8379 8345 – 8442	8086 – 8186 8147 – 8246 8207 – 8305 8266 – 8364 8325 – 8422	8086 – 8186 8273 – 8367 8448 – 8536 8614 – 8698 8772 – 8852	8086 – 8186 8352 – 8443 8596 – 8680 8823 – 8902 9036 – 9110	**
122	$P_{D_s^+}^{\Omega_b^-}$ $P_{\Xi_c^0}^{\Omega_b^0}$ $P_{\Xi_{bc}^0}^{\Omega_b^0}$ $P_{K^0}^{\Omega_{bc}^0}$	$c\bar{d}bss$	$\Omega_b^- D^+$ $\Omega_c^0 B^0$ $\Omega_{bc}^0 \bar{K}^0$	7916 7975	8091 – 8191 8157 – 8256 8222 – 8320 8286 – 8384 8350 – 8447	8091 – 8191 8151 – 8251 8212 – 8310 8271 – 8369 8330 – 8427	8091 – 8191 8278 – 8371 8453 – 8541 8618 – 8702 8776 – 8856	8091 – 8191 8357 – 8448 8600 – 8684 8826 – 8905 9039 – 9114	**
123	$P_{\bar{B}_c^-}^{\Omega_b^-}$ $P_{D_s^-}^{\Omega_b^0}$	$b\bar{c}sss$	$\Omega_b^- \bar{B}_c^-$ $\Omega_b^- D_s^-$	7946 8014	8121 – 8221 8229 – 8326 8334 – 8429 8437 – 8529 8536 – 8626	8121 – 8221 8221 – 8318 8318 – 8413 8413 – 8506 8506 – 8596	8121 – 8221 8285 – 8380 8342 – 8533 8459 – 8680 8737 – 8822	8121 – 8221 8356 – 8449 8576 – 8664 8784 – 8868 8982 – 9062	**
124	$P_{B_c^+}^{\Omega_b^-}$ $P_{\Xi_c^0}^{\Omega_b^0}$ $P_{\Xi_{bc}^0}^{\Omega_b^0}$	$c\bar{b}sss$	$\Omega_b^- B_c^+$ $\Omega_c^0 \bar{B}_s^0$	7946 8062	8121 – 8221 8229 – 8326 8334 – 8429 8437 – 8529 8536 – 8626	8121 – 8221 8221 – 8318 8318 – 8413 8413 – 8506 8506 – 8596	8121 – 8221 8222 – 8321 8321 – 8419 8420 – 8516 8517 – 8611	8121 – 8221 8266 – 8364 8409 – 8505 8549 – 8643 8686 – 8779	**
125	$P_{D_s^+}^{\Omega_b^-}$ $P_{\Xi_c^0}^{\Omega_b^0}$ $P_{\Xi_{bc}^0}^{\Omega_b^0}$ $P_{\phi(1020)}^{\Omega_{bc}^0}$	$c\bar{s}bss$	$\Omega_b^- D_s^+$ $\Omega_c^0 B_s^0$ $\Omega_{bc}^0 \phi(1020)$	8014 8062	8189 – 8289 8259 – 8358 8328 – 8426 8396 – 8493 8464 – 8560	8189 – 8289 8253 – 8352 8317 – 8415 8380 – 8478 8443 – 8540	8189 – 8289 8369 – 8463 8539 – 8628 8700 – 8785 8854 – 8935	8189 – 8289 8446 – 8538 8683 – 8768 8904 – 8984 9112 – 9189	
126	$P_{\bar{B}_c^-}^{\Lambda_c^+}$ $P_{\eta_c(1S)}^{\Sigma_b^0}$ $P_{\Xi_{bc}^0}^{\Xi_{bc}^+}$ $P_{\Xi_{bc}^0}^{\Xi_{bc}^-}$ $P_{\bar{D}^0}^{\Xi_{bc}^0}$	$b\bar{c}cd\bar{u}$	$\Lambda_c^+ \bar{B}_c^-$ $\Sigma_b^0 \eta_c(1S)$ $\Xi_{bc}^+ D^-$ $\Xi_{bc}^0 \bar{D}^0$	8560	8735 – 8835 8797 – 8896 8858 – 8957 8919 – 9017 8980 – 9077	8735 – 8835 8792 – 8891 8849 – 8947 8905 – 9003 8961 – 9058	8735 – 8835 8894 – 8990 9046 – 9138 9193 – 9281 9334 – 9420	8735 – 8835 8962 – 9056 9177 – 9266 9380 – 9465 9574 – 9655	*
127	$P_{B_c^+}^{\Lambda_c^+}$ $P_{\Xi_{cc}^0}^{\Xi_{cc}^+}$ $P_{\Xi_{cc}^0}^{\Xi_{cc}^-}$ $P_{\Xi_{cc}^0}^{\Xi_{cc}^0}$	$c\bar{b}cd\bar{u}$	$\Lambda_c^+ B_c^+$ $\Xi_{cc}^+ B^-$ $\Xi_{cc}^+ \bar{B}^0$	8560 8798 8902	8735 – 8835 8822 – 8920 8908 – 9004 8992 – 9087 9074 – 9168	8735 – 8835 8815 – 8914 8894 – 8991 8972 – 9068 9049 – 9143	8735 – 8835 8831 – 8930 8925 – 9023 9019 – 9115 9111 – 9207	8735 – 8835 8873 – 8971 9009 – 9105 9142 – 9237 9273 – 9367	**
128	$P_{B_c^+}^{\Sigma_c^{++}}$ $P_{\Xi_{cc}^0}^{\Xi_{cc}^+}$ $P_{B_c^-}^{\Xi_{cc}^+}$	$c\bar{b}cuu$	$\Sigma_c^{++} B_c^+$ $\Xi_{cc}^{++} B^-$	8728 8901	8903 – 9003 8987 – 9086 9070 – 9167 9151 – 9247 9232 – 9326	8903 – 9003 8981 – 9079 9057 – 9154 9133 – 9228 9207 – 9301	8903 – 9003 8997 – 9096 9089 – 9187 9181 – 9278 9272 – 9367	8903 – 9003 9038 – 9136 9171 – 9268 9302 – 9397 9430 – 9524	**
129	$P_{\bar{B}_c^-}^{\Sigma_c^{++}}$ $P_{\eta_c(1S)}^{\Sigma_c^0}$ $P_{\Xi_{bc}^0}^{\Xi_{bc}^+}$	$b\bar{c}cuu$	$\Sigma_c^{++} \bar{B}_c^-$ $\Sigma_b^+ \eta_c(1S)$ $\Xi_{bc}^+ \bar{D}^0$	8728 8795	8903 – 9003 8969 – 9069 9035 – 9134 9101 – 9198 9165 – 9262	8903 – 9003 8964 – 9064 9025 – 9124 9086 – 9183 9145 – 9242	8903 – 9003 9033 – 9131 9160 – 9255 9284 – 9376 9405 – 9495	8903 – 9003 9090 – 9186 9270 – 9363 9444 – 9534 9612 – 9699	*

130	$P_{B_c^0}^{\Sigma_c^0}$ $P_{\Xi_c^0}^{\Xi_c^+}$ $P_{\bar{B}_c^0}^{\Xi_{cc}^0}$	$c\bar{c}cd$	$\Sigma_c^0 B_c^+$ $\Xi_{cc}^0 \bar{B}_c^0$	8728 8799	8903 – 9003 8987 – 9086 9070 – 9167 9151 – 9247 9232 – 9326	8903 – 9003 8981 – 9079 9057 – 9154 9133 – 9228 9207 – 9301	8903 – 9003 8994 – 9093 9084 – 9182 9174 – 9270 9262 – 9358	8903 – 9003 9034 – 9133 9164 – 9261 9291 – 9386 9416 – 9511	**
131	$P_{\bar{B}_c^-}^{\Sigma_c^0}$ $P_{\eta_c(1S)}^{\Sigma_b^0}$ $P_{D_c^-}^{\Xi_b^0}$ $P_{D_c^-}^{\Xi_{bc}^0}$	$b\bar{c}cd$	$\Sigma_c^0 \bar{B}_c^-$ $\Sigma_b^- \eta_c(1S)$ $\Xi_{bc}^0 D^-$	8728 8800	8903 – 9003 8964 – 9063 9024 – 9122 9084 – 9182 9143 – 9240	8903 – 9003 8959 – 9058 9014 – 9113 9070 – 9168 9125 – 9222	8903 – 9003 9055 – 9151 9201 – 9294 9342 – 9431 9478 – 9565	8903 – 9003 9121 – 9215 9326 – 9416 9523 – 9609 9710 – 9793	*
132	$P_{\bar{B}_c^-}^{\Xi_c^+}$ $P_{\eta_c(1S)}^{\Xi_b^0}$ $P_{D_c^-}^{\Xi_{bc}^0}$ $P_{D_s^-}^{\Omega_{bc}^0}$ $P_{D_c^-}^{\Omega_{bc}^0}$	$b\bar{c}csu$	$\Xi_c^+ \bar{B}_c^-$ $\Xi_b^0 \eta_c(1S)$ $\Xi_{bc}^+ D_s^-$ $\Omega_{bc}^0 \bar{D}^0$	8742 8776	8917 – 9017 8983 – 9082 9049 – 9147 9114 – 9212 9179 – 9276	8917 – 9017 8978 – 9077 9039 – 9137 9099 – 9197 9159 – 9256	8917 – 9017 9071 – 9167 9219 – 9311 9361 – 9450 9498 – 9585	8917 – 9017 9137 – 9232 9345 – 9435 9543 – 9629 9732 – 9814	*
133	$P_{B_c^+}^{\Xi_c^+}$ $P_{\Xi_c^0}^{\Xi_{cc}^0}$ $P_{\bar{B}_s^0}^{\Xi_b^0}$ $P_{B_c^-}^{\Omega_{cc}^0}$	$c\bar{c}csu$	$\Xi_c^+ B_c^+$ $\Xi_{cc}^+ \bar{B}_s^0$ $\Omega_{cc}^+ B^-$	8742 8989	8917 – 9017 9001 – 9099 9084 – 9180 9165 – 9260 9245 – 9339	8917 – 9017 8994 – 9093 9071 – 9168 9146 – 9242 9220 – 9315	8917 – 9017 9010 – 9108 9101 – 9199 9191 – 9288 9281 – 9376	8917 – 9017 9050 – 9149 9181 – 9278 9310 – 9406 9438 – 9531	**
134	$P_{\bar{B}_c^-}^{\Xi_c^0}$ $P_{\eta_c(1S)}^{\Xi_b^-}$ $P_{D_c^-}^{\Omega_{bc}^0}$ $P_{D_s^-}^{\Xi_{bc}^0}$	$b\bar{c}cds$	$\Xi_c^0 \bar{B}_c^-$ $\Xi_b^- \eta_c(1S)$ $\Omega_{bc}^0 D^-$ $\Xi_{bc}^0 D_s^-$	8744 8781	8919 – 9019 8980 – 9079 9040 – 9138 9099 – 9197 9159 – 9256	8919 – 9019 8975 – 9074 9030 – 9129 9085 – 9184 9140 – 9238	8919 – 9019 9073 – 9169 9220 – 9313 9363 – 9452 9500 – 9587	8919 – 9019 9139 – 9233 9347 – 9437 9545 – 9630 9734 – 9816	*
135	$P_{B_c^+}^{\Xi_c^0}$ $P_{\Xi_c^+}^{\Xi_{cc}^0}$ $P_{\bar{B}_s^0}^{\Xi_b^0}$ $P_{B_c^-}^{\Omega_{cc}^0}$	$c\bar{c}cds$	$\Xi_c^0 B_c^+$ $\Xi_{cc}^+ \bar{B}_s^0$ $\Omega_{cc}^+ \bar{B}^0$	8744 8886	8919 – 9019 9003 – 9101 9085 – 9182 9167 – 9262 9247 – 9341	8919 – 9019 8996 – 9095 9073 – 9170 9148 – 9244 9222 – 9316	8919 – 9019 9011 – 9110 9103 – 9201 9193 – 9290 9283 – 9378	8919 – 9019 9052 – 9151 9183 – 9280 9312 – 9408 9439 – 9533	**
136	$P_{B_c^+}^{\Xi_{cc}^+}$ $P_{\Xi_b^0}^{\Xi_{bc}^0}$ $P_{D_c^-}^{\Xi_{bc}^0}$ $P_{\pi^-}^{bcc^+}$	$b\bar{c}ccd$	$\Xi_c^+ B_c^+$ $\Xi_b^0 D^0$ $bcc^+ \pi^-$	8798	8973 – 9073 9035 – 9134 9096 – 9195 9157 – 9255 9218 – 9315	8973 – 9073 9030 – 9129 9087 – 9186 9143 – 9241 9199 – 9297	8973 – 9073 9137 – 9232 9294 – 9385 9443 – 9531 9587 – 9671	8973 – 9073 9208 – 9301 9427 – 9515 9634 – 9717 9831 – 9910	**
137	$P_{B_c^0}^{\Xi_c^+}$ $P_{\Xi_c^0}^{\Xi_{cc}^0}$ $P_{D_c^+}^{\Xi_{bc}^0}$ $P_{\pi_d^0}^{bcc^+}$	$b\bar{d}cc$	$\Xi_{cc}^+ B^0$ $\Xi_{bc}^0 D^+$ $bcc^+ \pi_d^0$	8799	8974 – 9074 9032 – 9132 9091 – 9189 9148 – 9246 9206 – 9303	8974 – 9074 9028 – 9127 9082 – 9180 9135 – 9233 9188 – 9286	8974 – 9074 9138 – 9233 9295 – 9386 9444 – 9532 9588 – 9672	8974 – 9074 9209 – 9302 9428 – 9516 9635 – 9718 9831 – 9911	
138	$P_{B_c^0}^{\Xi_{cc}^+}$ $P_{\Xi_b^0}^{\Xi_{bc}^0}$ $P_{D_s^+}^{\Xi_{bc}^0}$ $P_{K_0}^{bcc^+}$	$b\bar{s}ccd$	$\Xi_{cc}^+ B_s^0$ $\Xi_{bc}^0 D_s^+$ $bcc^+ K^0$	8886	9061 – 9161 9123 – 9222 9185 – 9284 9246 – 9344 9307 – 9404	9061 – 9161 9118 – 9218 9175 – 9274 9232 – 9330 9288 – 9386	9061 – 9161 9221 – 9316 9374 – 9465 9520 – 9608 9661 – 9746	9061 – 9161 9290 – 9383 9504 – 9593 9707 – 9791 9900 – 9981	**
139	$P_{B_c^+}^{\Xi_{cc}^{++}}$ $P_{\Xi_b^+}^{\Xi_{bc}^0}$ $P_{D_c^0}^{\Xi_{bc}^0}$ $P_{\pi_u^0}^{bcc^+}$	$b\bar{u}cu$	$\Xi_{cc}^{++} B^+$ $\Xi_{bc}^- D^0$ $bcc^+ \pi_u^0$	8901	9076 – 9176 9134 – 9233 9191 – 9290 9248 – 9347 9305 – 9403	9076 – 9176 9129 – 9229 9182 – 9281 9235 – 9333 9287 – 9385	9076 – 9176 9235 – 9331 9387 – 9479 9533 – 9621 9674 – 9759	9076 – 9176 9304 – 9397 9517 – 9606 9720 – 9804 9912 – 9993	
140	$P_{B_c^0}^{\Xi_{cc}^{++}}$ $P_{\Xi_b^+}^{\Xi_{bc}^0}$ $P_{D_c^+}^{\Xi_{bc}^0}$ $P_{\pi^+}^{bcc^+}$	$b\bar{d}ccu$	$\Xi_{cc}^{++} B^0$ $\Xi_{bc}^+ D^+$ $bcc^+ \pi^+$	8902	9077 – 9177 9138 – 9237 9199 – 9297 9259 – 9357 9319 – 9416	9077 – 9177 9133 – 9233 9189 – 9288 9245 – 9343 9300 – 9398	9077 – 9177 9236 – 9332 9388 – 9480 9534 – 9622 9675 – 9760	9077 – 9177 9305 – 9398 9518 – 9607 9720 – 9805 9913 – 9994	**
141	$P_{B_c^+}^{\Omega_c^0}$ $P_{\Xi_c^+}^{\Xi_{cc}^0}$ $P_{\Xi_{cc}^0}^{\Xi_{bc}^0}$ $P_{\bar{B}_s^0}^{\Xi_{bc}^0}$	$c\bar{b}css$	$\Omega_c^0 B_c^+$ $\Omega_{cc}^0 \bar{B}_s^0$	8969	9144 – 9244 9229 – 9327 9312 – 9409 9394 – 9490 9475 – 9569	9144 – 9244 9222 – 9321 9299 – 9396 9375 – 9471 9450 – 9544	9144 – 9244 9235 – 9334 9326 – 9424 9415 – 9512 9504 – 9599	9144 – 9244 9276 – 9374 9405 – 9502 9533 – 9628 9659 – 9753	**
142	$P_{\bar{B}_c^-}^{\Omega_c^0}$ $P_{\eta_c(1S)}^{\Omega_b^0}$ $P_{D_s^-}^{\Omega_{bc}^0}$ $P_{\pi_u^0}^{\Omega_{bc}^0}$	$b\bar{c}css$	$\Omega_c^0 \bar{B}_c^-$ $\Omega_b^- \eta_c(1S)$ $\Omega_{bc}^0 D_s^-$	8969 9030	9144 – 9244 9208 – 9308 9272 – 9371 9336 – 9433 9398 – 9495	9144 – 9244 9203 – 9303 9262 – 9361 9321 – 9419 9379 – 9476	9144 – 9244 9281 – 9378 9414 – 9508 9543 – 9634 9668 – 9757	9144 – 9244 9341 – 9436 9528 – 9620 9709 – 9797 9883 – 9968	*
143	$P_{B_s^0}^{\Xi_{cc}^{++}}$ $P_{\Xi_b^+}^{\Xi_{bc}^0}$ $P_{D_s^+}^{\Xi_{bc}^0}$ $P_{K^+}^{bcc^+}$	$b\bar{s}ccu$	$\Xi_{cc}^{++} B_s^0$ $\Xi_{bc}^+ D_s^+$ $bcc^+ K^+$	8989	9164 – 9264 9225 – 9325 9286 – 9385 9347 – 9445 9407 – 9504	9164 – 9264 9221 – 9320 9277 – 9376 9333 – 9431 9389 – 9486	9164 – 9264 9319 – 9415 9468 – 9560 9611 – 9699 9749 – 9834	9164 – 9264 9386 – 9480 9595 – 9684 9794 – 9878 9983 – 10064	**

144	$P_{\bar{B}_c^0}^{\Xi_{cc}^+}$ $P_{\bar{B}_c^0}^{\Omega_{ccc}^+}$	$c\bar{c}cd$	$\Xi_{cc}^+ B_c^+$ $\Omega_{ccc}^+ \bar{B}^0$	9793	9968 – 10068 10038 – 10137 10107 – 10205 10175 – 10272 10243 – 10339	9968 – 10068 10032 – 10131 10096 – 10194 10160 – 10257 10222 – 10318	9968 – 10068 10053 – 10152 10137 – 10235 10220 – 10317 10303 – 10399	9968 – 10068 10090 – 10189 10211 – 10308 10330 – 10426 10448 – 10542	**
145	$P_{\bar{B}_c^0}^{\Xi_{cc}^+}$ $P_{bc}^{\Xi_{bc}^+}$ $\eta_c(1S)$ $P_{D^-}^{bcc^+}$	$b\bar{c}cd$	$\Xi_{cc}^+ \bar{B}_c^-$ $\Xi_{bc}^0 \eta_c(1S)$ $bcc^+ D^-$	9793	9968 – 10068 10022 – 10121 10076 – 10174 10129 – 10227 10182 – 10280	9968 – 10068 10018 – 10117 10067 – 10166 10117 – 10215 10166 – 10264	9968 – 10068 10095 – 10192 10218 – 10313 10339 – 10431 10456 – 10546	9968 – 10068 10150 – 10246 10325 – 10418 10495 – 10584 10658 – 10745	*
146	$P_{\bar{B}_c^0}^{\Xi_{cc}^{++}}$ $P_{bc}^{\Xi_{bc}^+}$ $\eta_c(1S)$ $P_{D^-}^{bcc^+}$	$b\bar{c}cu$	$\Xi_{cc}^{++} \bar{B}_c^-$ $\Xi_{bc}^+ \eta_c(1S)$ $bcc^+ \bar{D}^0$	9896	10071 – 10171 10128 – 10228 10186 – 10284 10242 – 10340 10299 – 10396	10071 – 10171 10124 – 10223 10177 – 10276 10229 – 10327 10281 – 10379	10071 – 10171 10195 – 10292 10316 – 10411 10434 – 10527 10549 – 10640	10071 – 10171 10249 – 10346 10421 – 10514 10587 – 10677 10748 – 10835	*
147	$P_{\bar{B}_c^0}^{\Xi_{cc}^{++}}$ $P_{bc}^{\Xi_{bc}^+}$ $P_{D^-}^{bcc^+}$	$c\bar{c}cu$	$\Xi_{cc}^{++} B_c^+$ $\Omega_{ccc}^+ B^-$	9896	10071 – 10171 10140 – 10239 10208 – 10306 10275 – 10372 10342 – 10438	10071 – 10171 10134 – 10233 10197 – 10295 10260 – 10357 10321 – 10418	10071 – 10171 10155 – 10254 10238 – 10336 10320 – 10418 10402 – 10498	10071 – 10171 10192 – 10291 10311 – 10409 10429 – 10525 10545 – 10640	**
148	$P_{\eta_b(1S)}^{\Lambda_c^+}$ $P_{bc}^{\Sigma_b^0}$ $P_{bc}^{\Xi_b^+}$ $P_{D^-}^{\Xi_b^0}$ $P_{bc}^{\Xi_b^-}$	$b\bar{b}cd$	$\Lambda_c^+ \eta_b(1S)$ $\Sigma_b^0 B_c^+$ $\Xi_{bc}^+ \bar{B}^0$ $\Xi_{bc}^0 B^-$	11685	11860 – 11960 11922 – 12021 11984 – 12082 12045 – 12142 12106 – 12202	11860 – 11960 11917 – 12017 11974 – 12073 12031 – 12128 12087 – 12184	11860 – 11960 11948 – 12046 12034 – 12132 12120 – 12216 12205 – 12300	11860 – 11960 11986 – 12085 12110 – 12207 12233 – 12328 12353 – 12447	*
149	$P_{\eta_b(1S)}^{\Sigma_c^{++}}$ $P_{bc}^{\Sigma_b^+}$ $P_{bc}^{\Xi_b^+}$ $P_{D^-}^{\Xi_b^-}$	$b\bar{b}cu$	$\Sigma_c^{++} \eta_b(1S)$ $\Sigma_b^+ B_c^+$ $\Xi_{bc}^- B^-$	11853 12085	12028 – 12128 12089 – 12188 12149 – 12247 12209 – 12306 12268 – 12365	12028 – 12128 12084 – 12183 12140 – 12238 12195 – 12293 12250 – 12347	12028 – 12128 12108 – 12207 12187 – 12285 12265 – 12362 12343 – 12439	12028 – 12128 12143 – 12242 12256 – 12354 12368 – 12464 12479 – 12574	*
150	$P_{\eta_b(1S)}^{\Sigma_c^0}$ $P_{bc}^{\Sigma_b^-}$ $P_{bc}^{\Xi_b^+}$ $P_{D^-}^{\Xi_b^0}$	$b\bar{b}dd$	$\Sigma_c^0 \eta_b(1S)$ $\Sigma_b^- B_c^+$ $\Xi_{bc}^0 \bar{B}^0$	11853 12090	12028 – 12128 12089 – 12188 12149 – 12247 12209 – 12306 12268 – 12365	12028 – 12128 12084 – 12183 12140 – 12238 12195 – 12293 12250 – 12347	12028 – 12128 12114 – 12213 12198 – 12296 12282 – 12379 12365 – 12461	12028 – 12128 12151 – 12250 12273 – 12370 12393 – 12488 12510 – 12604	*
151	$P_{\eta_b(1S)}^{\Xi_c^+}$ $P_{bc}^{\Xi_b^0}$ $P_{bc}^{\Xi_b^+}$ $P_{D^-}^{\Xi_b^0}$ $P_{bc}^{\Omega_{bc}^0}$	$b\bar{b}cs$	$\Xi_c^+ \eta_b(1S)$ $\Xi_b^0 B_c^+$ $\Xi_{bc}^0 \bar{B}_s^0$ $\Omega_{bc}^0 B^-$	11867 12066	12042 – 12142 12103 – 12202 12163 – 12261 12222 – 12320 12281 – 12378	12042 – 12142 12098 – 12197 12153 – 12252 12208 – 12306 12263 – 12360	12042 – 12142 12128 – 12227 12213 – 12311 12297 – 12394 12380 – 12476	12042 – 12142 12166 – 12264 12288 – 12385 12408 – 12503 12526 – 12620	*
152	$P_{\eta_b(1S)}^{\Xi_c^0}$ $P_{bc}^{\Xi_b^-}$ $P_{bc}^{\Omega_{bc}^0}$ $P_{D^-}^{\Xi_b^0}$ $P_{bc}^{\Xi_{bb}^0}$	$b\bar{b}cd$	$\Xi_c^0 \eta_b(1S)$ $\Xi_b^- B_c^+$ $\Omega_{bc}^0 \bar{B}_s^0$ $\Xi_{bc}^0 B^-$	11869 12071	12044 – 12144 12105 – 12204 12165 – 12263 12224 – 12322 12283 – 12380	12044 – 12144 12100 – 12199 12155 – 12254 12210 – 12308 12265 – 12362	12044 – 12144 12130 – 12229 12215 – 12313 12299 – 12396 12382 – 12478	12044 – 12144 12168 – 12266 12290 – 12387 12410 – 12505 12528 – 12622	*
153	$P_{bc}^{\Xi_b^0}$ $P_{bc}^{\Xi_b^-}$ $P_{D_s^-}^{\Xi_{bb}^0}$ $P_{D_s^0}^{\Omega_{bb}^0}$	$b\bar{c}bs$	$\Xi_b^0 \bar{B}_c^-$ $\Xi_{bb}^0 D_s^-$ $\Omega_{bb}^- \bar{D}^0$	12066	12241 – 12341 12332 – 12429 12421 – 12515 12507 – 12599 12591 – 12682	12241 – 12341 12325 – 12423 12407 – 12502 12487 – 12580 12565 – 12656	12241 – 12341 12398 – 12493 12547 – 12638 12690 – 12778 12828 – 12912	12241 – 12341 12465 – 12558 12674 – 12763 12873 – 12956 13061 – 13141	**
154	$P_{bc}^{\Xi_b^-}$ $P_{D_s^-}^{\Omega_{bb}^0}$ $P_{D_s^-}^{\Xi_{bb}^0}$	$b\bar{c}bd$	$\Xi_b^- \bar{B}_c^-$ $\Omega_{bb}^- D^-$ $\Xi_{bb}^- D_s^-$	12071	12246 – 12346 12337 – 12434 12425 – 12520 12511 – 12604 12596 – 12686	12246 – 12346 12330 – 12427 12412 – 12507 12492 – 12585 12570 – 12661	12246 – 12346 12358 – 12456 12468 – 12563 12574 – 12668 12679 – 12770	12246 – 12346 12407 – 12504 12563 – 12656 12713 – 12804 12860 – 12948	**
155	$P_{bc}^{\Sigma_b^+}$ $P_{D_s^-}^{\Xi_b^0}$ $P_{D_s^0}^{\Xi_{bb}^0}$	$b\bar{c}bu$	$\Sigma_b^+ \bar{B}_c^-$ $\Xi_{bb}^0 \bar{D}^0$	12085	12260 – 12360 12350 – 12448 12439 – 12533 12524 – 12617 12608 – 12699	12260 – 12360 12344 – 12441 12425 – 12520 12505 – 12598 12582 – 12674	12260 – 12360 12365 – 12463 12469 – 12565 12570 – 12664 12669 – 12762	12260 – 12360 12412 – 12509 12559 – 12653 12702 – 12794 12841 – 12931	**
156	$P_{bc}^{\Sigma_b^-}$ $P_{D_s^-}^{\Xi_b^0}$ $P_{D_s^0}^{\Xi_{bb}^0}$	$b\bar{c}bdd$	$\Sigma_b^- \bar{B}_c^-$ $\Xi_{bb}^- D^-$	12090	12265 – 12365 12355 – 12453 12443 – 12538 12529 – 12622 12613 – 12703	12265 – 12365 12348 – 12446 12430 – 12525 12509 – 12602 12587 – 12678	12265 – 12365 12418 – 12513 12564 – 12655 12704 – 12792 12839 – 12924	12265 – 12365 12483 – 12577 12688 – 12777 12883 – 12968 13068 – 13149	**

157	$P_{\eta_b(1S)}^{\Omega_c^0}$ $P_{B_c^+}^{\Omega_b^-}$ $P_{\bar{B}_s^0}^{\Omega_{bc}^0}$	$b\bar{b}css$	$\Omega_c^0 \eta_b(1S)$ $\Omega_b^- B_c^+$ $\Omega_{bc}^0 \bar{B}_s^0$	12094 12320	12269 – 12369 12328 – 12427 12386 – 12484 12444 – 12542 12501 – 12598	12269 – 12369 12323 – 12422 12377 – 12476 12430 – 12528 12483 – 12581	12269 – 12369 12350 – 12449 12430 – 12528 12510 – 12607 12588 – 12685	12269 – 12369 12386 – 12484 12501 – 12598 12614 – 12710 12726 – 12821	*
158	$P_{\bar{B}_c^-}^{\Omega_b^-}$ $P_{D_s^-}^{\Omega_{bb}^0}$	$b\bar{c}bss$	$\Omega_b^- \bar{B}_c^-$ $\Omega_{bb}^0 D_s^-$	12320	12495 – 12595 12580 – 12677 12662 – 12758 12743 – 12837 12822 – 12914	12495 – 12595 12573 – 12671 12649 – 12745 12724 – 12819 12798 – 12890	12495 – 12595 12608 – 12705 12718 – 12813 12825 – 12918 12931 – 13022	12495 – 12595 12657 – 12754 12814 – 12907 12965 – 13055 13112 – 13200	**
159	$P_{\eta_b(1S)}^{\Xi_{cc}^{++}}$ $P_{B_c^+}^{\Xi_{bc}^0}$ $P_{\bar{B}_s^0}^{bcc^+}$	$b\bar{b}ccd$	$\Xi_{cc}^+ \eta_b(1S)$ $\Xi_{bc}^0 B_c^+$ $bcc^+ \bar{B}_s^0$	12918	13093 – 13193 13146 – 13245 13199 – 13297 13251 – 13349 13303 – 13400	13093 – 13193 13142 – 13241 13190 – 13289 13239 – 13337 13287 – 13384	13093 – 13193 13170 – 13269 13247 – 13345 13323 – 13420 13398 – 13494	13093 – 13193 13204 – 13303 13314 – 13412 13423 – 13519 13530 – 13625	*
160	$P_{\eta_b(1S)}^{\Xi_{cc}^{++}}$ $P_{B_c^+}^{\Xi_{bc}^+}$ $P_{\bar{B}_s^0}^{bcc^+}$	$b\bar{b}ccu$	$\Xi_{cc}^{++} \eta_b(1S)$ $\Xi_{bc}^+ B_c^+$ $bcc^+ B^-$	13021	13196 – 13296 13248 – 13348 13300 – 13399 13352 – 13450 13403 – 13501	13196 – 13296 13244 – 13344 13292 – 13391 13340 – 13438 13387 – 13485	13196 – 13296 13272 – 13371 13348 – 13446 13423 – 13520 13497 – 13594	13196 – 13296 13306 – 13405 13415 – 13512 13522 – 13618 13628 – 13723	*
161	$P_{B_c^0}^{bcc^+}$ $P_{D_s^+}^{bbc^0}$	$b\bar{d}bcc$	$bcc^+ B^0$ $bbc^0 D^+$						**
162	$P_{B_c^-}^{bbc^0}$ $P_{\eta_c(1S)}^{bbc^-}$	$b\bar{c}bbc$	$bbc^0 \bar{B}_c^-$ $bbb^- \eta_c(1S)$						*
163	$P_{B_c^+}^{bbc^0}$ $P_{D_s^-}^{bbc^-}$	$b\bar{u}bbc$	$bbc^0 B^+$ $bbb^- D^0$						**
164	$P_{\eta_b(1S)}^{\Omega_{cc}^+}$ $P_{B_c^+}^{\Omega_{bc}^0}$ $P_{\bar{B}_s^0}^{bcc^+}$	$b\bar{b}ccs$	$\Omega_{cc}^+ \eta_b(1S)$ $\Omega_{bc}^0 B_c^+$ $bcc^+ \bar{B}_s^0$						*
165	$P_{\bar{B}_s^0}^{bcc^+}$ $P_{D_s^+}^{bbc^0}$	$b\bar{s}bcc$	$bcc^+ B_s^0$ $bbc^0 D_s^+$						**
166	$P_{\bar{B}_c^-}^{\Xi_{bc}^0}$ $P_{\eta_c(1S)}^{\Xi_{bb}^-}$ $P_{D_s^-}^{bbc^0}$	$b\bar{c}bcd$	$\Xi_{bc}^0 \bar{B}_c^-$ $\Xi_{bb}^- \eta_c(1S)$ $bbc^0 D^-$						*
167	$P_{B_c^0}^{\Omega_{cc}^+}$ $P_{D_s^+}^{\Omega_{bc}^0}$ $P_{\phi(1020)}^{bcc^+}$	$b\bar{s}ccs$	$\Omega_{cc}^+ B_s^0$ $\Omega_{bc}^0 D_s^+$ $bcc^+ \phi(1020)$						
168	$P_{B_c^0}^{bbc^0}$ $P_{D_s^+}^{bbb^-}$	$b\bar{d}bbc$	$bbc^0 B^0$ $bbb^- D^+$						**
169	$P_{B_c^+}^{\Omega_{cc}^0}$ $P_{D_s^0}^{\Omega_{bb}^-}$ $P_{K_-}^{bbc^0}$	$b\bar{u}bcs$	$\Omega_{cc}^0 B^+$ $\Omega_{bb}^- D^0$ $bbc^0 K^-$						**
170	$P_{B_c^+}^{\Xi_{bc}^+}$ $P_{D_s^0}^{\Xi_{bb}^0}$ $P_{\pi_0}^{bbc^0}$	$b\bar{u}bcu$	$\Xi_{bc}^+ B^+$ $\Xi_{bb}^0 D^0$ $bbc^0 \pi_u^0$						
171	$P_{B_c^0}^{\Xi_{bc}^+}$ $P_{D_s^+}^{\Xi_{bb}^0}$ $P_{\pi_0}^{bbc^0}$	$b\bar{d}bcu$	$\Xi_{bc}^+ B^0$ $\Xi_{bb}^0 D^+$ $bbc^0 \pi^+$						**
172	$P_{B_s^0}^{\Omega_{ccc}^{++}}$ $P_{D_s^+}^{bcc^+}$	$b\bar{s}ccc$	$\Omega_{ccc}^{++} B_s^0$ $bcc^+ D_s^+$						**
173	$P_{\bar{B}_c^-}^{\Xi_{bb}^0}$ $P_{D_s^0}^{bbc^+}$	$b\bar{c}bbu$	$\Xi_{bb}^0 \bar{B}_c^-$ $bbb^- \bar{D}^0$						**
174	$P_{\bar{B}_c^-}^{\Xi_{bb}^+}$ $P_{D_s^-}^{bbc^-}$	$b\bar{c}bbd$	$\Xi_{bb}^- \bar{B}_c^-$ $bbb^- D^-$						**

175	$P_{\eta_b(1S)}^{\Xi_{bc}^+}$ $P_{B_c^0}^{\Xi_{bb}^+}$ $P_{B_c^0}^{B_c^+}$ $P_{B_c^0}^{bbc^0}$	$b\bar{b}cu$	$\Xi_{bc}^+ \eta_b(1S)$ $\Xi_{bb}^0 B_c^+$ $bbc^0 B^-$						*
176	$P_{B_c^0}^{\Xi_{bc}^0}$ $P_{B_c^0}^{\Xi_{bb}^+}$ $P_{D_s^0}^{\Xi_{bb}^-}$ $P_{B_c^0}^{bbc^0}$	$b\bar{u}bcd$	$\Xi_{bc}^0 B^+$ $\Xi_{bb}^0 D^0$ $bbc^0 \pi^-$						**
177	$P_{B_c^0}^{\Omega_{bc}^0}$ $P_{D_s^+}^{\Omega_{bb}^-}$ $P_{K_0^0}^{bbc^0}$	$b\bar{d}bcs$	$\Omega_{bc}^0 B^0$ $\Omega_{bb}^0 D^+$ $bbc^0 \bar{K}^0$						**
178	$P_{\bar{B}_c^-}^{bbc^-}$	$b\bar{c}bbb$	$bbb^- \bar{B}_c^-$						**
179	$P_{B_s^0}^{\Xi_{bc}^0}$ $P_{D_s^+}^{\Xi_{bb}^-}$ $P_{K_0^0}^{bbc^0}$	$b\bar{s}bcd$	$\Xi_{bc}^0 B_s^0$ $\Xi_{bb}^- D_s^+$ $bbc^0 K^0$						**
180	$P_{B_c^0}^{\Omega_{cc}^+}$ $P_{D_s^+}^{\Omega_{bc}^0}$ $P_{K_0^0}^{bcc^+}$	$b\bar{d}ccs$	$\Omega_{cc}^+ B^0$ $\Omega_{bc}^0 D^+$ $bcc^+ \bar{K}^0$						**
181	$P_{\eta_b(1S)}^{bbc^+}$ $P_{B_c^+}^{bbc^0}$	$b\bar{b}bcc$	$bcc^+ \eta_b(1S)$ $bbc^0 B_c^+$						*
182	$P_{\eta_b(1S)}^{\Xi_{bc}^0}$ $P_{B_c^0}^{\Xi_{bb}^-}$ $P_{B_c^0}^{bbc^0}$	$b\bar{b}bcd$	$\Xi_{bc}^0 \eta_b(1S)$ $\Xi_{bb}^- B_c^+$ $bbc^0 \bar{B}^0$						*
183	$P_{\bar{B}_c^-}^{\Omega_{bb}^-}$ $P_{D_s^-}^{bbc^-}$	$b\bar{c}bbs$	$\Omega_{bb}^- \bar{B}_c^-$ $bbb^- D_s^-$						**
184	$P_{\eta_b(1S)}^{bbc^0}$ $P_{B_c^+}^{bbc^-}$	$b\bar{b}bbc$	$bbc^0 \eta_b(1S)$ $bbb^- B_c^+$						*
185	$P_{\bar{B}_c^-}^{\Sigma_b^0}$ $P_{D_s^-}^{\Xi_{bb}^0}$ $P_{\bar{D}^0}^{\Xi_{bb}^-}$	$b\bar{c}bdu$	$\Sigma_b^0 \bar{B}_c^-$ $\Xi_{bb}^0 D^-$ $\Xi_{bb}^- \bar{D}^0$						**
186	$P_{D_0^0}^{\Omega_{ccc}^{++}}$	$c\bar{u}ccc$	$\Omega_{ccc}^{++} D^0$						**
187	$P_{\eta_c(1S)}^{\Omega_{cc}^+}$ $P_{D_s^-}^{\Omega_{ccc}^{++}}$	$c\bar{c}ccs$	$\Omega_{cc}^+ \eta_c(1S)$ $\Omega_{ccc}^{++} D_s^-$						*
188	$P_{B_c^+}^{\Omega_{ccc}^{++}}$	$c\bar{b}ccc$	$\Omega_{ccc}^{++} B_c^+$						**
189	$P_{\bar{B}_c^-}^{bcc^+}$ $P_{\eta_c(1S)}^{bbc^0}$	$b\bar{c}bcc$	$bcc^+ \bar{B}_c^-$ $bbc^0 \eta_c(1S)$						*
190	$P_{\bar{B}_c^-}^{\Omega_{cc}^+}$ $P_{\eta_c(1S)}^{\Omega_{bc}^0}$ $P_{D_s^-}^{bcc^+}$	$b\bar{c}ccs$	$\Omega_{cc}^+ \bar{B}_c^-$ $\Omega_{bc}^0 \eta_c(1S)$ $bcc^+ D_s^-$						*
191	$P_{B_c^0}^{\Xi_{bc}^0}$ $P_{D_s^+}^{\Xi_{bb}^-}$ $P_{K_0^0}^{bbc^0}$	$b\bar{d}bcd$	$\Xi_{bc}^0 B^0$ $\Xi_{bb}^- D^+$ $bbc^0 \pi_d^0$						
192	$P_{\bar{B}_c^-}^{\Xi_{bc}^+}$ $P_{\eta_c(1S)}^{\Xi_{bb}^0}$ $P_{\bar{D}^0}^{bbc^0}$	$b\bar{c}bcu$	$\Xi_{bc}^+ \bar{B}_c^-$ $\Xi_{bb}^0 \eta_c(1S)$ $bbc^0 \bar{D}^0$						*
193	$P_{D_0^0}^{\Omega_{cc}^+}$ $P_{K_-}^{\Omega_{ccc}^{++}}$	$c\bar{u}ccs$	$\Omega_{cc}^+ D^0$ $\Omega_{ccc}^{++} K^-$						**

194	$P_{\bar{B}_c^-}^{\Omega_{bc}^0}$ $P_{\eta_c(1S)}^{\Omega_{bb}^-}$ $P_{D_s^-}^{bbc^0}$	$b\bar{c}bcs$	$\Omega_{bc}^0 \bar{B}_c^-$ $\Omega_{bb}^- \eta_c(1S)$ $b b c^0 D_s^-$						*
195	$P_{\bar{B}_c^-}^{\Omega_{ccc}^+}$ $P_{\eta_c(1S)}^{bbc^+}$ $P_{D_s^+}^{bcc^0}$	$b\bar{c}ccc$	$\Omega_{ccc}^+ \bar{B}_c^-$ $bcc^+ \eta_c(1S)$						*
196	$P_{D_s^+}^{\Omega_{cc}^+}$ $P_{K_0^+}^{\Omega_{ccc}^+}$ $P_{\bar{K}_0^-}^{bcc^0}$	$c\bar{d}ccs$	$\Omega_{cc}^+ D^+$ $\Omega_{ccc}^+ \bar{K}^0$						**
197	$P_{B_s^0}^{\Omega_{ccc}^+}$ $P_{D_s^+}^{bcc^+}$ $P_{D_s^0}^{bcc^0}$	$b\bar{d}ccc$	$\Omega_{ccc}^+ B^0$ $bcc^+ D^+$						**
198	$P_{B_s^+}^{\Omega_{ccc}^+}$ $P_{D_s^0}^{bcc^+}$ $P_{D_s^0}^{bcc^0}$	$b\bar{u}ccc$	$\Omega_{ccc}^+ B^+$ $bcc^+ D^0$						**
199	$P_{D_s^+}^{\Omega_{ccc}^+}$	$c\bar{d}ccc$	$\Omega_{ccc}^+ D^+$						**
200	$P_{B_s^+}^{\Omega_{cc}^+}$ $P_{D_s^0}^{\Omega_{bc}^0}$ $P_{K_0^-}^{bcc^+}$ $P_{\bar{K}_0^+}^{bcc^0}$	$b\bar{u}ccs$	$\Omega_{cc}^+ B^+$ $\Omega_{bc}^0 D^0$ $bcc^+ K^-$						**
201	$P_{D_s^+}^{\Omega_{ccc}^+}$	$c\bar{s}ccc$	$\Omega_{ccc}^+ D_s^+$						**
202	$P_{B_s^0}^{bbc^0}$ $P_{D_s^+}^{bbb^-}$ $P_{D_s^0}^{bbc^+}$	$b\bar{s}bbc$	$bbc^0 B_s^0$ $bbb^- D_s^+$						**
203	$P_{B_s^+}^{bcc^+}$ $P_{D_s^0}^{bbc^0}$ $P_{D_s^0}^{bbc^0}$	$b\bar{u}bcc$	$bcc^+ B^+$ $bbc^0 D^0$						**
204	$P_{B_s^0}^{\Xi_{bc}^+}$ $P_{D_s^+}^{\Xi_{bb}^0}$ $P_{K_0^+}^{\Xi_{bc}^0}$ $P_{\bar{K}_0^+}^{bbc^0}$	$b\bar{s}bcu$	$\Xi_{bc}^+ B_s^0$ $\Xi_{bb}^0 D_s^+$ $bbc^0 K^+$						**
205	$P_{\eta_c(1S)}^{\Omega_{ccc}^+}$	$c\bar{c}ccc$	$\Omega_{ccc}^+ \eta_c(1S)$						*
206	$P_{B_s^0}^{\Omega_{bb}^0}$ $P_{D_s^+}^{\Omega_{bb}^-}$ $P_{\phi(1020)}^{bbc^0}$	$b\bar{s}bcs$	$\Omega_{bc}^0 B_s^0$ $\Omega_{bb}^- D_s^+$ $bbc^0 \phi(1020)$						
207	$P_{D_s^+}^{\Omega_{cc}^+}$ $P_{\phi(1020)}^{\Omega_{ccc}^+}$	$c\bar{s}ccs$	$\Omega_{cc}^+ D_s^+$ $\Omega_{ccc}^+ \phi(1020)$						
208	$P_{\eta_b(1S)}^{\Omega_{ccc}^+}$ $P_{B_s^+}^{bcc^+}$ $P_{B_c^+}^{bcc^+}$	$b\bar{b}ccc$	$\Omega_{ccc}^+ \eta_b(1S)$ $bcc^+ B_c^+$						*
209	$P_{B_s^0}^{\Omega_{cc}^+}$ $P_{\bar{B}_s^0}^{\Omega_{ccc}^+}$ $P_{\bar{B}_s^0}^{bbc^0}$	$c\bar{b}ccs$	$\Omega_{cc}^+ B_c^+$ $\Omega_{ccc}^+ \bar{B}_s^0$						**
210	$P_{\eta_b(1S)}^{\Omega_{bc}^0}$ $P_{B_c^+}^{\Omega_{bb}^+}$ $P_{B_s^0}^{bbc^0}$ $P_{B_s^0}^{\Omega_{bc}^0}$	$b\bar{b}bcs$	$\Omega_{bc}^0 \eta_b(1S)$ $\Omega_{bb}^+ B_c^+$ $bbc^0 \bar{B}_s^0$						*

Table 223: Pentaquarks configurations, predictions and thresholds.

8 Summary and Conclusions

In this paper we use the HISH model in order to tame the zoo of exotic hadrons in particular tetraquarks and pentaquarks. We enlist 71 candidates of tetraquark states and 210 candidates of pentaquarks. For a great part of them we determine the corresponding HISH modefied Regge trajectory. Out of the 71 tetraquark states we compute a trajectory with 5 states, thus predicting 240 new tetraquarks. We added another additional 5 states for genuine and semi-genuine tetraquarks, with another 350 states. For 160 candidate states of the pentaquarks we determine for each 5 states on the J trajectory and 5 in the n trajectory thus predicting

altogether 1600 new pentaquark states.

The basic structure of the stringy mesons occurs also for the stringy tetraquarks. However, whereas for the mesons the predominantly decay mechanism is the breakup of the string into two strings, namely a transition from a meson to two mesons, for the tetraquarks there is an additional mechanism of the annihilation of a BV and an anti-BV. In the latter case the result of the decay of the tetraquark are two mesons, in the former the output is a baryon and an anti-baryon. Thus, for the tetraquarks, unlike for the mesons, the states on a trajectory are divided into two classes the lower mass one where the decay is via annihilation into two mesons and the higher mass one where in addition there is the mechanism of string breaking. In section (4.3) we have mentioned another mechanism that involves an annihilation of a quark from the di-quark and an anti-quark from the anti-diquark. This is the analog of a similar mechanism that takes place in the Zweig suppressed decay of heavy quarkonia [13].

The stringy structure of baryons is based on a single string connecting a quark to a BV which is attached to a di-quark. On the other hand for the pentaquarks there are two possible structures: one similar to the baryon with a single BV and the other with two strings connecting an anti-BV in the center to two BVs on both sides. These two structures provide a large number of options of the spectra and of the decay processes.

Our procedure of determining the HMRTs is based on the assumption that the first tetraquark state that can decay into a baryon and an anti-baryon is of a mass that is higher than that of the baryonic threshold by 40-150 MEV. This is based on the few cases with such a decay that have been already discovered. Using this assumption we can determine the approximated value of the intercept. It is clear that once there will be more such states found, we will be able to improve the determination of the corresponding intercept and slope and hence improvement of the whole trajectory.

According to our survey there are of the order of thousand candidates of tetraquarks and pentaquarks. This obviously calls for an intensive effort to experimentally identify these resonance states. This should be done in the running experiments and may also call for a new experiment designed specially for the exotic hadrons. This can obviously be of much lower energy than the one used in the LHC.

This was a data driven project, where we tried to unify all the available exotic candidates under the HISH framework in order to systematically predict tetraquark and pentaquark modified Regge trajectories. The overall result allows us to provide a "map" that locates exotic states energy-wise, guiding future searches for exotic candidates. As more data will be accumulated, we will be able to improve our model predictions. The assumptions that tetraquarks α' is similar to that of mesons, was in general good as can be seen from the global tetraquarks-mesons fit 7.3. The slope of $T_{c\bar{c}c\bar{c}}$ was the only one that didn't fit this assumption, and we fit it separately. This requires further research. Another interesting outcome, is that the predictions of the HMRTs of tetraquarks that decay to baryons that weren't found yet could potentially allow us to predict where to search for these baryons. This is also a result that should be analysed in future work. One important results from past papers [7], [32] is that the excitation in the two planes J and n are different. This implies multiple HMRTs for each state and could explain resonances that are close in energy, but doesn't rely exactly on the same trajectory. The results for the pentaquarks candidates were not far from the baryonic trajectories as we expected, but they remain inconclusive since there isn't enough data to determine if they rely on a trajectory. Another observation to note is that the pentaquarks configurations, as baryons, are ambiguous in their internal division (in which quarks occupy each of the endpoints). The multiple resonances observed with content $c\bar{c}uud$ may be explained as a mix of some of these configurations.

9 Open Questions

Applying the HISH model to the study of exotic hadrons and in particular tetraquarks and pentaquarks is still in a preliminary phase and there are many open questions related to it. Here we enumerate several such questions.

- Probably the most important question is whether the stringy description of exotic hadrons is the “right” way to view them and not just as a bound states of elementary particles. Of course the string picture includes particles at the endpoints of the strings but it is only with the strings that one can get a faithful description of the spectra and decay widths.
- The HISH model, both for ordinary hadrons, as well as for exotic ones, lacks a theoretical account of the intercept, namely, the Casimir energy. As was explained in section 2 hadron phenomenology implies a negative $\tilde{a} = a - S$, which provides a repulsion that balances the string tension for non-rotating strings. Ordinary bosonic string admits a positive intercept. The theory of QCD strings,namly, flux tubes has been only partially revealed. One may hope that acquiring more data about the experimental values of the intercepts will be useful in determining the full quantum theory of the stringy hadrons including controlling the repulsive Casimir forces.
- Whereas for the breaking of the string decay process we can determine the decay width using a string calculation, for the annihilation process we do not have yet an exact procedure which provides such a calculation and so far we have been using a “crude approximation” of it.
- In fact the zoo of exotic hadrons is divided into two classes: genuine exotic hadrons and molecules. In the stringy description the former are described by connected stringy diagrams whereas the latter by disconnected diagrams. The simplest molecules, in the HISH picture take the form of two disconnected strings. In this paper we have discussed only genuine exotic states. In our future research we intend to address the description of molecules in the HISH framework in particular the analog of the Van der Waals forces that bind separate ”atom strings” into molecules.
- One of the most interesting questions is: could there exist in nature a stable (against strong decays) exotic hadron. This means, for instance for a tetraquark, with mass that is lower than that of the two possible lightest daughter mesons. In [118] it was argued that the tetraquark (b, b, \bar{u}, \bar{d}) should be stable. This statement got a support from lattice [119] and large N_c [120] calculations. In this paper we have investigated charmed tetraquark and hence did not address this particular state. In the future, with a better insight on the intercepts, one should in principle be able to determine whether, and in what conditions, can a stable exotic charmed hadron exist.
- The HISH model that we have utilized is a simplified HISH model where we have not taken into account explicitly the electric charges[22] and spins [121] and [122] of the endpoint particles. These properties, in particular the spin, play an important role in the determinations of the trajectories of the exotic hadrons. In the present work we used the data about the intercepts, which depend on these properties, from the experimental results about non-exotic hadrons. The structure of the di-quarks attached to the BVs where not play any significant role apart from its total mass. The simplified model that we used should be improved by taking into account the latter properties.
- For the pentaquarks unlike the tetraquarks there are two possible structures. One based on a single BV and the other with an anti-BV and two BVs. It will be interesting, based

on theoretical calculations or on observational data to get a better understanding of who out or the two options is preferable. Distinguishing between the two options will be relevant for the constructions of stringy states with higher baryon number. This question was discussed recently in [29].

- At present exotic hadrons have been discovered in the LHC and in low energy charm and bottom factories. It is very probable that many more exotic hadrons will be discovered if special purpose experiments are constructed for that mission. For instance the breaking process of tetraquarks producing a baryon anti-baryon pairs, may hint that a proton anti-proton machine of low energies or may be adequate for that purpose.
- We have mentioned in section (3) that there may exist hadrons which are even more exotic than tetraquarks and pentaquarks. These include exotic glueballs, hadrons of higher number of quarks like heptaquarks etc and string states of hadrons with baryon number $B > 1$ like the sexaquarks [23].
- The phenomena of hadronization of quark gluon fluid, for instance in heavy ion collisions or in the evolution of the early universe incorporate productions of hadrons in the form of glueballs and hadrons. If the description of hadrons in terms of strings, in particular in the HISH model. there should be also exotic hadrons like tetraquarks and pentaquarks coming out of the quark gluon fluid. It will be interesting to search for them in these experiments and to determine their abundance in comparison with ordinary hadrons
- A very important aspect of elementary particle physics that the HISH model has not been capable yet to account for is the electro-weak interaction. This is a drawback of the model in the context of ordinary hadrons as well as for exotic ones. They challenge is use the holographic setup of multiflavor QCD-like theories and deduce from it the way the HISH model has to be modified to accommodate also the weak interactions. Related to his problem is the incorporation of leptons in the stringy picture of hadrons.

10 Acknowledgment

We would like to thank O. Andreev, S. Dubovsky, G. Farrar, M. Karliner, M. Peskin and especially D. Weissman, for useful discussions. We also thank O. Andreev, S. Nussinov, A. Sofer, D. Weissman and specially M. Karliner for their comments on the manuscript. This work was supported by a center of excellence of the Israel Science Foundation (grant number 2289/18). J.S would like to thank the c.c.p.p of NYU and the Simons Center at Stony Brook, where part of this work was done, for support.

References

- [1] Hua-Xing Chen, Wei Chen, Xiang Liu, and Shi-Lin Zhu. The hidden-charm pentaquark and tetraquark states. *Phys. Rept.*, 639:1–121, 2016.
- [2] A. Esposito, A. Pilloni, and A. D. Polosa. Multiquark Resonances. *Phys. Rept.*, 668:1–97, 2017.
- [3] Marek Karliner, Jonathan L. Rosner, and Tomasz Skwarnicki. Multiquark States. *Ann. Rev. Nucl. Part. Sci.*, 68:17–44, 2018.
- [4] Stephen Lars Olsen, Tomasz Skwarnicki, and Daria Ziemska. Nonstandard heavy mesons and baryons: Experimental evidence. *Rev. Mod. Phys.*, 90(1):015003, 2018.

- [5] Nora Brambilla, Simon Eidelman, Christoph Hanhart, Alexey Nefediev, Cheng-Ping Shen, Christopher E. Thomas, Antonio Vairo, and Chang-Zheng Yuan. The XYZ states: experimental and theoretical status and perspectives. *Phys. Rept.*, 873:1–154, 2020.
- [6] Nora Brambilla et al. Substructure of Multiquark Hadrons (Snowmass 2021 White Paper). 3 2022.
- [7] Jacob Sonnenschein and Dorin Weissman. Rotating strings confronting PDG mesons. *Journal of High Energy Physics*, 2014(8), aug 2014.
- [8] Jacob Sonnenschein and Dorin Weissman. A rotating string model versus baryon spectra. *JHEP*, 02:147, 2015.
- [9] Jacob Sonnenschein and Dorin Weissman. Glueballs as rotating folded closed strings. *Journal of High Energy Physics*, 2015(12):1–43, dec 2015.
- [10] Jacob Sonnenschein and Dorin Weissman. A tetraquark or not a tetraquark? a holography inspired stringy hadron (HISH) perspective. *Nuclear Physics B*, 920:319–344, jul 2017.
- [11] Jacob Sonnenschein. Holography inspired stringy hadrons. *Progress in Particle and Nuclear Physics*, 92:1–49, jan 2017.
- [12] Jacob Sonnenschein and Dorin Weissman. Quantizing the rotating string with massive endpoints. *Journal of High Energy Physics*, 2018(6), jun 2018.
- [13] Jacob Sonnenschein and Dorin Weissman. The decay width of stringy hadrons. *Nuclear Physics B*, 927:368–454, feb 2018.
- [14] P. D. B. Collins. *An Introduction to Regge Theory and High-Energy Physics*. Cambridge Monographs on Mathematical Physics. Cambridge Univ. Press, Cambridge, UK, 5 2009.
- [15] Johanna Erdmenger, Nick Evans, Ingo Kirsch, and Ed Threlfall. Mesons in Gauge/Gravity Duals - A Review. *Eur. Phys. J. A*, 35:81–133, 2008.
- [16] G. C. Rossi and G. Veneziano. Tetra-quarks, penta-quarks and the like: old and new views. *Nucl. Part. Phys. Proc.*, 312-317:140–145, 2021.
- [17] Keiji Kikkawa, Tsuneyuki Kotani, Masa-aki Sato, and Masakatsu Kenmoku. Semiclassical Approach to the Quark String Model and the Hadron Spectrum. 2. Baryons and Exotic Hadrons. *Phys. Rev. D*, 19:1011, 1979.
- [18] F. Bigazzi, A. L. Cotrone, L. Martucci, and L. A. Pando Zayas. Wilson loop, Regge trajectory and hadron masses in a Yang-Mills theory from semiclassical strings. *Phys. Rev. D*, 71:066002, 2005.
- [19] D. Ebert, R. N. Faustov, and V. O. Galkin. Spectroscopy and Regge trajectories of heavy baryons in the relativistic quark-diquark picture. *Phys. Rev. D*, 84:014025, 2011.
- [20] Oleg Andreev. Toward a stringy description for the QQ^-qq^- -quark system. *Phys. Rev. D*, 106(6):066002, 2022.
- [21] Yasuhiro Hayashi, Takahiro Ogino, Tadakatsu Sakai, and Shigeki Sugimoto. Stringy excited baryons in holographic quantum chromodynamics. *PTEP*, 2020(5):053B04, 2020.

- [22] Jacob Sonnenschein, Dorin Weissman, and Shimon Yankielowicz. The scattering amplitude of stringy hadrons: strings with opposite charges on their endpoints. *JHEP*, 07:156, 2020.
- [23] Glennys R. Farrar. Stable Sexaquark. 8 2017.
- [24] Jacob Sonnenschein and Dorin Weissman. Deciphering the recently discovered tetraquark candidates around 6.9 GeV. *The European Physical Journal C*, 81(1), jan 2021.
- [25] Feng-Kun Guo, Christoph Hanhart, Ulf-G. Meißner, Qian Wang, Qiang Zhao, and Bing-Song Zou. Hadronic molecules. *Rev. Mod. Phys.*, 90(1):015004, 2018. [Erratum: Rev.Mod.Phys. 94, 029901 (2022)].
- [26] T. Gutsche S. Eidelman, C. Hanhart, and R.E. Mitchell. Review of Particle Physics. *PTEP*, 2022:083C01, 2022.
- [27] M.Karliner and T. Skwarnicki. Review of Particle Physics. *PTEP*, 2022:083C01, 2022.
- [28] Oleg Andreev. $Q\bar{Q}qqq^-$ quark system, compact pentaquark, and gauge/string duality. *Phys. Rev. D*, 107(2):026023, 2023.
- [29] Oleg Andreev. $Q\bar{Q}qqq$ Quark System, Compact Pentaquark, and Gauge/String Duality (Part II). 6 2023.
- [30] Kasper Peeters, Jacob Sonnenschein, and Marija Zamaklar. Holographic decays of large-spin mesons. *Journal of High Energy Physics*, 2006(02):009–009, feb 2006.
- [31] Ofer Aharony. The non-ads/non-cft correspondence, or three different paths to qcd, 2003.
- [32] Jacob Sonnenschein and Dorin Weissman. Rotating strings confronting PDG mesons. *Journal of High Energy Physics*, 2014(8), aug 2014.
- [33] Y. Kinar, E. Schreiber, and J. Sonnenschein. Q anti-Q potential from strings in curved space-time: Classical results. *Nucl. Phys. B*, 566:103–125, 2000.
- [34] Martin Kruczenski, Leopoldo A. Pando Zayas, Jacob Sonnenschein, and Diana Vaman. Regge trajectories for mesons in the holographic dual of large-N(c) QCD. *JHEP*, 06:046, 2005.
- [35] Ofer Aharony and Zohar Komargodski. The Effective Theory of Long Strings. *JHEP*, 05:118, 2013.
- [36] Alexander M. Polyakov. Fine Structure of Strings. *Nucl. Phys. B*, 268:406–412, 1986.
- [37] Alan Chodos and Charles B. Thorn. Making the Massless String Massive. *Nucl. Phys. B*, 72:509–522, 1974.
- [38] I. Bars and Andrew J. Hanson. Quarks at the Ends of the String. *Phys. Rev. D*, 13:1744–1760, 1976.
- [39] Joseph Polchinski and Andrew Strominger. Effective string theory. *Phys. Rev. Lett.*, 67:1681–1684, 1991.
- [40] Jacob Sonnenschein and Dorin Weissman. Excited mesons, baryons, glueballs and tetraquarks: predictions of the holography inspired stringy hadron model. *The European Physical Journal C*, 79(4), apr 2019.

- [41] Simeon Hellerman and Ian Swanson. String Theory of the Regge Intercept. *Phys. Rev. Lett.*, 114(11):111601, 2015.
- [42] Edward Witten. Baryons and branes in anti-de Sitter space. *JHEP*, 9807:006, 1998.
- [43] A. Brandhuber, N. Itzhaki, J. Sonnenschein, and S. Yankielowicz. Baryons from supergravity. *JHEP*, 07:020, 1998.
- [44] Shigenori Seki and Jacob Sonnenschein. Comments on Baryons in Holographic QCD. *JHEP*, 01:053, 2009.
- [45] G. S. Sharov. Four various string baryon models and regge trajectories, 1998.
- [46] Gerard 't Hooft. Minimal strings for baryons, 2004.
- [47] G. S. Sharov. Quasirotational motions and stability problem in the dynamics of string hadron models. *Physical Review D*, 62(9), oct 2000.
- [48] V. P. Petrov and G. S. Sharov. Rotational stability of linear string baryon configuration, 1998.
- [49] G. S. Sharov. Quasirotational disturbances of linear string baryon configuration, 2001.
- [50] Jin Dai and Joseph Polchinski. The Decay of Macroscopic Fundamental Strings. *Phys. Lett. B*, 220:387–390, 1989.
- [51] David Mitchell, Bo Sundborg, and Neil Turok. Decays of Massive Open Strings. *Nucl. Phys. B*, 335:621–634, 1990.
- [52] A. Casher, H. Neuberger, and S. Nussinov. Chromoelectric Flux Tube Model of Particle Production. *Phys. Rev. D*, 20:179–188, 1979.
- [53] Jacob Sonnenschein and Dorin Weissman. Excited mesons, baryons, glueballs and tetraquarks: Predictions of the Holography Inspired Stringy Hadron model. *Eur. Phys. J. C*, 79(4):326, 2019.
- [54] Nadav Shrayer. Topics in the Study of Exotic Hadronic Strings 'msc thesis, tel aviv university publications'. 2021.
- [55] Alon Liberman. The location of the baryonic vertex in the HISH model 'msc thesis, tel aviv university publications'. 2019.
- [56] D. Bridges et al. Anti-proton Annihilations in Deuterium at Rest Into Two Pions: Evidence for $\bar{P}N$ Bound States Near Threshold. *Phys. Lett. B*, 180:313–318, 1986.
- [57] M. Ablikim et al. Observation of a resonance X(1835) in $J/\psi \rightarrow \gamma\pi^+\pi^-$. *Phys. Rev. Lett.*, 95:262001, 2005.
- [58] M. Ablikim et al. Observation and Spin-Parity Determination of the X(1835) in $J/\psi \rightarrow \gamma K_S^0 K_S^0 \eta$. *Phys. Rev. Lett.*, 115(9):091803, 2015.
- [59] Medina Ablikim et al. Observation of an anomalous line shape of the $\eta'\pi^+\pi^-$ mass spectrum near the $p\bar{p}$ mass threshold in $J/\psi \rightarrow \gamma\eta'\pi^+\pi^-$. *Phys. Rev. Lett.*, 117(4):042002, 2016.

- [60] R. J. Abrams, R. L. Cool, G. Giacomelli, T. F. Kycia, B. A. Leontic, K. K. Li, and D. N. Michael. Total cross-sections of K+- mesons and anti-protons on nucleons up to 3.3-GeV/c. *Phys. Rev. D*, 1:1917–1935, 1970.
- [61] J. Alspector, K. J. Cohen, W. C. Harrison, B. Maglich, F. Sannes, D. Van Harlingen, G. Cvijanovich, M. Matin, and J. Oostens. High-statistics investigation of the broad t and u peaks in anti-proton interactions. *Phys. Rev. Lett.*, 30:511–514, 1973.
- [62] D. Cutts, M. L. Good, P. D. Grannis, D. Green, Y. Y. Lee, R. Pittman, J. Storer, A. C. Benvenuti, G. C. Fischer, and D. D. Reeder. Anti-Proton-Proton Charge-Exchange Between 1-GeV/c and 3-GeV/c. *Phys. Rev. D*, 17:16, 1978.
- [63] A. V. Anisovich, C. A. Baker, C. J. Batty, D. V. Bugg, C. Hodd, H. C. Lu, V. A. Nikonov, A. V. Sarantsev, V. V. Sarantsev, and B. S. Zou. $I = 0$ $C = +1$ mesons from 1920 to 2410 MeV. *Phys. Lett. B*, 491:47–58, 2000.
- [64] D. Alde et al. Further Study of Mesons Which Decay Into $\omega\omega$. *Phys. Lett. B*, 241:600–604, 1990.
- [65] A. Adamo et al. Meson spectroscopy with anti-neutrons. *Phys. Lett. B*, 287:368–374, 1992.
- [66] D. V. Bugg, I. Scott, B. S. Zou, V. V. Anisovich, A. V. Sarantsev, T. H. Burnett, and S. Sutlief. Further amplitude analysis of $J/\psi \rightarrow \gamma(\pi^+\pi^-\pi^+\pi^-)$. *Phys. Lett. B*, 353:378–384, 1995.
- [67] V. A. Shchegelsky, A. V. Sarantsev, V. A. Nikonov, and A. V. Anisovich. The $K0(S)$ final state in two-photon collisions and SU(3) tensor nonets. *Eur. Phys. J. A*, 27:207–212, 2006.
- [68] Medina Ablikim et al. Observation of a near-threshold enhancement in the $\Lambda\bar{\Lambda}$ mass spectrum from $e^+e^- \rightarrow \phi\Lambda\bar{\Lambda}$ at \sqrt{s} from 3.51 to 4.60 GeV. *Phys. Rev. D*, 104(5):052006, 2021.
- [69] D. V. Bugg. Partial wave analysis of $\bar{p}p \rightarrow \bar{\Lambda}\Lambda$. *Eur. Phys. J. C*, 36:161–168, 2004.
- [70] P. D. Barnes et al. High statistics measurements of the anti-p p \rightarrow anti-Lambda Lambda and anti-p p \rightarrow Lambda Sigma0 + c.c. reactions at threshold. *Phys. Rev. C*, 62:055203, 2000.
- [71] D. Alde et al. Further Study of Mesons Which Decay Into $\omega\omega$. *Phys. Lett. B*, 241:600–604, 1990.
- [72] A. N. Aleev et al. Narrow baryonia with open and hidden strangeness. *Phys. Atom. Nucl.*, 56:1358–1366, 1993.
- [73] A. V. Evdokimov et al. First observation of a narrow charm-strange meson $D+(sJ)(2632) \rightarrow D+(s)\eta$ and $D0\ K+$. *Phys. Rev. Lett.*, 93:242001, 2004.
- [74] Roel Aaij et al. Amplitude analysis of the $B^+ \rightarrow D^+D^-K^+$ decay. *Phys. Rev. D*, 102:112003, 2020.
- [75] R. Aaij et al. First Observation of a Doubly Charged Tetraquark and Its Neutral Partner. *Phys. Rev. Lett.*, 131(4):041902, 2023.

- [76] N. Gabyshev et al. Study of decay mechanisms in $b^- \rightarrow \lambda_c^+ \bar{p} \pi^-$ decays and observation of low-mass structure in the $\lambda_c^+ \bar{p}$ system. *Phys. Rev. Lett.*, 97:242001, 2006.
- [77] B. Aubert et al. Observation of the decay $\bar{B}^0 \rightarrow \lambda_c^+ \bar{p} \pi^0$. *Phys. Rev. D*, 82:031102, 2010.
- [78] Roel Aaij et al. Observation of an exotic narrow doubly charmed tetraquark. *Nature Phys.*, 18(7):751–754, 2022.
- [79] M. Ablikim et al. Study of the process $e^+e^- \rightarrow \pi^0\pi^0 J/\psi$ and neutral charmonium-like state $Z_c(3900)^0$. *Phys. Rev. D*, 102(1):012009, 2020.
- [80] K. Chilikin et al. Observation of a new charged charmoniumlike state in $\bar{B}^0 \beta J/\psi K^- \pi^+$ decays. *Phys. Rev. D*, 90(11):112009, 2014.
- [81] S. K. Choi et al. Observation of a resonance-like structure in the $\pi^\pm \psi'$ mass distribution in exclusive $B \rightarrow K \pi^\pm \psi'$ decays. *Phys. Rev. Lett.*, 100:142001, 2008.
- [82] R. Mizuk et al. Dalitz analysis of $B \rightarrow K \pi^+ \psi'$ decays and the $Z(4430)^+$. *Phys. Rev. D*, 80:031104, 2009.
- [83] K. Chilikin et al. Experimental constraints on the spin and parity of the $Z(4430)^+$. *Phys. Rev. D*, 88(7):074026, 2013.
- [84] Roel Aaij et al. Observation of the resonant character of the $Z(4430)^-$ state. *Phys. Rev. Lett.*, 112(22):222002, 2014.
- [85] M. Ablikim et al. Observation of a Charged Charmoniumlike Structure $Z_c(4020)$ and Search for the $Z_c(3900)$ in $e^+e^- \rightarrow \pi^+\pi^- h_c$. *Phys. Rev. Lett.*, 111(24):242001, 2013.
- [86] M. Ablikim et al. Observation of $e^+e^- \beta \pi^0 \pi^0 h_c$ and a Neutral Charmoniumlike Structure $Z_c(4020)^0$. *Phys. Rev. Lett.*, 113(21):212002, 2014.
- [87] M. Ablikim et al. Observation of a charged charmoniumlike structure in $e^+e^- \rightarrow (D^*\bar{D}^*)^\pm \pi^\mp$ at $\sqrt{s} = 4.26\text{GeV}$. *Phys. Rev. Lett.*, 112(13):132001, 2014.
- [88] R. Mizuk et al. Observation of two resonance-like structures in the $\pi^+ \chi(c1)$ mass distribution in exclusive anti-B0 $\rightarrow K^- \pi^+ \chi(c1)$ decays. *Phys. Rev. D*, 78:072004, 2008.
- [89] X. L. Wang et al. Measurement of $e^+e^- \rightarrow \pi^+\pi^- \psi(2S)$ via Initial State Radiation at Belle. *Phys. Rev. D*, 91:112007, 2015.
- [90] Medina Ablikim et al. Measurement of $e^+e^- \rightarrow \pi^0\pi^0 \psi(3686)$ at \sqrt{s} from 4.009 to 4.600 GeV and observation of a neutral charmoniumlike structure. *Phys. Rev. D*, 97(5):052001, 2018.
- [91] M. Ablikim et al. Measurement of $e^+e^- \rightarrow \pi^+\pi^- \psi(3686)$ from 4.008 to 4.600 GeV and observation of a charged structure in the $\pi^\pm \psi(3686)$ mass spectrum. *Phys. Rev. D*, 96(3):032004, 2017. [Erratum: *Phys. Rev. D* 99, 019903 (2019)].
- [92] Roel Aaij et al. Evidence for an $\eta_c(1S)\pi^-$ resonance in $B^0 \rightarrow \eta_c(1S)K^+\pi^-$ decays. *Eur. Phys. J. C*, 78(12):1019, 2018.
- [93] Roel Aaij et al. Observation of New Resonances Decaying to $J/\psi K^+$ and $J/\psi \phi$. *Phys. Rev. Lett.*, 127(8):082001, 2021.

- [94] R. Aaij et al. Evidence of a J/ψ KS0 Structure in $B0 \rightarrow J/\psi\phi$ KS0 Decays. *Phys. Rev. Lett.*, 131(13):131901, 2023.
- [95] Roel Aaij et al. Observation of a Resonant Structure near the $Ds+Ds-$ Threshold in the $B+ \rightarrow Ds+Ds-K+$ Decay. *Phys. Rev. Lett.*, 131(7):071901, 2023.
- [96] Serguei Chatrchyan et al. Observation of a Peaking Structure in the $J/\psi\phi$ Mass Spectrum from $B^\pm \rightarrow J/\psi\phi K^\pm$ Decays. *Phys. Lett. B*, 734:261–281, 2014.
- [97] Roel Aaij et al. Observation of $J/\psi\phi$ structures consistent with exotic states from amplitude analysis of $B^+ \rightarrow J/\psi\phi K^+$ decays. *Phys. Rev. Lett.*, 118(2):022003, 2017.
- [98] C. P. Shen et al. Evidence for a new resonance and search for the $Y(4140)$ in the gamma gamma $\rightarrow \phi J/\psi$ process. *Phys. Rev. Lett.*, 104:112004, 2010.
- [99] Medina Ablikim et al. Observation of the $Y(4220)$ and $Y(4360)$ in the process $e^+e^- \rightarrow \eta J/\psi$. *Phys. Rev. D*, 102(3):031101, 2020.
- [100] X. L. Wang, Y. L. Han, C. Z. Yuan, C. P. Shen, and P. Wang. Observation of $\psi(4040)$ and $\psi(4160)$ decay into $\eta J/\psi$. *Phys. Rev. D*, 87(5):051101, 2013.
- [101] G. Pakhlova et al. Observation of a near-threshold enhancement in the $e+e^- \rightarrow \Lambda+(c)\bar{\Lambda}-(c)$ cross section using initial-state radiation. *Phys. Rev. Lett.*, 101:172001, 2008.
- [102] Georges Aad et al. Observation of an Excess of Dicharmonium Events in the Four-Muon Final State with the ATLAS Detector. *Phys. Rev. Lett.*, 131(15):151902, 2023.
- [103] Aram Hayrapetyan et al. Observation of new structure in the $J/\psi J/\psi$ mass spectrum in proton-proton collisions at $\sqrt{s} = 13$ TeV. *Nature Physics*, 6:2023.
- [104] Roel Aaij et al. Observation of structure in the J/ψ -pair mass spectrum. *Sci. Bull.*, 65(23):1983–1993, 2020.
- [105] . Amplitude analysis of the $b^+ \rightarrow d^+d^-k^+$ decay. *Physical Review D*, 102(11), dec 2020.
- [106] LHCb collaboration. First observation of a doubly charged tetraquark and its neutral partner, 2022.
- [107] . Observation of an exotic narrow doubly charmed tetraquark. *Nature Physics*, 18(7):751–754, jun 2022.
- [108] Boris A. Gelman and Shmuel Nussinov. Does a narrow tetraquark cc anti-u anti-d state exist? *Phys. Lett. B*, 551:296–304, 2003.
- [109] S. S. Agaev, K. Azizi, and H. Sundu. Near-threshold structures in the $D_s^+D_s^-$ mass distribution of the decay $B^+ \rightarrow D_s^+D_s^-K^+$. *Phys. Rev. D*, 107:094018, May 2023.
- [110] LHCb collaboration. Observation of a resonant structure near the $d_s^+d_s^-$ threshold in the $b^+ \rightarrow d_s^+d_s^-k^+$ decay, 2022.
- [111] . Observation of a peaking structure in the $j/\psi\phi$ mass spectrum from $b(+/-) \rightarrow j/\psi\phi k(+/-)$ decays. *Physics Letters B*, 734:261–281, jun 2014.
- [112] LHCb collaboration. Observation of structure in the j/ψ -pair mass spectrum. *Science Bulletin*, 65(23):1983–1993, dec 2020.

- [113] The CMS collaboration. Observation of new structures in the $j/\psi j/\psi$ mass spectrum in pp collisions at $\sqrt{s} = 13$ tev. *Cern*, Jul 2022.
- [114] . Observation of $j/\psi p$ resonances consistent with pentaquark states in $\lambda_b^0 \rightarrow j/\psi k^- p$ decays. *Physical Review Letters*, 115(7), aug 2015.
- [115] . Observation of a narrow pentaquark state, $p_c(4312)^+$, and of two-peak structure of the $p_c(4450)^+$. *Physical Review Letters*, 122(22), jun 2019.
- [116] R. Aaij et al. Observation of a $j/\psi \Lambda$ resonance consistent with a strange pentaquark candidate in $B^- \rightarrow j/\psi \Lambda \bar{p}$ decays. *Phys. Rev. Lett.*, 131:031901, Jul 2023.
- [117] K. Azizi, Y. Sarac, and H. Sundu. Investigation of the strange pentaquark candidate $p_{\psi s}^\Lambda(4338)^0$ recently observed by lhcb, 2023.
- [118] Marek Karliner and Jonathan L. Rosner. Discovery of doubly-charmed Ξ_{cc} baryon implies a stable $(bb\bar{u}\bar{d})$ tetraquark. *Phys. Rev. Lett.*, 119(20):202001, 2017.
- [119] Estia J. Eichten and Chris Quigg. Heavy-quark symmetry implies stable heavy tetraquark mesons $Q_i Q_j \bar{q}_k \bar{q}_l$. *Phys. Rev. Lett.*, 119(20):202002, 2017.
- [120] Andrzej Czarnecki, Bo Leng, and M. B. Voloshin. Stability of tetrons. *Phys. Lett. B*, 778:233–238, 2018.
- [121] F. A. Berezin and M. S. Marinov. Particle Spin Dynamics as the Grassmann Variant of Classical Mechanics. *Annals Phys.*, 104:336, 1977.
- [122] R. D. Pisarski and J. D. Stack. Spin Dependent Potential for Heavy Fermions on the Ends of a String. *Nucl. Phys. B*, 286:657–668, 1987.
- [123] Roel Aaij et al. Observation of five new narrow Ω_c^0 states decaying to $\Xi_c^+ K^-$. *Phys. Rev. Lett.*, 118(18):182001, 2017.

A Mesons Fits

In this section we detail the global fits that were done to mesons in order to use the results for predicting tetraquarks spectrum and widths as detailed in 6.3. The states that were used for the fits are detailed in table 229, which are the states for (J, M^2) plane. Table 232 contain the states used for the fits in the (n, M^2) plane¹³.

As explained in 6.5, for the tetraquarks predictions, we did a global for each of the planes - (J, M^2) , (n, M^2) and once for both. In the first two, we constrained the endpoint masses according to the quarks content (e.g. m_s was forced as m_1 and m_2 of ϕ/f' as well as m_1 of K^*). We also constrained α' of all light mesons to be the same, as well as the heavy mesons. In the common global fit, we constrained only the endpoint masses, but allowed the α' parameters to differ between the two planes, yet preserving the same light/heavy separation for each.

The degree-of-conformity of each global fit, as well as the parameters the fits emitted, are in table 224. It can be seen that the global fit used didn't change most of the parameters significantly, nor worsen χ^2_r significantly with respect to (n, M^2) fit. The only parameter that changed significantly is $m_{u/d}$, but its mass wasn't strict in the first place as discussed in [7].

For the global fit for both planes, we performed the fit once with the light/heavy slopes constrain and once without it. The parameters emitted almost didn't change. The results are presented in 224.

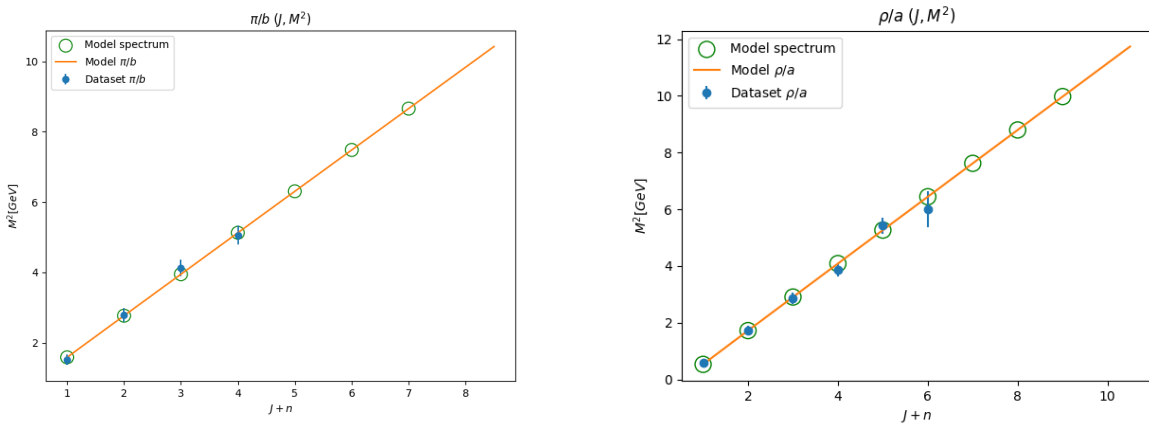
¹³Some of the states in the trajectories above were omitted, see [7] A.1 for full explanation.

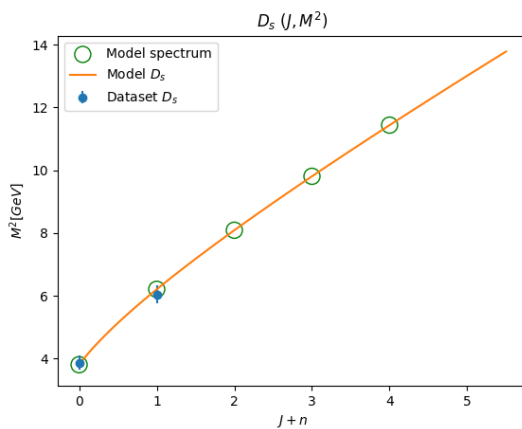
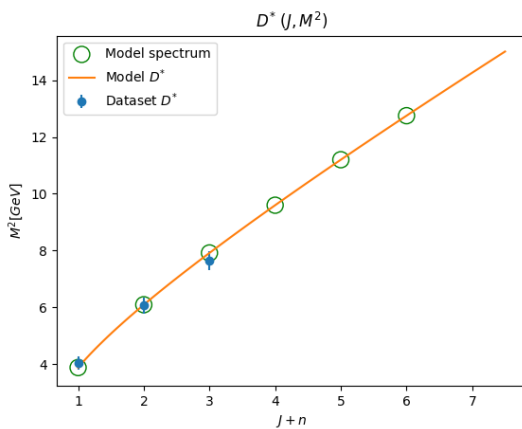
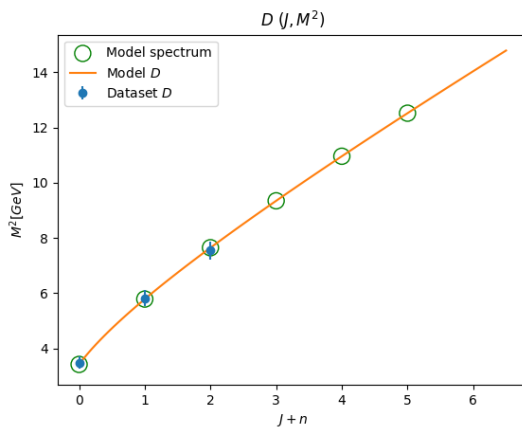
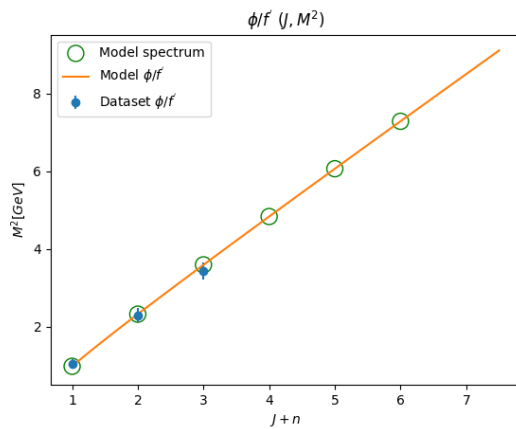
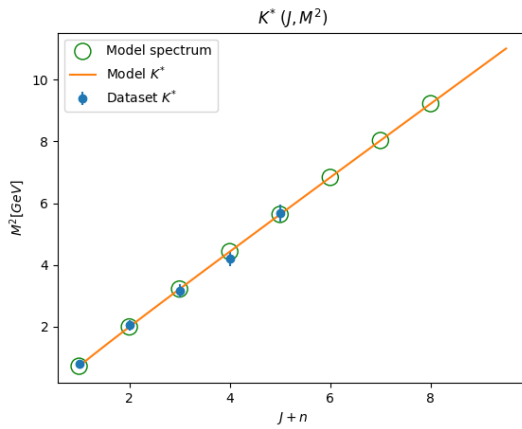
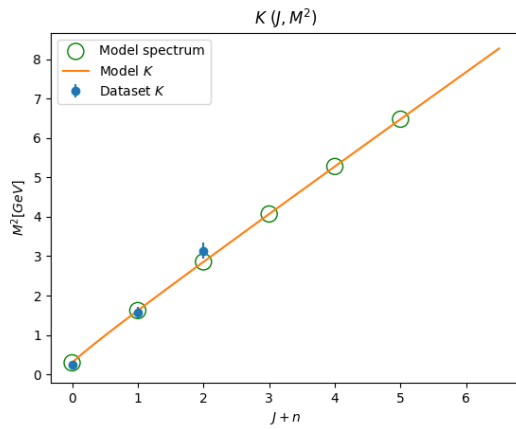
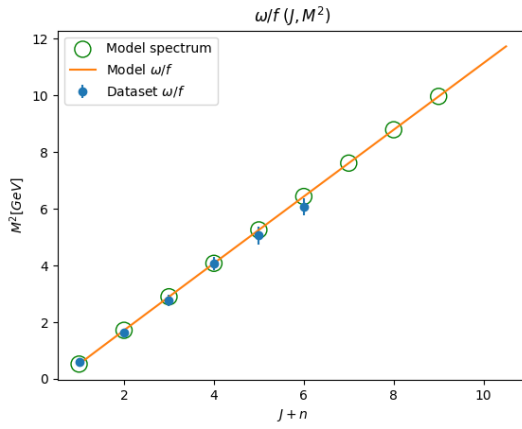
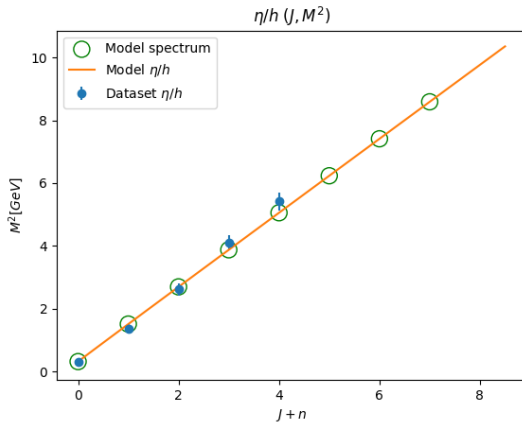
	χ^2_r	α'_{light} [GeV $^{-2}$]	$m_{u/d}$ [GeV]	m_s [GeV]	α'_{heavy} [GeV $^{-2}$]	m_c [GeV]	m_b [GeV]
(J, M^2)	0.60	0.85	0.05	0.25	0.80	1.43	4.73
(n, M^2)	1.35	0.91	0.01	0.51	0.49	1.29	4.76
(J, M^2)	1.63	0.83	0.013	0.36	0.65	1.11	4.71
(n, M^2)		0.86			0.45		

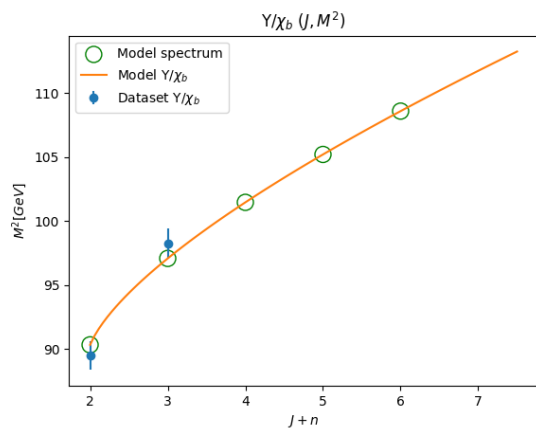
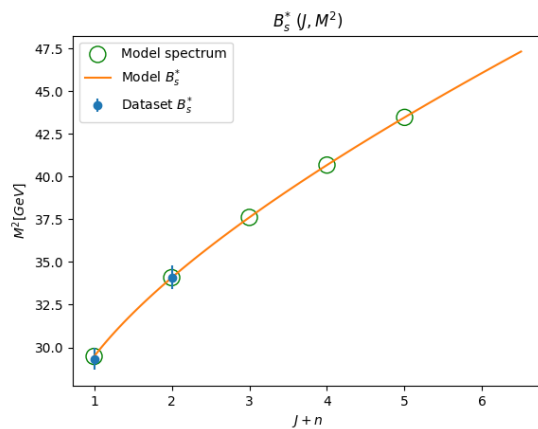
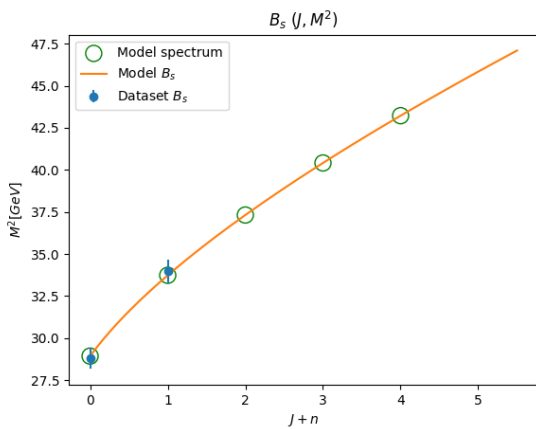
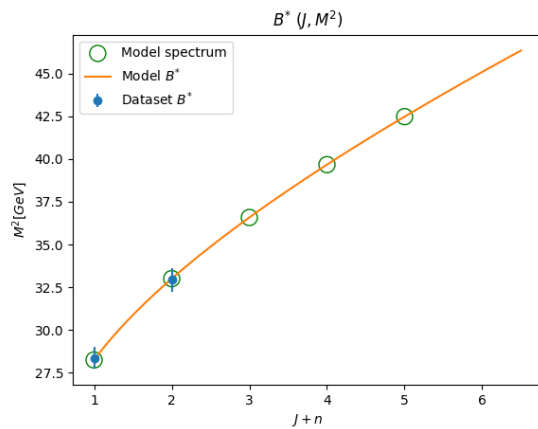
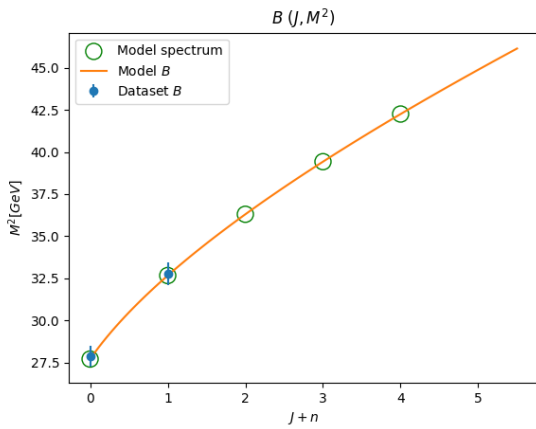
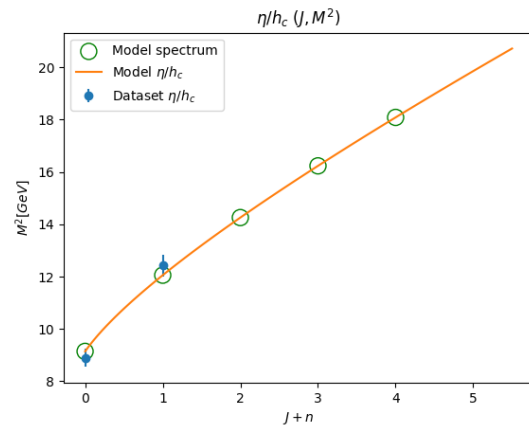
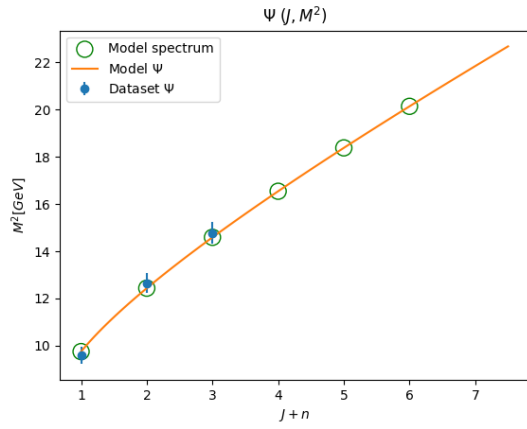
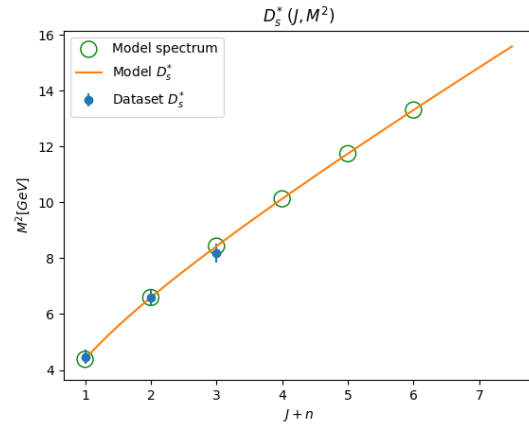
Table 224: The mesons global fit results for both planes - (J, M^2) and (n, M^2) . The first row are the HISH model parameters of the best fit in the (J, M^2) plane. The second row are the HISH model parameters of the best fit in the (n, M^2) plane, and the last row are the output parameters of the combined global fit in both planes, assuming the masses are common, but the slopes are different.

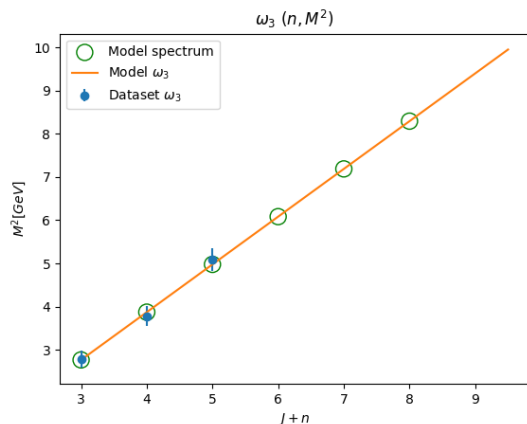
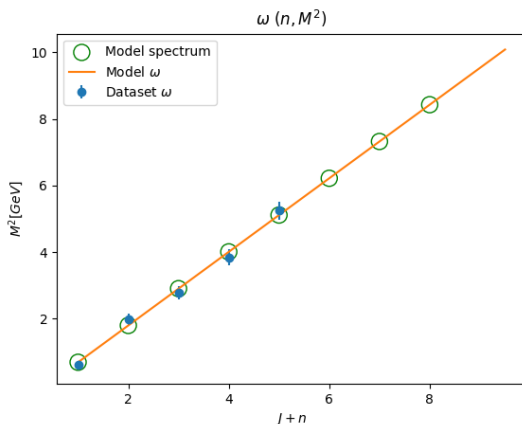
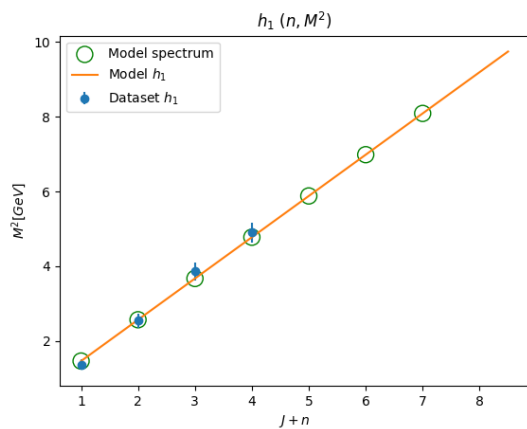
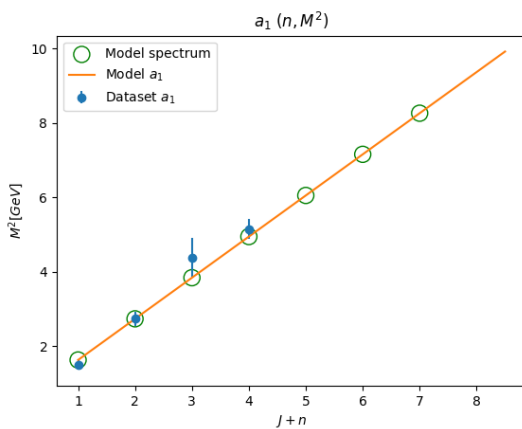
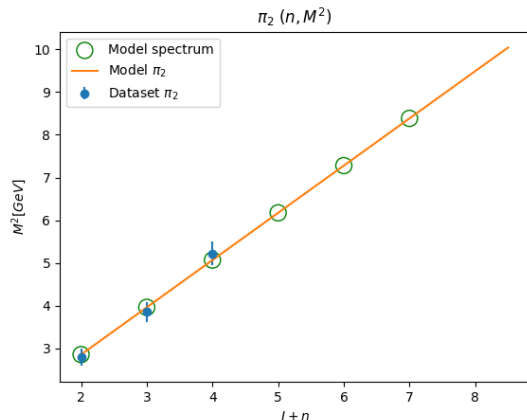
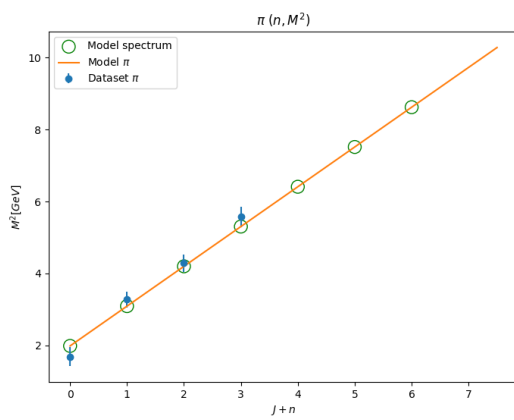
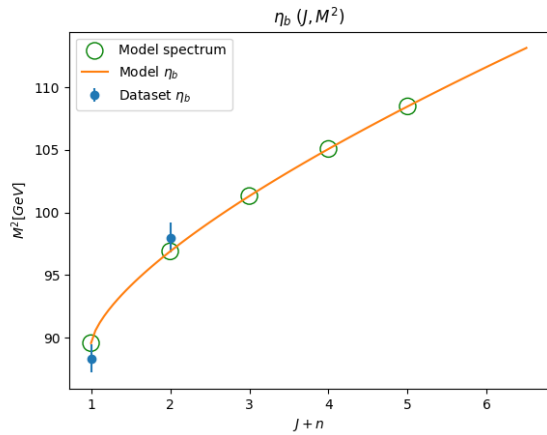
Traj.	a n/J only	a global	Traj.	a n/J only	a global	Traj.	a n/J only	a global
π/b	$a_J = -0.30$	-0.39	η_c/h_c	$a_J = -0.15$	-1.41	ω_3	$a_n = 0.50$	0.79
ρ/a	$a_J = 0.59$	0.51	B	$a_J = -0.41$	-0.35	ϕ	$a_n = 0.98$	0.69
η/h	$a_J = -0.23$	-0.30	B^*	$a_J = 0.50$	0.60	K	$a_n = -1.15$	-1.28
ω/f	$a_J = 0.60$	0.53	B_s	$a_J = -0.40$	-0.19	K^*	$a_n = 0.86$	0.76
K	$a_J = -0.09$	0.02	B_s^*	$a_J = 0.51$	0.76	K_0^*	$a_n = -0.22$	-0.34
K^*	$a_J = 0.61$	0.71	Υ/χ_b	$a_J = 1.97$	1.93	D_1^{*0}	$a_n = 0.64$	0.50
ϕ/f'	$a_J = 0.59$	0.86	η_b	$a_J = 1.00$	0.64	Ψ	$a_n = 1.39$	0.87
D	$a_J = -0.23$	-0.64	π	$a_n = -1.80$	-1.55	B_c	$a_n = 0.76$	0.44
D^*	$a_J = 0.61$	0.23	π_2	$a_n = -0.58$	-0.25	χ_{c2}	$a_n = 1.29$	1.04
D_s	$a_J = -0.20$	-0.44	a_1	$a_n = -0.48$	-0.30	Υ	$a_n = 0.88$	1.49
D_s^*	$a_J = 0.60$	0.39	h_1	$a_n = -0.32$	-0.12	χ_{b1}	$a_n = 1.37$	1.19
Ψ/χ_c	$a_J = 0.68$	-0.65	ω	$a_n = 0.38$	0.55			

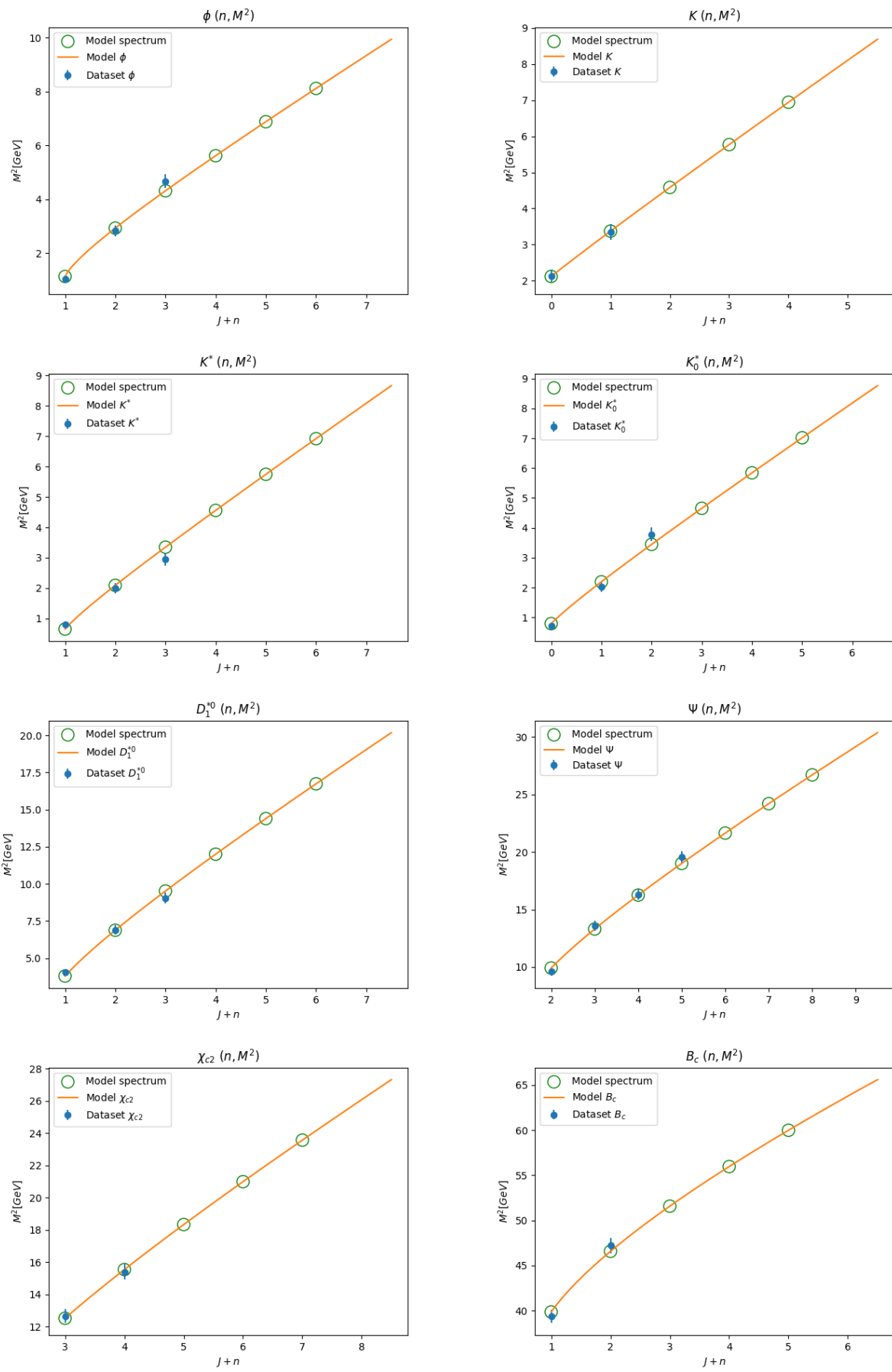
Table 225: Mesons global fits intercepts. a_J marks that the Traj was done in the (J, M^2) plane. "a global" column contains the results of the global fit for both planes.

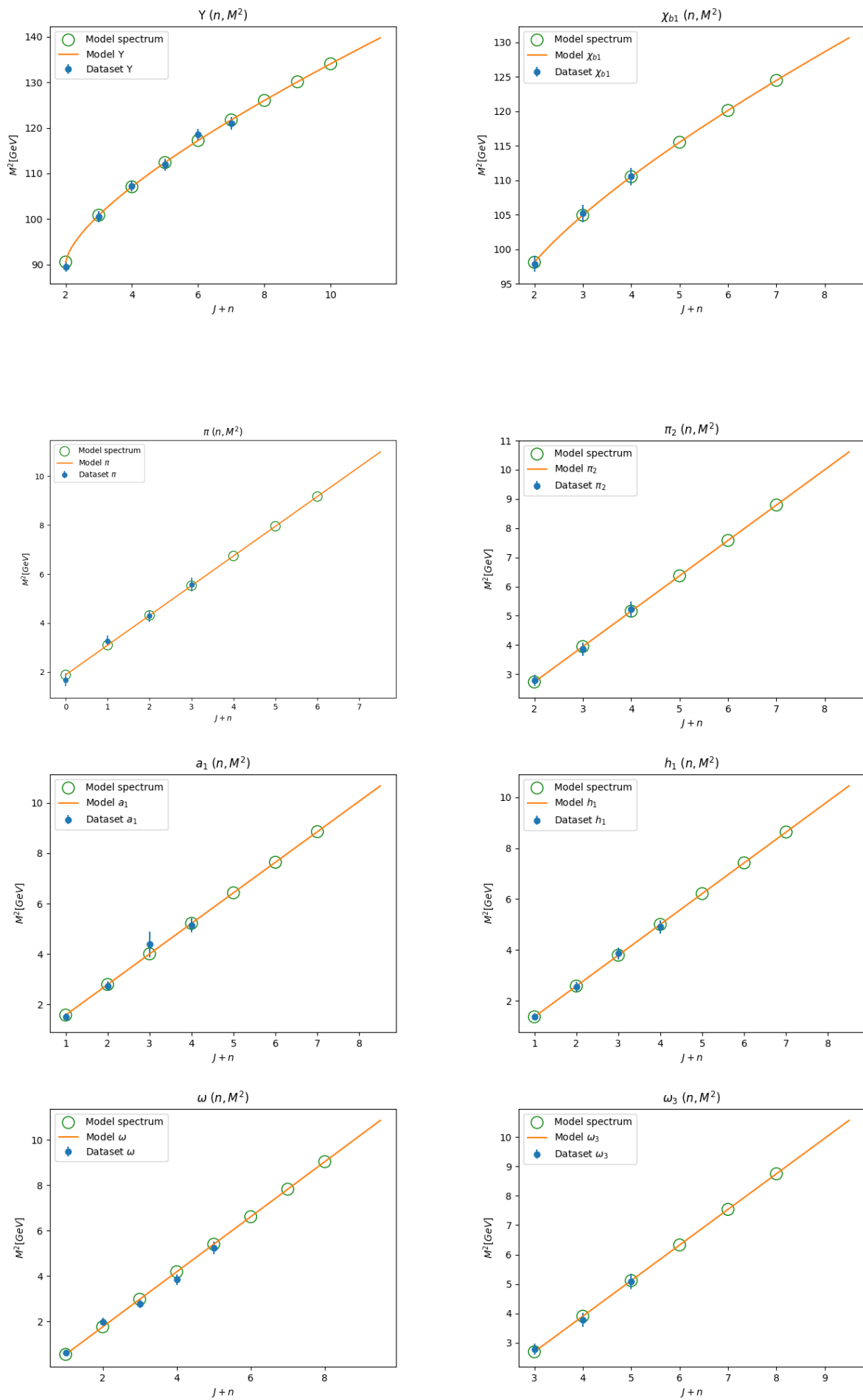


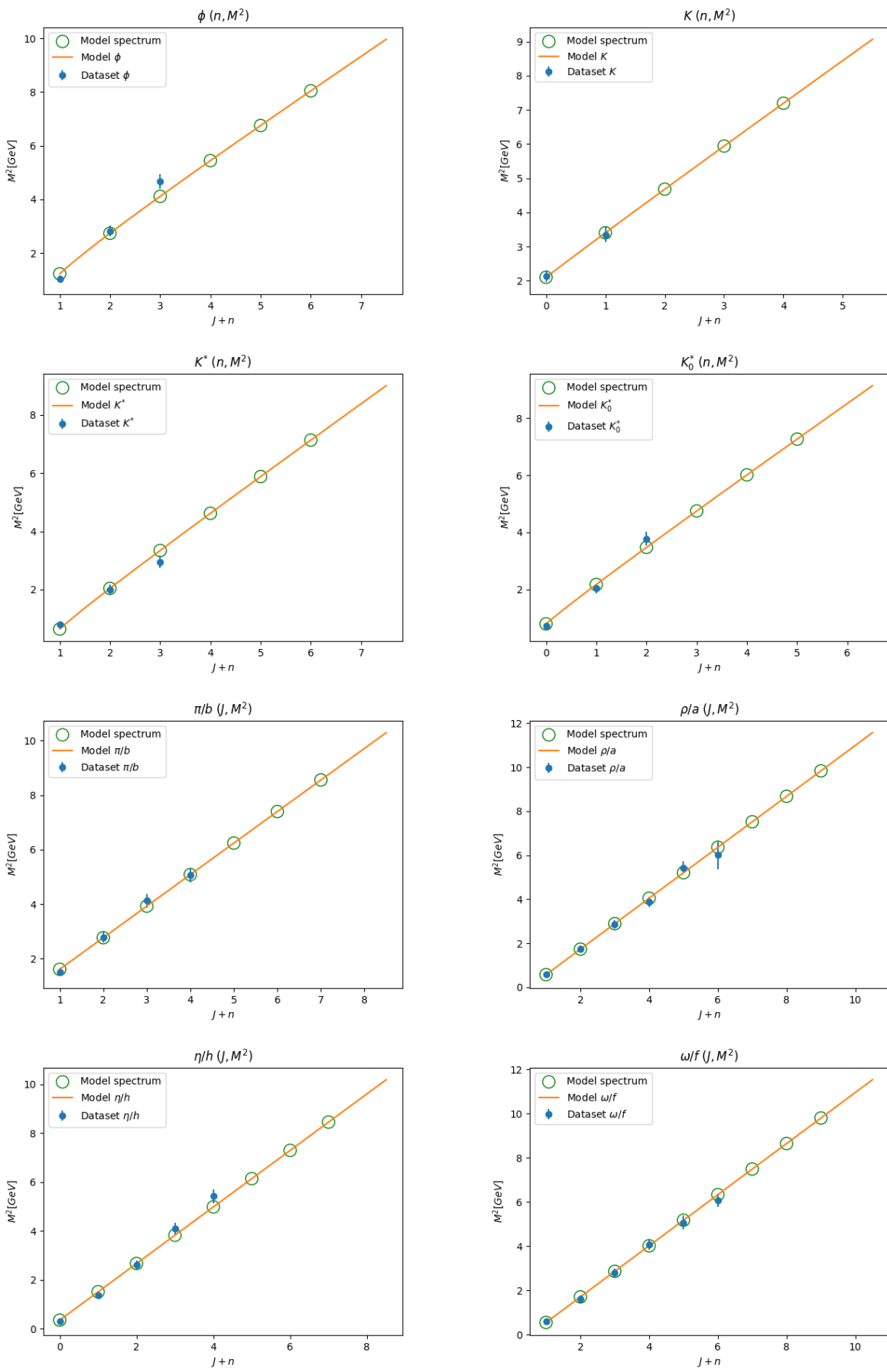


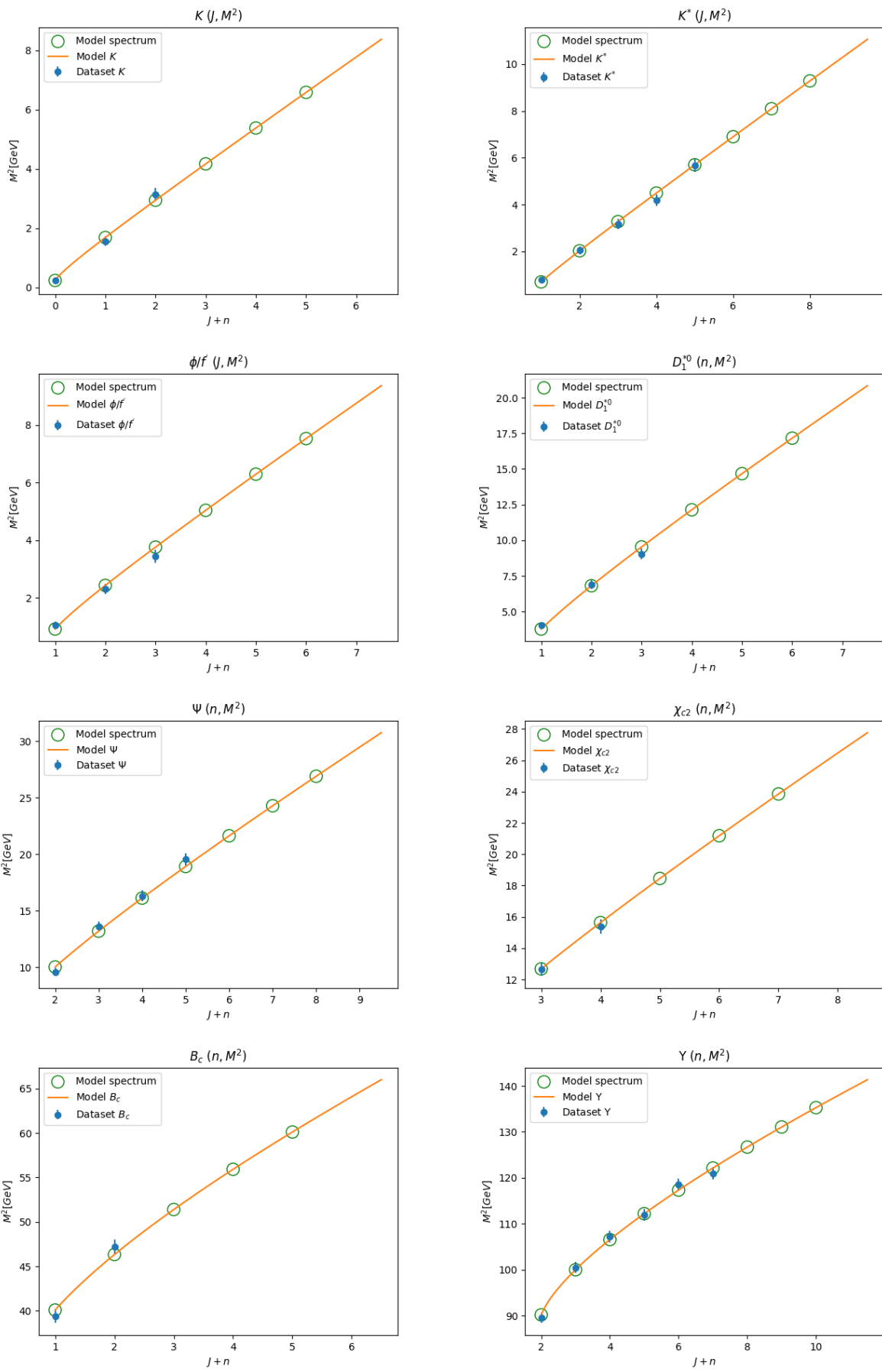


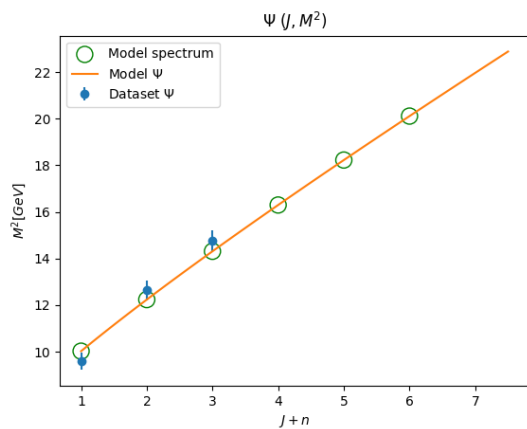
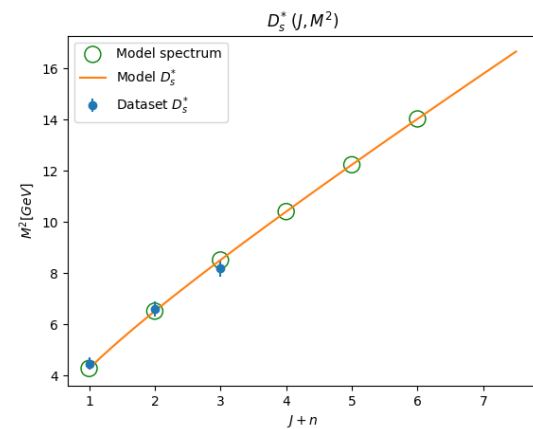
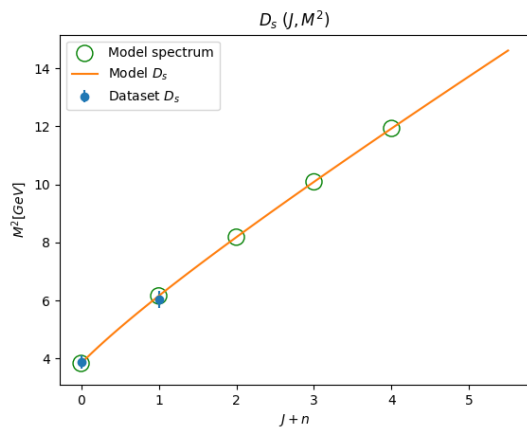
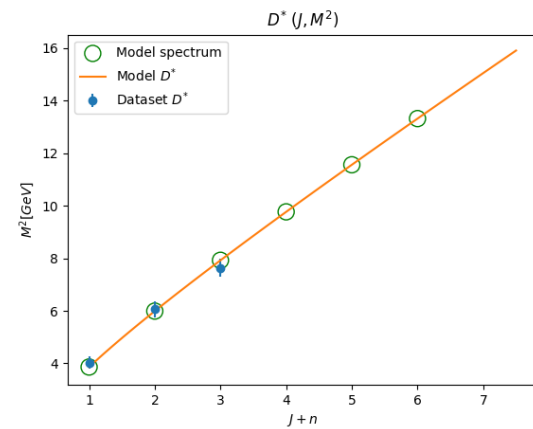
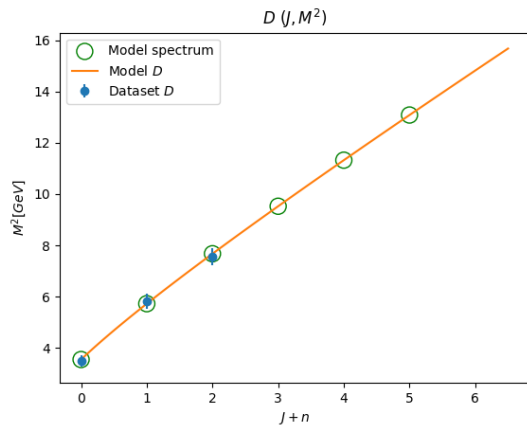
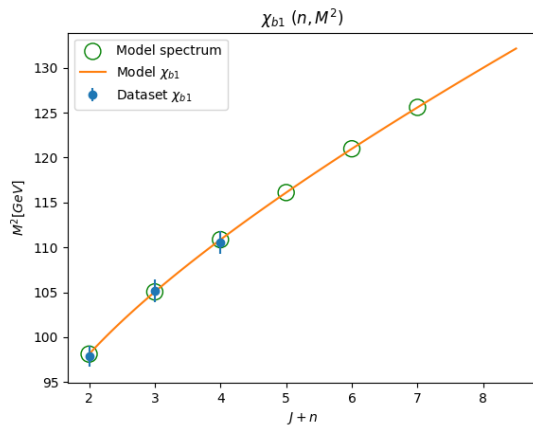
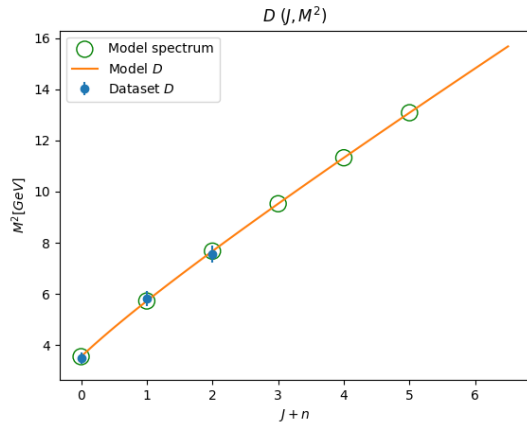
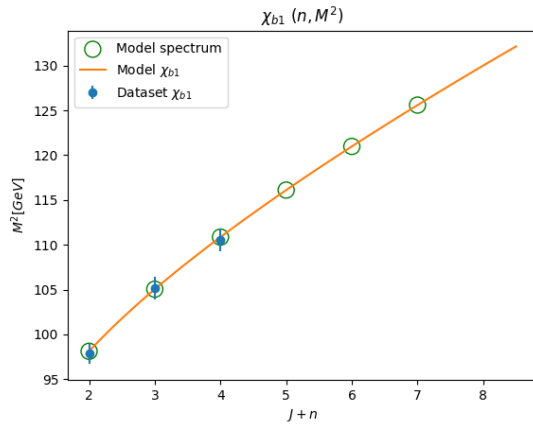


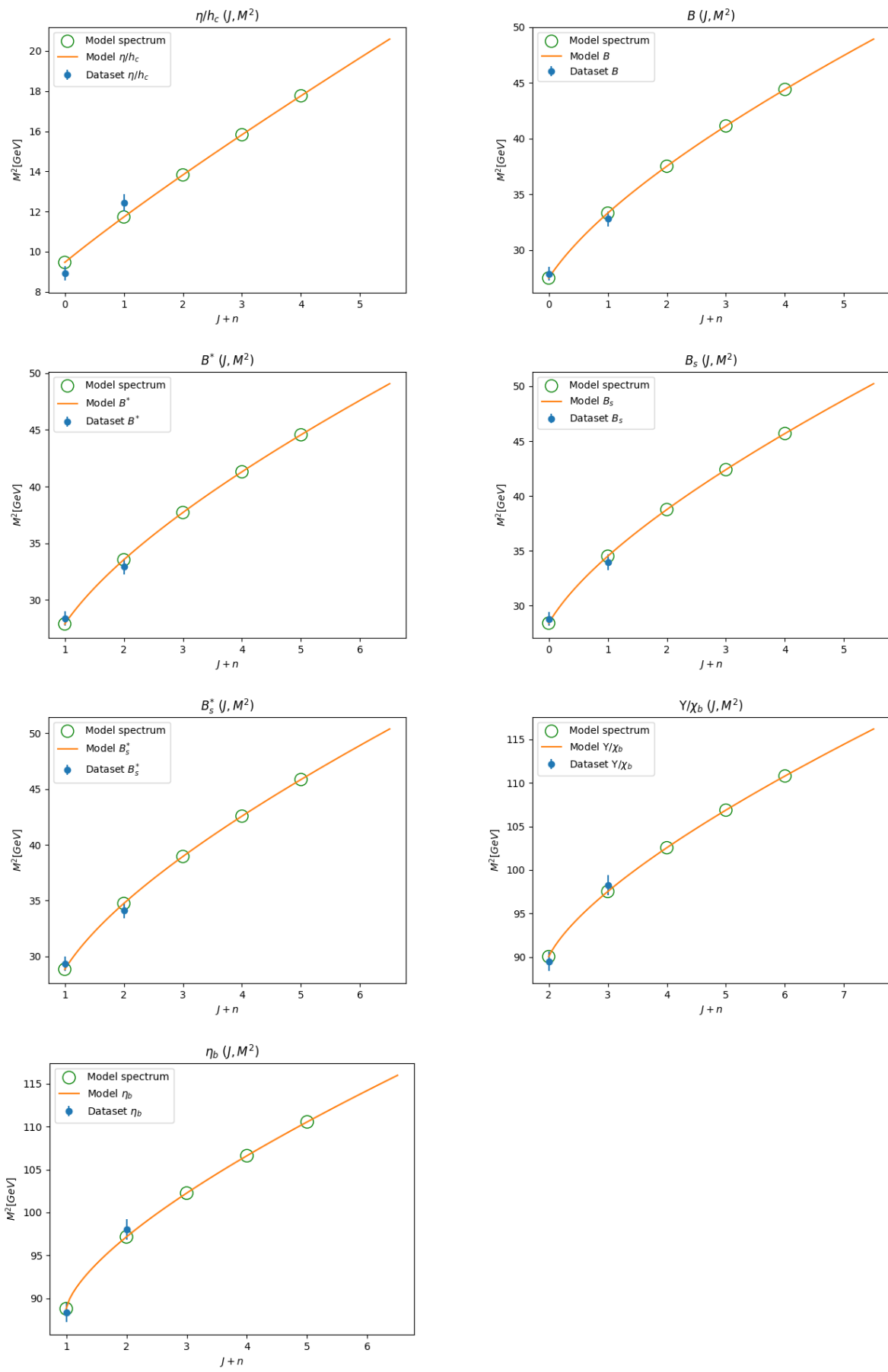












Meson	Content	States	I	J^{PC}	α'	a	m_1	m_2
π/b	$\frac{u\bar{d}}{\sqrt{2}}$ $\frac{u\bar{u}-d\bar{d}}{d\bar{u}}$	$b_1(1235)$ $\pi_2(1670)$ $b_3(2030)$ $\pi_4(2250)$	1	1^{+-} 2^{-+} 3^{+-} 4^{-+}	0.844	0.00	0.17	0.17
ρ/a	$\frac{u\bar{d}}{\sqrt{2}}$ $\frac{u\bar{u}-d\bar{d}}{d\bar{u}}$	$\rho(770)$ $a_2(1320)$ $\rho_3(1690)$ $a_4(2040)$ $\rho_5(2350)$ $a_6(2450)$	1	1^{--} 2^{++} 3^{--} 4^{++} 5^{--} 6^{++}	0.896	0.52	0.065	0.065
η/h	$c_1(u\bar{u} + d\bar{d}) + c_2 s\bar{s}$	$\eta(548)$ $h_1(1170)$ $\eta_2(1645)$ $h_3(2025)$ $\eta_4(2330)$	0	0^{-+} 1^{+-} 2^{-+} 3^{+-} 4^{-+}	0.745	-0.01	0.045	0.045
ω/f	$c_1(u\bar{u} + d\bar{d}) + c_2 s\bar{s}$	$\omega(782)$ $f_2(1270)$ $\omega_3(1670)$ $f_4(2050)$ $\omega_5(2250)$ $f_6(2510)$	0	1^{--} 2^{++} 3^{--} 4^{++} 5^{--} 6^{++}	0.909	0.45	0.06	0.06
K	$\frac{u\bar{s}}{d\bar{s}}$ $d\bar{s}$ $\bar{d}s$ $\bar{u}s$	K $K_1(1270)$ $K_2(1770)$	1/2	0^- 1^+ 2^-				
K^*	$\frac{u\bar{s}}{d\bar{s}}$ $d\bar{s}$ $\bar{d}s$ $\bar{u}s$	$K^*(892)$ $K_2^*(1430)$ $K_3^*(1780)$ $K_4^*(2045)$ $K_5^*(2380)$	1/2	1^- 2^+ 3^- 4^+ 5^-	0.885	0.50	0.060	0.220
ϕ/f'	$s\bar{s}/c_1(u\bar{u} + d\bar{d}) + c_2 s\bar{s}$	$\phi(1020)$ $f'_2(1525)$ $\phi_3(1850)$	0	1^{--} 2^{++} 3^{--}	1.078	0.82	0.400	0.400
D	$\frac{c\bar{d}}{c\bar{u}}$ $c\bar{u}$ $\bar{c}u$ $\bar{c}d$	$D^0(1865)$ $D_1^0(2420)$ $D_J(2740)$	1/2	0^- 1^+ 2^-	1.073	-0.07	0.08	1.640
D^*	$\frac{c\bar{d}}{c\bar{u}}$ $c\bar{u}$ $\bar{c}u$ $\bar{c}d$	D^* $D_2^*(2460)$ $D_3^*(2750)$	0	1^- 2^+ 3^-				
D_s	$\frac{c\bar{s}}{\bar{c}s}$	D_s^\pm $D_{s1}(2536)^\pm$	0	0^- 1^+				
D_s^*	$\frac{c\bar{s}}{\bar{c}s}$	$D_s^{*\pm}(2112)$ $D_{s2}^{*\pm}(2573)$ $D_{s3}^{*\pm}(2860)$	0	1^- 2^+ 3^-	1.093	0.89	0.400	1.580
Ψ/χ_c	$c\bar{c}$	$J/\Psi(1S)(3100)$ $\chi_{c1}(1P)(3510)$ $\Psi(3823)$	0	1^{--} 2^{++} $2^{--[a]}$	0.979	-0.09	1.500	1.500

η_c/h_c ¹⁴	$c\bar{c}$	$\eta_c(1S)$ $h_c(1P)$	0	0^{-+} 1^{+-}	0.88	0.00	1.500	1.500
B	$b\bar{u}$ $b\bar{d}$ $\bar{u}b$ $\bar{d}b$	B $B_1(5721)$	1/2	0^- 1^+				
B^*	$\bar{u}b$ $\bar{d}b$ $\bar{u}b$ $\bar{d}b$	B^* $B_2^*(5747)$	0	1^- 2^+				
B_s	$s\bar{b}$ $\bar{s}b$	B_s $B_{s1}(5830)^0$	0	0^- 1^+				
B_s^*	$s\bar{b}$ $\bar{s}b$	B_s^* $B_{s2}^*(5840)^0$	0	1^- 2^+				
Υ/χ_b	$b\bar{b}$	$\Upsilon(1S)(9460)$ $\chi_{b2}(1P)(9912)$ $\Upsilon(1D)(10164)$	0	1^{--} 2^{++} $2^{--[a]15}$	0.635	1.00	4.730	4.730
η_b	$b\bar{b}$	$\eta_b(1S)$ $\eta_b(1P)$	0	0^{-+} 1^{+-}				

Table 229: Mesons (J, M^2) fit states summarized from [7] and [40] and the global fit results we did for this paper in the (J^2, M^2) plane.

α' [GeV $^{-2}$]	$m_{u/d}$ [GeV]	m_s [GeV]	m_c [GeV]
0.884	0.060	0.400	1.5

Table 230

$a_{\pi/b}$	$a_{\rho/a}$	$a_{\eta/h}$	$a_{\omega/f}$	a_{K^*}	$a_{\phi/f'}$	a_D	$a_{D_s^*}$	a_Ψ
-0.33	0.52	-0.22	0.53	-0.33	0.52	-0.22	0.53	-0.06

Table 231

Meson	Content	States	I	J^{PC}	α'	a	m_1	m_2
π	$u\bar{d}$ $\frac{u\bar{u}-d\bar{d}}{\sqrt{2}}$ $d\bar{u}$	$\pi(1300)$ $\pi(1800)$ $\pi(2070)$ $\pi(2360)$	1	0^{-+}	0.823	0.00	0.225	0.225

¹⁴The values for α' and a are taken from [40] as explained in pages 40, 44.

π_2	$\frac{u\bar{d}}{\sqrt{2}}$ $\frac{u\bar{u}-d\bar{d}}{d\bar{u}}$	$\pi_2(1670)$ $\pi_2(2005)$ $\pi_2(2285)$	1	2^{-+}	0.823	0.26	0.225	0.225
a_1	$\frac{u\bar{d}}{\sqrt{2}}$ $\frac{u\bar{u}-d\bar{d}}{d\bar{u}}$	$a_1(1260)$ $a_1(1640)$ $a_1(2095)$ $a_1(2270)$	1	1^{++}	0.787	-0.14	0.100	0.100
h_1	$c_1(u\bar{u} + d\bar{d}) + c_2 s\bar{s}$	$h_1(1170)$ $h_1(1595)$ $h_1(1965)$ $h_1(2215)$	0	1^{+-}	0.850	-0.02	0.105	0.105
ω	$c_1(u\bar{u} + d\bar{d}) + c_2 s\bar{s}$	$\omega(782)$ $\omega(1420)$ $\omega(1650)$ $\omega(1960)$ $\omega(2290)$	0	1^{--}	1.085	0.95	0.305	0.305
ω_3	$c_1(u\bar{u} + d\bar{d}) + c_2 s\bar{s}$	$\omega_3(1670)$ $\omega_3(1950)$ $\omega_3(2255)$	0	3^{--}	1.085	1.10	0.305	0.305
ϕ	$c_1(u\bar{u} + d\bar{d}) + c_2 s\bar{s}$	$\phi(1020)$ $\phi(1680)$ $\phi(2170)$	0	1^{--}	1.098	1.00	0.515	0.515
K	$u\bar{s}$ $d\bar{s}$ $\bar{d}s$ $\bar{u}s$	$K(1460)$ $K(1830)^{16}$	1/2	0^-				
K^*	$u\bar{s}$ $d\bar{s}$ $\bar{d}s$ $\bar{u}s$	$K^*(892)$ $K^*(1410)$ $K^*(1680)$	1/2	1^-				
K_0^*	$u\bar{s}$ $d\bar{s}$ $\bar{d}s$ $\bar{u}s$	$K_0^*(700)$ $K_0^*(1430)$ $K_0^*(1950)$	1/2	0^+				
D_1^{*0}	$c\bar{u}$ $\bar{c}u$	$D_1^*(2007)^0$ $D_1^*(2600)^0$ $D_J^*(3000)^{017}$	1/2	1^-				
Ψ	$c\bar{c}$	$J/\Psi(1S)(3100)$ $\Psi(2S)(3686)$ $\Psi(4040)$ $\Psi(4415)$	0	1^{--}	0.482	0.81	1.425	1.425
B_c	$\bar{c}b$ $\bar{c}\bar{b}$	B_c $B_c(2S)$	0	0^-				
χ_{c2}	$c\bar{c}$	$\chi_{c2}(1P)$ $\chi_{c2}(2P)$	0	2^{++}				

Υ	$b\bar{b}$	$\Upsilon(1S)(9460)$ $\Upsilon(2S)(10023)$ $\Upsilon(3S)(10355)$ $\Upsilon(4S)(10579)$ $\Upsilon(10860)$ $\Upsilon(11020)$	0	1 ⁻⁻	0.458	1.00	4.73	4.73
χ_{b1}	$b\bar{b}$	$\chi_{b1}(1P)$ $\chi_{b1}(2P)$ $\chi_{b1}(3P)$	0	1 ⁺⁺	0.499	0.58	4.8	4.8

Table 232: Mesons (n, M^2) fit states summarized from [7] and [40] and the global fit results we did for this paper in the (n, M^2) plane.

B Baryons Fits

In this section we summarize the results from previous papers [32] and [40] for the HISH model parameters. We used these for the predictions and fits when confronting the pentaquarks data.

Baryon	Content	States	I	J^P
N	uud	n/p		$1/2^+$
	uud	$N(1680)$		$5/2^+$
	udd	$N(2220)$	1/2	$9/2^+$
	udd	$N(2700)$		$13/2^+$
N	uud	$N(1520)$		$3/2^-$
	uud	$N(2190)$	1/2	$7/2^-$
	udd	$N(2600)$		$11/2^-$
N	uud	$N(1535)$		$1/2^-$
	uud	$N(1720)$	1/2	$5/2^-$
	udd	$N(2060)$		
N	uud	$N(1675)$	1/2	$5/2^-$
	udd	$N(2250)$		$9/2^-$
Δ	uuu	$\Delta(1232)$		$3/2^+$
	uud	$\Delta(1950)$		$7/2^+$
	udd	$\Delta(2420)$	3/2	$11/2^+$
	ddd	$\Delta(2950)$		$15/2^+$
Δ	uuu	$\Delta(1930)$		$5/2^-$
	uud	$\Delta(2400)$	3/2	$9/2^-$
	udd	$\Delta(2750)$		$13/2^-$
	ddd			
Δ	uuu	$\Delta(1700)$	3/2	$3/2^-$
	uud	$\Delta(2200)$		$7/2^-$
	udd			
	ddd			

Δ	uuu uud udd ddd	$\Delta(1905)$ $\Delta(2300)$	$3/2$	$5/2^+$ $9/2^+$
Λ	uds	Λ		$1/2^+$
		$\Lambda(1520)$		$3/2^-$
		$\Lambda(1820)$	$1/2$	$5/2^+$
		$\Lambda(2100)$		$7/2^-$
		$\Lambda(2350)$		$9/2^+$
Σ	uus	Σ		$1/2^+$
	uds	$\Sigma(1670)$	0	$3/2^-$
	dds	$\Sigma(1915)$		$5/2^+$
Σ	uus	$\Sigma(1385)$		$3/2^+$
	uds	$\Sigma(1775)$	0	$5/2^-$
	dds	$\Sigma(2030)$		$7/2^+$
Ξ	uss	Ξ		$1/2^+$
	dss	$\Xi(1820)$	0	$3/2^-$
		$\Xi(2030)$		$5/2^+$
Λ_c^+	udc	Λ_c^+		$1/2^+$
		$\Lambda_c(2625)^+$	0	$3/2^-$
		$\Lambda_c(2880)^+$		$5/2^+$
Λ_c^+	udc	$\Lambda_c(2595)^+$	0	$1/2^-$
		$\Lambda_c(2860)^+$		$3/2^+$
Ξ_c	usc	Ξ_c	0	$1/2^+$
		$\Xi_c(2815)^+$		$3/2^-$
Ω_c	ssc	Ω_c^0	0	$1/2^{+18}$
		$\Omega_c(3065)^0$		$3/2^-$
Ω_c	ssc	$\Omega_c(2770)^0$	0	$3/2^{+19}$
		$\Omega_c(3120)^0$		$5/2^-$
Ξ_b	usb	Ξ_b^0	0	$1/2^+$
	dsb	$\Xi_b(6100)^0$		$3/2^-$
Λ_b	udb	Λ_b^0		$1/2^+$
		$\Lambda_b(5920)^0$	0	$3/2^-$
		$\Lambda_b(6152)^0$		$5/2^+$
Λ_b	udb	$\Lambda_b(5912)^0$	0	$1/2^-$
		$\Lambda_b(6146)^0$		$3/2^+$

Table 233: Baryon (J, M^2) fit results summarized from [32] and [40]

Baryon	Content	States	I	J^{PC}
N	uud udd	n/p $N(1440)$ $N(1880)$ $N(2100)$	$1/2$	$1/2^+$

N	uud udd	$N(1520)$ $N(1875)$ $N(2150)$	1/2	$3/2^-$
N	uud udd	$N(1680)$ $N(2000)$	1/2	$5/2^+$
N	uud udd	$N(1535)$ $N(1895)$	1/2	$1/2^-$
N	uud udd	$N(1720)$ $N(2040)$	1/2	$3/2^+$
N	uud udd	$N(1675)$ $N(2060)$	1/2	$5/2^-$
Δ	uuu uud udd ddd	$\Delta(1232)$ $\Delta(1600)$ $\Delta(1920)$	3/2	$3/2^+$
Δ	uuu uud udd ddd	$\Delta(1620)$ $\Delta(1900)$ $\Delta(2150)$	3/2	$1/2^-$
Δ	uuu uud udd ddd	$\Delta(1700)$ $\Delta(1940)$	3/2	$3/2^-$
Δ	uuu uud udd ddd	$\Delta(1905)$ $\Delta(2000)$	3/2	$5/2^+$
Δ	uuu uud udd ddd	$\Delta(1950)$ $\Delta(2390)$	3/2	$7/2^+$
Λ_c	udc	$\Lambda_c(2625)^-$ $\Lambda_c(2940)^-$	0	$3/2^-$
Ξ_c	usc dsc	Ξ_c $\Xi_c(2970)^-$	0	$1/2^+$
Λ_b	udb	Λ_b $\Lambda_b(6070)$	0	$1/2^+$
Ω_b	ssb	Ω_b^- $\Omega_b(6330)^{-20}$	0	$1/2^+$

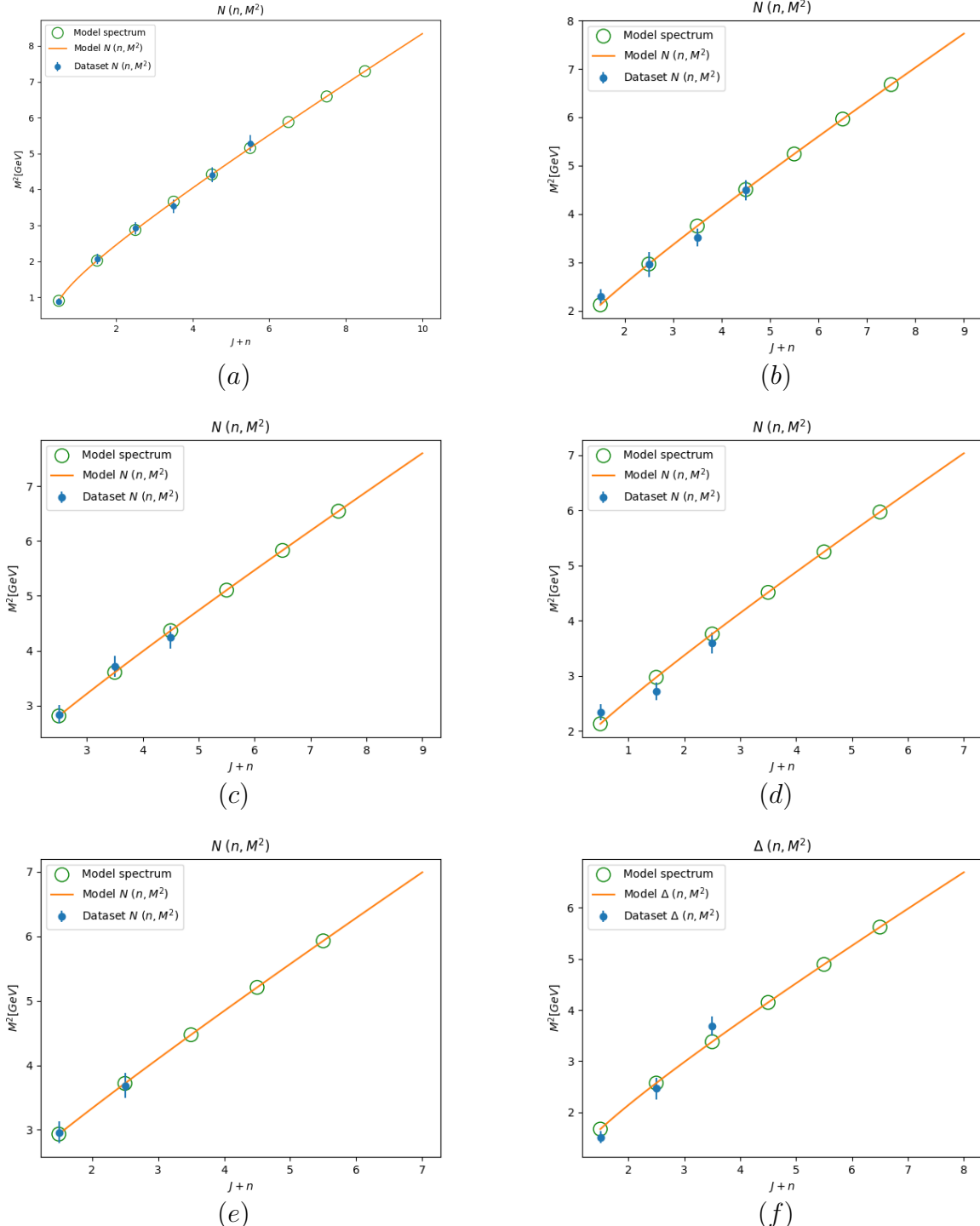
Table 234: Baryon (n, M^2) fit results summarized from [32] and [40].

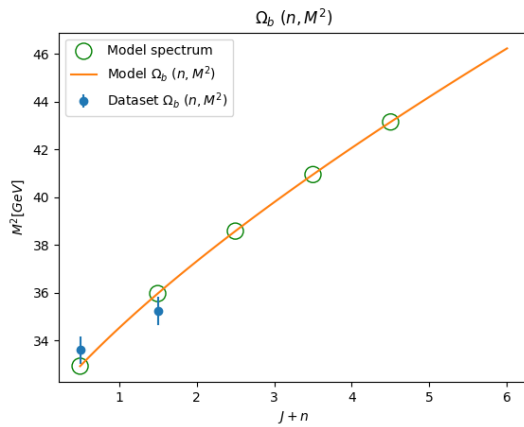
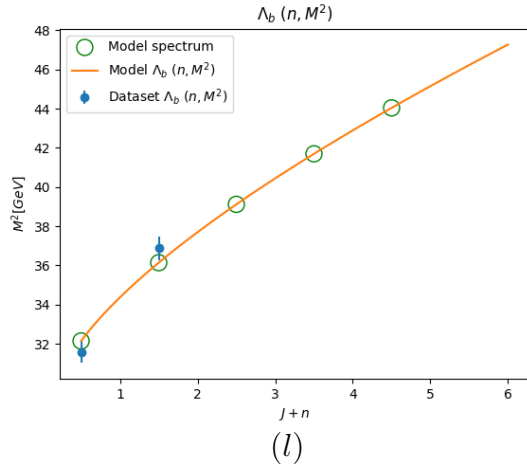
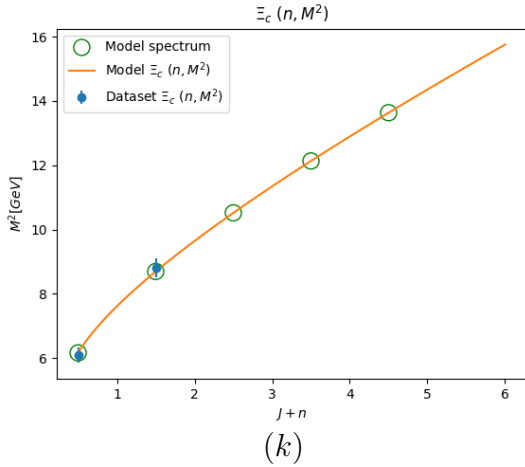
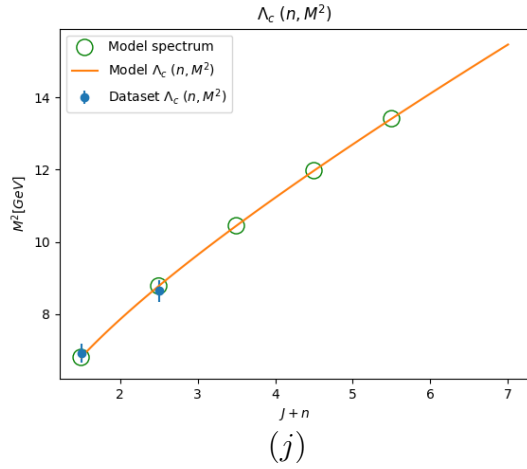
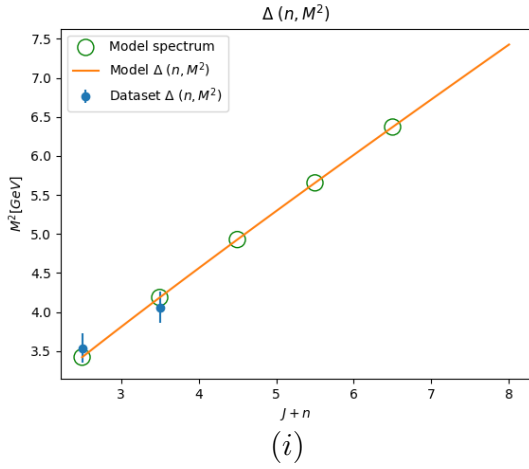
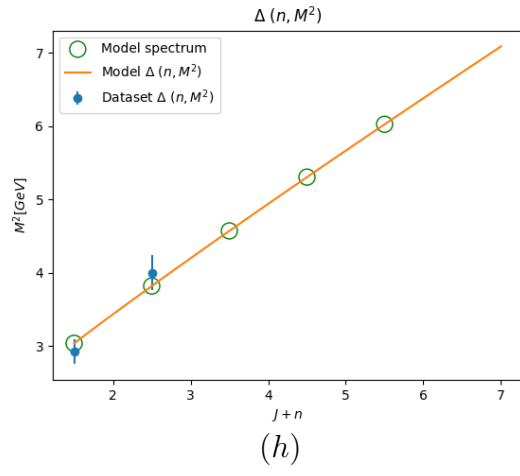
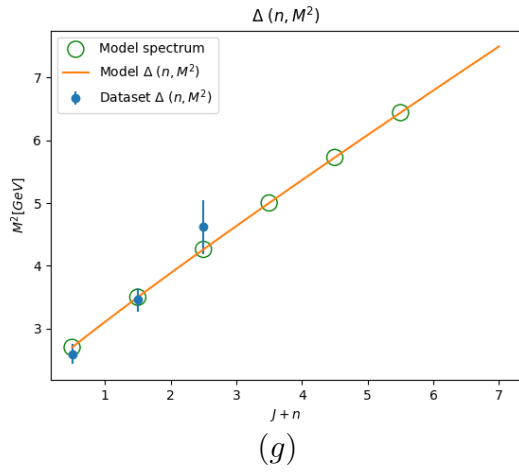
B.1 Baryons (n, M^2) Global Fit.

The fit procedure for the results of this section are at 6.6. Table 235 summarizes the output parameters for the results in this section. The χ^2_r value is 2.32 which is a good result for the accuracy that we expect from this model. The fits are displayed in 236, and the states used are detailed in 234.

χ^2_r	α'_L [GeV $^{-2}$]	α'_H [GeV $^{-2}$]	$m_{u/d}$ [GeV]	m_s [GeV]	m_c [GeV]	m_b [GeV]
2.32	1.6	1.025	0.07	0.39	1.16	4.7
$m_{BV_{u/d,u/d}}$	$m_{BV_{s,u/d}}$	$m_{BV_{s,s}}$	$m_{BV_{c,u/d}}$	$m_{BV_{c,s}}$	$m_{BV_{b,u/d}}$	$m_{BV_{b,s}}$
0.75	0.85	0.39	1.95	2.46	5.20	4.7

Table 235: The baryons global fit in (n, M^2) plane. α'_L and α'_H are the slopes for the light and heavy baryons respectively. The values for $m_{u/d}$, m_s , m_c and m_b were fixed according to the results of 1. The parameters $m_{BV_{q_1,q_2}}$ are the masses of the diquarks.





(n)

Table 236: The global (n, M^2) baryons fit results. The states used for this fit are listed in table 234.